Virginia Commonwealth University
VCU Scholars Compass

Theses and Dissertations | Graduate School

2018

# Metalloglycomics: Investigating the Interactions of Metal Complexes with Heparan Mimetics

Wyatt Johnson
*Virginia Commonwealth University*

Follow this and additional works at: https://scholarscompass.vcu.edu/etd

 Part of the Chemistry Commons

© The Author

Downloaded from
https://scholarscompass.vcu.edu/etd/5672

This Dissertation is brought to you for free and open access by the Graduate School at VCU Scholars Compass. It has been accepted for inclusion in Theses and Dissertations by an authorized administrator of VCU Scholars Compass. For more information, please contact libcompass@vcu.edu.

www.manaraa.com

# Metalloglycomics: Investigating the Interactions of Metal Complexes with Heparan Mimetics

A dissertation submitted in partial fulfillment of the requirements for the degree of Doctor of Philosophy in Chemical Biology at Virginia Commonwealth University

By

Wyatt E. Johnson

B.S. 2011 Pensacola Christian College
M.S. 2013 Pensacola Christian College

Director: Nicholas P. Farrell, Professor, Department of Chemistry, School of Humanities and Sciences, Virginia Commonwealth University

Virginia Commonwealth University
Richmond, VA
December, 2018

www.manaraa.com

# College of Humanities and Sciences
# Virginia Commonwealth University

This is to certify that the dissertation prepared by Wyatt E. Johnson entitled "Metalloglycomics: Investigating the Interactions of Metal Complexes with Heparan Mimetics" has been approved by his committee as satisfactory completion of the dissertation requirements for the degree of Doctor of Philosophy in Chemical Biology.

Nicholas P. Farrell, Ph.D., Director of Dissertation, Chemistry Department, College of Humanities and Sciences

Maryanne M. Collinson, Ph.D., Committee Chair, Chemistry Department, College of Humanities and Sciences

Umesh R. Desai, Ph.D., School of Pharmacy, Department of Medicinal Chemistry

Soma N. Dhakal, Ph.D., Chemistry Department, College of Humanities and Sciences

Matthew C.T. Hartman, Ph.D., Chemistry Department, College of Humanities and Sciences

M. Sammy El-Shall, Ph.D., Chair, Chemistry Department, College of Humanities and Sciences

Montserrat Fuentes, Ph.D., Dean, College of Humanities and Sciences

F. Douglas Boudinot, Ph.D., Dean, School of Graduate Studies

Date

www.manaraa.com

© Wyatt E. Johnson 2018

All Rights Reserved

www.manaraa.com

# Metalloglycomics: Investigating the Interactions of Metal Complexes with Heparan Mimetics

A dissertation submitted in partial fulfillment of the requirements for the degree of Doctor of Philosophy in Chemical Biology at Virginia Commonwealth University

By

Wyatt E. Johnson

B.S. 2011 Pensacola Christian College
M.S. 2013 Pensacola Christian College

Director: Nicholas P. Farrell, Professor, Department of Chemistry, School of Humanities and Sciences, Virginia Commonwealth University

Virginia Commonwealth University
Richmond, VA
December, 2018

www.manaraa.com

Acknowledgments

I wish to thank several people for their contributions to this work. First, I would like to thank my advisor, Dr. Farrell, for his direction and support of this project and giving me the opportunity to work in his research group, he has pushed me to be the best chemist I could be. This project allowed me to learn new techniques and study the exciting field of metalloglycomics through bioinorganic chemistry in a multi-disciplinary fashion. I would like to thank Dr. Qu for all of her help and guidance particularly through the use of NMR. I would also like to thank Dr. Turner for being an invaluable resource in the instrumentation lab. I am grateful to all of the members of the Farrell group, especially Erica for always being there when I had questions and Jamie for allowing me to discuss countless hours of chemistry with him. I am also grateful to the other members of the Farrell lab group: Daniel, Samantha, Sarah, Eric, Samantha, Tom, and David, and the visiting students who have always been available to help me. I would also like to thank my committee members for all of their helpful suggestions and for keeping me on track with my projects. Finally, I wish to thank my wife, Brittany, without her support both financially and emotionally I would not have been able to finish this degree, she always pushed me to be better; and I am eternally grateful that she was willing endure throughout my education process.



www.manaraa.com

Table of Contents





www.manaraa.com

List of Tables





www.manaraa.com

www.manaraa.com

List of Figures





www.manaraa.com

www.manaraa.com

www.manaraa.com

www.manaraa.com

List of Abbreviations

| | |
|---|---|
| μL | microliter |
| μm | micrometer |
| °C | degrees Celsius |
| c | cis |
| cisplatin | *cis*-diamminedichloroplatinum(II) |
| CD | circular dichroism |
| CID | collision induced dissociation |
| cm | centimeter |
| CPPS | cell penetrating peptide |
| CTR1 | copper transporter protein |
| $D_2O$ | deuterium oxide |
| DDD | Dickerson-Drew Dodecamer |
| DNA | deoxyribose nucleic acid |
| FDA | Food and Drug Administration |
| ESI | electrospray ionization |
| EtBR | ethidium bromide |
| GAG | glycosaminoglycan |
| GSH | glutathione |
| Hep | heparin |
| HMG | high mobility group |
| HPLC | high performance liquid chromatography |
| HS | heparan sulfate |
| HSPG | heparan sulfate proteoglycan |
| $IC_{50}$ | half maximal inhibitory concentration |
| ITC | isothermal calorimetry |
| M | molar |
| MB | methylene blue |
| m/z | mass-to-charge ratio |



www.manaraa.com

| | |
|---|---|
| min | minute |
| mM | millimolar |
| mm | millimeter |
| MS | mass spectrometry |
| ms | milliseconds |
| NC | noncovalent |
| NER | nucleotide excision repair |
| NMR | nuclear magnetic resonance |
| OAc | acetate |
| PPC | polynuclear platinum complex |
| Pt | platinum |
| ppm | parts per million |
| $TR_9$ | TAMRA-nonaarginine |
| UV | ultraviolet |
| VIS | visible |
| z | charge of an ion |



www.manaraa.com

Abstract

Metalloglycomics: Investigating the Interactions of Metal Complexes with Heparan Mimetics

By Wyatt E. Johnson

A dissertation submitted in partial fulfillment of the requirements for the degree of Doctor of Philosophy in Chemical Biology at Virginia Commonwealth University

**Virginia Commonwealth University, 2018**

Major Director: Nicholas P. Farrell, Professor, Department of Chemistry

Proteoglycans containing Heparan Sulfate (HS), a sulfated glycosaminoglycan (GAG), play a major role in the cell signaling process, interacting with many different proteins. HS is over expressed on the surface of many cancer cells. Enzymatic cleavage of HS-GAGs by heparanase causes release of angiogenic growth factors leading to tumor cell migration. Heparanase is also over-expressed in tumors with significant correlation between metastatic potential and heparanase activity. Proteoglycans and their associated enzymes are thus significant drug targets of high biological relevance.

A functional consequence of strong PPC-HS binding has been shown in proof-of-concept studies confirming inhibition of the model pentasaccharide, Fondaparinux, by bacterial Heparinase. Such metalloshielding by PPCs may also protect HS from enzymatic cleavage by the mammalian heparanase; preventing growth factors from binding to HS and/or preventing release of bound growth factors and thus inhibiting the metastatic response in the cancer cells. HS-GAGs are also receptors for cellular accumulation of cationic Polynuclear Platinum Complexes (PPCs) through high-affinity binding to the highly anionic HS. PPCs competitively inhibit uptake of TAMRA-R9, a fluorescent nona-arginine derivative, in CHO cells.

The previously reported series of Pt(II) complexes were investigated as DNA binders, initiating the apoptotic cascade. The result of PPC-DNA binding produces long range inter and intra-strand



www.manaraa.com

cross-links, that produce structural and conformational changes. Hydrogen bonding between phosphate oxygens and square planar Pt(II) nitrogen results in bidentate complexes by either backbone tracking or groove spanning of DNA. This complex forms a clamp like structure, called a phosphate clamp, similar to that of the arginine fork. Understanding this clamp allows us to investigate the structurally similar sulfate binding between metal complexes and target HSPG. HSPGs may allow significant research into both a novel cellular internalization of principal metals and "metalloshielding" of heparin by these compounds.

Previous studies have shown that a wide range of metal ions have high affinity to heparin. The trend of metal/heparin affinity is believed to be dependent on parameters consisting of the metal's overall size, spatial orientation of the ligands attached to each metal, the net charge and oxidation state of these metals, and number of binding sites. Studies have shown relative affinities of sulfate and carboxylate groups for the metal ions. These metal cations play an important role in the affinity, specificity, and stability of many protein/heparin interactions. The study of simple coordination compounds, like Pt, Mn, V, Ru and Co, will allow preliminary results which will extend into the PPCs mode of binding.

This thesis focuses on the concept of metalloglycomics and reviews the interactions of various metal complexes with heparin. The covalent and non-covalent interactions of metal complexes with heparin resulting in strong bonding are explained through spectroscopy and calorimetry. The cleavage inhibition of heparanase by metal complexes is also described. Sulfate cluster anchoring shields the sulfates from loss as seen in mass spectrometry. The study of metalloglycomics offers potential understanding into the relevance of metal-heparin interactions and possibilities into the development of new compounds as therapeutic agents.



www.manaraa.com

## Chapter 1: Introduction

### 1.1 Platinum Complexes

Cisplatin (*cis*-diamminedichloroplatinum(II)) was first synthesized in 1845, however, it was not until 1965 by Rosenberg that platinum complexes were shown to inhibit cell division and even later in 1969 that they were shown to possess anticancer properties.(1,2) Since 1978, cisplatin has been in clinical use for treatment in breast, ovarian, bladder, head and neck carcinomas.(3) Cisplatin is most well-known as part of the combination therapy that is used in the treatment of testicular cancer, with a cure rate over 90%.(3) While twenty-eight direct structural analogues of cisplatin have entered clinical trials, only cisplatin, carboplatin and oxaliplatin have been approved for use in the United States, Figure 1.1.(4) The remaining platinum complexes have failed to show improvement over the efficacy of cisplatin.(3)

Structurally, cisplatin consists of two inert ammine ligands and two labile chloride ligands. Platinum (II) exhibits a square planar geometry with a high affinity for nitrogen and sulfur molecules found commonly in proteins and DNA nucleobases. The accepted mechanism of cisplatin cytotoxicity is through DNA binding.(3) Extracellularly, replacement of the labile chlorides is limited due to the high chloride concentration, ~100 mM. Once cisplatin enters the cell, either through passive diffusion or active transport, the labile chlorides are replaced forming an aquated active platinum species.(6-9) Cisplatin, following aquation, acts as a soft Lewis acid and forms stable complexes with S or N donors found in proteins. Cisplatin forms bifunctional intra- or inter-strand cross-links with the N7 on guanine and to a lesser extent adenine bases.(10-14) The 1,2 intrastrand cross-link bends the DNA helix by 32-34$^{o}$ towards the cisplatin bound in the major grove, Figure 1.2.(15) These structural distortions can hinder the replication and transcription processes and lead to the initiation of the apoptotic cascade.(16)

While cisplatin and its analogs have been very successful anticancer drugs, their use is limited by developed or intrinsic resistance.(17, 18) Resistances may arise from multiple sources including a



www.manaraa.com

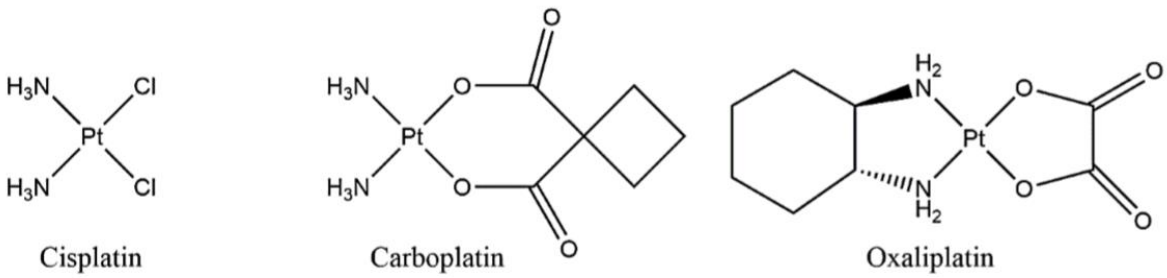


Figure 1.1 Structures of FDA approved platinum-based anticancer

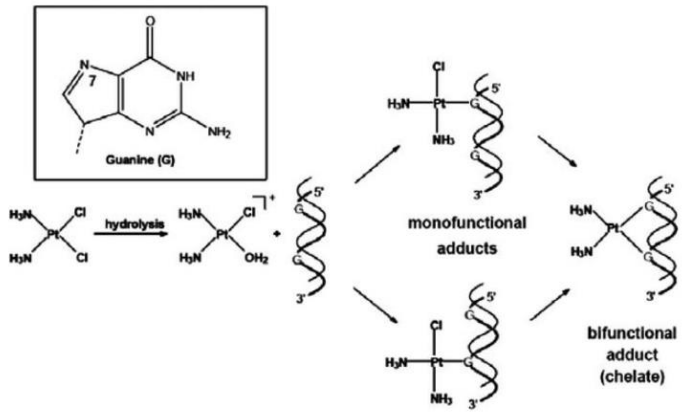


Figure 1.2 Pathways for GG intrastrand crosslinking of DNA by cisplatin. The insert shows the structure of guanine and the position of N7, the major Pt binding site. From Ref. 5



www.manaraa.com

decrease in cellular accumulation due to increased efflux, increase in deactivation of cisplatin by sulfur-containing molecules, Figure 1.3, and increased recognition and repair of cisplatin-DNA adducts, Figure 1.4.(19, 20) Reaction with human serum albumin (HSA), a single chain protein containing 17 disulfide bridges and one free thiol at Cys-34, is thought to be the main route for inactivation in human blood plasma. Another known biomolecule responsible for cisplatin inactivation is glutathione (GSH), an abundant thiol-containing tripeptide, which is present in a concentration of 1~10 mM intracellularly. Due to the centrality of DNA in both the development of the mechanism of action and resistance, new platinum compounds should produce different interactions than cisplatin leading to a greater antitumor efficacy.

The *cis* configuration of Pt(II) compounds was extensively studied since the *trans* configuration was shown to be clinically inactive. Structure-activity studies showed that a *cis* configuration was necessary for the Pt(II) complex to exhibit anticancer properties. The *trans* configuration of Pt(II) complexes is inactive due to the fast deactivation of the compound and their inability to induce DNA structural distortions. However, replacement of the ammine ligands with sterically hindered planar ammine ligands produces an equivalent cytotoxicity as cisplatin.(21) The steric effects of these ligands resulted in the formation of structurally unique cross-links, Figure 1.5, exhibiting cytotoxic activity toward cisplatin-resistant cell lines.(22-26) While certain trans Pt(II) complexes exhibit similar cytotoxicity to cisplatin, the reactivity potential of *trans* complexes with inactivating sulfur-containing nucleophiles increases due to the trans-influencing chlorides.(27) In an effort to optimize the pharmacological properties of *trans* compounds, another innovative approach was used, synthesizing cationic polynuclear platinum complexes (PPCs). A representative trinuclear complex, BBR364, was the first polynuclear platinum compound to enter clinical trials as an anticancer agent, Figure 1.6. BBR3464 binds to DNA through long range inter- and intra-strand cross-links, Figure 1.7.(30, 31) These lesions do not significantly bend the DNA and are therefore not recognized by high mobility group (HMG) and are a poor substrate for nucleotide excision repair (NER).(31) Upon binding to DNA, PPCs are capable of producing a B to A or Z transition.(4) Although BBR3464 resulted in a non-cross resistant cytotoxicity with



www.manaraa.com

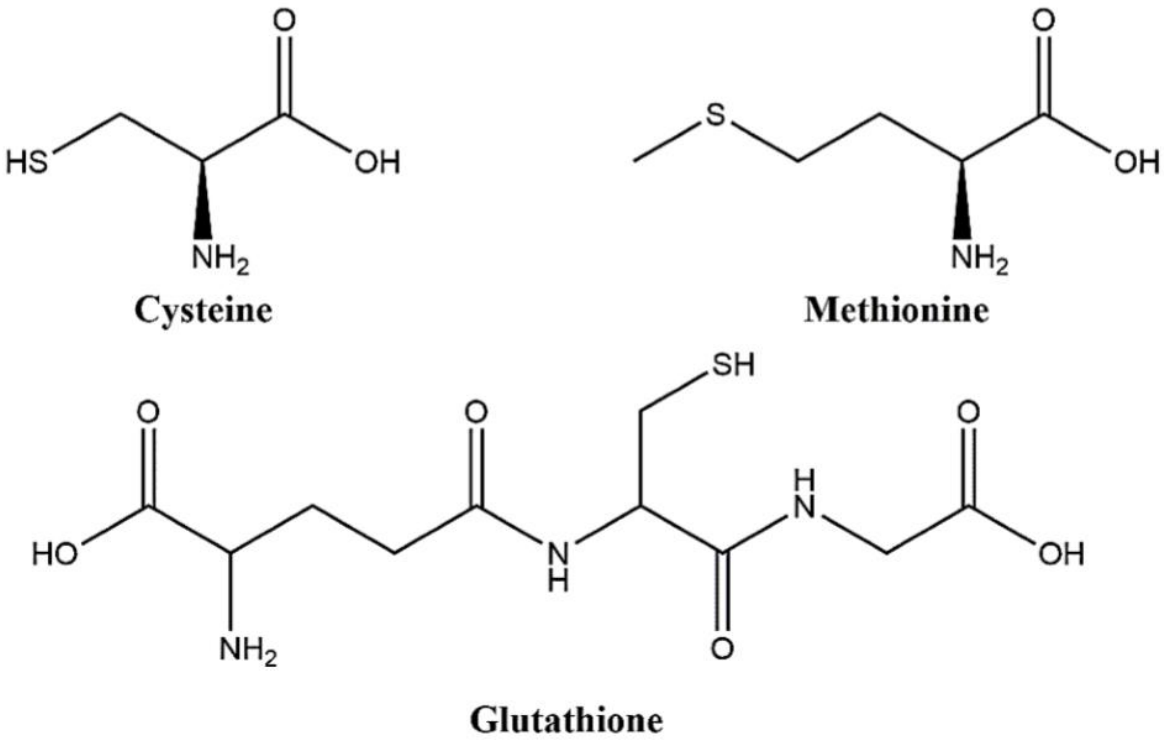


Figure 1.3 Structure of sulfur containing nucleophiles: Cysteine, methionine, and

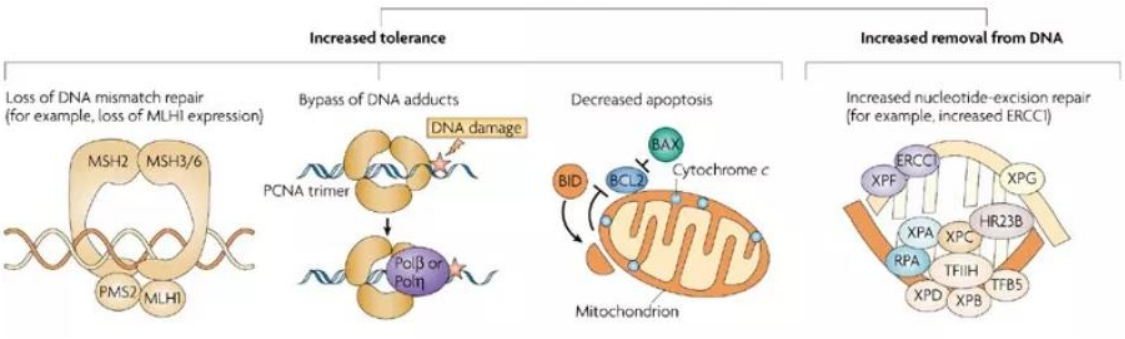


Figure 1.4 Resistance pathways for cisplatin and its analogs after DNA binding. From Ref. 8



www.manaraa.com

cisplatin by inducing a distinct mode of DNA binding, degradation into inactive metabolites by sulfur-containing nucleophiles was no exception for BBR3464 as with other covalently binding platinum compounds.(4) Replacement of the reactive chlorides by ammines or dangling ammines, Figure 1.8, negated the pharmacokinetic difficulties of inactivation by sulfur-containing nucleophiles.(32, 33) Replacement of Pt-Cl by substitution-inert ligands becomes unreactive toward sulfur nucleophiles, thus enhancing metabolic stability, and also allows study of non-covalent contributions. Non-covalent interactions showed a new mode of ligand-DNA recognition distinct from the conventional modes of intercalation and groove binding. Hydrogen bonding with phosphate oxygens results in either backbone tracking or groove spanning through formation of phosphate clamps where the $PtN_4$ coordination sphere forms bidentate N-O-N complexes with phosphate oxygen atoms condensing DNA.

One of the major requirements for the effectiveness of an anticancer therapeutic is the successful cellular uptake of the compound. A series of structure-activity relationship rules that define the favorable characteristics that a successful therapeutic agent should possess was broadly defined as: possess a zero net charge, contain two leaving groups or one bidentate leaving group, have chloride leaving groups or similar ligands, leaving groups oriented in the *cis*-configuration, no hydroxy or hydroxo ligands as it increases toxicity, and have inert non-leaving groups such as amines.(34-36) However, the previous assumption that platinum complexes need to be neutral to enter cells was contradicted by the higher cellular accumulation of the highly cationic PPCs over cisplatin.(37) Polynuclear platinum compounds have a remarkable cellular uptake that appears to be based on the charge of the compounds. Recently, the endocytic pathway has been utilized as a means to deliver the bioactive structure into the cell.(8) Cell penetrating peptides (CPPs), which consist of polycationic arginine rich oligopeptides, are capable of migrating across the membrane in a short time with the ability to assist other biomolecular compounds that may not readily migrate across the membrane.(34-36) For polyarginine CPPs, the effective arginine residues for cellular translocation ranged from 6 to 20 residues, with a maximal uptake of approximately 15 residues.(12) A length over 20 arginines increases the association to a level that is too high for the



www.manaraa.com

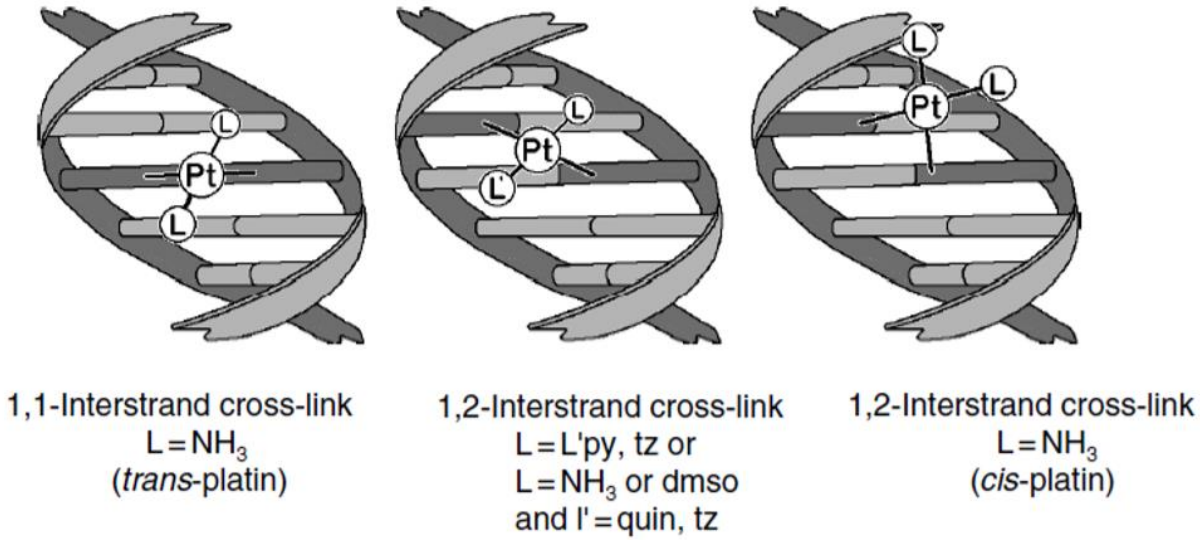


Figure 1.5 Unique cross-links formed by transplatin derivatives. From Ref. 29

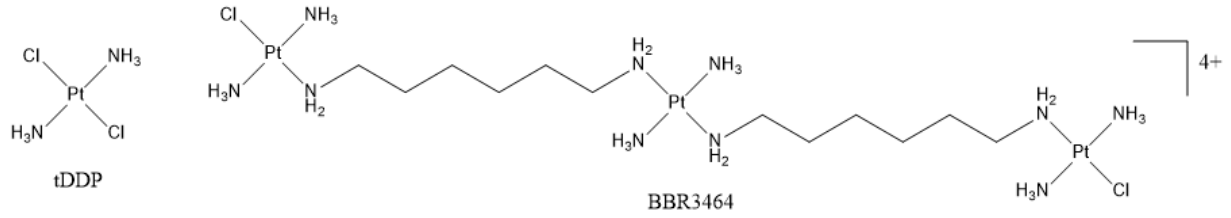


Figure 1.6 Structures of transplatin and BBR3464.



www.manaraa.com

effective release of the structure from the membrane. The cell surface contains an array of possible anionic binding sites, like phospholipids and polysaccharide constituents. While it has been well established that charged compounds do not readily cross the membrane without some sort of energetic assistance, which may come in the form of pumps or channels. Arginine rich peptides have been heavily studied because of their ability to translocate across the plasma membrane of living cells.(14)

The mechanism of PPCs cellular internalization and reactivity with DNA prompted studies into PPCs interactions with extracellular heparan sulfate proteoglycans (HSPG) as the mechanism of internalization and expand its studies into other transition metals to lower the cytotoxic profile.

### 1.2 Other Metal Complexes

In the early development of platinum complex analogs, other transition metals with similar reactivities as cisplatin were examined. A wide variety of ruthenium-based complexes exhibited anti-cancer properties.(38-43) NAMI-A, Figure 1.9, exerts antimetastatic effects which may occur through multiple mechanisms.(41-53) Superoxide dismutase (SOD) with an attached manganese performs the role of superoxide detoxification in the mitochondria. M40403, Figure 1.9, a SOD mimic, has been used as a cancer co-therapy with interleukin-2 (IL-2), an immune-stimulating cytokine drug. IL-2 shows enhanced efficacy when used in combination with M40403.(56-65) Metals like vanadium, while not specifically used in cancer treatments, have sparked increasing interest over their role in biological systems. The discovery of insulin-like properties of the vanadate ions stimulated research into the use of vanadium complexes as insulin mimics.(66-79) Many more examples of metal-containing drugs have been reported. Complexes containing gold, technetium, rhenium, gadolinium, lithium, bismuth, iron, calcium, lanthanum, gallium, tin, arsenic, rhodium, copper, zinc, aluminum, and lutetium have all been used in medicine.(80) More recently, cobalt complexes have been found to possess antiviral activity.



www.manaraa.com

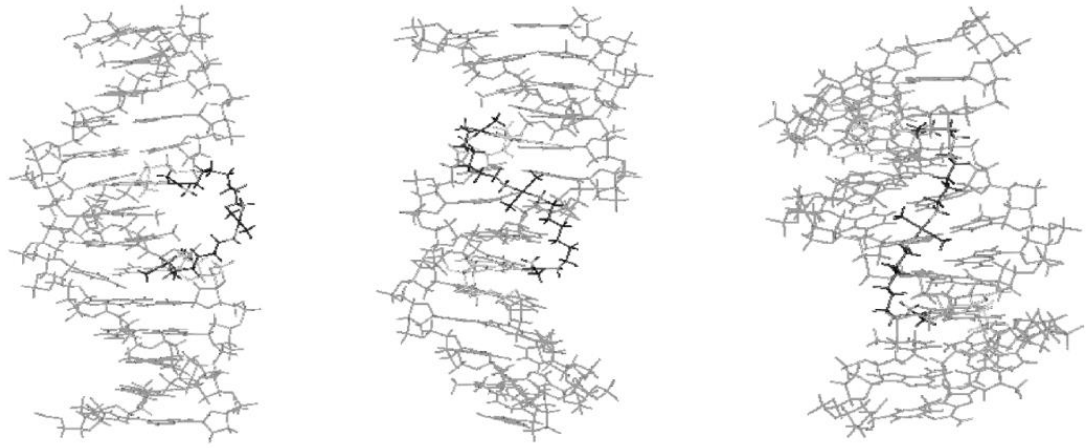

1,4-Interstrand cross-link 1,5-Interstrand cross-link 1,6-Interstrand cross-link

Figure 1.7 Structures from molecular modeling of the major DNA adducts of BBR3464. From Ref. 29

**Monoplatin-NC**

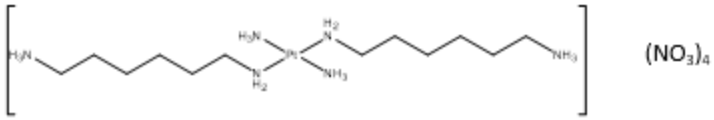

**Diplatin-NC**

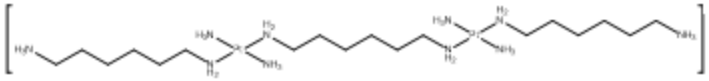

**BBR3464**

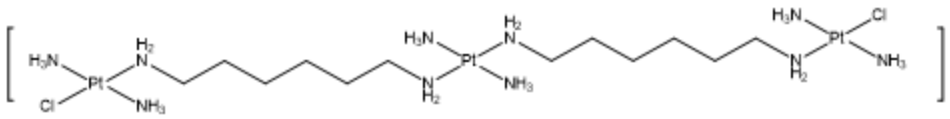

**AH44**

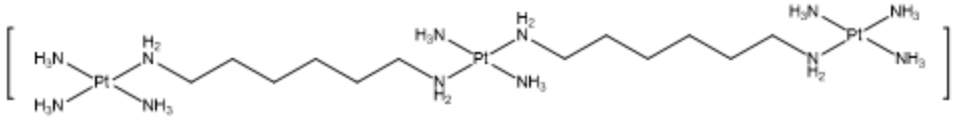

**Triplatin-NC**

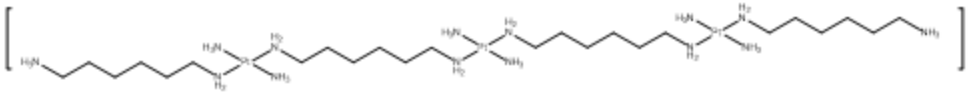

Figure 1.8 Structures of platinum complexes.



www.manaraa.com

The cobalt (III) ion in vitamin $B_{12}$ is one of a few organometallic complexes found naturally in the human body. Due to cobalt's role in biological processes, mechanisms have been developed to overcome cobalt overload, thus cobalt is less toxic to humans than non-essential metals like platinum. Cobalt (III), while normally unstable in water, can be stabilized against reduction by chelating ligands. One of the most promising applications of cobalt (III) complexes is the CTC series, Figure 1.10, that was shown to inhibit replication of Herpes Simplex Virus Type 1 (HSV-1).(81-87) Hexamminecoablt(III) chloride (Cohex), Figure 1.10, is an example of a classical Werner complex that is kinetically stable in aqueous solutions. While Cohex possesses the ability to hydrogen bond with the phosphate backbone of DNA, the mechanism of action is still not fully understood. Cohex also exhibits significant antiviral activity and acts at the point of viral entry. It is conjectured that the high positive charge density of Cohex allows it to disrupt the interaction of Sindbis virus glycoproteins with highly negatively charged, polysulfonated heparan sulfate receptors, Figure 1.11.(88, 89)

The acquired and intrinsic resistances to traditional platinum-based anticancer drugs have compelled research into the investigation of the properties of other transition metal-based compounds.(90-96) The less cytotoxic anticancer potential of cobalt complexes has been extensively studied over the last three decades with much time being devoted to the understanding of their mechanisms of action.(97, 98) This stimulated research into investigating cobalt-containing compounds as less toxic alternatives to platinum-based anticancer drugs. In 1952, the first biological studies were conducted with cobalt(III) complexes, verifying the low systemic toxicity, while some complexes (99) also exhibiting antibacterial properties, Figure 1.12.(100) Cohex has been found to have low to moderate toxicity, much less than cisplatin. The cytotoxicity of Cohex was measured against BHK cells and compared to that of cisplatin, Figure 1.13.(101) The Cohex cytotoxic effects are observed around 1 mM or higher, whereas cisplatin was cytotoxic at even the lowest concentration of 80 µM.



www.manaraa.com

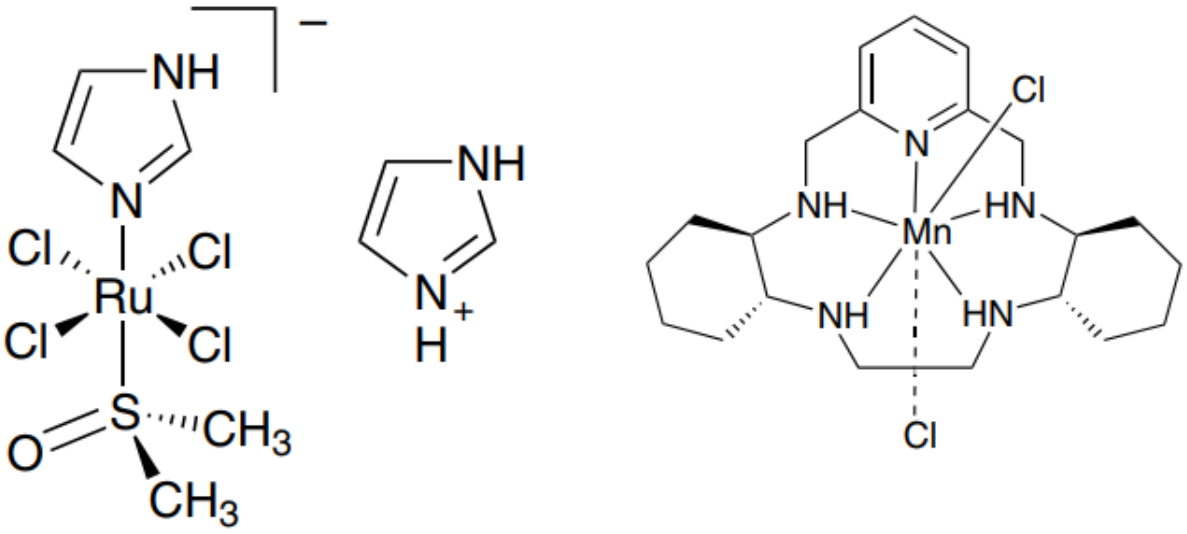


Figure 1.9 Structure of NAMI-A (left) and M40403 (right).

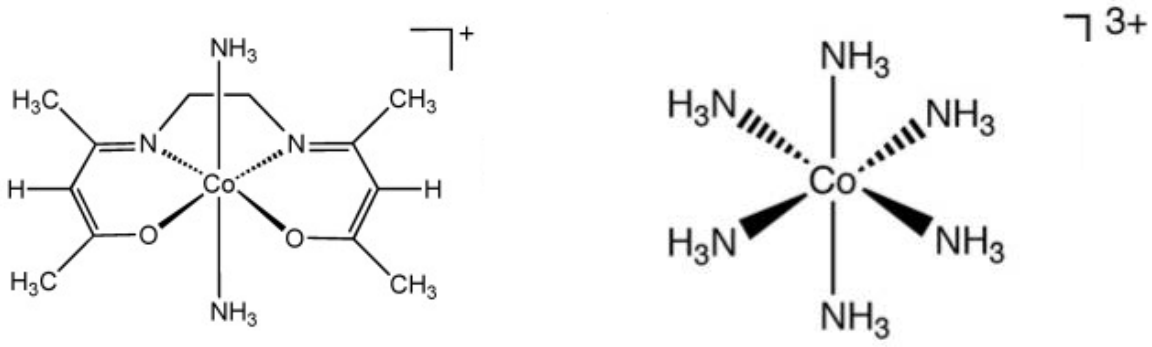


Figure 1.10 Structure of CTC (left) and Cohex (right).



www.manaraa.com

The most significant medical advancement in terms of cobalt compounds thus far, is the clinical development of Doxovir (CTC-96) for Herpes Simplex Virus 1, Figure 1.12.(102) The mechanism of action of Doxovir is still unknown, however it is speculated that Doxovir covalently binds to histidine residues in the active site of a viral enzyme which is crucial for Herpes replication, Figure 1.14.(103) The hexamminecobalt (III) cation was also discovered to complex with heparin interacting through all three of its valencies, which allowed for accurate determination of the content of anionic groups in sulfoglycosaminoglycans.(104)

Ruthenium complexes have also raised great interest and have been tested against a number of cancer cell lines.(105-112) Many Ru(III) compounds contain exchangeable ligands and require activation by the tumor microenvironment.(113) The antitumor properties of the Ru(III) complexes occur when they are reduced to Ru(II) under biological circumstances of low oxygen concentration, acidic pH and high levels of glutathione.(114-116) The first approved ruthenium complex in clinical trials, NAMI-A, [trans-$RuCl_4$(DMSO)(Im)] (Im = imidazole, DMSO = dimethylsulfoxide), Figure 1.9, has low potency in terms of direct cytotoxicity towards cancer cells *in vitro*; however, *in vivo*, it has significant efficacy in inhibiting tumor metastasis.(117-122) The mechanism of action of NAMI-A remains to be elucidated, but data suggests that NAMI-A is capable of binding to DNA and RNA. The fluorescent and photo-activating properties of Ru-polypyridyl complexes have been used in analyzing the abundance and degree of sulfation of HS and evaluating HS-growth factor interactions.(123) Ruthenium red, a polycationic stain, has been used to visualize acid polysaccharides on the outer surface of cells.(124) While the fluorescent properties of $[Ru(bipy)_3]^{2+}$ have been used to detect heparin and HS.(125) The application of less cytotoxic metal complexes can be expected to produce new patterns of metal ion binding with the HS chain. Further investigation is deserved to elucidate these lower cytotoxic complexes and their interactions with heparan sulfate.



www.manaraa.com

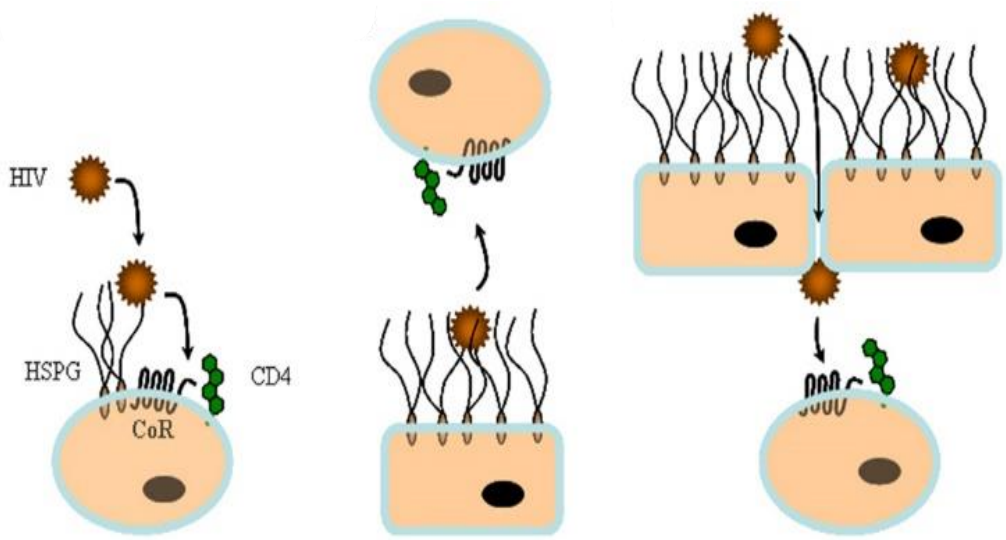


Figure 1.11 Heparan sulfate (HS) can play multiple roles during viral infection. On top of cells that express large amount of HS, HS can capture viral particles and facilitate in cis subsequent interaction with specific entry receptors. HS from non-permissive cells such as endothelia or epithelia can sequester HIV-1 and then mediate in trans infection by presenting the virus to permissive cells. HS can contribute to both attachment and transcytosis of HIV-1 through epithelia. From Ref. 88

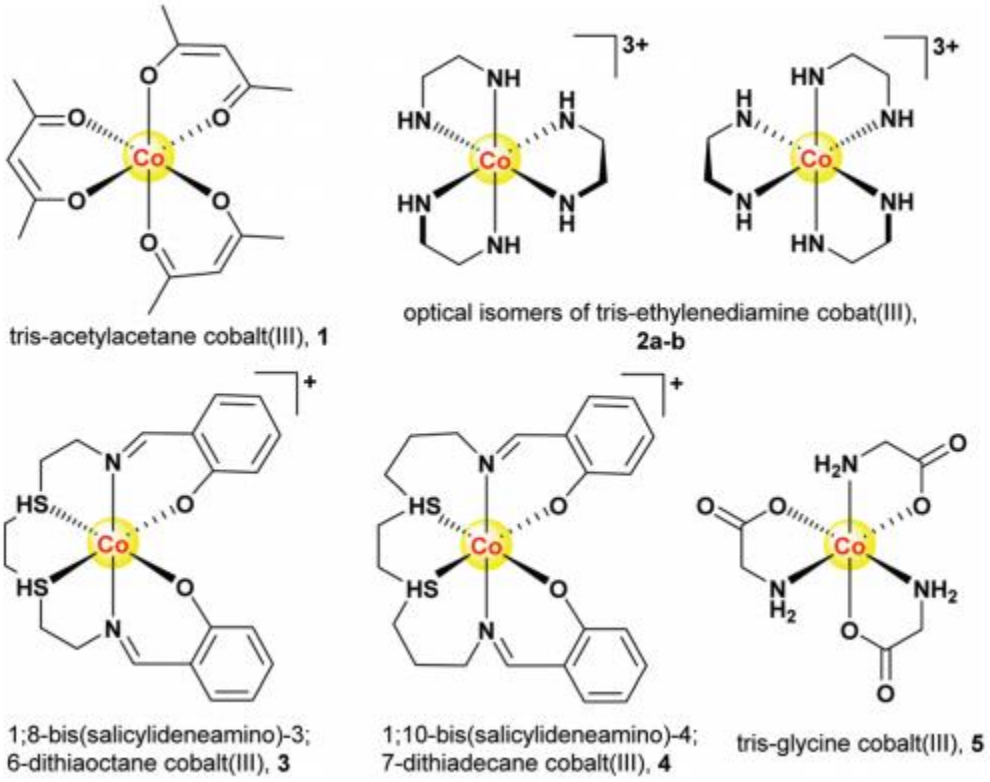


Figure 1.12. Chemical structures of cobalt(III) coordination complexes used in early biological studies. From Ref. 100



www.manaraa.com

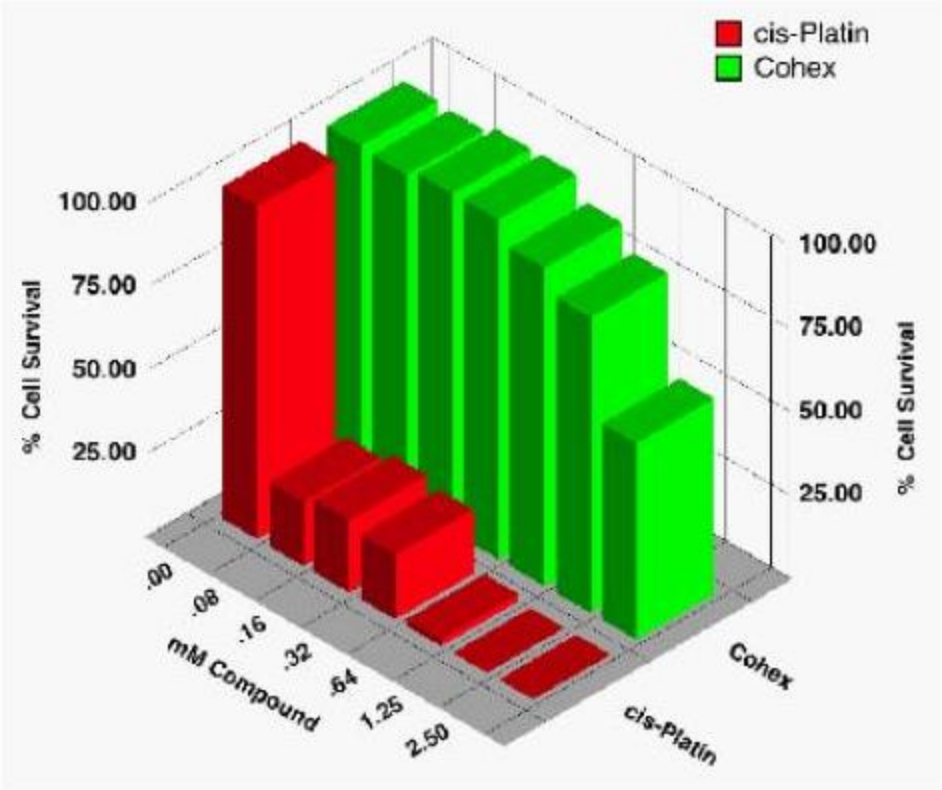


Figure 1.13 Comparison of cytotoxicity of Cohex against BHK cells with cisplatin. From Ref. 87

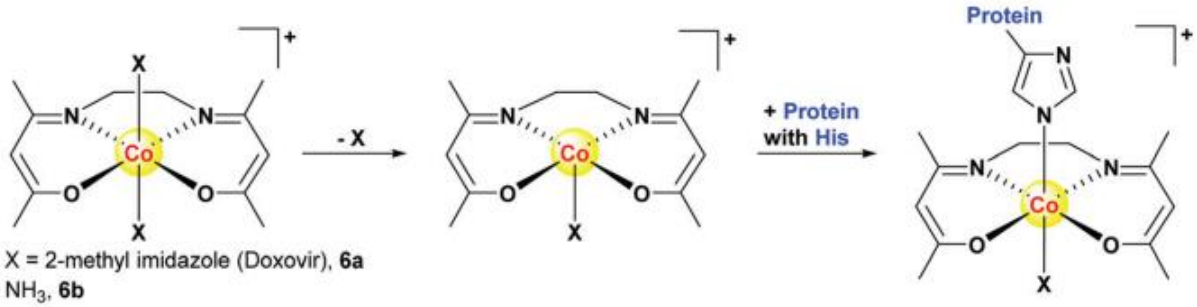


Figure 1.14. The proposed mechanism of action of Co(III)-acacen complexes, including Doxovir. It is postulated that one of the axial ligands is lost in a dissociative manner, followed by covalent binding to histidine residues within the active site of key enzymes or signalling proteins. From Ref. 102



www.manaraa.com

### 1.3 Glycosaminoglycans

Heparan sulfate proteoglycans (HSPGs) are polysulfated linear polysaccharides that are found on the cell surface and localized in mast cells.(126) These highly charged polysaccharides are made up of repeating 1-4 linked polysulfated disaccharide units comprised of glucosamine and hexuronic acid, with up to three sulfate moieties per unit. Two structurally similar polysaccharides, heparin and heparan sulfate (HS) are the most complex members of the glycosaminoglycan (GAG) family, which also consists of chondrotin sulfate, dermatan sulfate, and keratin sulfate.(127) Heparan sulfate is biosynthesized as a proteoglycan and strategically located on the cell surface and in the extracellular matrix.(127) The role of HS has been shown to include a variety of biological processes consisting of cell adhesion, cell growth regulation, blood coagulation, binding of cell surface proteins, and tumor metastasis.(127)

Heparin chains consist of repeating units of iduronic or glucuronic acids and D-glucosamine which may be irregularly substituted at the O- or N-sulfate or N-acetyl positions, Figure 1.15.(128) The sulfate residues act as the primary receptors for protein recognition which is affected by shape, sulfation pattern, and mobility of the heparin chain.(129) The iduronic acid residue can potentially adopt either $^{1}C_{4}$ chair or $^{2}S_{0}$ skew boat conformations with flexibility occurring around the glycosidic linkage.(130, 131) In heparin the $^{1}C_{4}$ to $^{2}S_{0}$ confomers ratio is 60:40 while the ratio in Fondaparinux is 40:60, more importantly when these fragments interact with a receptor the most favorable conformation is adopted, Figure 1.15.(132-134)

As with other major classes of macromolecules, the biological roles of glycans extend from negligible to crucial for the development, growth, functioning, or survival of the cell, Figure 1.16. The biological roles of glycans can be divided into two broad categories: the structural and modulatory properties of glycans and the specific recognition of glycans by other molecules either mediating cell-cell interactions or recognizing extracellular molecules. When conjugated with proteins, the proteoglycans are found in connective tissue with critical functions in cellular adhesion and migration. When in the extracellular matrix, proteoglycans form large complexes to



www.manaraa.com

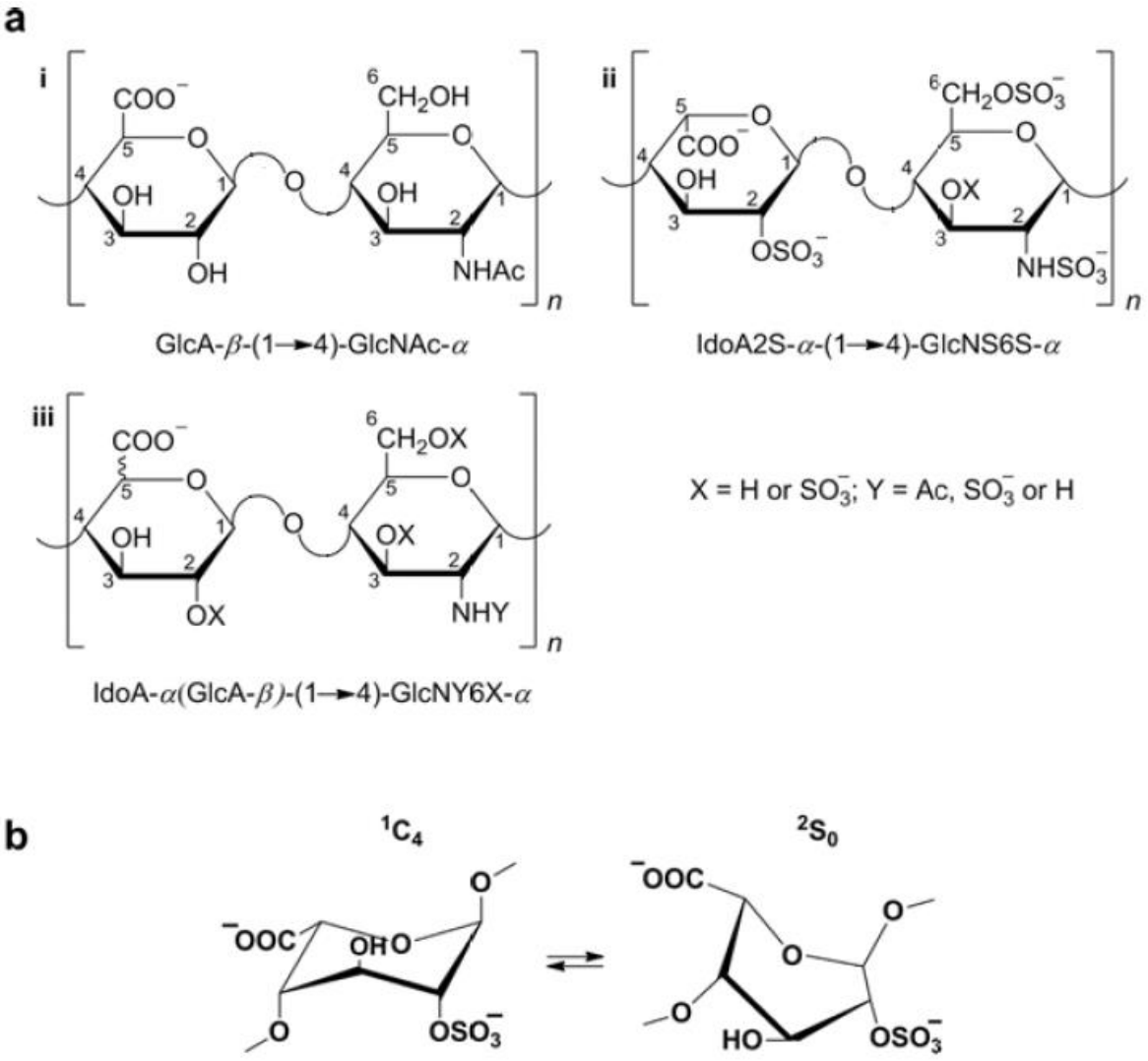


Figure 1.15. (a) Major repeating disaccharide unit of (i) heparan sulfate; (ii) heparin; and (iii) variable repeating disaccharide unit of heparin and heparan sulfate. (b) Equilibrium between the two major conformations found in IdoA(2S) residues of heparin and heparan sulfate. From Refs. 132-134



www.manaraa.com

other proteoglycans, to hyaluronan, and to fibrous matrix proteins such as collagen, affecting the activity and stability of proteins and signaling molecules within the matrix. Heparan sulfate is a sulfated glycosaminoglycan with numerous important biological activities associated with its interaction with diverse proteins, including growth factors, proteases, lipid-binding proteins, and adhesion proteins.

Heparan sulfate interacts with a range of proteins, growth factors, and enzymes. Recognition is affected by the glycosidic linkages, conformation, sulfate position, and associated cations.(135) Heparin is widely used as an anticoagulant drug based on its ability to accelerate the rate at which antithrombin inhibits serine proteases in the blood coagulation cascade. Fondaparinux (FPX), a synthetic glycosaminoglycan, is one example of the structure activity relationship required to produce an antithrombotic (AT) agent.(136) The variation of number and position of carboxylates and sulfates on the FPX chain confirmed these essential features for AT binding. The main example of HS–protein interactions is the binding to fibroblast growth factors (FGFs), a family of 23 structurally related polypeptides involved in developmental and physiological processes including cell proliferation, differentiation, morphogenesis and angiogenesis.(135, 136) Fibroblast Growth Factors (FGFs) are involved in differentiation, proliferation, and angiogenesis through high affinity interactions with their receptors. Heparan sulfate protects FGFs from degradation and assists their binding to receptors.(137) Again, heparan sulfate chain length, sulfation pattern, and conformation all play integral roles in their attachment to growth factors.(138) Binding of basic FGF to cell surface HSPG is necessary for its recruitment of high affinity FGF receptors and for its activity. In an initial step, these effects are exerted through binding to four highly related transmembrane tyrosine kinase receptors (FGFR1–FGFR4) resulting in FGF–FGFR dimerization, Figure 1.17.(139) This results in trans-autophosphorylation of FGFRs at intracellular tyrosine residues and the activation of the Ras/mitogen-activated protein kinase and/or phosphoinositide 3-kinases (PI3K)/Akt signaling networks.(140) Increased stimulation of receptor tyrosine kinases (RTKs) by growth factors is associated with the metastatic spread of cancerous cells.(141) Furthermore, heparan sulfate can be cleaved at the glycosidic bonds by both mammalian and



www.manaraa.com

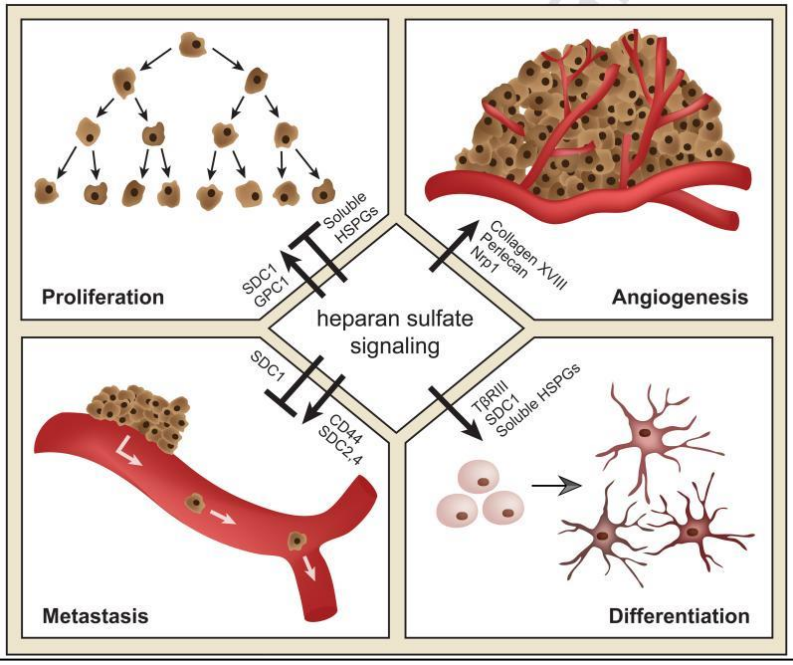


Figure 1.16: Involvement of heparin and heparan sulfate in important physiological processes. From Ref. 143

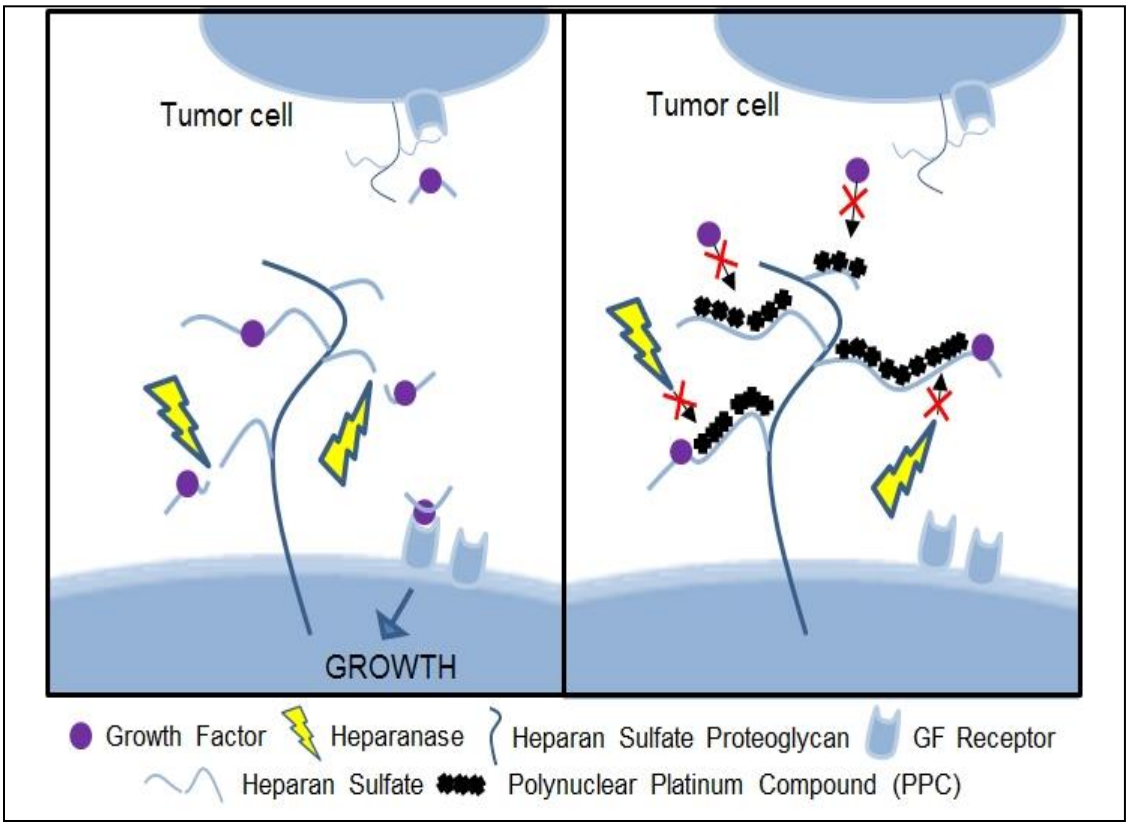


Figure 1.17 Free growth factors bind to the HSPGs and are cleaved by heparanse. Heparan Sulfate then mediates the dimerization between the growth factor and its receptor for accumulation into the cancer cell, resulting in growth. Proposed mechanism of metastatic and angiogenic hindrance from PPC binding.



www.manaraa.com

bacterial enzymes. In the mammalian case, enzymatic degradation by heparanase releases pro-tumorigenic growth factors.(142)

Due to the highly anionic nature of heparan sulfate, HS may associate with many physiological relevant cations which affects the conformation of the heparan sulfate chain.(143-145) Manganese deficiency in animals has significant effects on the production of hyaluronic acid, chondroitin sulfate, heparin, and other forms of mucopolysaccharides that are important for growth and maintenance of connective tissue, cartilage, and bone.(146) It was found that $Mn^{2+}$ had the strongest affinity toward heparin, in terms of decreasing affinities toward heparin, the relative relationships were $Mn^{2+} > Cu^{2+} > Ca^{2+} > Zn^{2+} > Co^{2+} > Na^{+} > Mg^{2+} > Fe^{3+} > Ni^{2+} > Al^{3+} > Sr^{2+}$.(147) Furthermore, $Mn^{2+}$ had the second highest number of heparin-binding sites at 66.(147) The insulin-like properties of vanadium salts have also attracted much attention in the cases of insulin resistances or deficiencies.(148-151) Vanadate's close resemblance to phosphates enables it to inhibit many of the enzymes that are involved in phosphate metabolism.(152) Recently, vanadium has been shown to activate the ERK pathway via phosphorylation of the EGF-R.(153, 154) $Cu^{2+}$ promotes angiogenesis and modulates vascular endothelium growth factor (VEGF) activity.(155, 156) The application of hard and soft acid and base concepts of these simple metals can be expected to produce new patterns of metal ion binding with the hard sulfate base on the HS chain.



www.manaraa.com

## 1.4 Inhibitors

The development of heparanase inhibitors for the treatment of highly malignant tumors is therefore of considerable interest. Heparanase inhibitors are a group of compounds inhibiting/decreasing heparanase enzymatic activity, which abolish degradation of heparanase on HS of extracellular matrix (ECM) and thus subsequential cascade. As an analog of the natural substrate of heparanase, heparin is commonly considered to be a potent inhibitor of heparanase as an alternative enzyme substrate. This activity is attributed to the high affinity heparin–enzyme interaction and the limited degradation of heparin. Heparin, as well as other sulfated polysaccharides, inhibits tumor cell heparanase, however, its use is limited due to its potent anticoagulant activity.(157-159) This drawback has stimulated research into the potential use of modified, nonanticoagulant species of heparin.(157-159) There are other examples of heparanase inhibitors as heparan sulfate mimics to produce an alternative enzyme substrate. Glycol-split N-acetyl heparin shows dramatically increased heparanase-inhibiting activity with substantial loss of the anticoagulant activity due to cleavage of C-2–C-3 bonds which are essential for binding to antithrombin, Figure 1.18.( 157-159) Heparanase enzyme activity can be inhibited by shorter but more extensively sulfated oligosaccharides, like PI-88, a highly sulfated phosphosulfomannan, Figure 1.18. The success of PI-88 inspired development of additional oligosaccharide-based heparanase inhibitors, mimicking GAGs as prototypes, like oligomannurarate sulfate, Figure 1.18. Suramin, Figure 1.18, is a polysulfonated naphthyl urea that inhibits heparanase with an $IC_{50}$ of 48 μM.( 157-159) Synthetic, linear, noncarbohydrate polyanionic polymers have also been studied as heparin mimetics. Besides heparanase substrate mimetics, development of small-molecular weight compounds directly inhibiting heparanase activity was also studied.( 157-159) The structure activity relationship study of this class of compounds led to 2-[4-propylamino-5-[5-(4-chloro)phenyl-benzoxazol-2-yl]phenyl]-2,3-dihydro-1,3-dioxo-1 H-isoindole-5-carboxylic acid, benzoxazol-5-yl-acetic acids, and 1,3-bis-[4-(1 H-benzoimidazol-2-yl)-phenyl]-urea, Figure 1.18, which displayed heparanase inhibitory activity and antiangiogenic effects.( 157-159) Currently, all heparanase inhibitors raise



www.manaraa.com

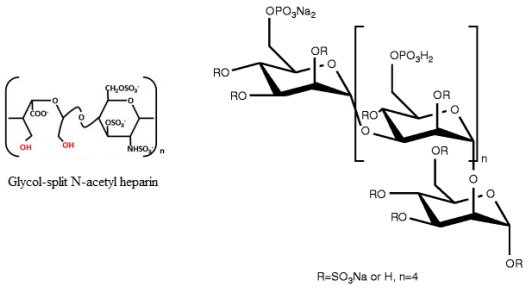

Glycol-split N-acetyl heparin

R=$SO_3Na$ or H, n=4

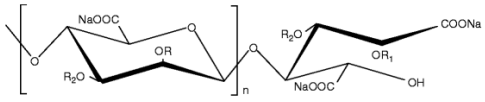

$R_1$=$SO_3Na$. $R_2$=$SO_3Na$ or H, n = 3–9

oligomannurarate sulfate

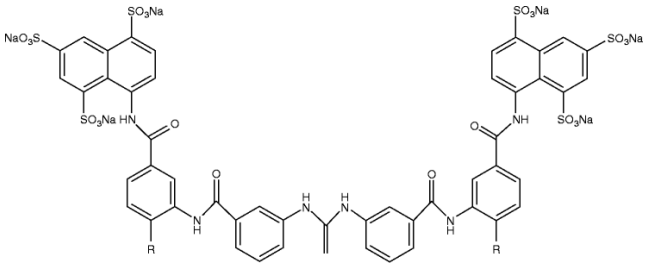

R=Me

Suramin

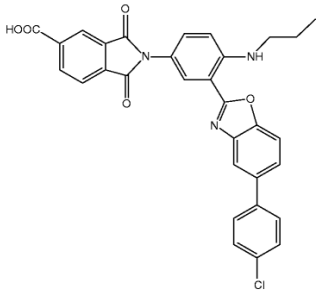

2-[4-propylamino-5-[5-(4-chloro)phenyl-benzoxazol-2-yl]phenyl]-2,3-dihydro-1,3-dioxo-1 H-isoindole-5-carboxylic acid

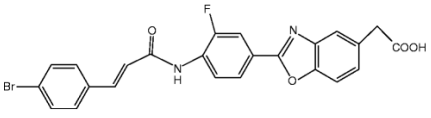

benzoxazol-5-yl-acetic acids

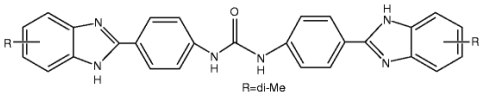

R=di-Me

1,3-bis-[4-(1 H-benzoimidazol-2-yl)-phenyl]-urea

Figure 1.18: Stuctures of Heparanase Inhibitors.



www.manaraa.com

specificity concerns, which gives rise to new approaches that develop effective and highly specific heparanase inhibitors.

The development of Growth Factor-Growth Factor Receptor inhibitors for the treatment of uncontrollable tumor growth is also of considerable interest, Figure 1.19.(160-164) This has led to the development of targeted agents for cancer treatment to target these pathways, strategies like monoclonal antibodies (mAbs) and protein kinase inhibitors that are designed to target the GFRs. mAb therapeutics act by directly blocking the function of GFRs and/or by antibody-dependent cytotoxicity.(165) Protein kinase inhibitors inhibit the cytoplasmic kinase activity of growth receptors and subsequently their downstream signaling cascades by rapidly crossing the cell plasma membranes and competing with phosphate donor adenosine tyrosine phosphate (ATP) and/or phosphorylation substrates.(166) Similar to heparanase inhibitors, heparin mimetics have also been used to inhibit growth factors by offering a different substrate than HSPGs. Resistances have been linked to the compensatory pathways mediated by other GFRs or mutations in downstream signaling pathways.(167) Targeting multiple GFs/GFRs offers significant therapeutic potential in cancer therapy, since overexpression of GFRs is also responsible for resistance to different drugs.



www.manaraa.com

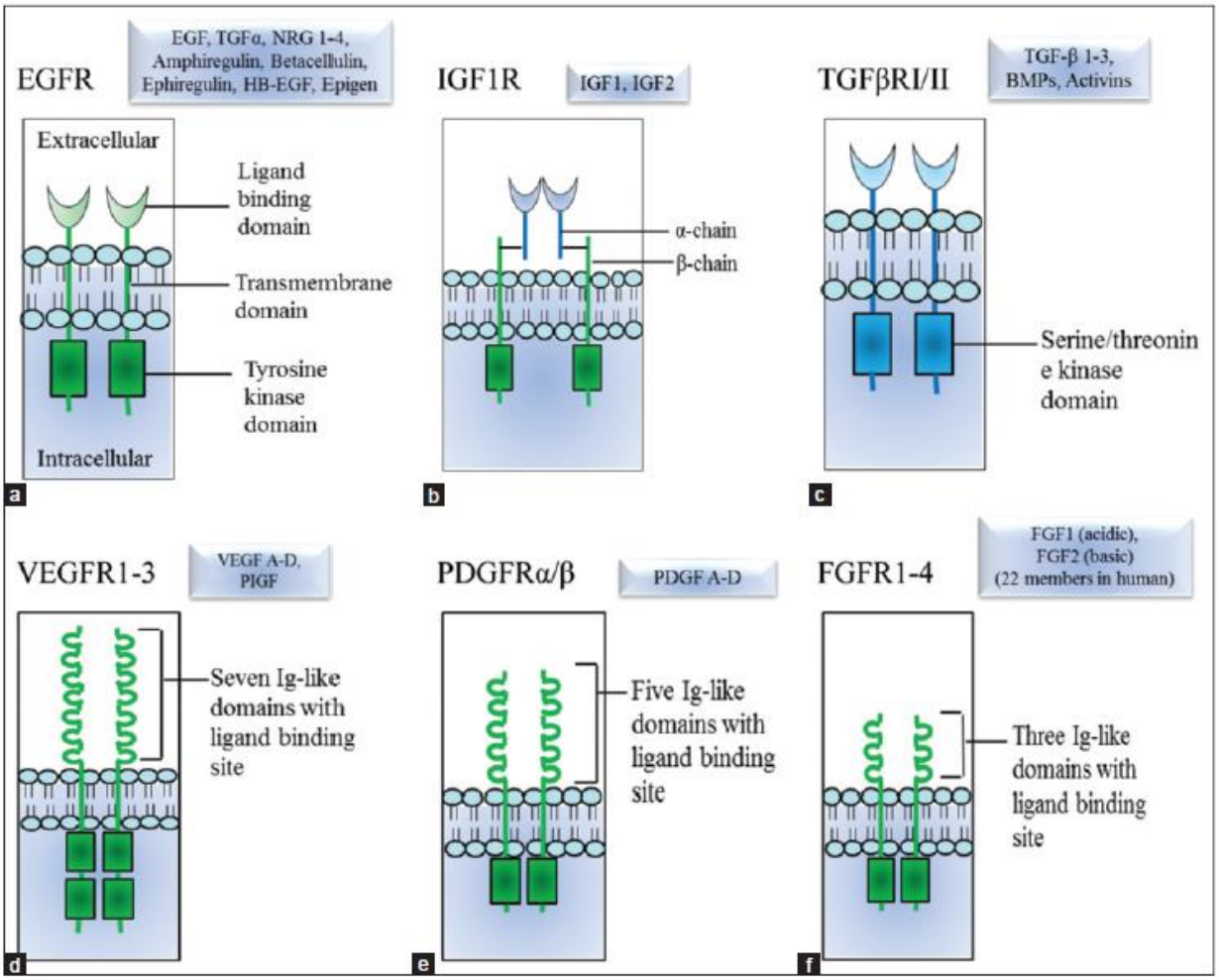


Figure 1.19: Schematic diagrams of membrane bound growth factor receptors and their ligands involve in cancer progression. Ligands are shown in boxes. (a) Epidermal growth factor receptor (ErbB/Her); (b) insulin-like growth factor receptor; (c) transforming growth factor-beta receptor; (d) vascular endothelial growth factor receptor; (e) platelet derived growth factor receptor, and (f) fibroblast growth factor receptor. ErbB2 (HER2) binds no known epidermal growth factor-like ligands, and ErbB3 shows no tyrosine kinase activity. They relay signals by forming heterodimer with other ErbB proteins from EGFR family. TGFβRIII does not pose any intracellular tyrosine kinase domain. From Ref. 161-167

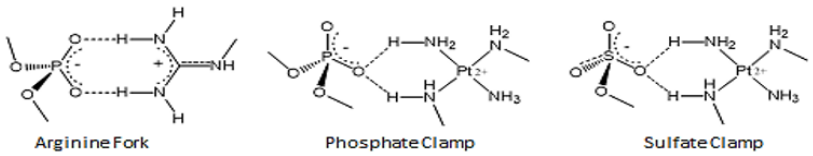


Figure 1.20 Structural analogies between phosphate and sulfate clamps and the arginine fork. From Ref. 170



www.manaraa.com

### 1.5 Metallogylcomics

Heparan sulfate has the highest negative charge density of any known biological macromolecule, sometimes referred to as "extracellular DNA", because of its signaling ability, helical nature and high content of negatively charged sulfate and carboxylate groups with an average of 2.7 sulfate groups per disaccharide.(168) The highly anionic nature of HS means it associates with physiologically relevant cations.(169) Therefore, HS may be a ligand receptor for anti-cancer cationic metal complexes revealing a new mechanism of cellular accumulation with implications for tumor selectivity.(170, 171) The interaction of PPCs with DNA is through the phosphate clamp, analogous to the arginine fork, Figure 1.20.(172) The discovery of the phosphate clamp as a biologically relevant binding motif suggested analogies with the isostructural sulfate. While these interactions are similar, the sulfate-Pt interactions are weaker due to the negative charge being more dispersed on a sulfate monoester from delocalization involving three non-ester oxygen atoms compared to the phosphate diester with only two non-ester oxygen atoms.(173) This sulfate clamp binding will affect protein recognition in strict analogy to inhibition of protein-DNA interactions upon formation of Pt-DNA adducts, allowing extension to the consequences of strong PPC-HS binding on the function of HS. Sulfate cluster binding is delocalized but will result in neutralization of the sulfate charge and further physically protect the sulfate groups from their receptors. "Metalloshielding" of HS by metal complexes through the binding of sulfate clusters, Figure 1.17, could act on the processes of tumor growth and metastasis, expanding into the relevance of metal complexes with HS.

Cellular internalization of PPCs are critical to their function as DNA binders. Interestingly, cellular accumulation differs dramatically between the 6+ and 8+ congeners.(32, 170) The cellular accumulation is higher than for cisplatin and actually increases with charge, further, accumulation is higher in transformed mast cells in comparison to the parent cells, suggesting possible tumor selectivity and overcoming acquired resistances of reduced platinum accumulation.(170)



www.manaraa.com

Discovery of HSPG-mediated cellular accumulation of PPCs has expanded this research to understanding PPC–HS interactions and the functional consequences of such binding. Metalloshielding could protect HS from the action of glycan-degrading enzymes and/or protein recognition, similar to DNA-protein inhibition. Invasiveness of tumor cells involves many events including adhesion to basement membrane, degradation of the basement membranes through the action of HPSE, and migration in response to growth factors. Cellular invasion through ECM requires degradation of the matrix by HPSE, and cell motility in response to growth factors. The end-point of inhibition of HPSE activity and growth factor binding to HS through modulation of growth factor signaling is the prevention of cell invasion and angiogenesis.

Understanding the structure activity relationship of metal-heparin binding interactions may extend as a model for coordination complexes and their interactions to heparan sulfate. The ability to vary oxidation state, coordination number and geometry, and lability of ligands allows investigation into the structure and function on heparin. Furthermore, this sulfate-cluster interaction will result in neutralization of the sulfate charge and protect the sulfate groups from interacting with their receptors. Metalloshielding may prevent HS function through inhibition of enzyme and protein recognition to HS. This prevention may occur through two potential approaches either as heparanase cleavage inhibition or growth factor binding inhibition, Figure 1.21.



www.manaraa.com

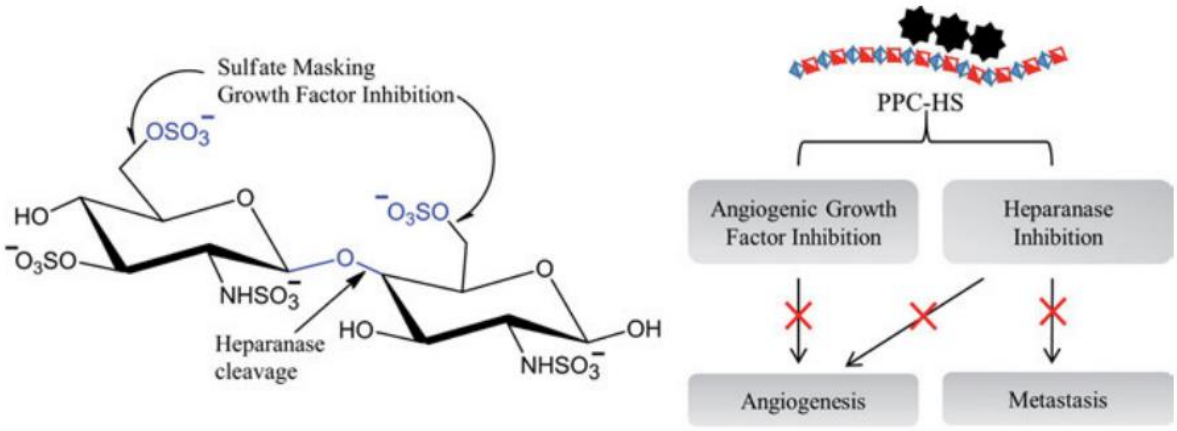


Figure 1.21: Potential chemical approaches to inhibition of HS-associated enzyme and protein recognition and activation through sulfate masking. From Ref. 103

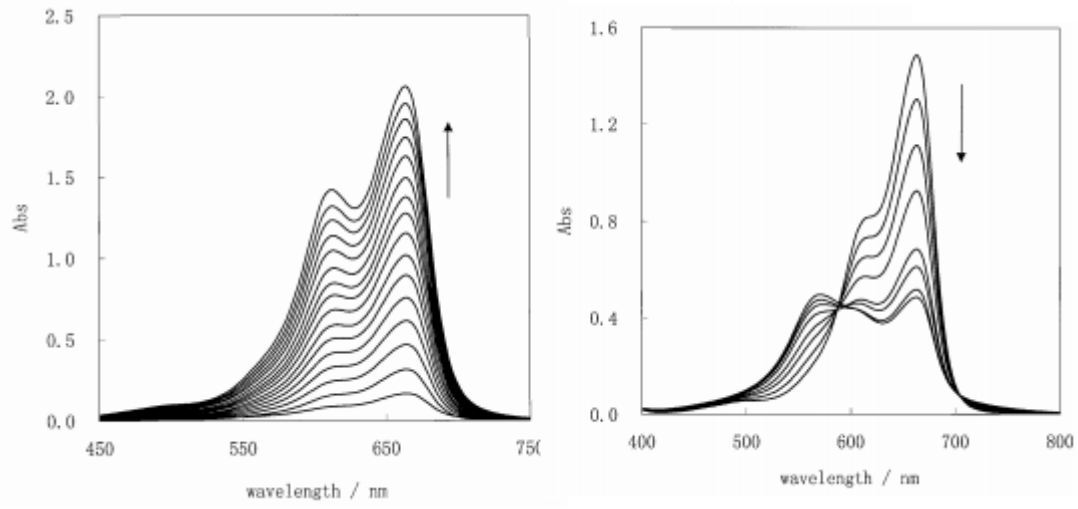


Figure 1.22: Left: Absorption spectra of MB solutions at different concentration levels. The concentrations (from bottom to top) were as follows: 0.4, 0.8, 1.2, 1.6, 2.0, 2.4, 2.8, 3.2, 3.6, 4.0, 4.4, 4.8, 5.2, 5.6, 6.0, and 6.4 x $10^{-5}$ mol/L. Right: Absorption spectra of a mixture of MB (2.0 x $10^{-5}$ mol/L) and CHS. The concentrations of CHS (from above to bottom at 664 nm) were as follows: 0.0, 0.2, 0.4, 0.6, 0.8, 1.0, 1.2, and 1.4 x $10^{-5}$ mol/L. From Ref. 180



www.manaraa.com

### 1.6 My contributions to the field of metalloglycomics

Pt-DNA interactions have been widely studied with much of our understanding of M-HS binding arising from these previous studies, for example the phosphate clamp and its isostructural sulfate clamp.(173) Pt-DNA interactions undergo a "pre-association" or non-covalent interaction before the covalent interaction is observed, this same "pre-association" may be extended to M-HS binding.(174) Furthermore, the previous assumption that platinum complexes need to be neutral to enter cells was contradicted by the higher cellular accumulation of the highly cationic PPCs over cisplatin.(175) The mechanism of PPCs cellular internalization and reactivity with DNA prompted studies into PPCs interactions with extracellular heparan sulfate proteoglycans (HSPG) as the mechanism of internalization and inhibition of function of HS, Figure 1.21. The less cytotoxic anticancer potential of other metal ammine complexes may be examined to elucidate the structure-function relationship of interactions with HS.

In these studies, we chose to examine multiple substrates. We examined multiple types of heparin, one maintained specific chain lengths while the other ranged between 3-18 kDa, however, both types possessed great heterogeneity of sulfate number and pattern to more closely mimic the heterogeneity of mammalian HS. Fondaparinux was chosen as a well-defined substrate in order to more accurately obtain binding parameters and association constants with the metal complexes, also FPX possesses a single point of cleavage when obtaining heparinase cleavage data.

Since HS interacts mainly through the sulfate regions, we verified that the key binding sites of our metal complexes were also through these sulfate regions. Previously, the interaction of Methylene Blue (MB) with heparin has been frequently investigated using spectroscopic techniques.(176-179) In water, MB aggregates with heparin through charge neutralization, increasing the frequency of MB dimer formation through π−π stacking.(180) The MB−heparin aggregation reduces the absorbance of the sample since there are fewer MB molecules in solution. Higher heparin concentrations disperse the MB−heparin aggregate due to the electrostatic repulsion between heparin chains allowing MB to self-aggregate, resulting in an increase in absorbance at 570 nm,



www.manaraa.com

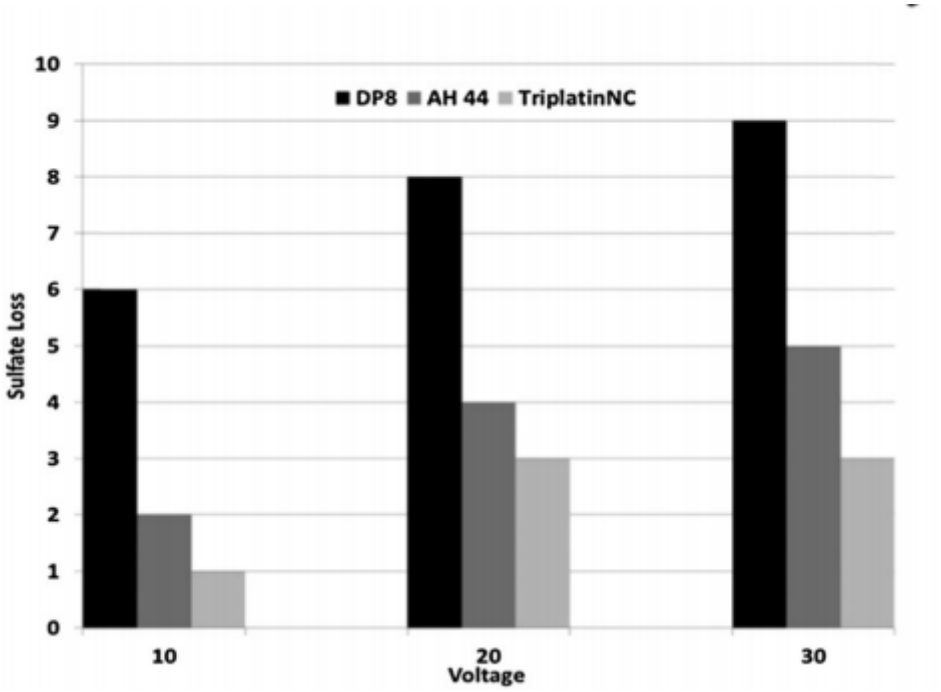


Figure 1.23: Sulfate loss in the octasaccharide DP8 by binding to polynuclear platinum complexes at varying ESI-MS/MS voltages. From Ref. 181

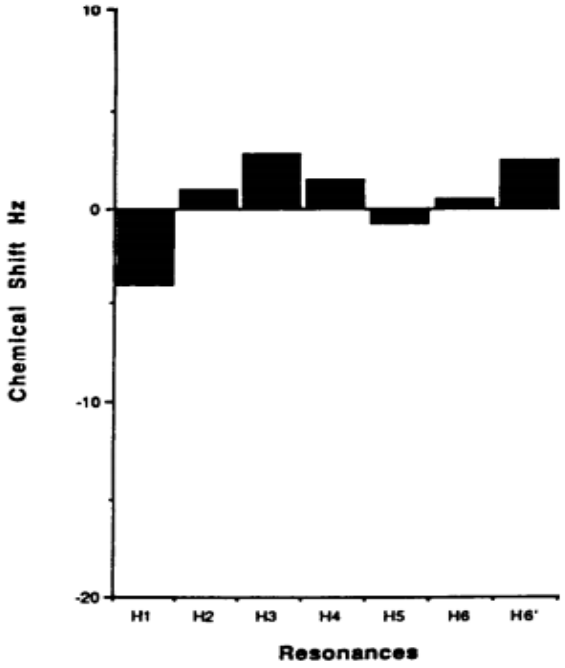


Figure 1.24. $^{1}$H NMR chemical shifts for D-Glucosamine-6-O-sulfate plus 1.3 equivalent Zn (OAc). From Ref. 186



www.manaraa.com

Figure 1.22.(181) In this work, I developed a competitive assay using MB as a reporter to verify interactions with the sulfate regions, increasing the concentration of metal complexes protected more heparin/FPX chains from interacting with MB. This inhibition of MB interaction increased the amount of free, unbound MB in solution concomitantly increasing the absorbance. This absorbance increase allowed for the calculation of $IC_{50}$s of the concentration of metal complexes required to inhibit MB from interacting with heparin/FPX, furthermore, the apparent dissociation constants were also calculated.

Confirming the potential for high-affinity binding to the sulfates of heparin, ESI-MS was previously employed on a model DP8 octasaccharide in the presence of the highly charged 6+ (AH44) and 8+ (TriplatinNC) ions. (182) This non-covalent interaction is the first demonstration of a platinum compound interaction with a sulfated polysaccharide. The sulfate moieties on heparin are quite labile and the spectrum of free octasaccharides showed a series of peaks corresponding to sequential sulfate loss. In contrast, the initial MS of the Pt-heparin adducts shows little loss compared to the unprotected heparin. ESI-MS/MS of the 1:1 adducts at increasing energies also shows stabilization toward sulfate loss, Figure 1.23.(181) The stabilization is dependent on size and charge of the non-covalent platinum compound with the 8+ compound significantly more effective. Various metal ions have also been shown to induce a conformational contraction in heparins structure due to the number of metal ion adducts, the ionic radii, and the ionic valence of metal ions through TOF-MS.(182) This observation suggests a conformational change of heparin induced by metal ions that may alter the interactions of heparin and heparin-binding proteins. (182) ESMS of heparin fragments as ammonium salts may also provide a valuable method for their analysis in combination with binding and inhibition assays providing an opportunity to derive structural requirements, such as size, charge density, and sequence, in relation to biological activity; while MS/MS analysis may provide complete sequence reporting for highly sulfated heparin chains if the precursor molecular ion has its acidic groups deprotonated through $Na^+/H^+$ exchange.(183, 184) To confirm sulfate interactions with metal complexes, I employed ESI-MS in this work to determine stoichiometry and sulfate protection.



www.manaraa.com

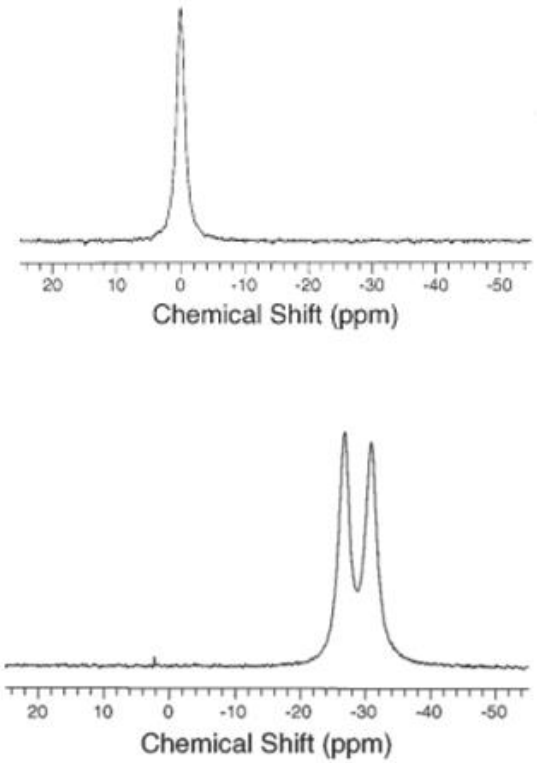


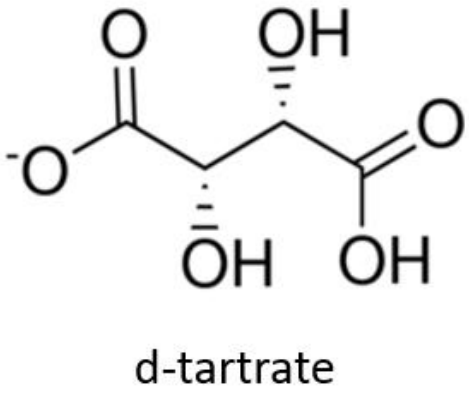


d-tartrate

Figure 1.25. Top Left: $^{59}$Co NMR spectrum of 10 mM (+/-)-$[Co(en)_3]Cl_3$ solution. Left Bottom: $^{59}$Co NMR spectrum of 10 mM (+/-)-$[Co(en)_3]Cl_3$ solution combined with 50 mM sodium d-tartrate. Right: Structure of d-tartrate. From Ref. 187



www.manaraa.com

NMR has also been used in order to ascertain which residues in heparin may be responsible for its metal binding capacities.(185) $^{1}$H NMR produced very small shifts of D-Glucosamine-6-O-sulfate when interacted with zinc acetate, Figure 1.24.(186) The main shifts were observed at the H6 and the anomericprotons, which corresponds to the sulfate as the key binding site.(4) Since $^{59}$Co possesses a relatively high magnetogyric ratio with a magnetic mixing of its occupied and excited *d* orbitals, it experiences substantial paramagnetic deshielding, >15,000 ppm, that will reveal even minute changes in its chemical environment.(187) The cobalt chemical shift for the cobalt atom in $[Co(en)_3]^{3+}$ hydrogen–deuterium isotopomers show about a 5 ppm shift for each hydrogen atom that is replaced by a deuterium atom.(188) Furthermore, with a nuclear spin number of 7/2 associated with a quadrupole moment that provides a very efficient relaxation mechanism, $^{59}$Co spectra possess broad solution phase resonances. Therefore, the nuclear quadrupole moment of $^{59}$Co requires the cobalt atom to occupy a highly symmetric environment in order to yield line widths of 100–200 Hz. The cobalt ion in the cobalt complex $[Co(en)_3]^{3+}$ resides in an octahedrally symmetric environment and possesses a relatively narrow line width, however, when the racemic$[Co(en)_3]^{3+}$ ion pairs with d-tartrate ion, this results in diastereomeric ion pairs having clearly separated $^{59}$Co NMR resonances that differ in chemical shift by about 5–6 ppm, Figure 1.25.(188) In this work, I followed each proton shift of D-glucosamine-6-O-sulfate when bound to metal complexes at a 1:1 mixing using $^{1}$H NMR. To verify that these cobalt compounds may interact covalently with the monomer, I also employed $^{59}$Co NMR and compared the obtained shifts with previously published spectra. Since we verified that these metal complexes interact with heparin/FPX through the sulfate regions, we continued with studies to elucidate the mechanism of internalization and inhibition of function on HS.

Previously, our lab investigated the internalization of PPCs mediated through HSPGs and association to the final target of DNA.(189) In this work, we obtained estimations of associations between metal complexes on heparin/FPX vs DNA using Fluorescence Polarization (FP) and Ethidium Bromide (EtBr). FP demonstrated similar affinities of metal complexes for heparin as for DNA. EtBr verified this data through FPX sequestering of the metal complexes from DNA. In



www.manaraa.com

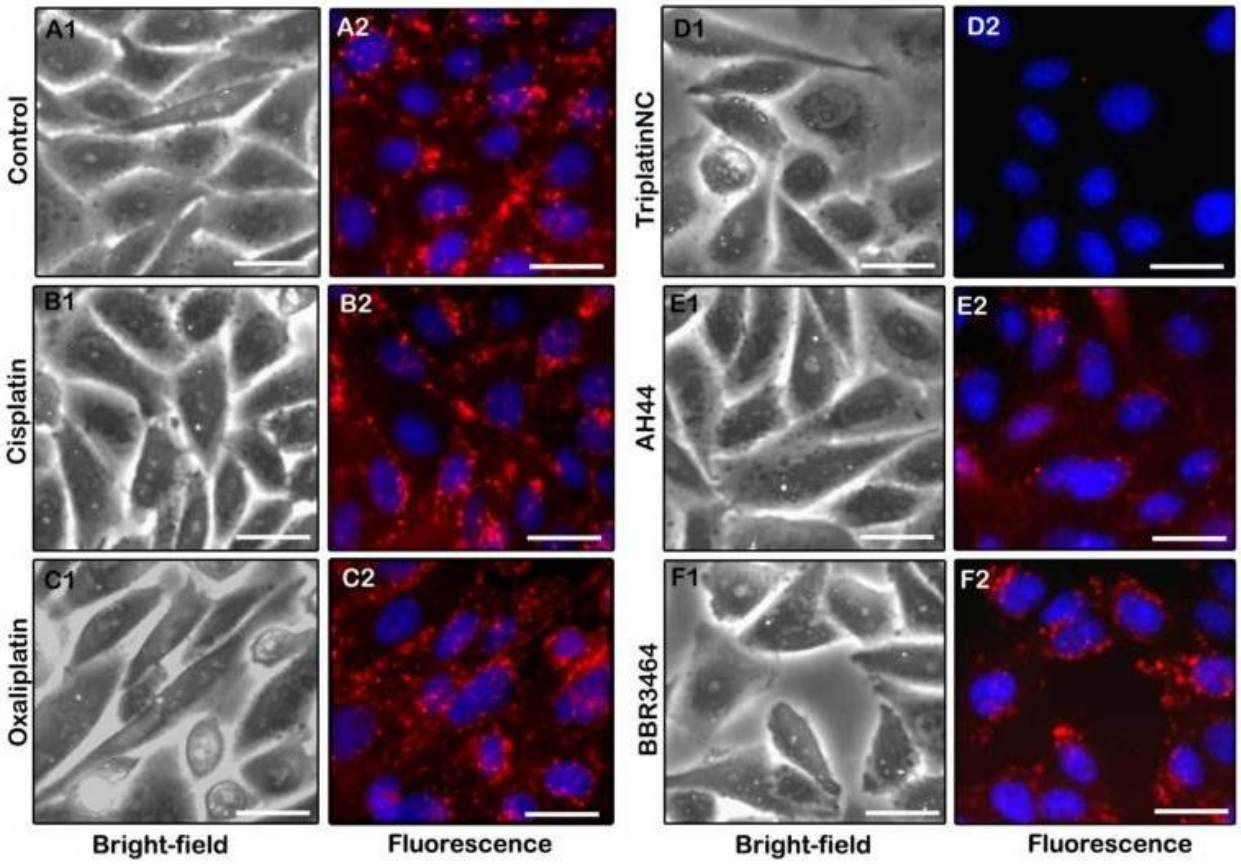


Figure 1.26. Competition of TAMRA-R9 internalization and Platinum compound in wt CHO cells. Compounds (10 μM) were added 5 min prior to the addition of TAMRA-R9 (1.0 μM) and analyzed by fluorescence microscopy. Cells were counterstained with Hoescht 33342. Panels: (A) Control; (B) Cisplatin; (C) Oxaliplatin; (D) TriplatinNC; (E) AH44; (F) BBR3464. Bar = 10 μm. From Ref. 189



www.manaraa.com

order to probe the metal-HS interaction nonaarginine was chosen since it binds to cell surface HS. The interaction of TAMRA-$R_9$ with HS has been investigated using spectroscopic techniques.(189, 190) Cellular uptake of TAMRA-$R_9$ in the presence of platinum drugs was examined, upon drug incubation, TAMRA-$R_9$ cell entry was prevented in a charge-dependent manner, Figure 1.26.(189) Furthermore, the affinity of TAMRA–$R_9$ for soluble heparin was also quantitated by direct titration monitored by fluorescence spectroscopy.(190) To determine the value of the equilibrium dissociation constant ($K_d$), binding data were fitted by nonlinear regression analysis to the equation: $K_d^n$ = [heparin][TAMRA–$R_9$]$^n$/[heparin·$n$TAMRA–$R_9$].(190) Because heparin ($M_r$ 3000) and TAMRA–$R_9$ ($M_r$ 1836) are essentially homopolymers of similar mass, the value of $n$ is likely to be near unity, for $n$ = 1, $K_d$ = 109 ± 13 nM.(190) In this work, I developed a competitive assay using TAMRA-$R_9$ as a reporter to indirectly determine the metalloshielding ability of these metal complexes on heparin, increasing the concentration of metal complexes protected more heparin chains from interacting with TAMRA-$R_9$. This inhibition of TAMRA-$R_9$ interaction increased the amount of free, unbound TAMRA-$R_9$ in solution concomitantly decreasing the fluorescence. This fluorescence decrease allowed for the calculation of $IC_{50}$s of the concentration of metal complexes required to inhibit TAMRA-$R_9$ from interacting with heparin.

Direct analysis of metal-heparin/FPX interactions was performed to confirm the strength of binding using Isothermal Titration Calorimetry (ITC) and Surface Plasmon Resonance (SPR). Previously, growth factor-homogeneous heparin mimetic interactions were measured using ITC, Figure 1.27.(191) Binding parameters were obtained with calculated dissociation constants in the nM range.(191) While growth factor-heterogeneous heparin mimetic interactions were measured using ITC, Figure 1.28, the binding parameters were obtained with calculated dissociation constants in the µM range.(192) In this work, I developed and refined the ITC assay to determine association constants of metal complexes-heparin/FPX that were in the same range as growth factors-HS. SPR was also used to more closely mimic cell surface bound HSPGs and their interactions with metal complexes, which were also in the range of previously reported growth factors-heparin interactions as calculated from SPR in the nM range.(193)



www.manaraa.com

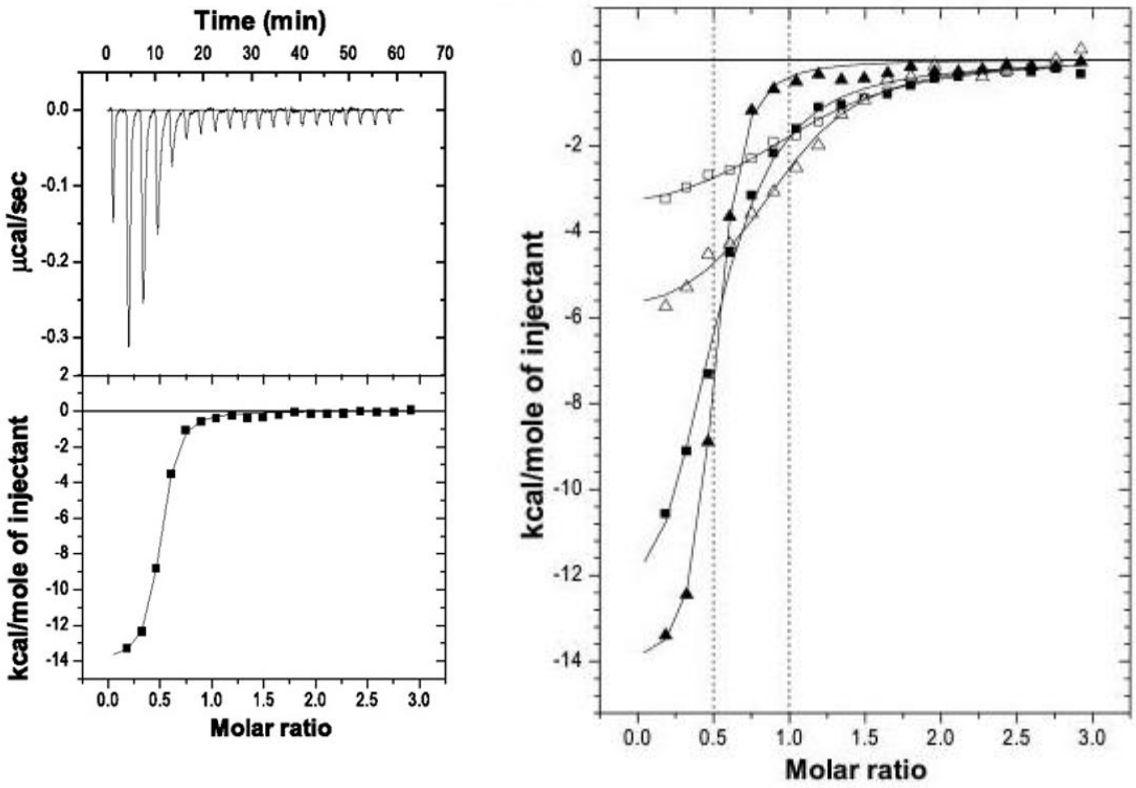


Figure 1.27: ITC titrations of FGF with heparin mimetics. Left: Sample titration of FGF2 with HM8. Top panel: raw heating power data; the first peak represents a small pre-injection (5 µl) that is omitted in the integrated data. Bottom panel: data after peak integration and concentration normalization. Curve fit of the data to a single site binding model. Right: Isotherms for binding of HM6 (open squares) or HM8 (filled squares) to FGF1, and for binding of HM6 (open triangles) or HM8 (filled triangles) to FGF2. Dotted vertical lines indicate the equivalence point of the titrations with HM6and HM8 at a molar ratio (HM:FGF) of 1 and 0.5. The sample cell contained 5 µM FGF, and HM were titrated from a 65 µM stock solution. From Ref. 191



www.manaraa.com

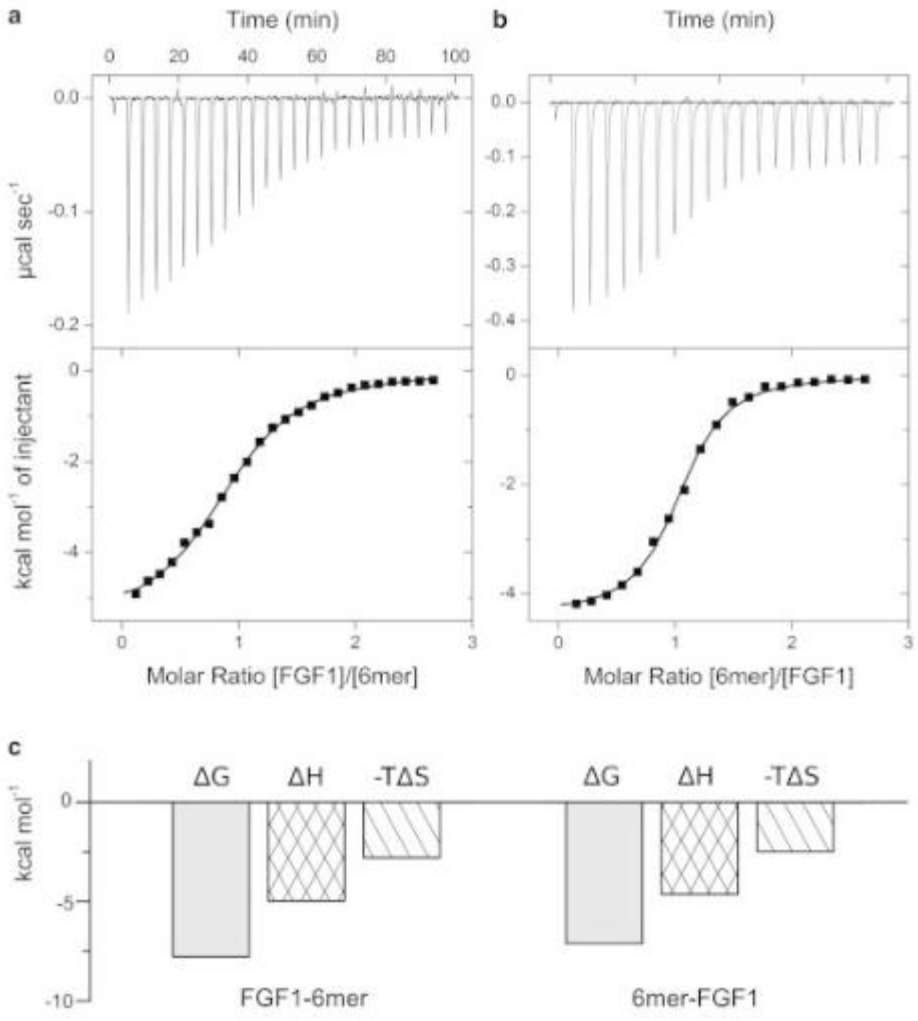


Figure 1.28. Analysis of FGF1-heparin hexasaccharide interaction by direct (a) and reverse (b) titrations. In the direct titration, 100 µM FGF1 was titrated into 7 µM hexasaccharide and in the reverse titration, 100 µM heparin was titrated into 12.5 µM FGF1. (Upper panel) Calorimetric titration trace with the integrated isotherms (shown in lower panel). (Solid lines) Best fit to the noncooperative McGhee-von Hippel model. (c) Thermodynamic dissection of the interaction between FGF1 and heparin hexasaccharide. (Shading) Free energy of binding (ΔG); (crosshatch) enthalpy of binding (ΔH); (diagonal shading) entropy of binding (−TΔS). From Ref. 192



www.manaraa.com

HSs are acted upon by the bacterial enzyme heparinase, used to mimic the cleavage of mammalian heparanase. Degradation by heparanase releases angiogenic and growth factors leading to tumor cell migration, growth, and angiogenesis. Heparanase overexpression is associated with tumor progression and there is significant correlation between metastatic potential and heparanase activity.(194-197) To examine the efficacy of metalloshielding in blocking heparinase and heparanase action on HS-containing proteoglycans we used the sulfated pentasaccharide, Fondaparinux as a model HS-like substrate. FPX is a substrate for both bacterial heparinases and human heparanase and has been used in assay development for screening the efficiency and kinetics of potential heparanase inhibitors.(198, 199) FPX is an ideal substrate because it is homogeneous with a single point of cleavage by either enzyme which leads to the formation of only two products. $^{1}$H NMR and colorimetric assays for enzymatic activity have been developed.(199) These assays were adapted to examine the inhibitory effect of metal complexes on the enzymatic (heparinase) degradation of Fondaparinux.(200) $^{1}$H NMR follows the proton shift, mainly the anomeric protons, after cleavage, while the colorimetric assay follows the creation of a double bond that absorbs at 584 nm. Furthermore, cellular invasion through the extracellular matrix (ECM) requires degradation of the matrix by HPSE, and cell motility in response to growth factors. The ability of metal complexes to inhibit cell invasion through matrigel basement membrane was also accessed using a Boyden-chamber assay.(201) Previously, inhibition of heparinase cleavage is effective in a charge and concentration-dependent manner for the metal compounds, Figure 1.29.(200)



www.manaraa.com

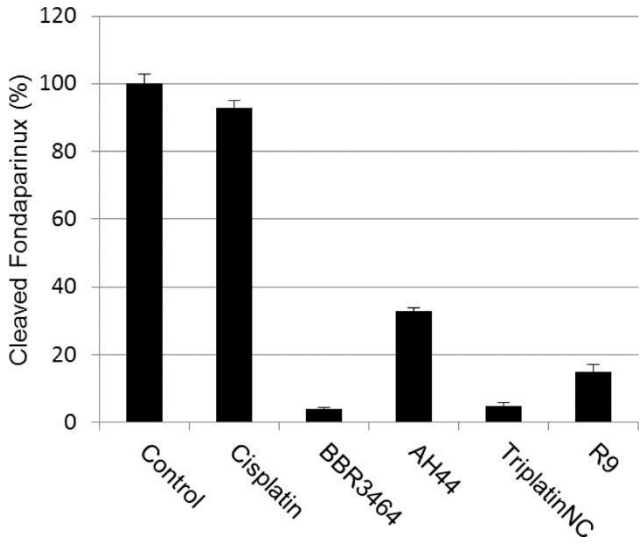


Figure 1.29. Inhibition of heparinase I Fondiparinux cleavage (3h incubation) by polynuclear platinum complexes and the arginine-rich $R_9$ protein (1:3 stoichiometry). From Ref. 200



www.manaraa.com

## 1.7 Thesis Outline

The study of coordination complexes with HS-GAGs has several applications in the field of bioinorganic chemistry distinct from the well-studied protein and DNA/RNA interactions. Extending from simple to polynuclear, metal complexes were chosen to examine the effects on the structure and function of HS, Figure 1.17. The application of hard and soft acid and base concepts can be expected to produce new patterns of metal ion binding with the hard sulfate base on the HS chain. Further, electrostatic and hydrogen-bonding interactions should provide opportunities for "non-covalent" interactions compared to "covalent" interactions.

Chapter 2 describes work that I collaborated on and that was published in Chemistry: A European Journal, investigating the interactions of PPCs with the well-defined pentasaccharide fondaparinux. Chapter 3 describes work that I collaborated on and that was published in Inorganic Chemistry, investing the interactions of simple metal complexes with heterogeneous heparin. Chapter 4 describes work that I collaborated on, investigating the interactions of simple covalent cobalt complexes with fondaparinux. Chapter 5 describes work that I collaborated on, investigating the interactions of simple non-covalent cobalt complexes with fondaparinux. Chapter 6 describes work that I collaborated on, investigating the interactions of simple metal complexes with fondaparinux. Chapter 7 details the synthesis and characterization of Werner's Complex.

Published work will be included in a format as close as possible to that in which it was published.

## 1.8 References


1. B. Rosenberg, L. Van Camp, T. Krigas. *Nature* **1965**, 205, 698-699.
2. B. Rosenberg, L. VanCamp, J. E. Trosko, V. H. Mansour. *Nature* **1969**, 222, 385-386.
3. E. R. Jamieson, S. J. Lippard. *J. Chem. Rev*. **1999**, 99, 2467-2498.
4. N. P. Farrell. *Met Ions Biol Syst*. **2004**, 42, 251-296.
5. I. Kostova. *Recent Patents on Anti-Cancer Drug Discovery*. **2006**, 1, 1-22.




www.manaraa.com

6. S. Ishida, D. J. Thiele, I. Herskowitz. *Proc. Natl. Acad. Sci*. **2002**, 99, 14298-14302.

7. X. Lin, T. Okuda, A. Holzer, S. B. Howell. *Molecular Pharmacology* **2002**, 62, 1154-1159.

8. P. A. Andrews, S. B. Howell. *Cancer Cell - Mon. Rev*. **1990**, 2, 35-43.

9. N. Nagai, R. Okuda, M. Kinoshita, H. Ogata. *J. Pharm. Pharmacol* **1996**, 48, 918-924.

10. J. Reedijk. *Inorg. Chim. Acta* **1992**, 873, 198-200.

11. F. A. Blommaert, H .C. M. van Dijk-Knijnenburg, F. Dijt, L. den Engelse, A. Baan, F. Berends, A. M. J. Fichtinger-Schepman. *Biochemistry* **1995**, 34, 8474-8480.

12. Y. Jung, S. J. Lippard. *Chemical Reviews* **2007**, 107, 1387-1407.

13. A. M. J. Fichtinger-Schepman, J. L. van der Veer, J. H. L. den Hartog, P. H. M. Lohman, J. Reedijk. *Biochemistry* **1985**, 24, 707-713.

14. L. R. Kelland. *Crit. Rev. Oncol. Hematol*. **1993**, 15, 191-219.

15. S. F. Bellon, J. H. Coleman, S. J. Lippard. *Biochemistry* **1991**, 30, 8026-8035.

16. P. Jordan, M. Carmo-Fonseca. *Cell Mol Life Sci* **2000**, 57, 1229-1235.

17. R. Agarwal, S. B. Kaye. *Nature Reviews Cancer* **2003**, 3, 502-516.

18. G. N. Kaluderovic, R. Pascheke. *Current Medicinal Chemistry* **2011**, 18, 4738-4752.

19. L. Galluzi, L. Senovilla, I. Vitale, J. Michels, I. Martins, O. Kepp, M. Castedo, G. Kroemer. *Oncogene* **2012**, 31, 1869-1883.

20. R. J. Parker, A. Eastman, F. Bostick-Bruton, E. Reed. *J. Clin. Invest* **1991**, 87, 772-777.

21. R. J. Knox, F. Friedlos, A. Lydall, J. J. Roberts. *Cancer Research* **1986**, 46, 1972-1979.

22. S. G. Chaney, S. L. Campbell, B. Temple, E. Bassett, Y. Wu, M. Faldu. *Journal of Inorganic Biochemistry* **2004**, 98, 1551-1559.

23. B. Stordal, N. Pavlakis, R. Davey. *Cancer Treatment Reviews* **2007**, 33, 347-357.

24. S. J. Lippard. Metals in Medicine. In *Bioinorganic Chemistry*; University Science Books: Mill City, **1994**; pp 505-583.



www.manaraa.com

25. M. E. Gore, I. Fryatt, E. Wiltshaw, T. Dawson, B. A. Robinson, A. H. Calvert. *British Journal of Cancer* **1989**, 60, 767-769.

26. C. P. Saris, P. J. M. van de Vaart, F. A. Blommaert. *Carcinogenesis* **1996**, 17, 2763-2769.

27. K. J. Barnham, M. I. Djuran, P. del Soccoro Murdoch, J. D. Ranford, P. J. Sadler. *Inorganic Chemistry* **1996**, 35, 1065-1072.

28. L. Kelland. *Nature Reviews* **2007**, 7, 573-584.

29. N. Farrell. In *Comprehensive Coordination Chemistry*; Elsevier: Amsterdam, **2003**; Vol. 9, 809-840.

30. J. Kasparkova, J. Zehnulova, N. Farrell, V. Brabec. *J. Biol. Chem* **2002**, 277, 48076-48086.

31. A. Hegmans, S. J. Berners-Price, M. S. Davies, D. S. Thomas, A. S. Humphreys, N. Farrell. *J. Am. Chem. Soc* **2004**, 126, 2166-2180.

32. A. L. Harris, X. Yang, A. Hegmans, L. Povirk, J. J. Ryan, L. Kelland, N. P. Farrell. *Inorg. Chem*. **2005**, 44, 9598-9600.

33. Y. Qu, A. Harris, A. Hegmans, P. Kabolizadeh, H. Penazova, N. Farrell. *J. Inorg. Biochem* **2004**, 98, 1591-1598.

34. A. Ziegler, J. Seelig. *Biochemistry* **2007,** 46, (27), 8138-8145.

35. S. R. Schwarze, K. A. Hruska, S. F. Dowdy. *Trends Cell Biol* **2000,** 10, (7), 290-295.

36. M. Lindgren, M. Hallbrink, A. Prochiantz, U. Langel. *Trends Pharmacol Sci* **2000,** 21, (3), 99-103.

37. T. A. Connors, M. Jones, W. C. J. Ross, P. D. Braddock, A. R. Khokhar, M. L. Tobe. *Chem-Biol. Interact*. **1972**, 5, 415-424.

38. E. Alessio, G. Mestroni, A. Bergamo, G. Sava. *Metal Ions in Biological Systems*, **2004**, 42, 323–347.

39. A. Bergamo, G. Sava. *Dalton Transactions*, **2007**, 1267–1272.

40. M. A. Jakupec, M. Galanski, V. B. Arion, C. G. Hartinger. *Dalton Transactions*, **2008**, 183–194.



www.manaraa.com

41. A. F. A. Peacock, P. J. Sadler. *Chemistry, an Asian Journal*, **2008**, 3, 1890–1899.

42. M. J. Clark. *Coordination Chemistry Reviews*, **2003**, 236, 209–233.

43. M. J. Clarke, F. Zhu, D. R. Frasca. *Chemical Reviews*, **1999**, 99, 2511–2533.

44. G. Mestroni, E. Alessio, G. Sava. **1998**, Int. Patent WO 98/000431.

45. M. Bacac, A. C. G. Hotze, K. van der Schilden, J. G. Haasnoot, S. Pacor, E. Alessio, G. Sava, J. Reedijk. *Journal of Inorganic Biochemistry*, **2004**, 98, 402–412.

46. M. Brindell, D. Piotrowska, A. A. Shoukry, G. Stochel, R. van Eldik. *Journal of Biological Inorganic Chemistry*, **2007**, 12, 809–818.

47. B. Gava, S. Zoret, P. Spessotto, M. Cocchietto, G. Sava. *Journal of Pharmacology and Experimental Therapeutics*, **2006**, 317, 284–291.

48. M. Bouma, B. Nuijen, M. T. Jansen, G. Sava, A. Flaibani, A. Bult, J. H. Beijnen. *International Journal of Pharmaceutics*, **2002**, 248, 239–246.

49. L. Messori, P. Orioli, D. Vullo, E. Alessio, E. Iengo. *European Journal of Biochemistry*, **2000**, 267, 1206–1213.

50. L. Messori, F. G. Vilchez, R. Vilaplana, F. Piccioli, E. Alessio, B. Keppler. *Metal Based Drugs*, **2000**, 7, 335–342.

51. A. Bergamo, L. Messori, F. Piccioli, M. Cocchietto, G. Sava. *Investigational New Drugs*, **2003**, 21, 401–411.

52. M. Ravera, S. Baracco, C. Cassino, D. Colangelo, G. Bagni, G. Sava, D. Osella. *Journal of Inorganic Chemistry*, **2004**, 98, 984–990.

53. L. Messori, F. Kratz, E. Alessio. *Metal Based Drugs*, **1996**, 3, 1–9.

54. A. Casini, G. Mastrobuoni, M. Terenghi, C. Gabbiani, E. Monzani, G. Moneti, L. Casella, L. Messori. *Journal of Biological Inorganic Chemistry*, **2007**, 12, 1107–1117.

55. E. Gallori, C. Vettori, E. Alessio, F. G. Vilchez, R. Vilaplana, P. Orioli, A. Casini, L. Messori. *Archives of Biochemistry and Biophysics*, **2000**, 376, 156–162.

56. M. Brindell, I. Stawoska, J. Supel, A. Skoczowski, G. Stochel. *Journal of Biological Inorganic Chemistry*, **2008**, 13, 909–918.



www.manaraa.com

57. S. L. Church, J. W. Grant, L. A. Ridnour et al., "Increased manganese superoxide dismutase expression suppresses the malignant phenotype of human melanoma cells," Proceedings of the National Academy of Sciences of the United States of America, **1993**, vol. 90, no. 7, pp. 3113–3117.

58. K. Ishikawa, K. Takenaga, M. Akimoto et al., "ROS-generating mitochondrial DNA mutations can regulate tumor cell metastasis," Science, **2008**, vol. 320, no. 5876, pp. 661–664.

59. W. S. Wu, "The signaling mechanism of ROS in tumor progression," Cancer and Metastasis Reviews, **2006**, vol. 25, no. 4, pp. 695–705.

60. K. H. Kim, A. M. Rodriguez, P. M. Carrico, and J. A. Melendez, "Potential mechanisms for the inhibition of tumor cell growth by manganese superoxide dismutase," Antioxidants and Redox Signaling, **2001**, vol. 3, no. 3, pp. 361–373.

61. J. C. Copin, Y. Gasche, and P. H. Chan, "Overexpression of copper/zinc superoxide dismutase does not prevent neonatal lethality in mutant mice that lack manganese superoxide dismutase," Free Radical Biology and Medicine, **2000**, vol. 28, no. 10, pp. 1571–1576.

62. R. M. Lebovitz, H. Zhang, H. Vogel et al., "Neurodegeneration, myocardial injury, and perinatal death in mitochondrial superoxide dismutase-deficient mice," Proceedings of the National Academy of Sciences of the United States of America, **1996**, vol. 93, no. 18, pp. 9782–9787.

63. Y. Li, T. T. Huang, E. J. Carlson et al., "Dilated cardiomyopathy and neonatal lethality in mutant mice lacking manganese superoxide dismutase," Nature Genetics, **1995**, vol. 11, no. 4, pp. 376–381.

64. S. Melov, J. A. Schneider, B. J. Day et al., "A novel neurological phenotype in mice lacking mitochondrial manganese superoxide dismutase," Nature Genetics, **1998**, vol. 18, no. 2, pp. 159–163.

65. M. Fujimura, Y. Morita-Fujimura, M. Kawase et al., "Manganese superoxide dismutase mediates the early release of mitochondrial cytochrome C and subsequent DNA fragmentation after permanent focal cerebral ischemia in mice," Journal of Neuroscience, **1999**, vol. 19, no. 9, pp. 3414–3422.

66. Lyonnet, B., Martz, M., and Martin, E. L'emploi Therapeutique des derives du vanadium. La Presse Medicale, **1899**, 32, 191–192.



www.manaraa.com

67. E. L. Tolman, E. Barris, M. Burns, A. Pansini, R. Partridge. *Life Sciences*, **1979**, 25, 1159–1164.

68. G. R. Dubyak, A. Kleinzeller. *The Journal of Biological Chemistry*, **1980**, 255, 5306–5312.

69. Y. Shechter, S. J. Karlish. *Nature*, **1980**, 284, 556–558.

70. C. E. Heyliger, A. G. Tahiliani, J. H. McNeill. *Science*, **1985**, 227, 1474–1477.

71. P. Poucheret, S. Verma, M. D. Grynpas, J. H. McNeill. *Molecular and Cellular Biochemistry*, **1998**, 188, 73–80.

72. K. H. Thompson, C. Orvig. *Metal Ions in Biological Systems*, **2004**, 41, 221–252.

73. K. H. Thompson, J. H. McNeill, C. Orvig. *Chemical Reviews*, **1999**, 99, 2561–2571.

74. K. H. Thompson, C. Orvig. *Journal of Inorganic Biochemistry*, **2006**, 100, 1925–1935.

75. K. H. Thompson, J. Lichter, C. LeBel, M. C. Scaife, J. H. McNeill, C. Orvig. *Journal of Inorganic Biochemistry*, **2009**, 103, 554–558.

76. D. C. Crans. *Journal of Inorganic Biochemistry*, **2000**, 80, 123–131.

77. H. Sakurai, Y. Yoshikawa, H. Yasui. *Chemical Society Reviews*, **2008**, 37, 2383–2392.

78. M. Hiromura, H. Sakurai. *Chemistry & Biodiversity*, **2008**, 5, 1615–1621.

79. B. Mukherjee, B. Patra, S. Mahapatra, P. Banerjee, A. Tiwari, M. Chatterjee. *Toxicology Letters*, **2004**, 150, 135–143

80. J. C. Dabrowiak. *Metals in Medicine*. **2009**.

81. P. A. Asbell, S. P. Epstein, J. A. Wallace, D. Epstein, C. C. Stewart, R. M. Burger. *Cornea* **1998**, 17, 550–557.

82. T. Takeuchi, A. Böttcher, C. M. Quezada, T. J. Meade, H. B. Gray. *Bioorg. Med. Chem.* **1999**, 7, 815–819.

83. J. A. Schwartz, E. K. Lium, S. J. Silverstein. *J. Virol*. **2001**, 75, 4117–4128.

84. S. P. Epstein, Y. Y. Pashinsky, D. Gershon, I. Winicov, C. Srivilasa, K. J.; Kristic, P. A. Asbell. *BMC Opthalmol*. **2006**, 6, 22.



www.manaraa.com

85. A. Böttcher, T. Takeuchi, K. I. Hardcastle, T. J. Meade, H. B. Gray, D. Cwikel, M. Kapon, Z. Dori. *Inorg. Chem*. **1997**, 36, 2498–2504.

86. A. Y. Louie, T. J. Meade. *Proc. Natl. Acad. Sci*. USA **1998**, 95, 6663–6668.

87. P. H. Wooley, J. D. Whalen. *Agents Actions* **1992**, 35, 273–279.

88. R. V. Gessner, G. J. Quigley, A. H. Wang, G. A. van der Marel, J. H. van Boom, A. Rich. *Biochemistry* **1985**, 24, 237–240.

89. J. B. Delehanty, J. E. Bongard, D. C. Thach, D. A. Knight, T. E. Hickey, E. L. Chang. *Bioorg. Med. Chem*. **2008**, 16, 830–837.

90. A. Bergamo, C. Gaiddon, J. H. M. Schellens, J. H. Beijnen, G. Sava. *J. Inorg. Biochem*. **2012**, 106, 90–99.

91. A. Bergamo, G. Sava. *Dalton Trans*. **2011**, 40, 7817– 7823.

92. C. R. Chitambar. *Future Med. Chem*. **2012**, 4, 1257– 1272.

93. I. Kostova. *Anti-Cancer Agents Med. Chem*. **2009**, 9, 827– 842.

94. I. Ott. *Coord. Chem. Rev*. **2009**, 253, 1670–1681.

95. Z. Y. Wang. *Cancer Chemother. Pharmacol*. **2001**, 48(Suppl 1), S72–S76.

96. M .D. Hall, T. W. Failes, N. Yamamoto, T. W. Hambley. *Dalton Trans*. **2007**, 3983–3990.

97. M. C. Heffern, N. Yamamoto, R. J. Holbrook, A. L. Eckermann, T. J. Meade. *Curr. Opin. Chem. Biol*. **2013**, 17, 189–196.

98. J. B. Delehanty, J. E. Bongard, D. C. Thach, D. A. Knight, T. E. Hickey, E. L. Chang. *Bioorg. Med. Chem*. **2008**, 16, 830–837.

99. A. Bergamo, G. Sava. *Dalton Trans*. **2011**, 40, 7817– 7823.

100. F. P. Dwyer, E. C. Gyarfas, W. P. Rogers, J. H. Koch. *Nature* **1952**, 170, 190–191.

101. P. A. Wender, W. C. Galliher, E. A. Goun, L. R. Jones, T. H. Pillow. *Advanced Drug Delivery Reviews* **2008,** 60, (4-5), 452-472.

102. J. A. Schwartz, E. K. Lium, S. J. Silverstein. *J. Virol*. **2001**, 75, 4117–4128.

103. A. Y. Louie, T. J. Meade. *Proc. Natl. Acad*. Sci. U.S.A., **1998**, 95, 6663–6668.

104. S. M. Bykchov, V. N. Kharlamova. *Bull. Exper. Biol. Med*. **1974**, 78, 28–31.

105. C. X. Zhang, S. J. Lippard. *Curr Opin Chem Biol*. **2003,** 7, 481–489.



www.manaraa.com

106. I. Kostova. *Curr Med Chem*. **2006,** 13, 1085–1107.

107. G. S. Smith, B. Therrien. *Dalton Trans*. **2011**, 40, 10793–10800.

108. P. Liu, J. Jia, Y. Zhao, K. Wang. *Mini-Rev Med Chem*. **2015**, 16, 272–289.

109. J. Furrer, G. Süss-Fink. *Coord Chem Rev*. **2016**, 309, 36–50.

110. A. Levina, A. Mitra, P. A. Lay. *Metallomics* **2009**, 1, 458–470.

111. C. G. Hartinger, M. A. Jakupec, S. Zorbas-Seifried, M. Groessl, A. Egger; W. Berger, H. Zorbas, P. J. Dyson, B. K. Keppler. *Chem Biodiversity* **2008**, 5, 2140–2155.

112. I. Dragutan, V. Dragutan, A. Demonceau. *Molecules* **2015**, 20, 17244–17274.

113. C. G. Hartinger, M. Groessl, S. M. Meier, A. Casini, P. J. Dyson. *Chemical Society Reviews* **2013**, 42, 6186–6199.

114. E. S. Antonarakis, A. Emadi. *Cancer Chemother Pharmacol* **2010**, 66, 1–9.

115. A. I. Minchinton, I. F. Tannock. *Nat Rev Cancer* **2006**, 6, 583–592.

116. A. Bergamo, S. Zorzet, B. Gava, A. Sorc, E. Alessio, E. Iengo, G. Sava. *Anti-cancer drugs* **2000**, 11, 665–672.

117. S. L. Jones. *Arch Psychiat Nurs*. **1999**, 13, 109-110.

118. G. Sava, R. Gagliardi, M. Cocchietto, K. Clerici, I. Capozzi, M. Marrella, E. Alessio, G. Mestroni, R. Milanino. *Pathol Oncol Res*. **1998**, 4, 30–36.

119. M. Bacac, M. Vadori, G. Sava. *S. Cancer Immunol, Immun*. **2004**, 53, 1101–1110.

120. A. Bergamo, B. Gava, E. Alessio, G. Mestroni, B. Serli, M. Cocchietto, S. Zorzet, G. Sava. *Int J Oncol*. **2002**, 21, 1331–1338.

121. M. Debidda, B. Sanna, A. Cossu, A. M. Posadino, B. Tadolini, C. Ventura, G. Pintus. *Int J Oncol*. **2003**, 23, 477–482.

122. S. L. Jones. *Arch Psychiat Nurs*. **1999**, 13, 109-110.

123. Y. Yu, H. Li, Y. Yang, Y. Ding, Z. Wang, G. Li. *Anal. Chem*. **2016**, 88, 12287–12293.

124. A. Ziegler, J. Seelig. Biophys. J. **2008**, 94, 2142–2149.

125. L. N. Waller, N. Fox, K. F. Fox, A. Fox, R. L. Price. *J. Microbiol. Methods* **2004**, 58, 23–30.

126. D. L. Rabenstein. *Nat Prod Rep* **2002,** 19, (3), 312-31.

127. B. Mulloy, M. J. Forster. *Glycobiology* **2000**, *10*, 1147–1156.



www.manaraa.com

128. B. Mulloy, D. T. Crane, A. F. Drake, D. B. Davies. *Biochem. J*. **1997**, *328*, 51–61.

129. U. R. Desai, H. M. Wang, T. R. Kelly, R. J. Linhardt. *Carbohydr. Res.* **1993**, *241*, 249–259.

130. E. A. Yates, F. Santini, M. Guerrini, A. Naggi, G. Torri, B. Casu. *Carbohydr. Res.* **1896**, 294, 15–27.

131. D. R. Ferro, A. Provasoli, M. Ragazzi, G. Torri, B. Casu, G. Gatti, J. C. Jacquinet, P. Sinay, M. Petitou, J. Choay. *J. Am. Chem. Soc.* **1986**, *108*, 6773–6778.

132. D. R. Ferro, A. Provasoli, M. Ragazzi, B. Casu, G. Torri, V. Bossennec, B. Perly, P. Sinaÿ, M. Petitou, J. Choay. *Carbohydr. Res.* **1990**, *195*, 157–167.

133. E. A. Yates, C. J. Terry, C. Rees, T. R. Rudd, L. Duchesne, M. A. Skidomore, R. Levy, N. T. K. Thanh, R. J. Nichols, D. T. Clarke, D. G. Fernig. *Biochem. Soc. Trans*. **2006**, *34*, 427–430.

134. J. Kreuger, D. Spillmann, J. P. Li, U. Lindahl. *J. Cell Biol.* **2006**, *174*, 323–327.

135. D. J. D. Johnson, W. Li, T. E. Adams, J. A. Huntington. *EMBO J.* **2006**, *25*, 2029–2037.

136. M. Guerrini, M. Hricovíni, G. Torri. *Curr. Pharm. Des.* **2007**, *13*, 2045–2056.

137. J. Wesche, K. Haglund, E. M. Haugsten. *Biochem. J*. **2011**, *437*, 199–213.

138. W. Jorgen, H. Kaisa, M. H. Ellen. *Biochem. J*. **2011**, 437, 199–213.

139. J. H. Dey, F. Bianchi, J. Voshol, D. Bonenfant, E. J. Oakeley, N.E. *Cancer Res*. **2010**, 70, 4151–4162.

140. M. Koziczak, T. Holbro, N. E. Hynes. *Oncogene*. **2004**, 23, 3501–3508.

141. P. Chiodelli, A. Bugatti, C. Urbinati, M. Rusnati. *Molecules* **2015**, *20*, 6342–6388.

142. F. Zhang, X. Liang, J. M. Beaudet, Y. Lee, R. J. Linhardt. *J. Biom. Technol. Res.* **2014**, *1*, 6000101.

143. Y. Seo, M. R. Schenauer, J. A. Leary. *Int. J. Mass Spectrom.* **2011**, *303*, 191– 198.

144. I. Stevic, N. Parmar, N. Paredes, L. R. Berry, A. K. C. Chan. *Cell Biochem. Biophys.* **2011**, *59*, 171– 178.

145. H. Xie, Y. J. Kang. *Curr. Med. Chem.* **2009**, *16*, 1304– 1314.



www.manaraa.com

146. S. H. Zlotkin, S. Atkinson, G. Lockitch. *Clin Perinatol* **1995**; 22: 223-240.

147. L. D. D'Andrea, A. Romanelli, R. Di Stasi, C. Pedone. *Dalt. Trans.* **2010**, *39*, 7625– 7636.

148. G. Boden, X. Chen, J. Ruiz, G. D. van Rossum, S. Turco. *Metabolism*, **1996**; 45: 1130-1135.

149. N. Cohen, M. Halberstam, P. Shlimovich, C. J. Chang, H. Shamoon, L. Rosetti. *J Clin Invest*. **1995**; 95: 2501-2509.

150. A. B. Goldfine, D. Simonson, F. Folli, M. E. Patti, C. R. Kahn. *J Clin Endocrinol Metab*. **1995**; 80: 3312-3320.

151. M. Halberstam, N. Cohen, P. Shlimovich, L. Rosetti, H. Shamoon. *Diabetes*, **1996**; 45: 659-666.

152. E. G. De Master, R. A. Mitchell. *Biochemistry*, **1973**; 12: 3616-3621.

153. J. M. Samet, L. M. Graves, J. Quay, L. A. Dailey, R. B. Devlin, A. J. Ghio, W. Wu, P. A. Bromberg, W. Reed,. *Am. J. Physiol*. **1998**, 275: L551–L558.

154. W. Wu, L. M. Graves, I. Jaspers, R. B. Devlin, W. Reed, J. M. Samet. *Am. J. Physiol*. **1999**, 277: L924–L931.

155. J. B. Connell, H. Lortat-Jacob. *Front Immunol*. **2013**; 4, 385.

156. N. Ilan, M. Elkin, I. Voldavsky. *Int J Biochem Cell Biol*. **2006**, 38, 2018–2039.

157. H. Q. Miao, H. Liu, E. Navarro, P. Kussie, Z. Zhu. *Curr Med Chem*. **2006**, 13, 2101–2111.

158. H. J. Zhao, H. Y. Liu, Y. Chen, X. Xin, J. Li, Y. Hou, Z. Zhang, X. Zhang, C. Xie, M. Geng, J. Ding. *Cancer Res.* **2006**, 66, 8779–8787.

159. E. Witsch, M. Sela, Y. Yarden. *Physiology (Bethesda)* **2010**, 25, 85-101.

160. R. L. Elliott, G. C. Blobe. *J Clin Oncol.* **2005**, 23, 2078-2093.

161. H. L. Goel, A. M. Mercurio. *Nat Rev Cancer* **2013**, 13, 871-882.

162. J. B. Demoulin, A. Essaghir. *Cytokine Growth Factor Rev.* **2014**, 25, 273-283.



www.manaraa.com

163. M. V. Dieci, M. Arnedos, F. Andre, J. C. Soria. *Cancer Discov.* **2013**, 3, 264-279.

164. G. Adams, L. M. Weiner. *Nat Biotechnol.* **2005**, 23, 1147-1157.

165. P. Workman, V. G. Brunton, D. J. Robins. *Semin Cancer Biol.* **1992**, 3, 369-381.

166. R. Nahta, L. X. Yuan, B. Zhang, R. Kobayashi, F. J. Esteva. *Cancer Res.* **2005**, 65, 11118-11128.

167. J. Kreuger, D. Spillmann, J. P. Li, U. Lindahl. *J. Cell Biol*. **2006**, 174, 323–327.

168. T. R. Rudd, S. E. Guimond, M. A. Skidmore, L. Duchesne, M. Guerrini, G. Torri, C. Cosentino, A. Brown, D. T. Clarke, J. E. Turnbull, D. G. Fernig, E. A. Yates. *Glycobiology* **2007**, 17, 983–993.

169. A. L. Harris, J. J. Ryan, N. P. Farrell. *Pharmacol*. **2006**, 69, 666–672. 99.

170. A. L. Harris, X. Yang, A. Hegmans, L. Povirk, J. J. Ryan, L. Kelland, N. P. Farrell. *Inorg. Chem*. **2005**, 44, 9598–9600.

171. M. M. Fuster, J. D. Esko. *Nature Reviews* **2005**, 5, 526–542.

172. M. D. Hall, M. Okabe, D. W. Shen, X. J. Liang, M. M. Gottesman. *Annu Rev Pharmacol Toxicol*. **2008**, 48, 495–535.

173. H. Silva, F. Frézard, E. J. Peterson, P. Kabolizadeh, J. J. Ryan, N. P. Farrell. *Mol. Pharmaceutics* **2012**, *9*, 1795– 1802.

174. E. J. Peterson, A. G. Daniel, S. J. Katner, L. Bohlmann, C-W. Chang, A. Bezos, C. R. Parish, M. von Itzstein, S. J. Berners-Price, N. P. Farrell, Antiangiogenic platinum through glycan targeting. Chem. Sci. **2017** 8, 241– 252.

175. S. M. Fuchs, R. T. Raines. *Biochemistry* **2004**, *43*, 2438– 2444.

176. Q. C. Jiao, Q. Liu, C. Sun, H. He. *Talanta* **1999**, *48*, 1095– 1101.

177. L. Tan, S. Yao, Q. Xie. *Talanta* **2007**, *71*, 827– 832.

178. J. Wang, A. S. Jeevarathinum, K. Humpries, A. Jhunjhunwala, F. Chen, A. Hairiri, B. R. Miller, J. V. Jokerst. *Bioconj. Chem.* **2018**.

179. L. Zhang, N. Li, F. Zhao, K. Li. *Anal. Sci.* **2004**, *20*, 445– 50



www.manaraa.com

180. J. Wang, A. S. Jeevarathinum, K. Humpries, A. Jhunjhunwala, F. Chen, A. Hairiri, B. R. Miller, J. V. Jokerst. *Bioconj. Chem.* **2018**.

181. L. Zhang, N. Li, F. Zhao, K. Li. *Anal. Sci.* **2004**, *20*, 445– 50.

182. J. B. Mangrum, B. J. Engelmann, E. J. Peterson, J. J. Ryan, S. J. Berners-Price, N. P. Farrell. *Chem. Commun.* **2014**, 50, 4056–4058.

183. Y. Seo, M. R. Schenauer, J. A. Leary. *Int. J. Mass Spectrom*., **2011**, 303, 191–198.

184. W. G. Chai, J. L. Luo, C. K. Lim, A. M. Lawson. *Anal. Chem*., **1998**, 70, 2060–2066.

185. M. J. Kailemia, K. Li, M. Ly, R. J. Linhardt, I. J. Amster. *Anal. Chem.* **2012**, 84, 5475–5478.

186. B. Mulloy, M. J. Forster, C. Jones, D. B. Davies. *Biochem J*. **1993**; 293: 849-858.

187. H. Silva, F. Frézard, E. J. Peterson, P. Kabolizadeh, J. J. Ryan, N. P. Farrell. *Mol Pharm*. **2012**, 9(6): 1795-1802.

188. K. Saxena, U. Schieborr, O. Anderka, E. Duchardt-Ferner, B. Elshorst, S. L. Gande, J. Janzon, D. Kudlinzki, S. Sreeramulu, M. K. Dreyer, K. U. Wendt, C. Herbert, P. Duchaussoy, M. Bianciotto, P. A. Driguez, G. Lassalle, P. Savi, M. Mohammadi,F. Bono, H. Schwalbe. *J Biol Chem*. **2010**; 285 (34): 26628-26640.

189. H. H. Chen, M. T. Kuo. *Metal-Based Drugs* **2010**, 430939.

190. N. P. Farrell. Drugs of The Future **2012**, 37, 795–806.

191. E. J. Peterson, A. G. Daniel, S. J. Katner, L. Bohlmann, C-W. Chang, A. Bezos, C. R. Parish, M. von Itzstein, S. J. Berners-Price, N. P. Farrell, Antiangiogenic platinum through glycan targeting. Chem. Sci. **2017** 8, 241– 252.

192. A. T. Jones. *International Journal of Pharmaceutics* **2008,** 354, (1-2), 34-38.

193. A. L. Harris, X. Yang, A. Hegmans, L. Povirk, J. J. Ryan, L. Kelland, N. P. Farrell. *Inorg. Chem.* **2005,** 44, (26), 9598-9600.

194. M. Tang, A. J. Waring, M. Hong. *Journal of the American Chemical Society* **2007,** 129, (37), 11438-11446.

195. P. A. Wender, W. C. Galliher, E. A. Goun, L. R. Jones, T. H. Pillow. *Advanced Drug Delivery Reviews* **2008,** 60, (4-5), 452-472.



www.manaraa.com

196. D. L. Rabenstein. *Nat Prod Rep.* **2002,** 19, (3), 312-331.

197. N. P. Farrell, A. K. Gorle, E. J. Peterson, S. J. Berners-Price. *Met. Ions Life Sci*. **2018**, 18, 109–140.

198. E. Hammond, A. Khurana, V. Shridhar, K. Dredge. *Front. Oncol*. **2014**, 4, 1–15.

199. A. M. Gomes, M. P. Stelling, M. S. G. Pavão. *BioMed Res. Int.* **2013**, 1–11.

200. C. Pisano, I. Vlodavsky, N. Ilan, F. Zunino. *Biochem. Pharmacol*. **2014**, 89, 12– 19.

201. F. Levy-Adam, N. Ilan, I. Vlodavsky. *Sem. Cancer Biol*. **2010**, 20, 153–160.



www.manaraa.com

This work was published in Chemistry: A European Journal with the following contributions: Synthesis by Daniel Lee, Molecular modeling and DFT calculations by Gerard Daniel, NMR cleavage inhibition by Anil Gorle and Eric Ginsburg, MB, ITC, and MS by Wyatt Johnson, EtBR and Biological evaluation by Samantha Katner. Text by Anil Gorle, Wyatt Johnson, and Samantha Katner.

## Chapter 2: Substitution-Inert Polynuclear Platinum Complexes as Metalloshielding Agents for Heparan Sulfate

**Anil Kumar Gorle*, Samantha J. Katner, Wyatt E. Johnson, Daniel E. Lee, A. Gerard Daniel, Eric Ginsburg, Mark von Itzstein*, Susan J. Berners-Price*, and Nicholas P. Farrell**

*Institute for Glycomics, Griffith University, Gold Coast Campus, Southport, Queensland, 4222, (Australia)

Department of Chemistry and Massey Cancer Center, Virginia Commonwealth University (VCU), Richmond, Virginia 23284, United States

Chemistry: A European Journal, 2018, 24 (25), 6606-6616.



www.manaraa.com

## 2.1 Abstract:

Cleavage of heparan sulfate proteoglycans (HSPGs) by the enzyme heparanase modulates tumour-related events including angiogenesis, cell invasion, and metastasis. Metalloshielding of heparan sulfate (HS) by positively charged polynuclear platinum complexes (PPCs) effectively inhibits physiologically critical HS functions. Studies using bacterial P. heparinus heparinase II showed that a library of Pt complexes varying in charge and nuclearity and the presence or absence of a dangling amine inhibits the cleavage activity of the enzyme on the synthetic pentasaccharide, Fondaparinux (FPX). Charge-dependent affinity of PPC for FPX was seen in competition assays with methylene blue and ethidium bromide. The dissociation constant (Kd) of TriplatinNC for FPX was directly measured by isothermal titration calorimetry (ITC). The trend in DFT calculated interaction energies with heparin fragments is consistent with the spectroscopic studies. Competitive inhibition of TAMRA-$R_9$ internalization in human carcinoma (HCT116) cells along with studies in HCT116, wildtype CHO and mutant CHO-pgsA745 (lacking HS/CS) cells confirm that HSPG-mediated interactions play an important role in the cellular accumulation of PPCs.

## 2.2 Introduction:

The heparanase/heparan sulfate proteoglycan (HPSE/HSPG) interaction is central to many initiating processes of the angiogenesis cascade.(1, 2) Heparanase degrades heparan sulfate (HS) into shorter fragments at the cell surface and within the extracellular matrix through its β-endoglycosidase activity. These considerations, combined with glycan overexpression on many tumour surfaces make proteoglycans significant drug targets of high biological relevance.(1, 2) The sulfate residues are the critical recognition features for HS interaction with protein substrates such as growth factors. We have recently shown that sulfate cluster masking, or "metalloshielding", by clinically relevant anticancer polynuclear platinum complexes (PPCs)—Triplatin (BBR3464) and its substitution- inert analogue TriplatinNC—is an effective way to



www.manaraa.com

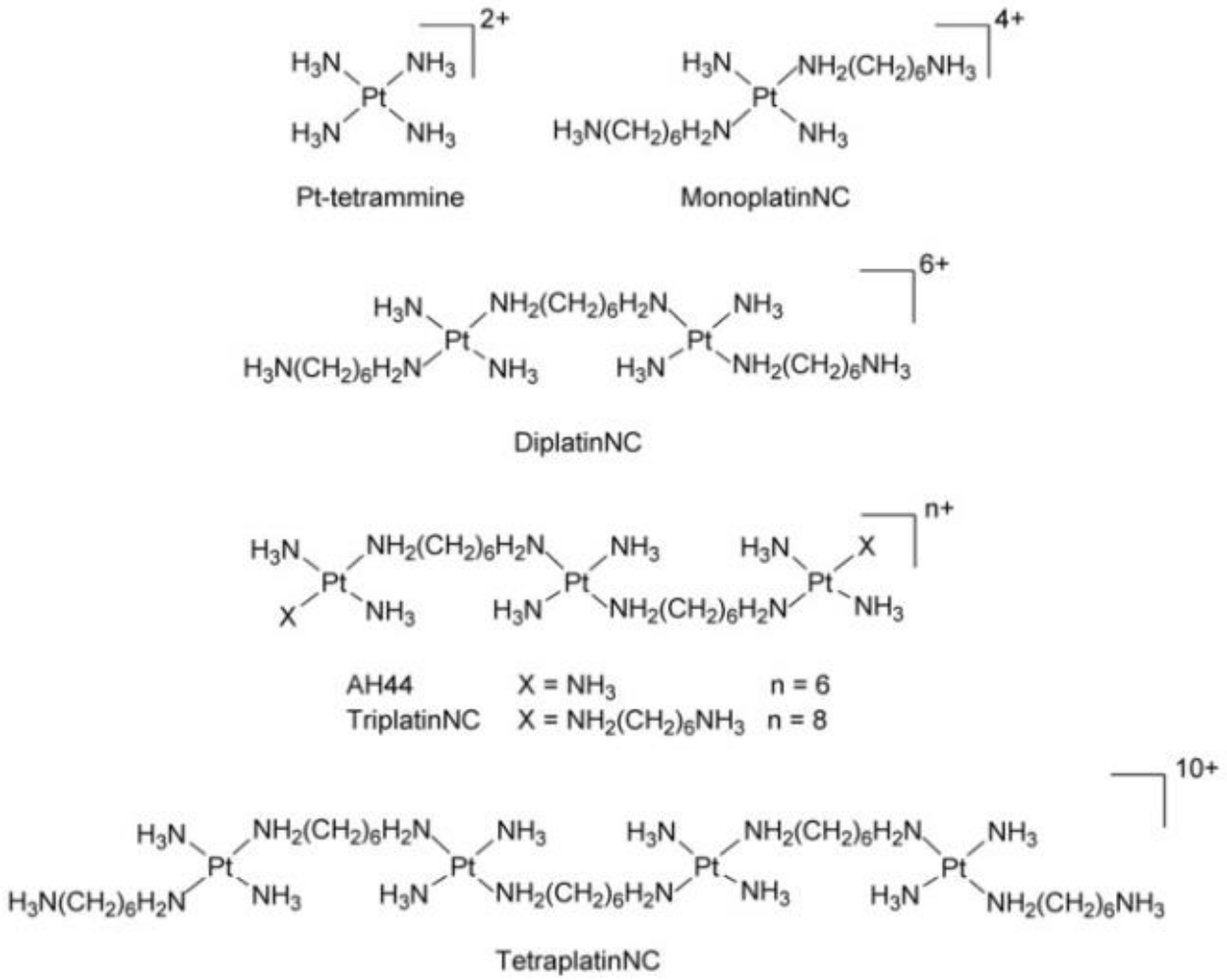


Scheme 2.1. Structures of the Polynuclear Platinum Compounds (PPC Library). Counter- anions omitted for clarity. All compounds with the exception of $[Pt(NH_3)_4]Cl_2$ were synthesised and used as nitrate salts.



www.manaraa.com

protect HS from the actions of its associated enzymes and proteins.(3-5) By protecting the substrate, the shielding concept is a complementary and attractive alternative to the time-consuming synthesis of small oligosaccharides, which are generally designed to act as competitive inhibitors toward heparanase.(1, 2) In this sense, the substrate protection is analogous to that of metal complex–DNA interactions with effects on protein recognition.

To define the detailed structure–activity relationships involved in inhibition of the HPSE/HSPG interaction through sulfate cluster masking by PPCs, it is necessary to consider the role of HS as ligand in coordination chemistry. The heterogeneity of heparin and HS, especially with respect to sulfation patterns, raises challenges for systematic approaches to this understanding.(6, 7) In this respect, we have previously used Fondaparinux (FPX) for mechanistic studies.(3, 4) FPX is a well- defined, highly sulfated synthetic glycosaminoglycan- based fragment that has been used clinically as an antithrombotic agent since the 1940s.(8) It is a substrate for both bacterial heparinases and human heparanase and is useful in screening the efficiency and reaction kinetics of potential heparanase inhibitors.(9-11) Fondaparinux is also an ideal substrate for mechanistic studies because it is homogeneous, has low molecular weight, and represents a single point of cleavage for both mammalian and bacterial enzymes.(9, 11) The course of FPX hydrolysis can conveniently be determined by $^{1}$H NMR spectroscopy because the anomeric protons are sensitive reporters of the cleavage reaction by both heparanase and the bacterial heparinases.(10, 12)

To develop structure–activity relationships, we have synthesised a small focused library of PPCs (Scheme 2.1) to examine the effects of charge and dangling amine on their interactions with FPX and the biological consequences thereof. In this paper we describe cleavage inhibition studies in the presence/absence of the PPC library using bacterial heparinase (*P. heparinus* heparinase II) and confirm the generality of the metalloshielding concept for the structurally distinct enzymes.3, 4 All complexes except the "control" mononuclear Pt- tetraammine $[Pt(NH_3)_4]^{2+}$ completely blocked the enzyme activity on FPX. Competition assays with methylene blue (MB) and ethidium bromide (EtBr) as reporter molecules describe approaches to measure the affinity of each compound for FPX binding and compare the results with the extensively studied



www.manaraa.com

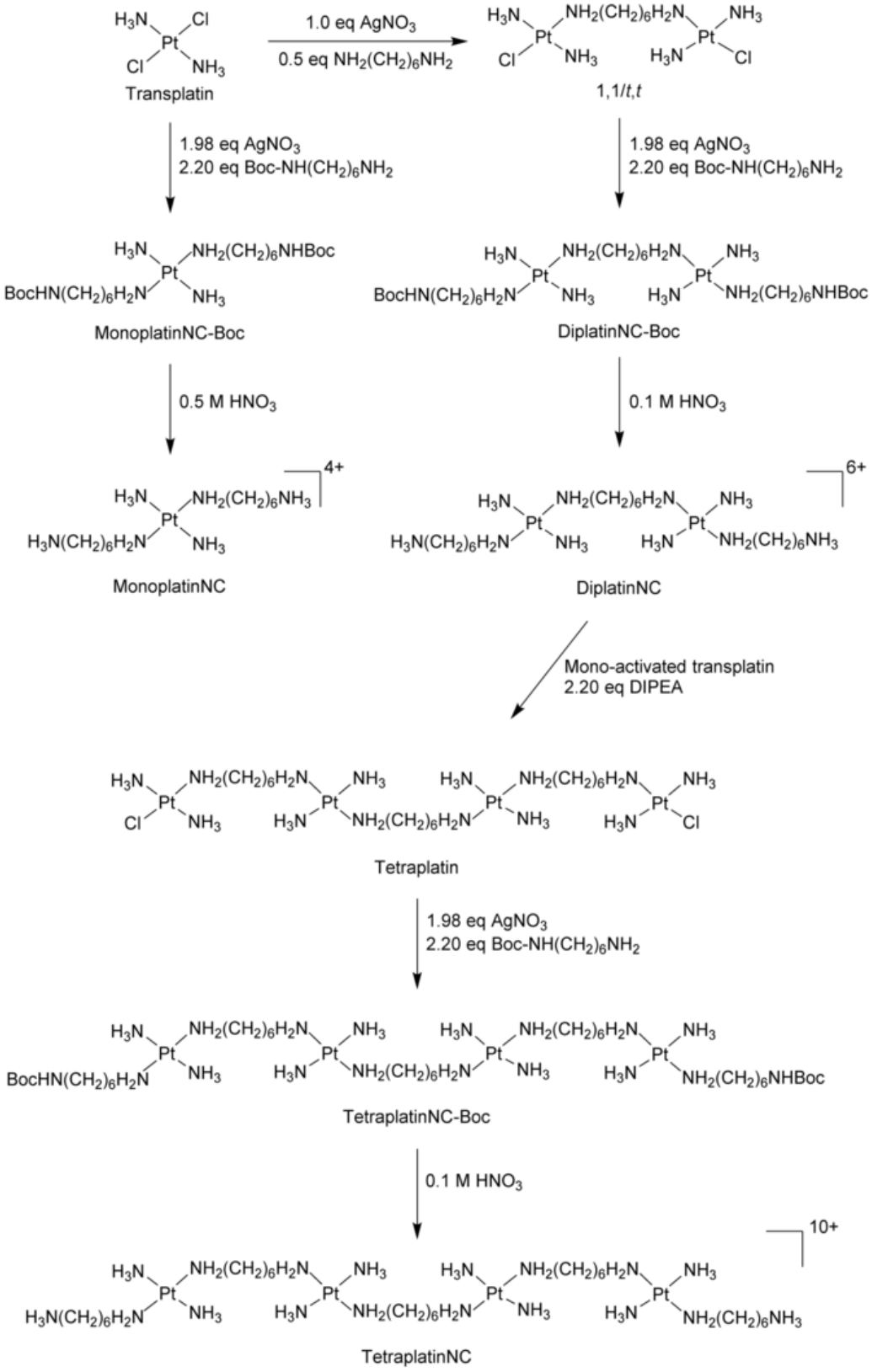


Scheme 2.2. Synthesis of MonoplatinNC, DiplatinNC and TetraplatinNC.



www.manaraa.com

DNA interactions. The combined data is correlated with calculated energies of interaction for PPC–heparin fragments from DFT. These studies contribute to the systematic development of metalloglycomics—the study of the effects of metal ions and coordination compounds on oligosaccharides—expanding the study of bioinorganic chemistry to the third major biomolecule after the well- studied proteins and nucleic acids.(13)

## 2.3 Results and Discussion:

### Synthesis of the PPC library

The library of PPC compounds used in this study is shown in Scheme 2.1. The compounds were chosen to examine variation in total positive charge, nuclearity (mono/di/tri Pt units) and the presence or absence of a dangling amine. The modular nature of PPCs lends itself to systematic synthetic procedures as illustrated for the newly reported compounds MonoplatinNC, DiplatinNC, and TetraplatinNC in Scheme 2.2.

### Inhibition of enzyme activity on FPX by PPCs

Cleavage inhibition studies were performed on the sulfated pentasaccharide Fondaparinux (FPX), as a model HS- like substrate, using the bacterial enzyme (*P. heparinus* heparinase II). The assay was performed as reported previously, where the effect of enzyme on FPX cleavage was monitored by following the anomeric region of the $^{1}$H NMR spectrum of FPX.(4, 10) Cleavage of FPX by the enzyme results in the formation of a trisaccharide unit and a double- bond containing disaccharide unit. Consistent with the formation of a double bond after enzyme treatment, the signal for $H_{D4}$ ($\delta$=4.06 ppm in FPX) shifts to $\delta$=5.89 ppm ($H_{D4'}$) and the signal for $H_{D5}$ disappears. Scheme 2.3 shows the enzymatic cleavage products of FPX when treated with *P. heparinus* heparinase II and Figure 2.1 shows the cleavage of FPX in the absence of Pt compounds over 24 h (positive control).



www.manaraa.com

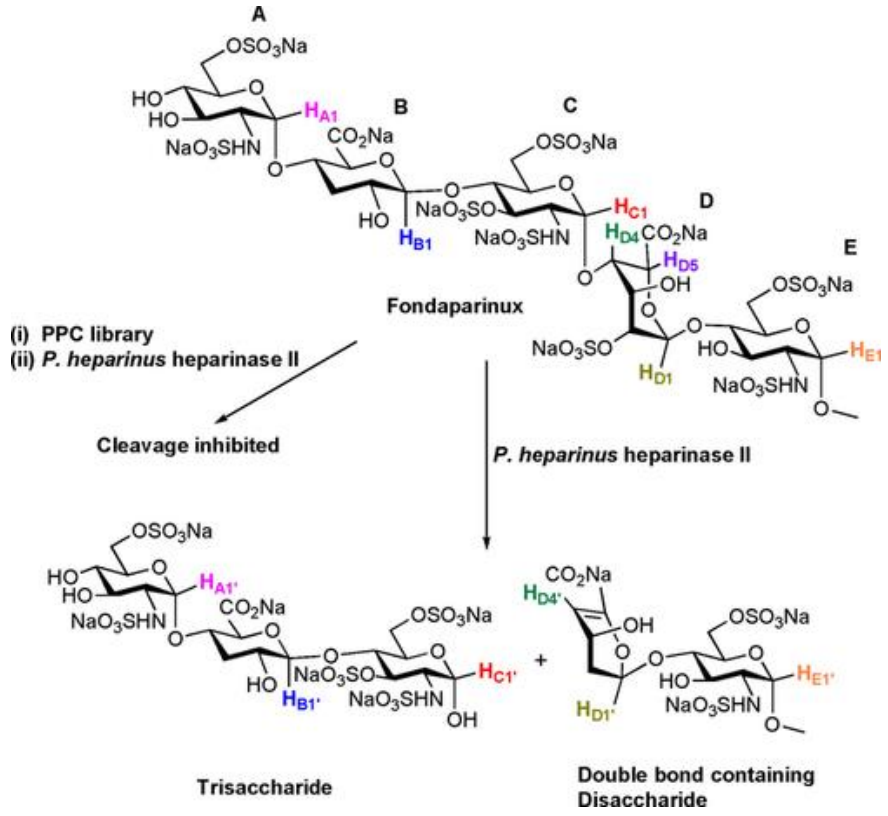


Scheme 2.3. Structures of Fondaparinux and cleavage products by *P. heparinus* heparinase II. In the presence of PPCs, cleavage was completely inhibited.

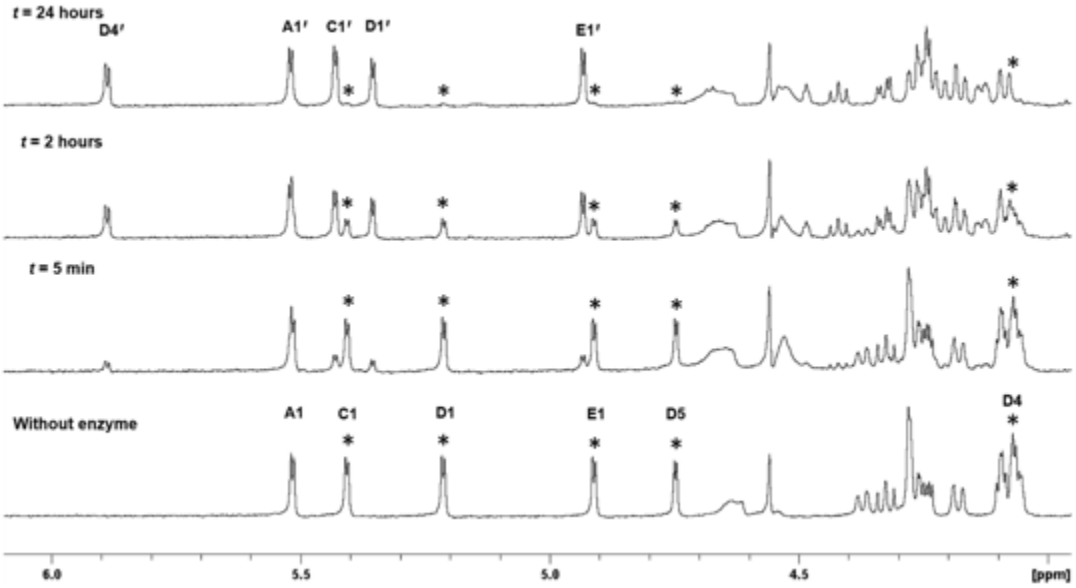


Figure 2.1. Cleavage of FPX by *P. heparinus* heparinase II. FPX was incubated with *P. heparinus* heparinase II, and $^{1}$H NMR spectra were recorded without enzyme and at different time points after addition of enzyme. Decrease of $^{1}$H NMR peaks of interest are indicated with asterisks. Olefinic proton at □ 5.89 ppm obtained due to cleavage of Fondaparinux labelled as D4´ (see scheme 1).



www.manaraa.com

To evaluate the ability of the PPC library to inhibit the enzymatic cleavage of FPX, the substrate was pre- incubated with each of the Pt complexes in a 1:1 stoichiometric ratio for 10 min prior to the addition of the enzyme. Figure 2.2 a shows the anomeric region of the $^{1}$H NMR spectra of FPX in the presence of one equivalent of each of the Pt complexes. Upon addition of the enzyme to each sample, reactions were followed for the next 24 h by $^{1}$H NMR spectroscopy (Figure 2.2 b). All Pt complexes completely inhibited FPX cleavage, with the exception of the mononuclear $[Pt(NH_3)_4]^{2+}$, for which weak signals corresponding to cleavage were observed. MonoplatinNC differs from the Pt- tetraammine by the presence of dangling amine groups, giving an overall higher charge (see Scheme 2.1). The different behaviour of these two mononuclear complexes in cleavage inhibition indicates the importance of dangling amines. Following on from our first demonstration,4 PPCs can now be considered a *class* of inhibitors of heparanase/heparinase cleavage. Charge dispersion, either through dangling amines or multiple Pt- tetraammine coordination spheres, is needed for the effective inhibition of enzymatic cleavage of HS substrates. Di- and tetra- saccharide fragments inhibit the function of *B. eggerthii* heparinase II (bacterial enzyme) on FPX.(10) The tetra- saccharide completely inhibited FPX cleavage, whereas the di-saccharide inhibited the cleavage for the first 60 min of enzyme exposure after which only minor levels of cleavage of FPX was observed.(10) Thus, the metalloshielding approach is an attractive alternative to the time- and material- costly synthesis of oligosaccharide mimetics.

**The nature of the PPC–FPX and PPC–HS interactions**

**NMR Studies**

The NMR chemical shift changes of FPX in the presence of stoichiometric ratios of PPCs were analysed to delineate the critical features for effective metalloshielding (Table 2.1). Highly positively charged PPCs induce changes to the chemical shifts of the anomeric protons of GlcNS(6S), GlcNS(3S)(6S), IdoA(2S) and GlcNS(6S) residues of FPX (Rings A, C, D and E, respectively, Scheme 2.3), suggesting the importance of delocalized positive charge of PPC for the favourable interaction with HS fragments. MonoplatinNC produced only slight chemical shift



www.manaraa.com

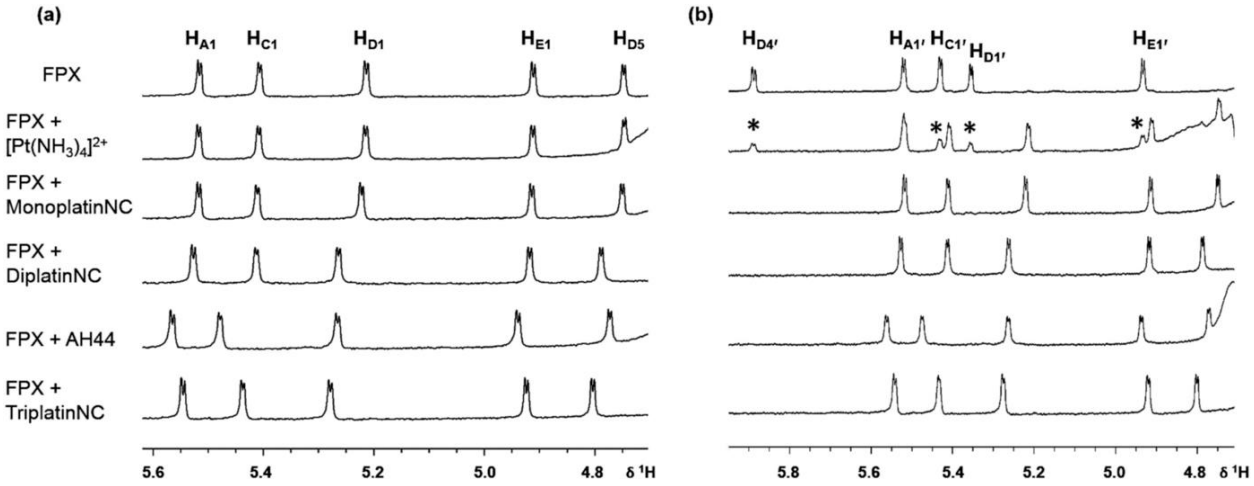


Figure 2.2. Anomeric region of the $^1$H NMR spectra of 1:1 mixtures of FPX and various PPCs a) after 10 min incubation in 20 mM Tris buffer, pH 7.5; b) 24 h after treatment with *P. heparinus* heparinase II enzyme. Peaks indicated with asterisks in (b) represent FPX cleavage products in the presence of the mononuclear complex, $[Pt(NH_3)_4]^{2+}$.

| Compound | $\Delta\delta=\delta$(FPX : PPC)−$\delta$(FPX)[a] | | | | |
|---|---|---|---|---|---|
| | A1 | C1 | D1 | E1 | D5 |
| $[Pt(NH_3)_4]^{2+}$ | 0.0 | 0.0 | 0.0 | 0.0 | 0.0 |
| MonoplatinNC | 0.0 | 0.01 | 0.01 | 0.0 | 0.0 |
| DiplatinNC | 0.01 | 0.01 | 0.05 | 0.0 | 0.04 |
| AH44 | 0.05 | 0.07 | 0.05 | 0.02 | 0.03 |
| TriplatinNC | 0.03 | 0.03 | 0.06 | 0.01 | 0.06 |

Table 2.1. $^1$H NMR chemical shift changes [$\Delta\delta=\delta$(FPX : PPC)−$\delta$(FPX)] after incubation of Pt complexes with FPX for 10 min at 37 °C.

[a] For assignment of the anomeric protons see Scheme **3**.



www.manaraa.com

changes whereas no discernible shifts were seen for $[Pt(NH_3)_4]^{2+}$. TriplatinNC and AH44 caused the largest changes, with AH44 significantly affecting the anomeric protons of the terminal and central glucosamine units, suggesting a favourable interaction between AH44 and sulfate groups of Ring A and Ring C, and showing the effect of the third Pt centre, with presumably more complex–FPX contacts. The $H_{D1}$ and $H_{D5}$ protons of IdoA(2S) (Ring D) are also significantly affected by the trinuclear complexes. DiplatinNC, which carries the same 6+ charge as AH44, but contains dangling amine groups on both the Pt centres, induces significant shifts only to these two protons. IdoA(2S) residues of HS are highly conformationally flexible and can adopt both the $^1C_4$ chair and $^2S_0$ skew boat conformations, whereas GlcNS residues prefer only $^4C_1$ chair conformation.(14, 15) The ratio of $^1C_4$ and $^2S_0$conformers of the IdoA(2S) residue of FPX in solution is about 35:65.(14-16) The results suggest that PPCs change the ring conformation and/or induce conformational changes to the important glycosidic linkages of the IdoA(2S) residue. The NMR changes observed for the FPX anomeric protons in the 1:1 adducts of FPX–PPC validate the reasons for effective inhibition of the enzymatic cleavage.

**Protection of FPX against sulfate loss**

Previous ESI-MS studies showed that AH44 (6+) and TriplatinNC (8+) protect the sulfate groups of an octasaccharide (DP8) against dissociation through the formation of sTable 2.1:1 adducts.3 In the present work we used ESI-MS to study the protection from sulfate loss of 1:1 PPC–FPX adducts in the gas phase (Figure 2.3). The most abundant charge state observed in previous MS studies of FPX was 3−, with three sulfo groups being cleaved and cation/$H^+$ exchange reducing $SO_3$ loss.(17) Under our conditions, ESI-MS spectra of free FPX also showed the sequential loss of three sulfate moieties, whereas under the same conditions and in the presence of PPCs, sulfate groups of FPX are protected in a manner dependent on charge and number of Pt centres. Consistent with the high affinity FPX binding of TriplatinNC, no significant sulfate loss occurred. The same was true for AH44, whereas for 1:1 FPX adducts of DiplatinNC (6+) there was also significant protection, with only peaks of low intensity observed corresponding to loss of one and two



www.manaraa.com

$SO_3$ groups. For the lower charged MonoplatinNC (4+), loss of two and three sulfate groups is observed, but again by far the most dominant peak was the parent ion.



www.manaraa.com

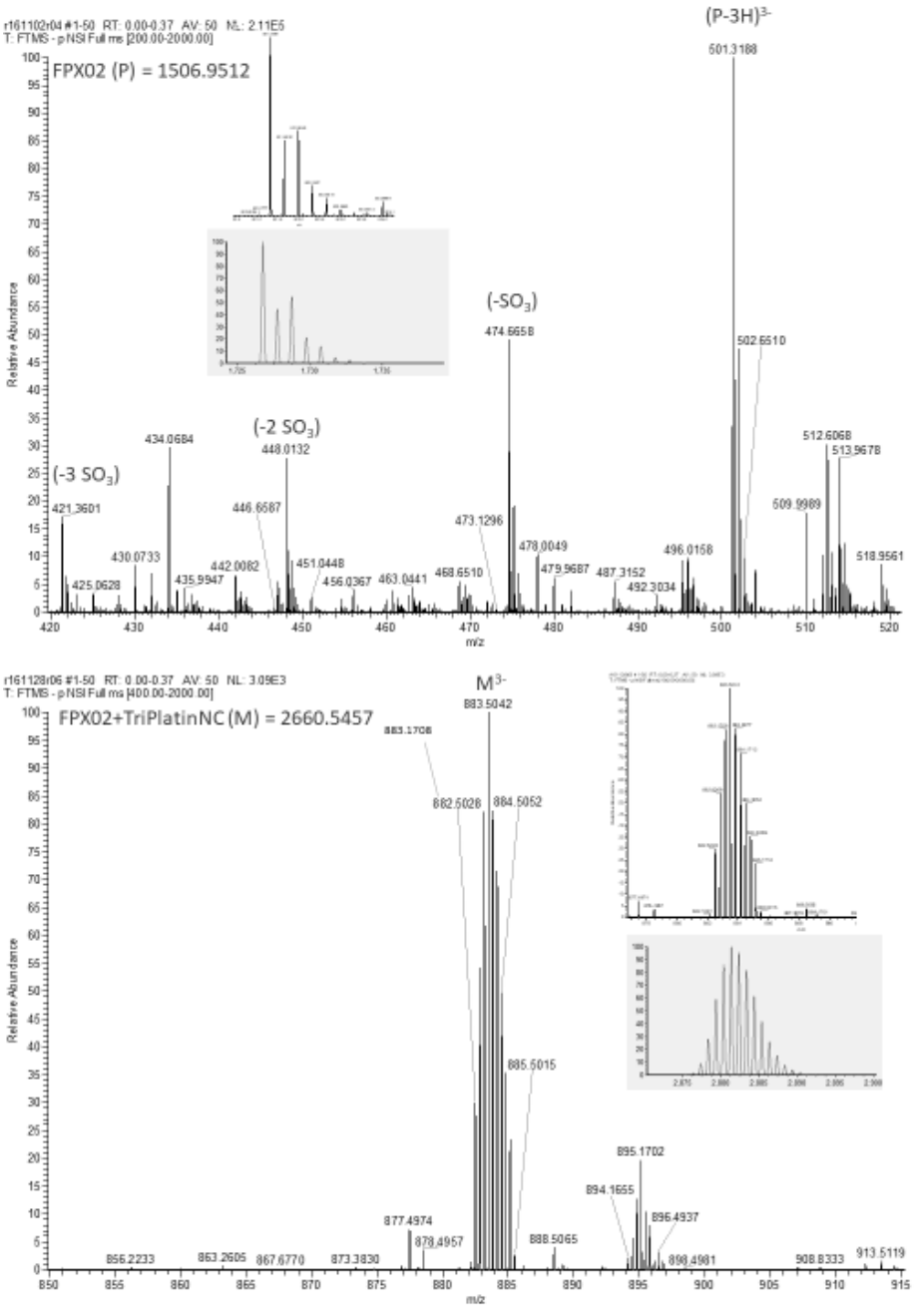


Figure 2.3. ESI-MS with inset showing actual isotopic distribution (top) and theoretical isotopic distribution (bottom). **A) Free FPX showing sequential sulfate loss. B) 1:1 adduct of FPX-TriplatinNC showing no sulfate loss.** C) FPX-AH44 showing no sulfate loss. D) FPX-DiplatinNC showing sequential loss of two sulfates. E) FPX-MonoplatinNC showing sequential loss of three sulfates.



www.manaraa.com

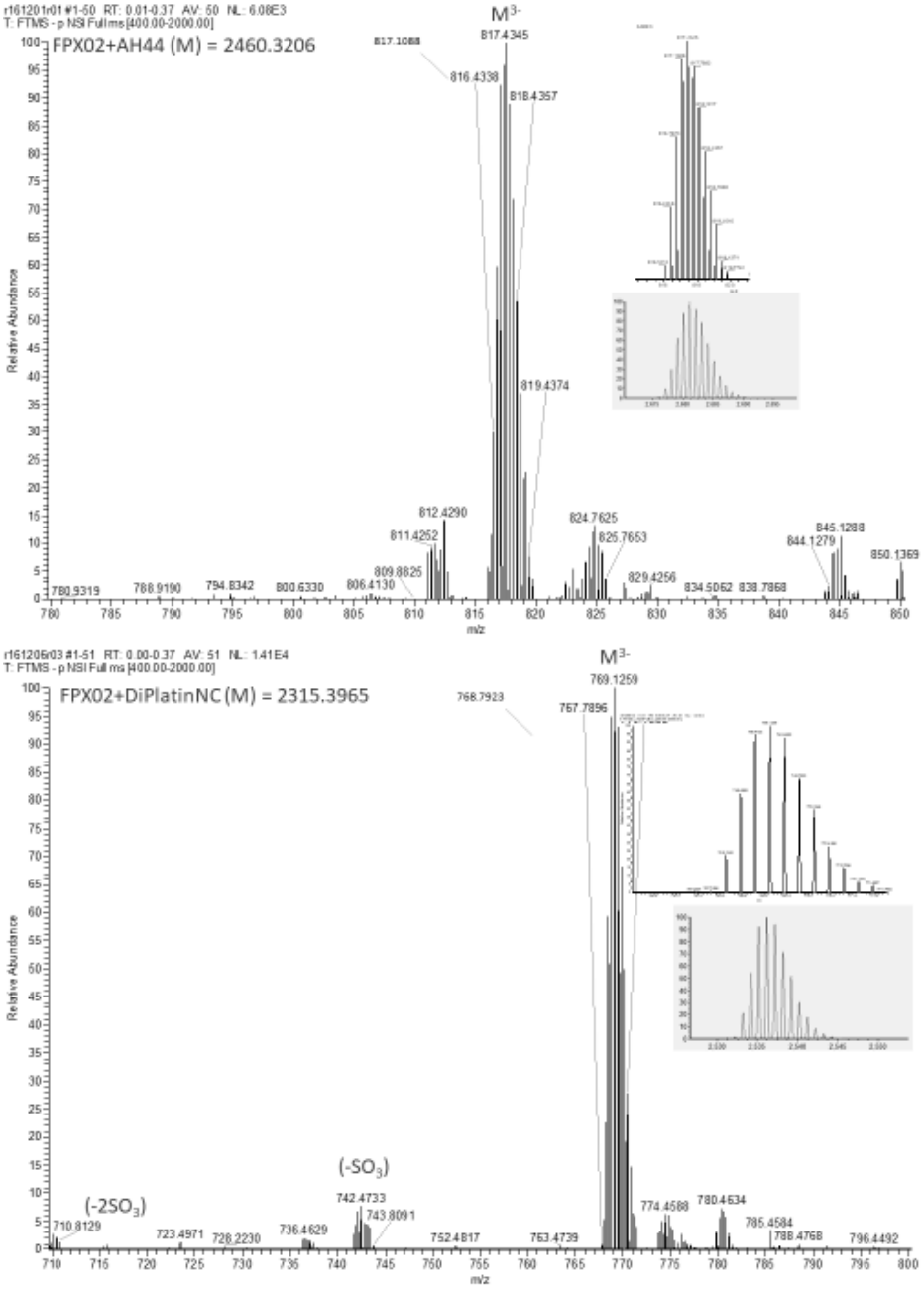


Figure 2.3. ESI-MS with inset showing actual isotopic distribution (top) and theoretical isotopic distribution (bottom). A) Free FPX showing sequential sulfate loss. B) 1:1 adduct of FPX-TriplatinNC showing no sulfate loss. **C) FPX-AH44 showing no sulfate loss. D) FPX-DiplatinNC showing sequential loss of two sulfates**. E) FPX-MonoplatinNC showing sequential loss of three sulfates.



www.manaraa.com

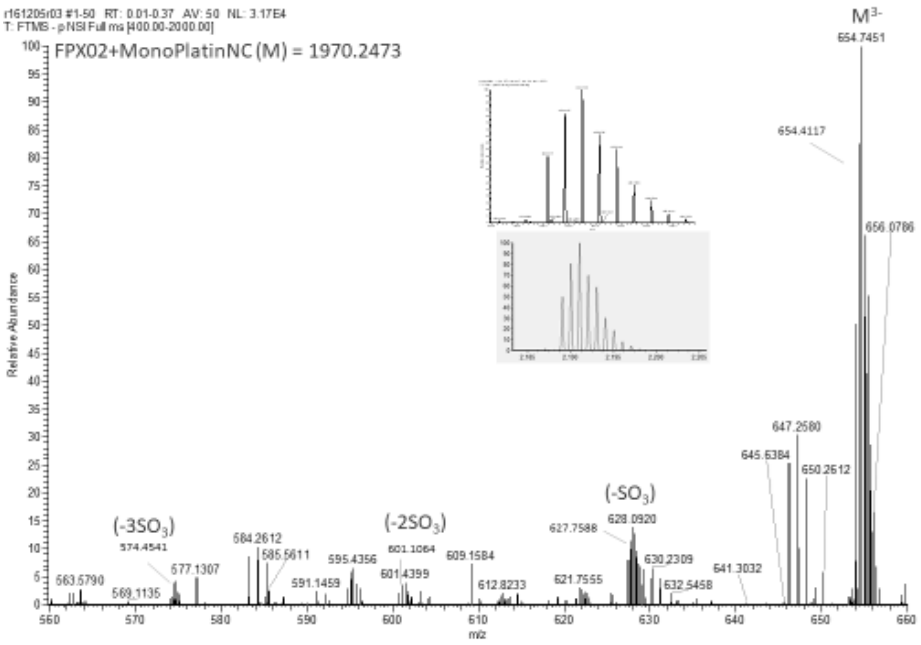


Figure 2.3. ESI-MS with inset showing actual isotopic distribution (top) and theoretical isotopic distribution (bottom). A) Free FPX showing sequential sulfate loss. B) 1:1 adduct of FPX-TriplatinNC showing no sulfate loss. C) FPX-AH44 showing no sulfate loss. D) FPX-DiplatinNC showing sequential loss of two sulfates. **E) FPX-MonoplatinNC showing sequential loss of three sulfates.**



www.manaraa.com

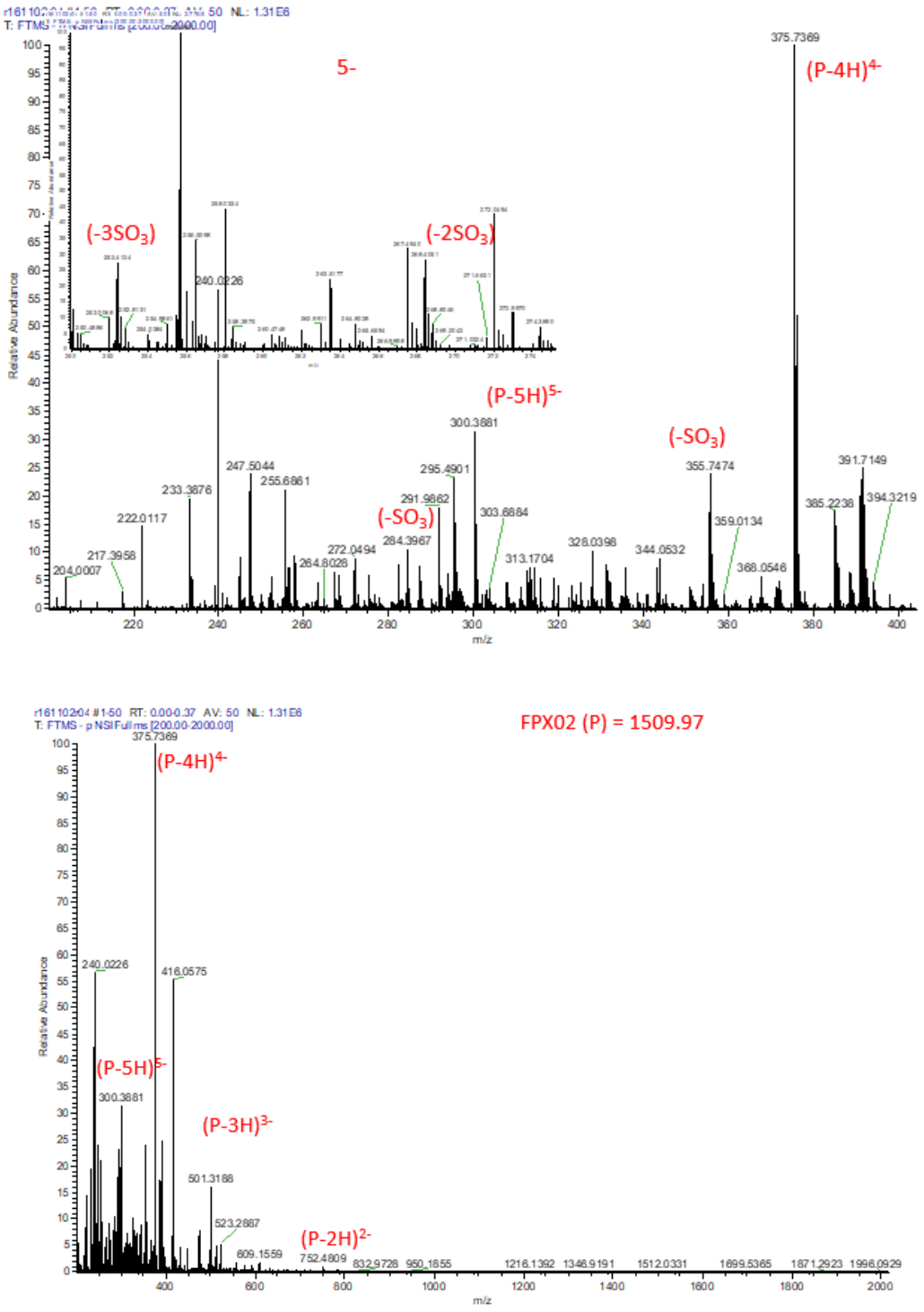


Figure 2.4. ESI-MS of Free FPX showing multiple charge states with sequential sulfate loss.



www.manaraa.com

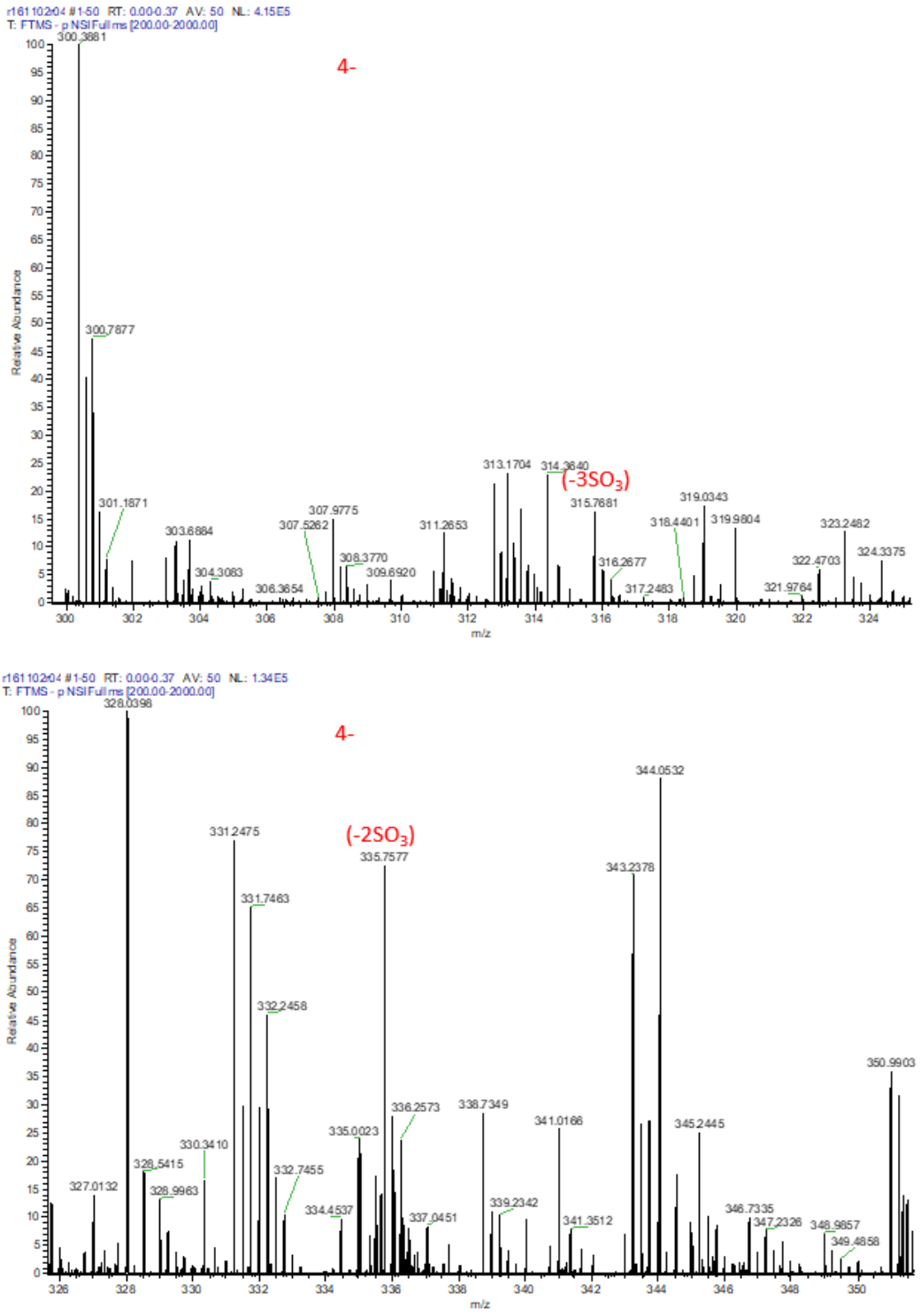


Figure 2.4. ESI-MS of Free FPX showing multiple charge states with sequential sulfate loss.



www.manaraa.com

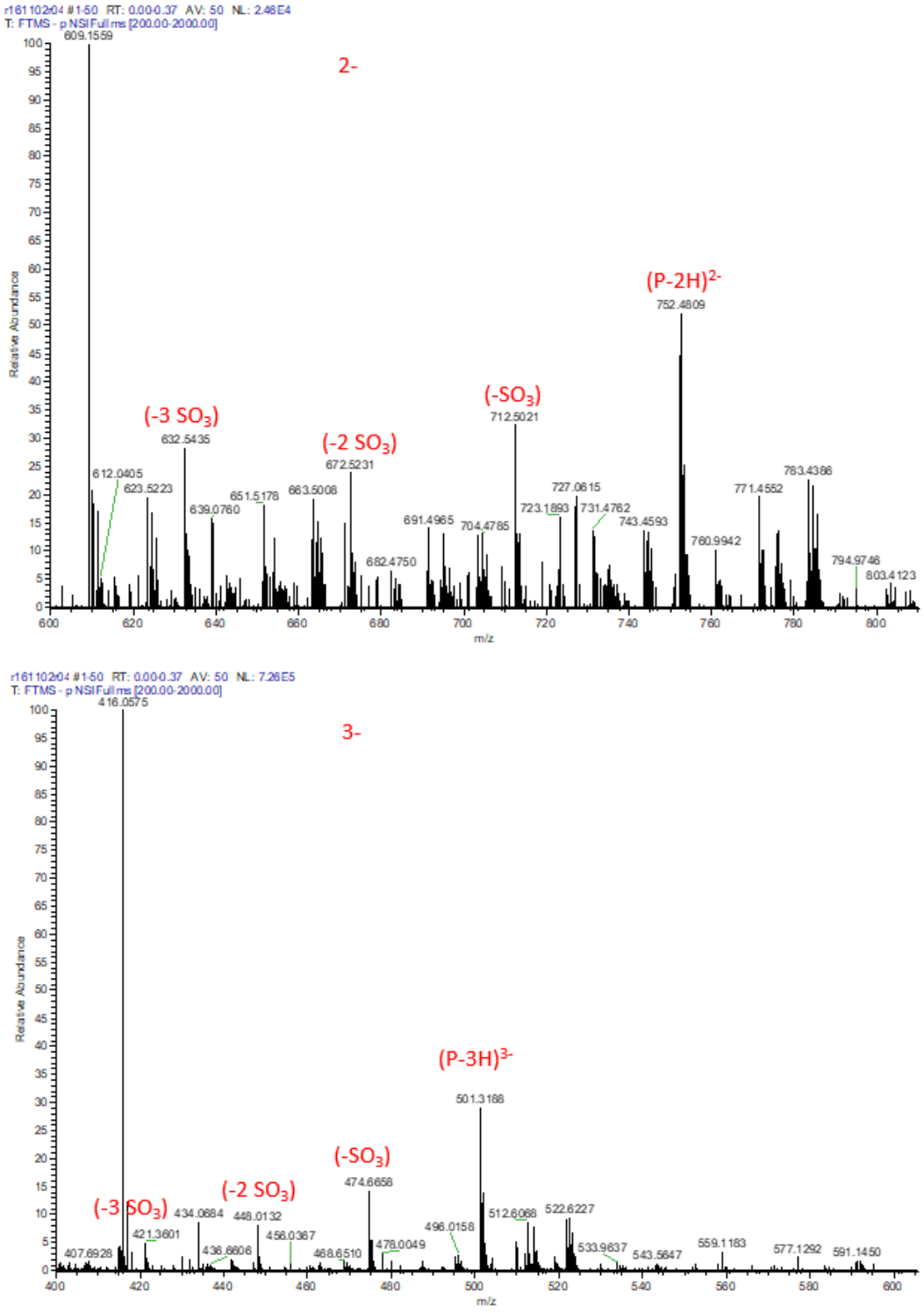


Figure 2.4. ESI-MS of Free FPX showing multiple charge states with sequential sulfate loss.



www.manaraa.com

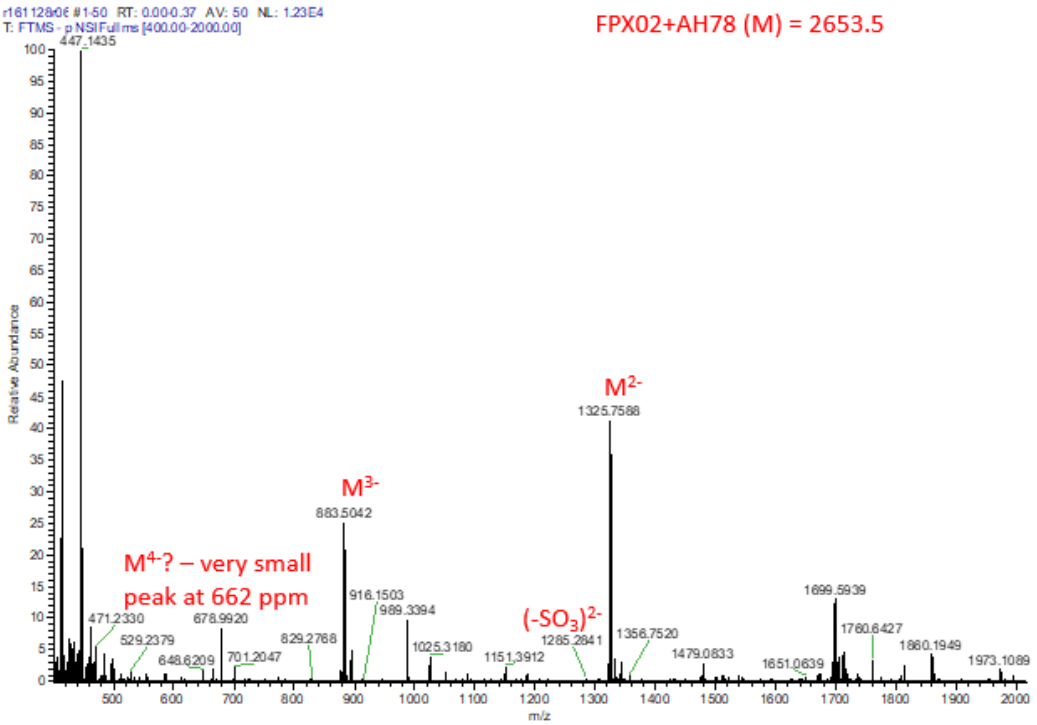


Figure 2.5. ESI-MS of FPX + AH78 showing multiple charge states with sulfate loss.

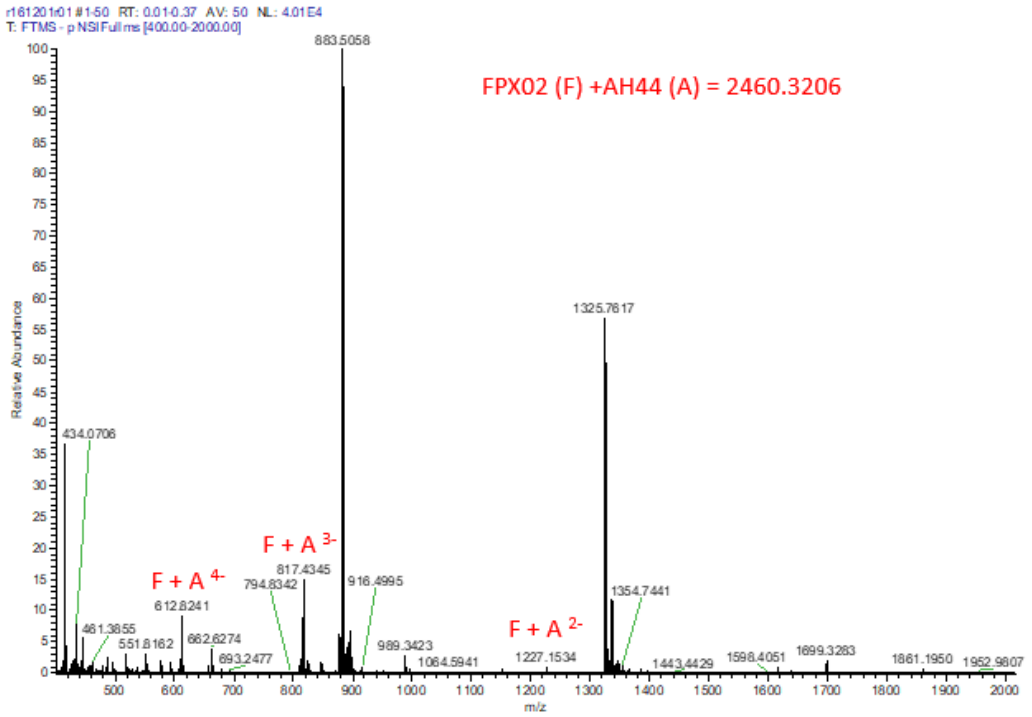


Figure 2.6. ESI-MS of FPX + AH44 showing multiple charge states with contamination of AH78 from previous runs.



www.manaraa.com

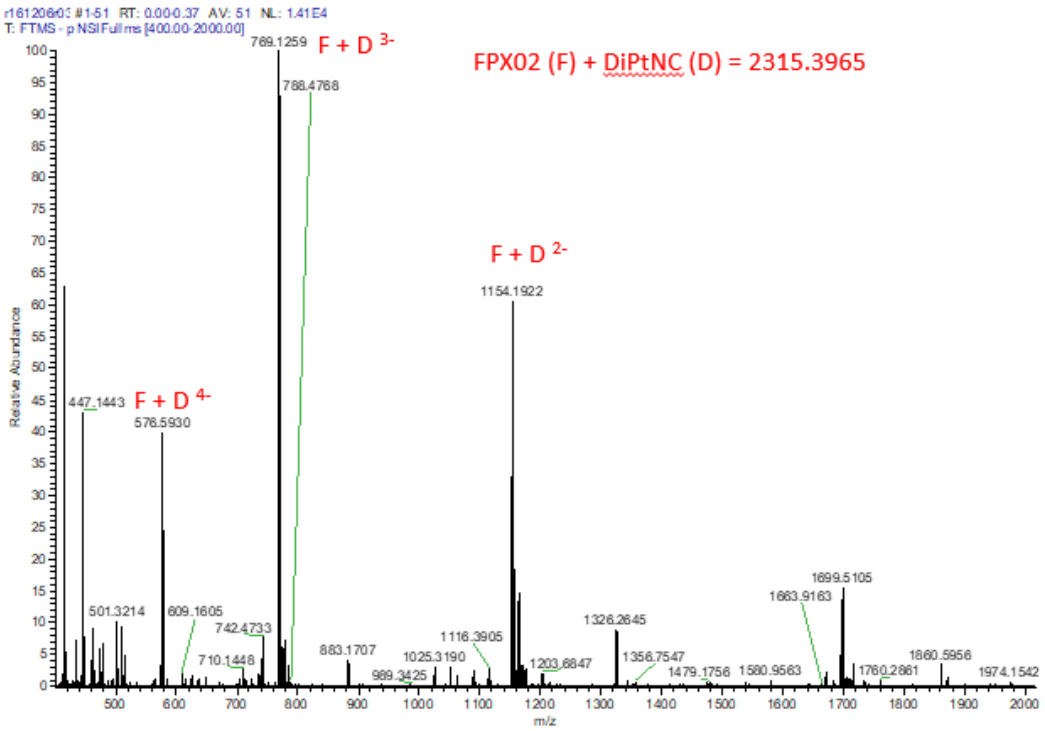


Figure 2.7. ESI-MS of FPX + DiPtNC showing multiple charge states.

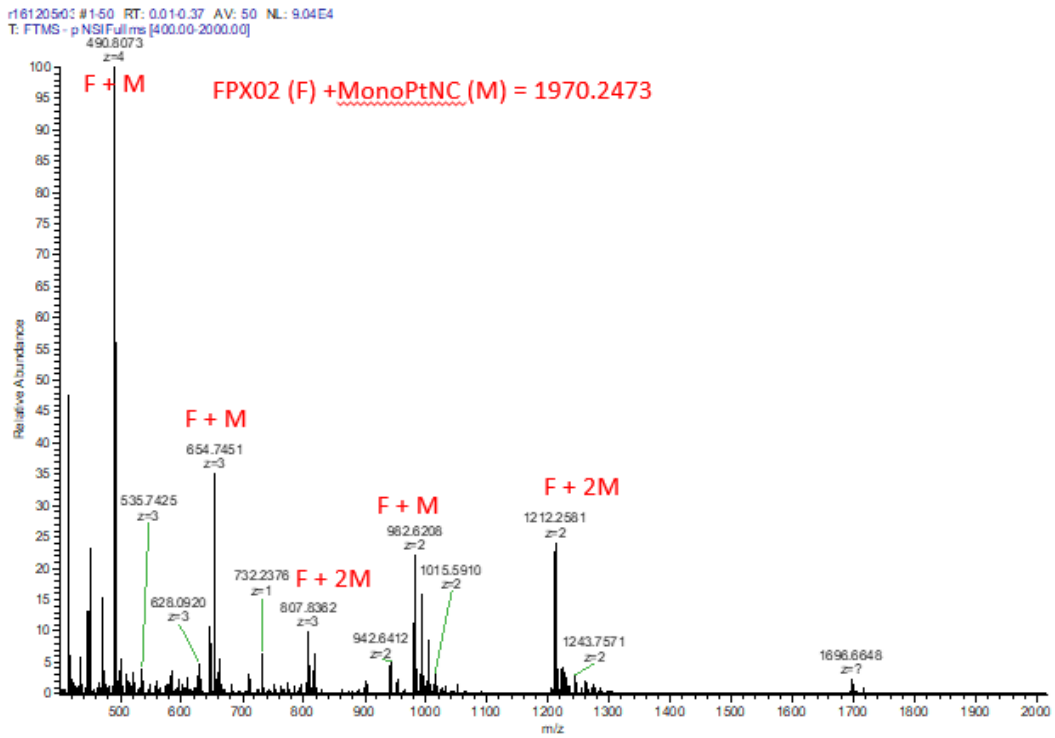


Figure 2.8. ESI-MS of FPX + MonoPtNC showing multiple charge states with sequential sulfate loss, and a 1:2 FPX:Pt binding stoichiometry.



www.manaraa.com

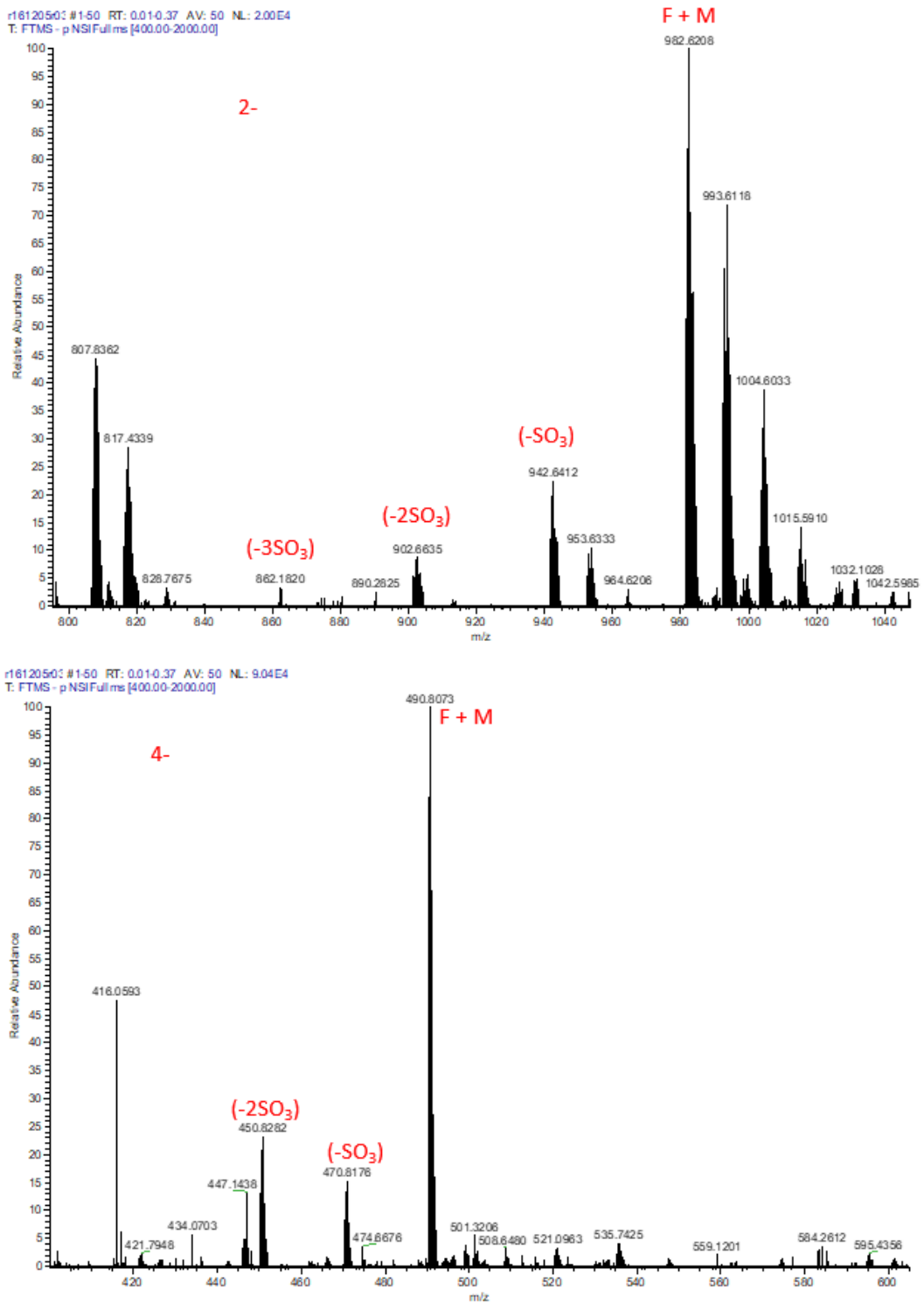


Figure 2.8. ESI-MS of FPX + MonoPtNC showing multiple charge states with sequential sulfate loss, and a 1:2 FPX:Pt binding stoichiometry.



www.manaraa.com

**DFT modelling of PPC–HS interactions**

DFT studies were performed to delineate the effect of structural differences of PPCs in their binding to various heparin fragments.(4) Interaction energies and comparison with individual phosphate and sulfate are given in Table 2.2. Based on the previously reported interactions of the heparin trimer with $[Pt(NH_3)_4]^{2+}$, and heparin hexamer with TriplatinNC,(4) we have now modelled the association of MonoplatinNC and DiplatinNC with a heparin tetramer [IdoA(2S)-Glc(NS)(6S)]$_2$, as well as the association of AH44 with the analogous heparin hexamer [IdoA(2S)- Glc(NS)(6S)]$_3$. As previously described,4 the model fragments were derived from the NMR- based structure PDB1HPN of the heparin dodecamer, comprising repeats of the disaccharide units.(14, 18) The interaction energies as measured by DFT increase in the order Pt-tetraammine < MonoplatinNC < DiplatinNC < AH44 < TriplatinNC.

The heparin tetramer–MonoplatinNC model was designed such that the carbon chain of one of the dangling amine groups stretched over the hydrophobic groove that is formed in the middle by the hydrocarbon rings of the tetramer. The *trans* geometry of the Pt coordination sphere in MonoplatinNC means that the other dangling amine is placed at the edge of the helix, with the free amine (- $CH_2NH_3^+$) interacting with *N*- sulfate of GlcNS(6S), which is in the middle of two IdoA(2S) residues. The optimised structure is shown in Figure 2.9 a. The hydrocarbon chain along the groove is seen to be involved in establishing van der Waals contact with hydrogen atoms from two of the sugar residues. Moreover, the chain stretches all the way to the other side of the helix, facilitating interaction of the free amine with *N*- sulfate and *O*- sulfate of terminal GlcNS(6S) and IdoA(2S) residues, respectively, and also with a carboxylate group of the middle IdoA(2S) residue. The interaction energy of the complex is −142 kcal mol$^{-1}$ and is almost three times that of the previously reported Pt- tetraammine- trimer interaction (Table 2.2).(4) The higher interaction energy of MonoplatinNC compared to that of the Pt- tetraammine again emphasises the importance of favourable interactions arising from the dangling amine ligands.

Based on the above structure, the interaction of DiplatinNC with heparin tetramer was designed by introducing the second Pt centre at the dangling amine that traverses the groove. The optimised



www.manaraa.com

| Fragment | Compound | Charge | $E_{int}$ in water (kcal mol$^{-1}$) |
|---|---|---|---|
| phosphate[a] | MonoplatinNC | 4+ | −4.2 |
| sulfate[a] | | | −1.2 |
| heparin trimer [a,b] | $[Pt(NH_3)_4]^{2+}$ | 2+ | −53 |
| heparin tetramer[c] | MonoplatinNC | 4+ | −142 |
| heparin tetramer[c] | DiplatinNC | 6+ | −171 |
| heparin hexamer[d] | AH44 | 6+ | −202 |
| heparin hexamer[a,d] | TriplatinNC | 8+ | −250 |

Table 2.2. Interaction energies of isolated phosphate and sulfate anions and heparin fragments with Pt coordination spheres in the PPC library (see Scheme **1**). [a] From Ref. **4**. [b] [GlcNS(6S)- IdoA(2S)-GlcNS(6S)]. [c] [IdoA(2S)- GlcNS(6S)]$_2$. [d] [IdoA(2S)- GlcNS(6S)]$_3$.



www.manaraa.com

structure of this interaction and the surface maps are shown in Figure 2.9 b. The second Pt centre forms H- bonds with the *N*- sulfate of the terminal GlcNS(6S), the carboxylate of the middle IdoA(2S) and *O*- sulfate of the terminal IdoA(2S) residues of the tetramer. The calculated interaction energy is −171 kcal $mol^{-1}$. The overlay of the optimised structures of the association complexes formed by the tetramer with MonoplatinNC and DiplatinNC and the free tetramer reveals the structural change that results following the interactions (Figure 2.10). It is noticeable that, compared to free tetramer, the outer rings have moved in towards the Pt complex to facilitate the interactions. MonoplatinNC induces more bending than DiplatinNC because the bulkier second Pt centre needs to be accommodated among the negatively charged sulfate groups of the terminal residues of the tetramer.

The structure of AH44 with hexamer reveals that the introduction of a third Pt centre, rather than the dangling ammine of DiplatinNC, results in strong cluster binding with three sulfate groups from terminal GlcNS(6S) and the central IdoA(2S) and GlcNS(6S) residues (Figure 2.9 c). The interaction energy of this model is −202 kcal $mol^{-1}$, which is greater than the interaction energies of MonoplatinNC and DiplatinNC models (Table 2.2), indicating the favourable interaction of the third Pt centre. For AH44, the hydrogen bonding cluster formation results in tighter binding compared with the cluster formation involving free amine (- $CH_2NH_3$) groups of DiplatinNC.

As shown in the surface maps (Figure 2.9), electrostatic and hydrophobic interactions facilitate the tight fit of PPCs with heparin fragments. Although the tetramer and hexamer sequences do not match exactly that of FPX, the observation of sulfate clusters involving the IdoA(2S) residue is consistent with the chemical shift changes observed and suggest that the Pt coordination spheres may reside close to this residue.

**Measurement of the FPX–PPC binding interaction**

The NMR studies of the FPX–PPC interaction show significant chemical shift changes indicative of strong binding, which is sufficient to inhibit cleavage of FPX by heparinase. To assess the strength of the noncovalent FPX–PPC interaction for the different compounds in the PPC library, two different competitive inhibition assays were developed (Figure 2.11 a). The first was based on



www.manaraa.com

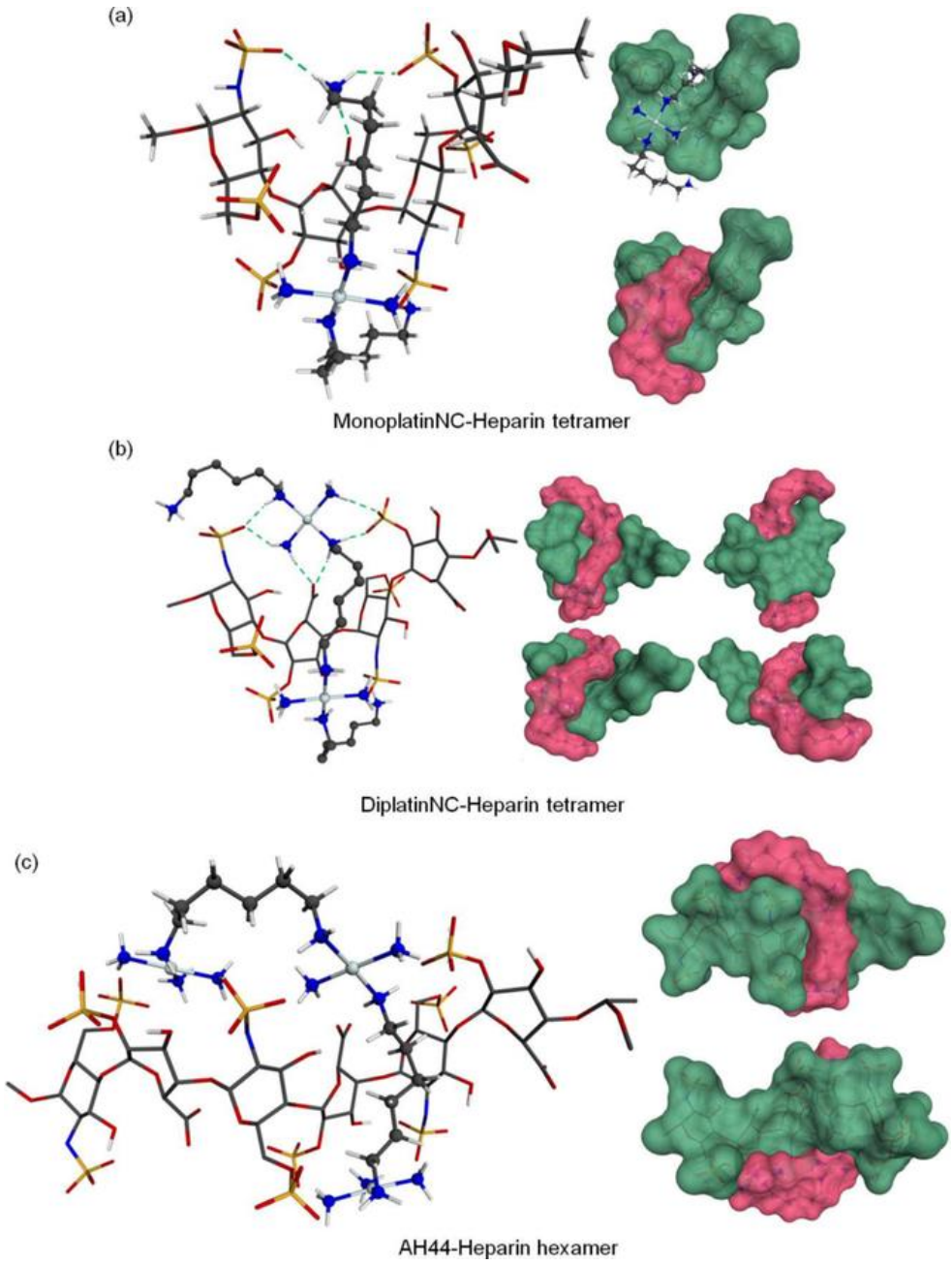


Figure 2.9. a) *Left*: Optimised structure of heparin tetramer (stick) interacting with MonoplatinNC (ball and stick): hydrogen bonding interactions of the free amine of the dangling amine are represented by green dashed lines. The favourable van der Waals interactions among the hydrogens can be inferred. *Right*: Solvent accessibility maps using a probe of 1.4 Å: These shows how well the Pt complex fits the pockets and grooves in heparin. b) *Left*: Optimised structure of heparin tetramer (stick) interacting with DiplatinNC (ball and stick): hydrogen bonding interactions of the second Pt centre are represented by green dashed lines. *Right*: Solvent accessibility maps using a probe of 1.4 Å: Top, bottom and side views show how well the Pt complex fits the pockets and grooves of the heparin unit. c) *Left*: Optimised structure of heparin hexamer (stick) interacting with AH44 (ball and stick). *Right*: Solvent accessibility maps using a probe of 1.4 Å: These maps show the relationship of AH44 (magenta) to the heparin hexamer (green).



www.manaraa.com

a spectroscopic investigation of the interaction of methylene blue (MB) with heparin and HS.(6, 19) The second measured the displacement of intercalated ethidium bromide (EtBr) from DNA, which is a useful assay to gauge the relative strengths of coordination compounds to oligosaccharides (heparin/HS) versus oligonucleotides (DNA/RNA).(4, 6) To confirm the direct strength of the FPX–PPC interactions, isothermal titration calorimetry (ITC) assays were also performed.

**Methylene blue reporter assay**

The cationic dye methylene blue (MB) has been used to quantify sulfate content on heparin.(19-22) The MB absorbance at 664 nm decreases proportionally with increasing heparin concentration, allowing the calculation of binding constants.(6, 19) The addition of increasing concentrations of FPX to a solution containing MB also resulted in the gradual decrease of MB absorbance (Figure 2.11 b, left). The association constant between MB and FPX was determined by the Scatchard plot and the value ($4.0\pm0.1\times10^4$ $M^{-1}$) is two orders of magnitude lower compared with the previously reported association constant between MB and the chondroitin sulfate (CS) polymer ($1.73\times10^6$ $M^{-1}$).(19) We then studied the effect of metalloshielding on the MB–FPX interaction by adding aliquots of MB to a solution containing FPX pre- incubated with varying concentrations of PPCs. PPCs are competitive inhibitors of the MB–FPX interaction, as evidenced by the higher absorbance of MB with increasing platinum complex concentration (Figure 2.11 b and Figure 2.12). The ability of PPCs to metalloshield FPX against MB binding may be reported as an $IC_{50}$ value, the concentration required to inhibit 50 % binding of MB to FPX. By using MB as a reporter, the apparent dissociation constant ($K_{d(app)}$) between PPCs and FPX may then be calculated. The results are shown in Table 2.3 and illustrate the systematic decrease in $IC_{50}$ with increase in positive charge. TriplatinNC, having the highest overall charge (8+), required the lowest concentration to inhibit 50 % of MB binding to FPX, and the lowest apparent dissociation constant. Slightly higher affinity was again also correlated with the number of Pt centres. Both AH44 and DiplatinNC have the same 6+ charge, but AH44 with one more Pt centre gave slightly lower $IC_{50}$ and $K_{d(app)}$ values.



www.manaraa.com

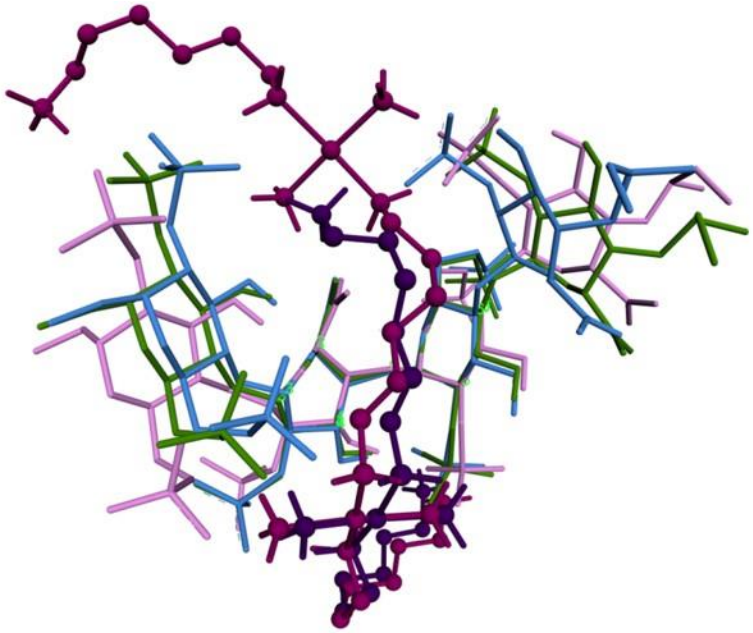

Figure 2.10. Overlay of optimized free heparin tetramer (pink), heparin tetramer (turquoise) in complex with MonoplatinNC (purple) and heparin tetramer (green) in complex with DiplatinNC (violet). The alignment was centred at the middle two rings.



www.manaraa.com

**Ethidium bromide (EtBr) reporter assay**

To compare the PPC–FPX interactions with the well- studied PPC–DNA interactions(5, 23, 24)an ethidium bromide (EtBr) competition assay was developed applying EtBr as the reporter.(4)This assay exploits the decrease in fluorescent properties when the intercalator is removed from DNA under the influence of DNA–PPC binding. Upon FPX addition to the EtBr–PPC–DNA system, the intercalator binds back to DNA as FPX sequesters the PPC (Figure 2.11 a).(4) The comparative binding of different PPCs for DNA and FPX was estimated based on the FPX concentrations required to sequester the PPC from DNA, thus allowing EtBr to intercalate, with a concomitant increase in its fluorescence. Given that the ability to displace EtBr from DNA differs amongst the complexes themselves, the concentration for any individual PPC required to produce an initial ≥50 % decrease in fluorescence was normalised as the modified EtBr–PPC–DNA fluorescence ([$PPC_d$]) and 100 % fluorescence was control EtBr–DNA. The data are presented in the form of an $EC_{50}$ value, which reflects the concentration of FPX, [$FPX_r$], required to restore EtBr fluorescence to 50 % of the control EtBr–DNA sample in the absence of either PPC or FPX (Figure 2.11 c and Table 2.3). Note that FPX has no effect on EtBr–DNA fluorescence. This allows a discussion of the $EC_{50}$ as a ratio index of [$PPC_d$]/[$FPX_r$] (Table 2.3). The ratio index suggests that above 1, PPCs have more affinity for FPX than DNA, whereas below 1 PPCs have more affinity for DNA than FPX. Thus, AH44 has similar affinities for DNA as FPX, with ratio index of 0.97, while MonoplatinNC, DiplatinNC, and TriplatinNC all had slightly higher affinities for FPX than DNA. $[Pt(NH_3)_4]^{2+}$ has a very high ratio index but this reflects its very weak binding to DNA(25) and thus was eliminated from the comparison of strongly binding DNA compounds (Figure 2.13).

**Isothermal titration calorimetry (ITC)**

ITC assays were performed to determine the binding constants between FPX and different PPCs. Hydrogen bonding and electrostatic interactions contribute to the enthalpy term, whereas changes in conformational freedom and solvation upon complex formation contribute to the entropy term.(26, 27) The entropic term reflects the desolvation as a principal contributor.(27) Figure



www.manaraa.com

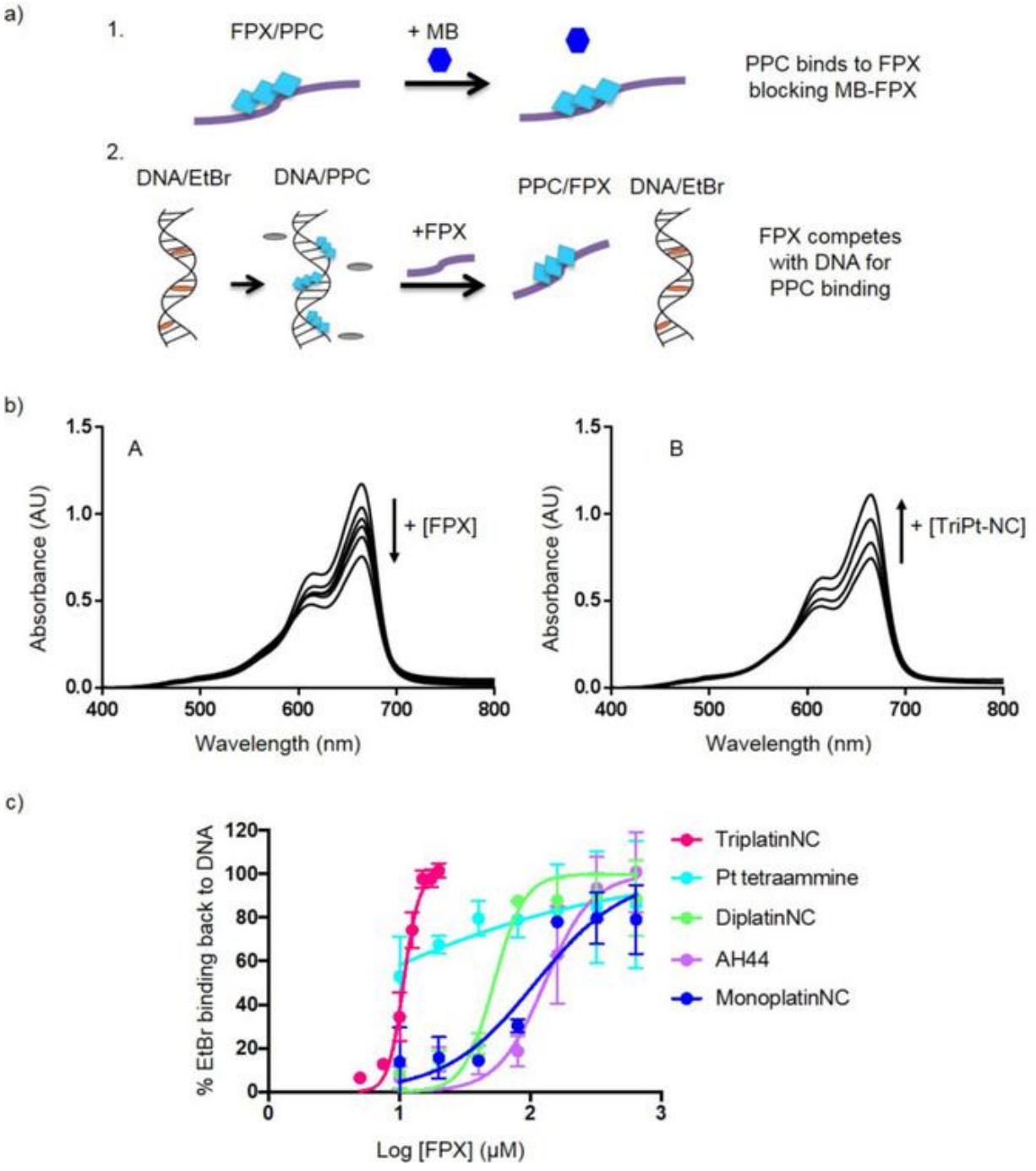


Figure 2.11. PPC–HS binding interaction as measured by EtBr and methylene blue (MB) reporter assays. a) Schematic representation of PPC competitive inhibition of MB binding to FPX and sequestering of DNA bound PPC by FPX. b) A; absorption spectra of a mixture of MB (18.6 μM) and FPX. The concentrations of FPX (from top to bottom at 664 nm) were as follows: 0, 1, 2, 3, 5, 10, and 15 μM. B; absorption spectra of a mixture of MB (18.6 μM), FPX (15 μM), and TriplatinNC. The concentrations of TriplatinNC (from above to bottom at 664 nm) were as follows: 14, 10, 5, and 0.5 μM. c) Curve graph for the $EC_{50}$ values measured by EtBr reporter assay showing the preference of PPCs for FPX, samples were normalised to the controls (no FPX as 0 % and EtBr–DNA as 100 %). TriplatinNC data was taken from Ref. **4**.



www.manaraa.com

2.14 shows the ITC analysis by direct titration for the binding of FPX to TriplatinNC, with similar plots for other compounds from the PPC library shown in Figure 2.14. The derived dissociation constants are given in Table 2.4 and the derived thermodynamic binding parameters are given in Table 2.4. The PPCs follow the same trend seen in the MB assay. The dissociation constants again show the same charge- dependency with the $K_d$ value for TriplatinNC approximately three orders of magnitude higher than that of $[Pt(NH_3)_4]^{2+}$ and AH44 having slightly greater affinity than DiplatinNC. Few ligand–heparin(HS) data have been reported. ITC has been used in heparin-growth factor interaction assays and in defining the thermodynamic parameters obtained from these interactions. The $K_d$ of a synthetic hexasaccharide with a homogeneous sulfation pattern interacting with FGF1 and FGF2 gave values of 54 to 855 nM, respectively.(28) On the other hand, a mixture of heterogeneous heparin chains showed a $K_d$ of 1.1 to 3 μM for interaction with FGF-1.(29, 30) Considering the $K_d$ for FPX–TriplatinNC from Table 2.4 as approximately 40 nM (0.4 μM), the strength of this interaction is broadly similar to that seen for FGF–oligosaccharide interactions.

**Summary**

Indirect and direct assays give an estimate of the strength of the FPX–PPC interaction. The set of assays developed give an estimate of strength of binding and relative FPX(HS)/DNA affinities. Given clear variations in the quantitation of dissociation constants, care should be taken in extrapolating across the assays discussed due to the inherent differences in the nature of these assays. Thus, whereas ITC is a "two- body" system, the MB and EtBr competition assays become "three- body and four- body" systems, respectively, and are consequently more difficult to interpret. Nevertheless, the trends are consistent within each assay and strongly reflect a charge dependence. In general, we suggest that use of complementary assays in this manner should be encouraged to provide an overall picture of the metal complex–heparin(HS) interaction.(13)

**Correlation of FPX binding with HSPG- mediated cellular accumulation of PPCs**

The nature of the PPC–FPX interactions may also be relevant in considering the molecular details of PPC cellular accumulation mediated by HS proteoglycans. Polyarginine cellular uptake is



www.manaraa.com

| Compound | MB assay[a] | | ITC assay[b] | EtBr assay[c] | |
|---|---|---|---|---|---|
| | $IC_{50}$ (μM) | $K_{d(app)}$ (μM) | $K_d$ (μM) | $EC_{50}$ (μM)[d] | Ratio index[e] |
| $[Pt(NH_3)_4]^{2+}$ | 64±8 | 30±4 | 40±13 | NA | NA |
| MonoplatinNC | 25.5±0.5 | 12.1±0.3 | 14±1 | 108.90 | 1.15 |
| DiplatinNC | 16.6±0.4 | 7.9±0.2 | 3.4±0.9 | 52.60 | 1.19 |
| AH44 | 13.5±0.5 | 6.4±0.2 | 0.95±0.2 | 128.30 | 0.97 |
| TriplatinNC | 10.2±0.4 | 4.8±0.2 | 0.04±0.01 | 10.74 | 1.17 |

Table 2.3. FPX–PPC dissociation constants as measured by methylene blue (MB), ethidium bromide (EtBr) reporter assays and isothermal titration calorimetry (ITC).
[a] MB $IC_{50}$ indicates PPC concentration required to competitively inhibit 50 % of the MB dye from binding to FPX. Association constants were calculated from the MB assay for PPCs binding to FPX using a two ligand- one binding site Scatchard model. [b] ITC analysis reported in Table S1. [c] TriplatinNC data was taken from Ref. **4**. [d] $EC_{50}$ is the concentration of FPX required to restore EtBr–DNA fluorescence, and was calculated from the normalisation of 0 μM FPX as 0 % and DNA–EtBr only as 100 %. [e] Ratio index calculated from the $[PPC_d]/[FPX_r]$ where $[PPC_d]$ is the concentration required to produce an initial <50 % decrease in fluorescence and $[FPX_r]$ is the concentration required to restore EtBr fluorescence to 50 % of the control EtBr–DNA sample in absence of either PPC or FPX (see text).



www.manaraa.com

mediated by cell surface heparan sulfate proteoglycans (HSPGs).(31, 32) The conceptualization of PPCs as "polyarginine mimics" led to the inhibition of the HSPG- mediated cellular internalisation and nucleolar localization of the fluorescent- labelled nona- arginine peptide (TAMRA- $R_9$) and identification of HSPGs as receptors for PPC cellular internalisation.(33, 34) In contrast to the mononuclear clinical platinum agents such as cisplatin and oxaliplatin, PPCs uniquely utilise this internalisation mechanism, which could provide an approach for selective uptake into tumours with high levels of HSPGs.(34, 35)

TAMRA- $R_9$ entry into human colorectal carcinoma (HCT 116) cells was examined in the presence of different PPCs, which prevented cell entry of the peptide in a charge- dependent manner (Figure 2.15 a). A complete inhibition of TAMRA- $R_9$ fluorescence was observed in the cells containing TetraplatinNC (10+) and TriplatinNC (8+), whereas the lesser- charged analogues AH44 (6+) and DiplatinNC (6+) reduced the fluorescence somewhat. MonoplatinNC (4+) failed to reduce any fluorescence. Differential accumulation of PPCs into wild type CHO- $K_1$ and mutant CHO- 745 (lacking HS and CS) confirmed the proteoglycan mediation (Figure 2.16).

The relative cellular accumulation of the PPC library in HCT 116 cells suggest the involvement of dangling amine- dependent and size- dependent mechanisms (Figure 2.15 b). TriplatinNC′s higher cellular accumulation compared with AH44 is consistent with previous results.(34, 36) DiplatinNC, TriplatinNC, and TetraplatinNC showed similar cellular accumulation, even though their overall charges ranged from 6+ to 10+, suggesting an influence of the dangling amine. There is no strict correlation between TAMRA- $R_9$ inhibition and cellular accumulation—as evidenced in the comparison between DiplatinNC and AH44 (Figure 2.15 a and b). Likewise, although MonoplatinNC failed to inhibit TAMRA- $R_9$internalisation, it showed the highest cellular accumulation compared with the other PPCs, and showed higher accumulation into wildtype compared with mutant CHO cells (Figure 2.S7). The smaller size may allow it to use multiple entry pathways including a size- dependent one.(37, 38) Small mononuclear platinum drugs like cisplatin, carboplatin, and oxaliplatin reportedly use the hCTR1 copper influx transporter for cell entry.(39) Furthermore, the cellular accumulation and cytotoxicity of the



www.manaraa.com

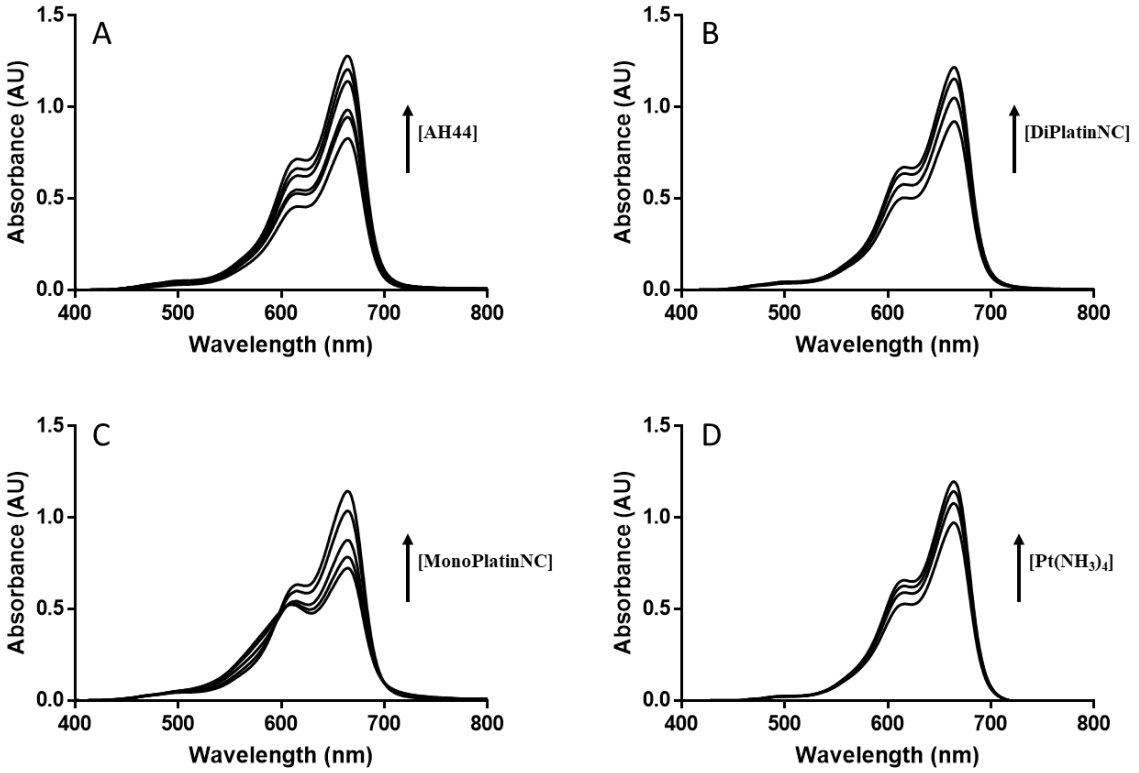


Figure 2.12. Absorption spectra of a mixture of MB (18.6 µM), FPX (15 µM), and PPCs. A) The concentrations of [AH44] (from above to bottom at 664 nm) were as follows: 30, 20, 15, 12, 6, and 1 µM; B) The concentrations of [DiplatinNC] (from above to bottom at 664 nm) were as follows: 30, 20, 15, and 10 µM; C) The concentrations of [MonoplatinNC] (from above to bottom at 664 nm) were as follows: 50, 30, 20, 10, and 1 µM; D) The concentrations of $[Pt(NH_3)_4]^{2+}$ (from above to bottom at 664 nm) were as follows: 250, 100, 50, and 20 µM. Charges omitted for clarity.

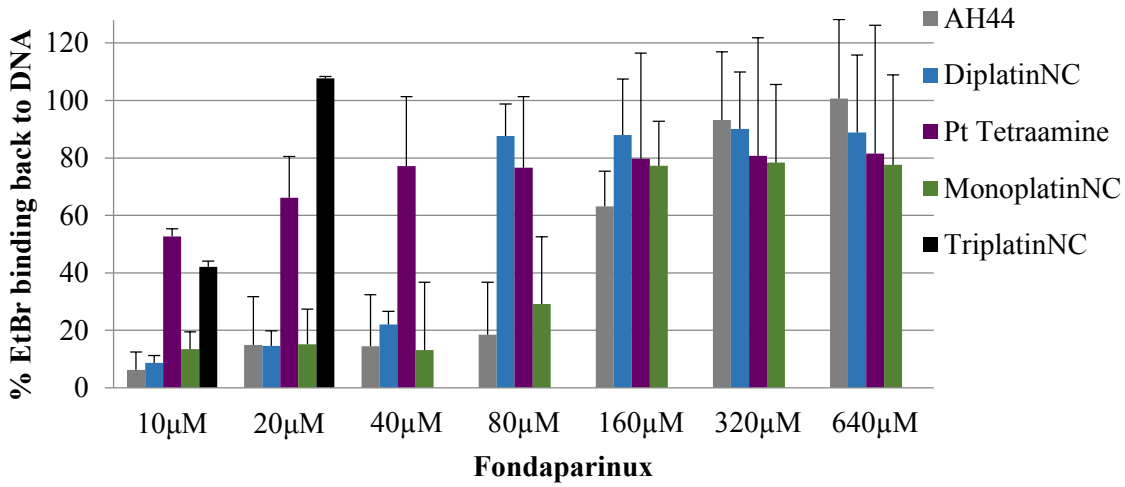


Figure 2.13. Competitive inhibition of PPC-DNA binding by FPX as measured by EtBr reporter assay with 12.5 µM EtBr, 10µM ct-DNA and PPC (12.5µM TriplatinNC, 125µM AH44, 62.5µM DiplatinNC, 125µM MonoplatinNC and 500µM Pt tetraammine) were incubated for 1h and then increasing concentrations of FPX from 10-640µM were added and incubated again for an another 1h and read at 530/590 nm.



www.manaraa.com

covalently binding Triplatin (BBR3464) is also affected by copper status.(40 The relative cytotoxicity of the PPC library in HCT 116 cells was investigated using MTT viability assays (Figure 2.15 c). The PPC cytotoxicity was unpredictably related to their cellular uptake (Table 2.5).

**Summary**

This section extrapolated the enzyme inhibition and biophysical studies of the FPX–PPC interaction to correlate with HSPG- mediated PPC cellular accumulation, considering FPX as a small but well- defined HS model.(6, 34) Although there is clear evidence of proteoglycan mediation for this class of molecules, there is no strict correlation with cellular accumulation. In general, while HSPGs clearly affect cellular internalisation, the results emphasise that multiple complementary pathways exist for small molecule internalisation and, for platinum complexes, no single pathway is "all or nothing".(36-38) The proteoglycan mediation is unique to the PPC class and, coupled with the overexpression of glycans on many tumour cell surfaces,(1, 35) the results do suggest potential avenues for tumour selectivity of PPC agents based on differential uptake.

## 2.4 Conclusions:

The results presented in this study demonstrate that the library of PPC complexes, with the exception of the mononuclear $[Pt(NH_3)_4]^{2+}$, completely inhibits cleavage of the model HS substrate (FPX) by the bacterial *P. heparinus* heparinase II enzyme. Combined with previous results using both bacterial heparinase I and human heparanase,(3, 4) PPCs are a structurally distinct class of broad- spectrum heparanase cleavage inhibitors acting through metalloshielding. Oligosaccharide mimetics have been widely studied for their ability to act as inhibitors of the heparanase enzyme, and a number have entered clinical trials.(41, 42)Metalloshielding is an attractive alternative to design of heparanase inhibitors and indeed the Phase I and Phase II clinical results of Triplatin could be reinterpreted in light of these new glycan- related findings.(5, 13)



www.manaraa.com

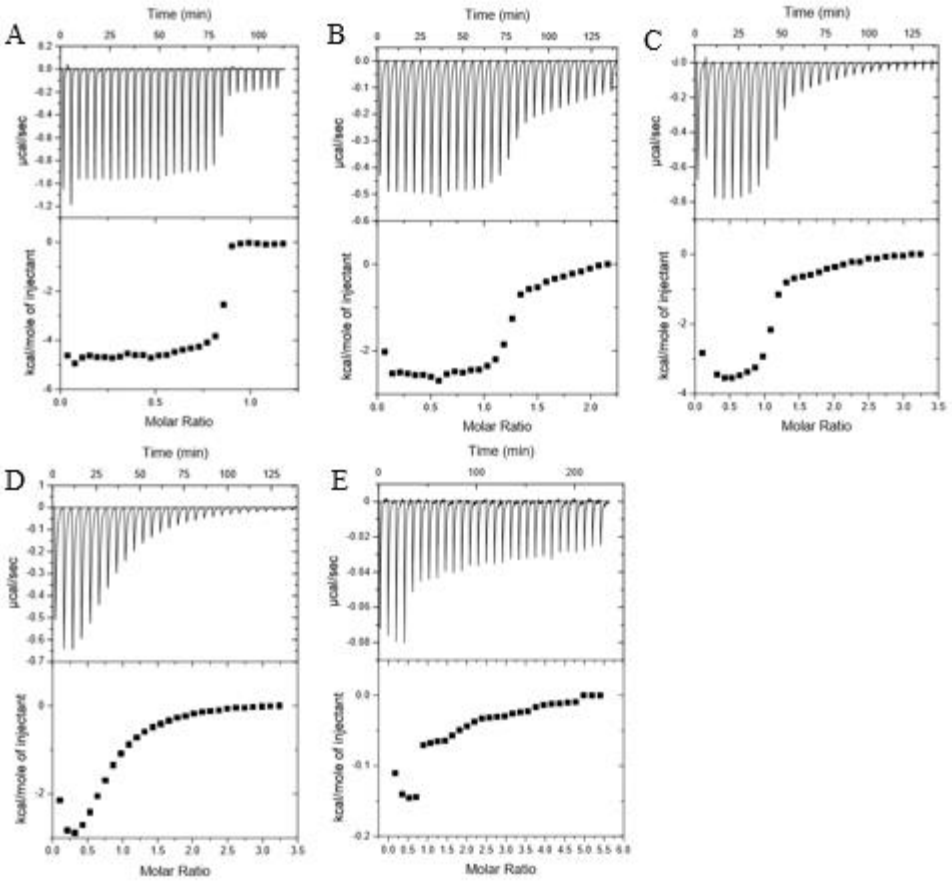


Figure 2.14. ITC analysis of FPX by direct titration of A) [TriPlatinNC], B) [AH44], C) [DiPlatinNC], D) [MonoPlatinNC], and E) $[Pt(NH3)_4]^{2+}$. A trace of calorimetric titration (upper panel) and integrated isotherms (lower panel). The first peak represents a pre-injection that was omitted in the binding calculations.



www.manaraa.com

The focused small library studied here begins to elucidate structure–activity relationships. The stark contrast between $[Pt(NH_3)_4]^{2+}$ and MonoplatinNC in inhibiting the HS cleavage emphasises the importance of dangling amine moieties as well as increased charge dispersion. The relative efficacy of the polynuclear set again shows that positive charge dispersion through dangling amines and Pt coordination spheres play important roles in masking the HS fragments and protecting them against enzymatic cleavage. The ability to form a "sulfate clamp" from the interaction of am(m)ines in a Pt coordination unit are a priori likely to be more effective in masking than the single positive charge of the dangling amine—nevertheless the two structural features do contribute to the overall effect.

As part of our approach to metalloglycomics, we have developed direct and indirect assays to study the nature and strength of "noncovalent" interactions on the biomolecule.(6, 13)Consistent trends emerge—affinity is related to charge and in general these substitution- inert complexes show broadly similar affinity to FPX and DNA. Heparin is often considered as having higher negative charge density compared with that of polyanionic DNA, with an average negative charge of 2.7 per disaccharide compared to that of two negative charges per base pair for DNA.(7)

In this latter aspect, at least for substitution- inert complexes, the approaches to inhibition of HS or DNA function are formally analogous—both protect the "substrate" from enzyme and/or protein processing. High- affinity DNA binding through the phosphate clamp efficiently inhibits transcription factors such as TBP (TATA box binding proteins) and restriction enzymes.(5, 23, 33) The $K_d$ values found for PPC–FPX interactions are broadly similar to those found for growth factor–oligosaccharide interactions.(28-30) This suggests that metalloshielding will also be effective in inhibition of oligosaccharide- protein function as shown for the effect of TriplatinNC on FGF- heparin interactions.(4) Overall, the results demonstrate the utility of the metalloglycomics concept in developing new classes of molecules for study of glycan structure and function. It is clear that oligosaccharides represent a viable alternative cellular target to oligonucleotides and the results further emphasise the unique dual- function nature of the PPC series compared with the mononuclear clinical agents.



www.manaraa.com

| Complex | ITC | | | |
|---|---|---|---|---|
| | $K_d$ | ΔG [c] (kJ mol$^{-1}$) | ΔH (kJ mol$^{-1}$) | TΔS (kJ mol$^{-1}$) |
| Pt-tetraammine | 40.3 ± 13.0 [a] | -0.65 ± 0.01 | -0.16 ± 0.03 | 0.49 |
| MonoplatinNC | 13.9 ± 1.24 [a] | -6.62 ± 0.20 | -3.83 ± 0.11 | 2.79 |
| DiplatinNC | 3.40 ± 0.89 [a] | -7.45 ± 0.28 | -3.97 ± 0.15 | 3.49 |
| AH44 | 0.943 ± 0.18 [a] | -8.21 ± 0.12 | -2.63 ± 0.04 | 5.58 |
| TriplatinNC | 35.7 ± 15.3 [b] | -10.15 ± 1.11 | -4.63 ± 0.05 | 5.52 |

Table 2.4. ITC analysis showing the obtained binding parameters: dissociation constants ($K_d$); free energy of binding (ΔG); enthalpy of binding (ΔH); and entropy of binding (-TΔS) between PPCs and FPX, best fit to a one site model. The standard error from 3 measurements is indicated.
[a] $K_d$ measured in µM
[b] $K_d$ measured in nM
[c] Gibbs Free Energy calculated from the enthalpy and entropy of binding



www.manaraa.com

## 2.5 Experimental Section:

Synthesis and materials

$[Pt(NH_3)_4]Cl_2$ was prepared by published methods.(43) TriplatinNC and AH44 (as nitrate salts) were prepared as described previously.(23, 24) Fondaparinux (GlcNS(6S)- GlcA- GlcNS(3S)(6S)- IdoA(2S)- GlcNS(6S)- OMe) was sourced from Sigma–Aldrich.

Synthesis of new compounds

**MonoplatinNC**: A mixture of *trans*- diamminedichloro- platinum (1 mmol) and $AgNO_3$ (1.98 mmol) in anhydrous DMF (18 mL) was stirred overnight with protection from light, and AgCl was then filtered off. A solution of the mono- Boc- 1,6- hexanediamine (2.2 mmol) in anhydrous DMF (2 mL) was added to the filtrate. The mixture was stirred for three days at ambient temperature, protected from light. The solvent was then removed under reduced pressure and the residue was dissolved in $H_2O$ (100 mL) at 50 °C and filtered through a membrane filter to remove any reduced silver and platinum. The filtrate was evaporated to dryness and the residue was suspended in 0.5 M $HNO_3$ (25 mL) and stirred for two days at room temperature. The mixture was filtered through Celite to remove any unreacted starting materials and reduced silver/platinum. The volume of the filtrate was reduced to almost dryness and acetone was added to force the precipitation of the product. The formed precipitate (92.3 % yield) was filtered off then washed with acetone and dried under vacuum. $^1$H NMR (300 MHz, $D_2O$): $\delta$=3.00 (t, $J$=6.6 Hz, 4H 4 H), 2.67 (t, $J$=7.2 Hz 4 H), 1.67 (m, 8 H), 1.39 ppm (m, 8 H); $^{195}$Pt NMR (300 MHz $D_2O$): $\delta$=−2658 ppm; elemental analysis calcd (%) for $C_{12}H_{40}N_{10}O_{12}Pt$: C 20.25, H 5.67, N 19.68; found: C 20.20; H 5.54; N 19.44.

**DiplatinNC- Boc**: The nitrate salt of $[\{trans\text{-}\ PtCl(NH_3)_2\}_2\{\mu\text{-}\ H_2N(CH_2)_6NH_2\}]^{2+}$ (1,1/*t*,*t*) was synthesised from *trans*- diamminedichloroplatinum as previously reported.(44) To 1,1/*t*,*t* (1 mmol) dissolved in DMF (50 mL), $AgNO_3$ (1.98 equiv) was added. The reaction was protected from light and stirred for 16 h, then AgCl was removed by filtering through Celite. Mono- Boc- 1,6- hexanediamine (2.2 equiv) was added to the filtrate and the reaction was stirred for two days



www.manaraa.com

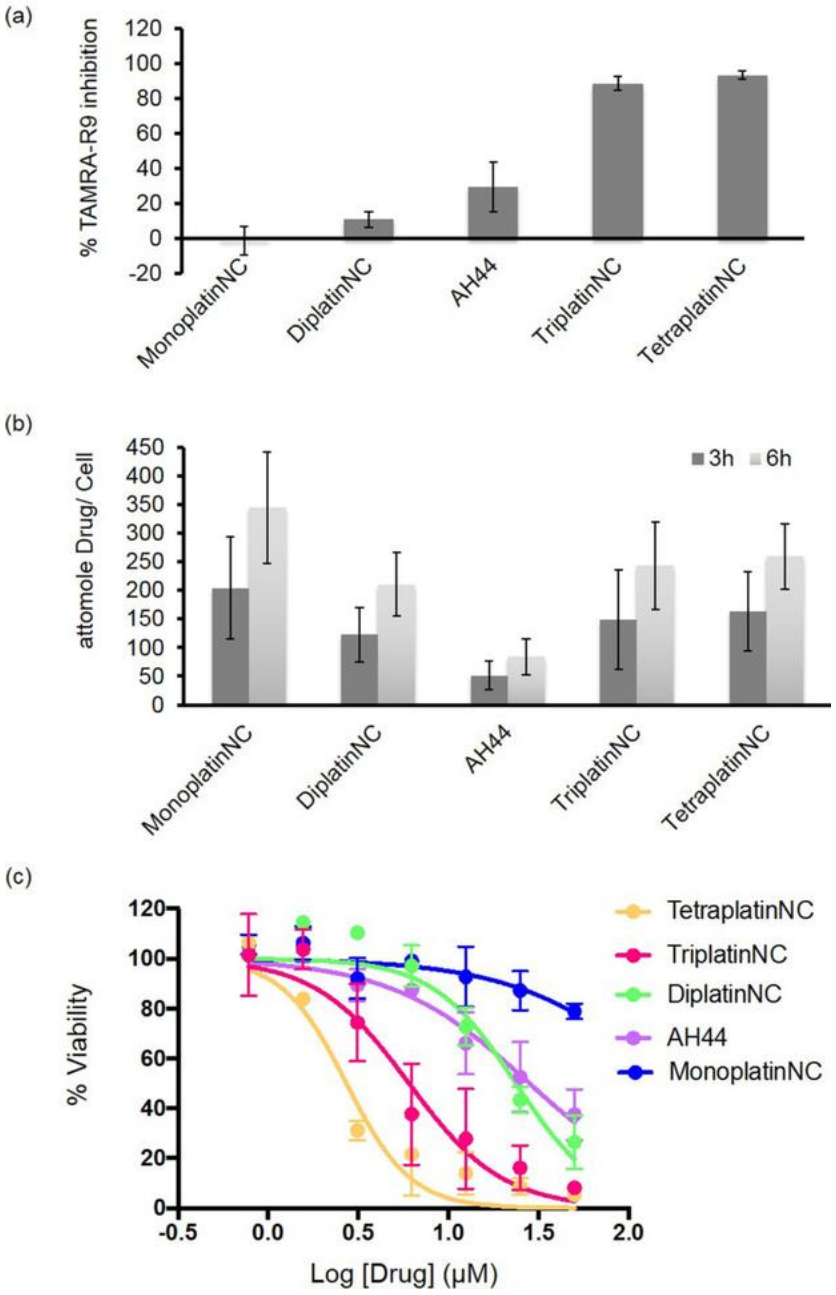


Figure 2.15. An evaluation of PPCs cell uptake, accumulation, and overall cytotoxicity in colorectal carcinomas cells (HCT 116). a) PPCs (10 μM) competition with TAMRA- $R_9$(1 μM) uptake was compared by the presence of fluorescence dye using flow cytometry. b) Cellular accumulation of PPCs (10 μM) at 3 and 6 h prior to collection was analysed using ICP- MS for Pt content. Pt readings were normalised to cell number and number of Pt- centres for each compound. c) MTT assays were employed to determine overall cytotoxicity of PPCs for a 72 h compound incubation.



www.manaraa.com

at room temperature. The solution was evaporated to dryness under reduced pressure and the residue was dissolved in $H_2O$ (100 mL) at 60 °C and filtered through Celite to remove any reduced platinum and silver. The filtrate was evaporated to dryness and acetone was added to precipitate the product. The precipitate was collected through filtration then washed with acetone and dried under vacuum to obtain the product (64 % yield). $^1$H NMR (300 MHz, $D_2O$): $\delta$=3.05 (t, $J$=9.0 Hz 4 H), 2.65 (m, 8 H), 1.60 (m, 12 H), 1.40 ppm (m, 30 H).

**DiplatinNC**: DiplatinNC- Boc (0.1 mmol) was suspended in 0.1 M $HNO_3$ (25 mL) and stirred for four days at 50 °C, at which time the suspension had turned into a clear almost colourless solution. Completion of Boc- deprotection was confirmed by $^1$H NMR spectroscopic analysis. The solution was filtered through Celite to remove any unreacted starting material. The filtrate was evaporated to almost dryness and acetone was added to force the precipitation of the product. The residue was collected through filtration and washed with methanol and acetone. The crude product (yield 93 %) was recrystallised in water. $^1$H NMR (600 MHz, $D_2O$): $\delta$=3.00 (t, $J$=9.9 Hz 4 H), 2.65 (m, 8 H), 1.65 (m, 12 H), 1.37 ppm (m, 12 H); $^{195}$Pt NMR (600 MHz, $D_2O$): $\delta$=−2651 ppm; elemental analysis calcd (%) for $C_{18}H_{62}N_{16}O_{18}Pt_2$: C 18.31, H 5.29, N 18.98; found: C 18.51, H 5.27, N 18.47.

**Tetraplatin**: A mixture of *trans*- diamminedichloroplatinum (2.2 mmol) and $AgNO_3$ (1.1 mmol) in anhydrous DMF (18 mL) was stirred overnight at −20° C in the dark to produce, upon warming to room temperature and filtration, mono- activated transplatin. This solution was then added to a mixture of DiplatinNC (1 mmol) and *N*,*N*- diisopropylethylamine (DIPEA) (2.2 mmol) in DMF (20 mL). The reaction mixture was stirred for two days at ambient temperature. The solution was then evaporated to dryness under reduced pressure. The residue was dissolved in a minimum amount of $H_2O$ and filtered through a syringe filter to remove any unreacted starting materials. The filtrate was then evaporated to ca. 1 mL under reduced pressure and acetone (25 mL) was added to precipitate the product. The precipitate (46 % yield) was collected through filtration, washed with acetone and dried under vacuum. $^1$H NMR (300 MHz, $D_2O$): $\delta$=2.62 (m, 12 H), 1.61 (m, 12 H), 1.13 ppm (m, 12 H); $^{195}$Pt NMR (300 MHz, $D_2O$): $\delta$=−2405, −2663 ppm; elemental



www.manaraa.com

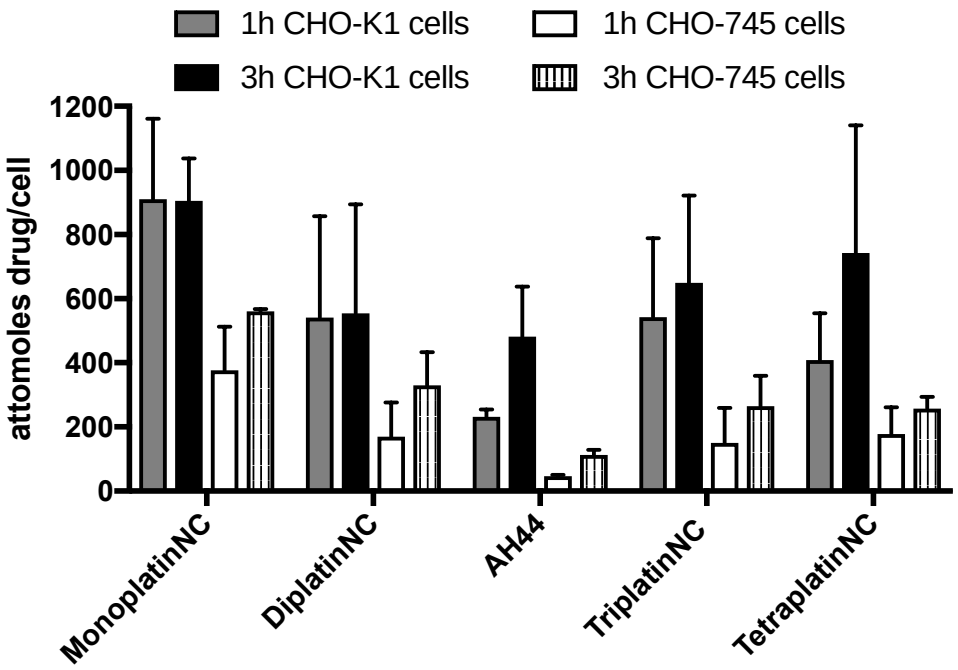


Figure 2.16. Cellular accumulation of PPCs in wt (CHO K1) and mutant CHO-pgsA-745 cells (lack of both heparan sulfate and chondrotin sulfate). Platinum complexes were incubated for 1 and 3 hours prior to cell collection for Pt detection on ICP-MS. Pt readings were normalized to cell number and number of Pt-centers per compound. See Materials and Methods.

| Compound | $IC_{50}$ (μM) | Charge |
|---|---|---|
| MonoplatinNC | >50 | 4+ |
| DiplatinNC | 24±5 | 6+ |
| AH44 | 30±13 | 6+ |
| TriplatinNC | 7±4 | 8+ |
| TetraplatinNC | 3.0±0.7 | 10+ |

Table 2.5. Cytotoxicity of noncovalent PPCs in HCT116 cells (*n*=2).



www.manaraa.com

analysis calcd (%) for $C_{18}H_{72}Cl_2N_{20}O_{18}Pt_4$: C 12.66; H 4.25; N 16.40; found: C 13.04; H 4.20; N 16.36.

**TetraplatinNC**: To Tetraplatin (1 mmol) dissolved in DMF (20 mL), $AgNO_3$ (1.98 equiv) was added. The reaction was protected from light and stirred for 16 h, then AgCl formed during the reaction was removed by filtering through Celite. Mono- Boc- 1,6- hexanediamine (2.2 equiv) was added to the filtrate and the mixture was stirred for two days at room temperature. The solution was evaporated to dryness under reduced pressure and the residue was dissolved in $H_2O$ (100 mL) at 60 °C and filtered through Celite to remove any reduced platinum and silver. The filtrate was evaporated to dryness. The residue was suspended in 0.1 M $HNO_3$ (25 mL) and stirred for four days at 50 °C, at which time the suspension had turned into a clear almost colourless solution. Completion of Boc- deprotection was confirmed by $^1$H NMR spectroscopic analysis. The solution was filtered through Celite to remove any unreacted starting material. The filtrate was evaporated to almost dryness and acetone was added to force the precipitation of the product. The residue was collected through filtration and washed with methanol and acetone. The crude product (yield 84 %) was recrystallised in water. $^1$H NMR (300 MHz, $D_2O$): $\delta$=2.95 (t, $J$=8.4 Hz 4 H), 2.62 (m, 16 H), 1.61 (m, 20 H), 1.35 ppm (m, 20 H); $^{195}$Pt NMR ($D_2O$): $\delta$=−2652 ppm; elemental analysis calcd (%) for $C_{30}H_{106}N_{28}O_{30}Pt_4$: C 17.00; H 5.04; N 18.50; found: C 17.27; H 5.02; N 18.21.

Molecular modelling and DFT calculations

All DFT computations were performed using the Guassian 09 suite of programs, with the dispersion corrected density functional MO6L, as described in detail elsewhere.(4) The heparin models were constructed based on the NMR structure, 1HPN.(14, 18) There are two models in the original PDB file, each corresponding to all the iduronic acid residues in either a $^2S_0$ or $^1C_4$ conformation. The structure resulting from the IdoA(2S) in a $^2S_0$ form has sulfate groups well separated compared to the structure from the $^1C_4$ conformation of IdoA(2S). Through an initial visual assessment of a crude model, the $^2S_0$ form was found to be more suitable for Pt-tetraammine interactions,4 and the structure containing all the IdoA(2S) residues in $^2S_0$ confirmation has been used to study the interactions of PPC library with heparin.



www.manaraa.com

NMR cleavage inhibition assay

$^{1}$H NMR spectroscopy was performed in 250 µL Shigemi tubes with an Avance 600 MHz Ultrashield NMR spectrometer (Bruker) with a $^{1}$H/$^{13}$C/$^{15}$N gradient cryoprobe system; data were collected and analysed with the TOPSPIN software (Bruker). The HDO signal was suppressed using a 2 s rf- field during the relaxation delay. The assay was performed according to the previous reports.(4, 10) FPX (300 µM) was pre- incubated for 10 min with each of the Pt compounds (300 µM) in the PPC library (Scheme 2.1) and then was incubated with *P. heparinus* heparinase II (0.4 U, 4 µL, Sigma–Aldrich) at 37 °C in deuterated Tris buffer (Tris- $D_{11}$ (20 mM), NaCl (100 mM) and $CaCl_2{\cdot}2H_2O$ (10 mM)), pH 7.5. $^{1}$H NMR spectra were recorded for each sample prior to addition of enzyme and at different time points thereafter. A control experiment was performed under the same conditions in the absence of PPC library to confirm the activity of the enzyme on FPX.

**Competitive binding assays**

**FPX–PPC binding (methylene blue reporter method)**

All binding studies were performed in triplicate with an Agilent 8453 diode array spectrophotometer in a sub- micro quartz cuvette with a path length of 10 mm. Aqueous solutions of methylene blue chloride (at a constant concentration of 18.6 µM) and fondaparinux (1–15 µM) were prepared for determination of optimal MB- FPX binding. A concentration of 15 µM of FPX was then used for evaluating the inhibition of MB binding by PPCs. Varying concentrations of PPCs were incubated with constant concentration of FPX (15 µM) for 15 min at 23 °C. To each sample was added MB to a final concentration of 18.6 µMand the absorbance was measured.
The Scatchard model(19) was applied to calculate the binding constant between MB and FPX by plotting $\frac{n}{[L]}$ versus *n*, where $\frac{n}{[L]} = \frac{(A_{max}-A)}{(A-A_{min})C_x}$ , [*L*]=concentration of free methylene blue, and *n* is average number of binding sites [Eq.1]:

$$n = \frac{(A_{max} - A)}{\Delta\varepsilon C_x} \quad (1)$$



www.manaraa.com

where $\Delta\epsilon$ is the calculated difference in molar absorptivity between free and bound methylene blue in water at 664 nm; $C_x^=$concentration of heparin added.

$IC_{50}$ and $K_{a(app)}$ values for binding of PPCs to FPX were calculated by converting the MB absorption values into a normalised value (minimum and maximum absorbance) and the $K_{a(app)}$ was determined by using Equation 2

$$\frac{1}{K_{a(app)}} = IC_{50} \times \frac{2K_{dL}[S_L - (B_L)_0]^\circ}{[(B_L)_0^2 + 2S_L K_{dL} - 3S_L(B_L)_0]} \quad (2)$$

where $K_{dL}$ is the dissociation constant for the labelled ligand (MB) and binding site (FPX), $S_L$ is the total concentration of the labelled ligand, and $(B_L)_o$ is the equilibrium of labelled ligand value when competitor concentration is zero.

**FPX competition with PPC–DNA (EtBr reporter method)**

All samples were read in a 96 well plate at 530/590 nm using a microplate reader (BioTek instruments). Ethidium bromide (EtBr) at 5 mM in water was diluted in HEPES buffer (80 mMHEPES, pH 7.2) and incubated with calf thymus (ct) DNA for 5 min at 25 °C to a final control concentration of 12.5 μM EtBr and 10 μM DNA in a final volume of 100 μL. In separate wells, the concentration of each individual PPC (dissolved in water and diluted in HEPES buffer) needed to *decrease* EtBr fluorescence by at least or greater than 50 % after 1 h incubation was calculated to be the following: TriplatinNC 12.5 μM, DiplatinNC 62.5 μM, AH44 125 μM, MonoplatinNC 125 μM, and $[Pt(NH_3)_4]^{2+}$ 500 μM and denominated as $[PPC_d]$. This concentration was normalised as the modified (0 %) EtBr–PPC–DNA fluorescence and 100 % fluorescence was the control EtBr- DNA. Next, 10 μL of varying concentrations of FPX (0–640 μM) in HEPES buffer were added to 90 μL of a combined solution of platinum complex, DNA and EtBr such that the final concentrations were $[PPC_d]$, 12.5 μM (EtBr) and 10 μM (DNA). After 1 h, the fluorescence was read, allowing the calculation of $[FPX_r]$, the concentration of FPX required to *restore* EtBr fluorescence to 50 % of the control EtBr- DNA sample. Samples were normalised to the controls



www.manaraa.com

([$PPC_d$] and no FPX as 0 % and EtBr- DNA only as 100 %) to calculate $EC_{50}$ values using Prism software as per Table 2.3. The ratio index was calculated from the drug concentration divided by the $EC_{50}$ value.

**Isothermal titration calorimetry**

ITC data were collected with a VP- ITC Microcalorimeter (MicroCal, LLC). All samples were degassed for 5 min with a ThermoVac (MicroCal, LLC). For all titrations, injections of Pt complexes were pipetted automatically into the reaction cell containing 1.3 mL of FPX at 300 s intervals from a 300 μL syringe, while stirring at 75 rpm. In all experiments, 100 mMcacodylate buffer (pH 7.4) was used at 25 °C and the thermal reference cell contained 1.3 mL of 100 mM cacodylate buffer (pH 7.4). Integration of the thermogram peaks was carried out using the software supplied with the calorimeter (Origin 7.0). The heats were fitted to a one- site model using Origin 7.0 to determine $K_d$, $\Delta H$, and $\Delta S$. $\Delta G$ was obtained by using the Gibbs free energy equation.

**Mass spectrometry**

Mass spectra were acquired with a Thermo Electron Corporation Orbitrap Velos mass spectrometer (Waltham, MA). Samples were introduced by flow injection at flow rates of 0.5 to 0.7 μL $min^{-1}$ by using a syringe pump. Electrospray source conditions were kept constant with a capillary temperature of 230 °C and capillary voltage between 2.3 and 2.5 kV. FPX and Pt compounds were reconstituted in deionised water to a stock concentration of 40 μM. Samples were mixed at a 1:1 molar ratio and were incubated at room temperature for 20 min. Samples were diluted with addition of Milli- Q methanol for a final concentration of 1:10 methanol/water.

Biological Evaluation

**Cell lines and cell culture**

The human colorectal cancer cell line HCT 116 was obtained from the American Type Tissue Collection. HCT116 cells were cultured in RPMI 1640 media (Invitrogen) with 10 % fetal bovine serum (FBS) and 1 % penicillin/streptomycin (Gibco) at 37 °C with 5 % $CO_2$.



www.manaraa.com

**MTT cell viability assay**

HCT116 cells were seeded in 96- well plates ($5\times10^3$ cells/well) in supplemented media (100 μL). After incubation overnight, the cells were treated with varying concentrations of the indicated Pt compound, in sets containing four replicates for each concentration. After drug exposure for 72 h, 1 mM MTT (3- (4,5- dimethylthiazol- 2- yl)- 2,5- diphenyltetrazolim bromide) (Sigma) was added to each well and incubated for 4 h. The MTT reagent was removed, and 100 μL of DMSO was added to each well. All incubations were performed at 37 °C with 5 % $CO_2$. Spectrophotometric readings were determined at 570 nm with a microplate reader (Bio- Tek instruments). Percentage cell survival was determined as treated/untreated controls × 100. Data are reported as the average of two independent experiments ± SD.

**Cellular accumulation**

HCT116 cells were seeded in 100 mm dishes ($1\times10^6$ cells/dish) in supplemented media (20 mL). After incubation for 24 h, cells were treated with 10 μM of the indicated Pt compounds for 3 and 6 h incubations (37 °C with 5 % $CO_2$). The cells were then washed twice with PBS, harvested with 0.25 % trypsin (Gibco), and washed with 10 mL of PBS. The cell pellets were digested in 1 mL of nitric acid for 72 h and diluted with $H_2O$ (2 mL). The solutions were filtered through a 0.45 GHP filter. Platinum analysis was performed with a Varian 820 inductively coupled plasma mass spectrometer (ICP- MS). The standards were prepared with $K_2PtCl_4$ in concentrations of 10, 50, 100, 150, and 250 ppb. The blank was 7 % nitric acid. Data was normalized to number of platinum centres per drug.

**Cellular internalization**

HCT116 cells were seeded in 6- well plates ($5\times10^5$ cells/well) in supplemented media (3 mL). After incubation for 24 h, cells were treated with 10 μM of the indicated Pt compounds and incubated for 5 min before the addition of TAMRA- $R_9$ (1.0 μM) and further incubation for 1 h at 37 °C with 5 % $CO_2$. Cells were washed three times with PBS, harvested with 0.25 % trypsin (Gibco), and washed twice with cold PBS. The cells were passed through a cell strainer (40



www.manaraa.com

μMFlowmi) and then analysed at 488 nm (excitation) and 585±42 nm bandwidth emission with a Becton Dickinson FACSCanto II Analyzer flow cytometer (BD Biosciences).

**2.6 Acknowledgements:**

The work was supported by grants from NIH (RO1CA78754) to NPF and the Australian Research Council (DP150100308) to SBP, MvI and NPF. This project has been partly supported by pilot funding from the VCU Massey Cancer Center with funding in part from NIH- NCI Cancer Center Support Grant P30 CA016059.

**2.7 References:**

1. P. Chiodelli, A. Bugatti, C. Urbinati, M. Rusnati, *Molecules* **2015**, 20, 6342–6388.
2. C. Pisano, I. Vlodavsky, N. Ilan, F. Zunino, *Biochem. Pharmacol.* **2014**, 89, 12–19.
3. J. B. Mangrum, B. J. Engelmann, E. J. Peterson, J. J. Ryan, S. J. Berners-Price, N. P. Farrell, *Chem. Commun.* **2014**, 50, 4056–4058.
4. E. J. Peterson, A. G. Daniel, S. J. Katner, L. Bohlmann, C.-W. Chang, A. Bezos, C. R. Parish, M. von Itzstein, S. J. Berners-Price, N. P. Farrell, *Chem. Sci.* **2017**, 8, 241–252.
5. N. P. Farrell, *Chem. Soc. Rev.* **2015**, 44, 8773–8785.
6. S. J. Katner, W. E. Johnson, E. J. Peterson, P. Page, N. P. Farrell, *Inorg. Chem*. Submitted for Publication.
7. I. Capila, R. J. Linhardt, *Angew. Chem. Int. Ed.* **2002**, 41, 390–412; *Angew. Chem.* **2002**, 114, 426–450.
8. M. Petitou, C. A. A. van Boeckel, *Angew. Chem. Int. Ed.* **2004**, 43, 3118–3133; *Angew. Chem.* **2004**, 116, 3180–3196.



www.manaraa.com

9. J. C. Wilson, A. E. Laloo, S. Singh, V. Ferro, *Biochem. Biophys. Res. Commun.* **2014**, 443, 185–188.

10. L. Bohlmann, C. W. Chang, I. Beacham, M. von Itzstein, *ChemBioChem* **2015**, 16, 1205–1211.

11. E. Hammond, C. P. Li, V. Ferro, *Anal. Biochem.* **2010**, 396, 112–116.

12. G. Torri, B. Casu, G. Gatti, M. Petitou, J. Choay, J. C. Jacquinet, P. Sinay, *Biochem. Biophys. Res. Commun.* **1985**, 128, 134–140.

13. N. P. Farrell, A. K. Gorle, E. J. Peterson, S. J. Berners-Price, in *Metal Ions in Life Sciences, Vol. 18*(Eds.: A. Sigel, H. Sigel, E. Freisinger, R. K. O. Sigel), Walter de Gruyter, GmbH Berlin, Germany, **2018**, pp109–140s.

14. B. Mulloy, M. J. Forster, *Glycobiology* **2000**, 10, 1147–1156.

15. M. Hricovíni, M. Guerrini, A. Bisio, G. Torri, M. Petitou, B. Casu, *Biochem. J.* **2001**, 359, 265–272.

16. D. R. Ferro, A. Provasoli, M. Ragazzi, C. Torri, B. Casu, G. Gatti, J.-C. Jacquinet, P. Sinay, M. Petitou, J. Choay, *J. Am. Chem. Soc.* **1986**, 108, 6773–6778.

17. M. J. Kailemia, K. Li, M. Ly, R. J. Linhardt, I. J. Amster, *Anal. Chem.* **2012**, 84, 5475–5478.

18. B. Mulloy, M. J. Forster, C. Jones, D. B. Davies, *Biochem. J.* **1993**, 293, 849–858.

19. L. Zhang, N. Li, F. Zhao, K. Li, *Anal. Sci.* **2004**, 20, 445–450.

20. Q. C. Jiao, Q. Liu, C. Sun, H. He, *Talanta* **1999**, 48, 1095–1101.

21. L. Tan, S. Yao, Q. Xie, *Talanta* **2007**, 71, 827–832.

22. H. Chu, N. R. Johnson, N. S. Mason, Y. A. Wang, *J. Controlled Release* **2011**, 150, 157–163.

23. A. Prisecaru, Z. Molphy, R. G. Kipping, E. J. Peterson, Y. Qu, A. Kellett, N. P. Farrell, *Nucleic Acids Res.* **2014**, 42, 13474–13487.

24. Y. Qu, R. G. Kipping, N. P. Farrell, *Dalton Trans.* **2015**, 44, 3563–3572.



www.manaraa.com

25. N. Carte, F. Legendre, E. Leize, N. Potier, F. Reeder, J. C. Chottard, A. V. Dorsselaer, *Anal. Biochem.* **2000**, 284, 77–86.

26. A. Brown, *Int. J. Mol. Sci.* **2009**, 10, 3457–3477.

27. S. Leavitt, *Curr. Opin. Struct. Biol.* **2001**, 11, 560–566.

28. K. Saxena, U. Schieborr, O. Anderka, E. Duchardt-Ferner, B. Elshorst, S. L. Gande, J. Janzon, D. Kudlinzki, S. Sreeramulu, M. K. Dreyer, K. U. Wendt, C. Herbert, P. Duchaussoy, M. Bianciotto, P.-A. Driguez, G. Lassalle, P. Savi, M. Mohammadi, F. Bono, H. Schwalbe, *J. Biol. Chem.* **2010**, 285, 26628–26640.

29. A. Brown, C. J. Robinson, J. T. Gallagher, T. L. Blundell, *Biophys. J.* **2013**, 104, 1720–1730.

30. A. K. Powell, E. A. Yates, D. G. Fernig, J. E. Turnbull, *Glycobiology* **2004**, 14, 17R–30R.

31. S. M. Fuchs, R. T. Raines, *Biochemistry* **2004**, 43, 2438–2444.

32. S. M. Fuchs, R. T. Raines, *Cell. Mol. Life Sci.* **2006**, 63, 1819–1822.

33. E. J. Peterson, V. R. Menon, L. Gatti, R. Kipping, D. Dewasinghe, P. Perego, L. F. Povirk, N. P. Farrell, *Mol. Pharmaceutics* **2015**, 12, 287–297.

34. H. Silva, F. Frézard, E. J. Peterson, P. Kabolizadeh, J. J. Ryan, N. P. Farrell, *Mol. Pharm.* **2012**, 9, 1795–1802.

35. M. M. Fuster, J. D. Esko, *Nat. Rev. Cancer* **2005**, 5, 526–542.

36. A. L. Harris, X. Yang, A. Hegmans, L. Povirk, J. J. Ryan, L. Kelland, N. P. Farrell, *Inorg. Chem.* **2005**, 44, 9598–9600.

37. M. D. Hall, M. Okabe, D. Shen, X. Liang, M. M. Gottesman, *Annu. Rev. Pharmacol. Toxicol.* **2008**, 48, 495–535.

38. H. Burger, W. J. Loos, K. Eechoute, J. Verweij, R. H. Mathijssen, E. A. Wiemer, *Drug Resist. Updates* **2011**, 14, 22–34.

39. S. B. Howell, R. Safaei, C. A. Larson, M. J. Sailor, *Mol. Pharmacol.* **2010**, 77, 887–894.

40. P. Kabolizadeh, J. Ryan, N. Farrell, *Biochem. Pharmacol.* **2007**, 73, 1270–1279.



www.manaraa.com

41. V. Ferro, L. Liu, K. Johnstone, N. Wimmer, T. Karoli, P. Handley, J. Rowley, K. Dredge, C. P. Li, E. Hammond, K. Davis, L. Sarimaa, J. Harenberg, I. Bytheway, *J. Med. Chem.* **2012**, 55, 3804–3813.

42. J. Ritchie, V. Ramani, Y. Ren, A. Naggi, G. Torri, B. Casu, S. Penco, C. Pisano, P. Carminati, M. Tortoreto, F. Zunino, I. Vlodavsky, R. Sanderson, Y. Yang, *Clin. Cancer Res.* **2011**, 17, 1382–1393.

43. D. G. Kauffman, D. O. Cowan, in *Inorg. Synth., Vol. 7* (Ed.: J. Klienberg), McGraw-Hill Book Co., Inc., **1963**, pp. 239–245.

44. N. P. Farrell, Y. Qu, L. Feng, B. V. Houten, *Biochemistry* **1990**, 29, 9522–9531.

45. Z. Gao, H. Luo, L. Chen, J. Shen, K. Chen, H. Jiang, X. Shen, *Sci. China Ser.B Chem.* **2005**, 48, 122.



www.manaraa.com

This work was published in Inorganic Chemistry with the following contributions:

Synthesis by Daniel Lee and Eric Ginsburg, MB, TAMRA-$R_9$, and ITC by Wyatt Johnson, SPR by Phillip Page, FP by Erica Peterson, EtBR and CD by Samantha Katner. Text by Wyatt Johnson, Phillip Page, Erica Peterson, and Samantha Katner.

**Chapter 3: Comparison of Metal–Ammine Compounds Binding to DNA and Heparin. Glycans as Ligands in Bioinorganic Chemistry**

**Samantha J. Katner, Wyatt E. Johnson, Erica J. Peterson, Phillip Page*, and Nicholas P. Farrell**

Department of Chemistry and Massey Cancer Center, Virginia Commonwealth University (VCU), Richmond, Virginia 23284, United States

* Reichert Technologies, Depew, New York 14043, United States

Inorganic Chemistry, 2018, 57 (6), 3116-3125.



www.manaraa.com

### 3.1 Abstract:

We present spectroscopic and biophysical approaches to examine the affinity of metal–ammine coordination complexes for heparin as a model for heparan sulfate (HS). Similar to nucleic acids, the highly anionic nature of heparin means it is associated in vivo with physiologically relevant cations, and this work extends their bioinorganic chemistry to substitution-inert metal–ammine compounds (M). Both indirect and direct assays were developed. M compounds are competitive inhibitors of methylene blue (MB)–heparin binding, and the change in the absorbance of the dye in the presence or absence of heparin can be used as an indirect reporter of M–heparin affinity. A second indirect assay uses the change in fluorescence of TAMRA-$R_9$, a nonaarginine linked to a fluorescent TAMRA moiety, as a reporter for M–heparin binding. Direct assays are surface plasmon resonance (SPR) and isothermal titration calorimetry (ITC). The $K_d$ values for TriplatinNC–heparin varied to some extent depending on the technique from 33.1 ± 2 nM (ITC) to 66.4 ± 1.3 nM (MB absorbance assay) and 340 ± 30 nM (SPR). The differences are explained by the nature of the technique and the use of heparin of differing molecular weight. Indirect probes using the displacement of ethidium bromide from DNA or, separately, fluorescently labeled oligonucleotide (DNA-Fl) can measure the relative affinities of heparin and DNA for M compounds. These assays showed essentially equivalent affinity of TriplatinNC for heparin and DNA. The generality of these methods was confirmed with a series of mononuclear cobalt, ruthenium, and platinum compounds with significantly lower affinity because of their smaller overall positive charge but in the order $[Co(NH_3)_6]^{3+} > [Ru(NH_3)_6]^{3+} > [Pt(NH_3)_4]^{2+}$. The results on heparin can be extrapolated to glycosoaminoglycans such as HS, emphasizing the relevance of glycan interactions in understanding the biological properties of coordination compounds and the utility of the metalloglycomics concept for extending bioinorganic chemistry to this class of important biomolecules.



www.manaraa.com

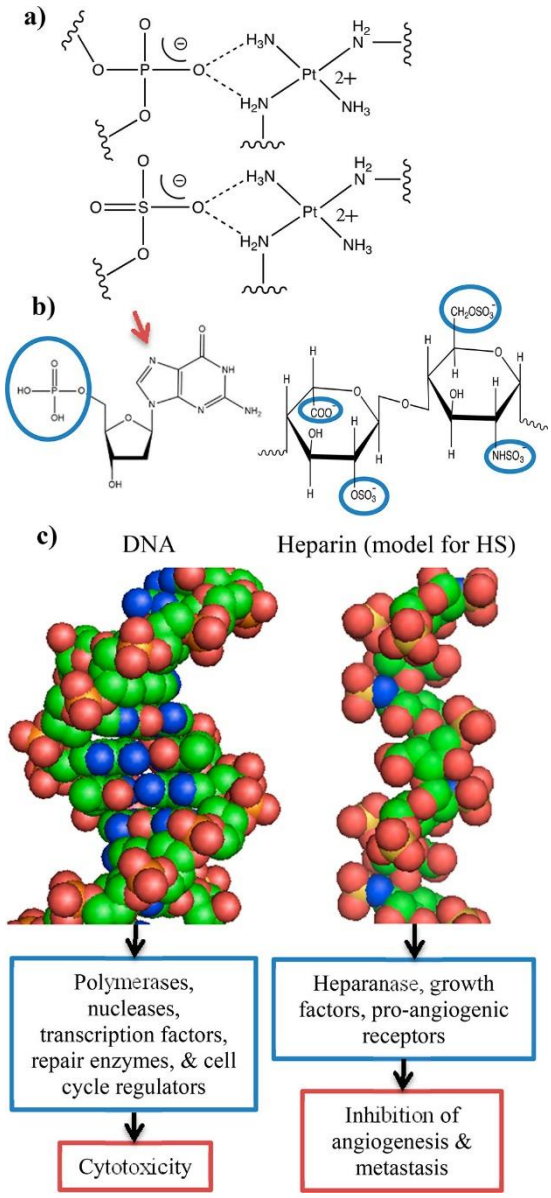


Figure 3.1. (a) Proposed structural analogy of the phosphate clamp to DNA (top) and the sulfate clamp to heparin or a sulfated glycan (bottom) formed by PPCs. (b) Blue circles on the repeating IdoA(2S)–GlcNS(6S) dimer in heparin (right) and 2′-deoxyguanosine 5′-monophosphate (left) in DNA indicating possible electrostatic interaction sites, and a red arrow showing the favored GuanineN7 site of covalent binding. (c) DNA (PDB: 309D) and heparin (PDB: 1HPN) having high negative charge densities, and glycans such as HS having different protein recognition and signaling pathways (blue boxes). Inhibition of these pathways results in different biological consequences (red boxes).



www.manaraa.com

### 3.2 Introduction:

Glycosaminoglycans (GAGs) such as heparan sulfate (HS) are linear polysaccharides composed of repeating disaccharide units of alternating uronic acid and hexosamine residues. When conjugated with proteins, heparan sulfate proteoglycans (HSPGs) are found on the cell surface and extracellular matrix with critical functions in cellular adhesion and migration.(1,2) HS is structurally related to heparin, a free GAG chain produced by mast cells that may be deployed as an immune defense mechanism.(3,4) Heparin usually remains highly sulfated, whereas HS displays varying degrees of sulfation.(1,2) HS has a multitude of protein partners, mediated through hydrogen-bonding and electrostatic interactions between sulfated regions of the polysaccharide and the basic amino acids of the protein.(5−7) Specifically, HSPGs interact with pro-angiogenic growth factors such as fibroblast growth factor (FGF) to induce dimerization for subsequent activation of its receptor.(5,8) FGF-2 directly stimulates tumor and endothelial cell proliferation, migration, and survival.(6) In addition to protein interactions, heparin and HSPGs are cleaved at glycosidic bonds by bacterial and mammalian enzymes (heparinase and heparanase, respectively). This HS cleavage leads to degradation of the extracellular matrix and release of growth factors for tumor angiogenesis.(9) Heparanase has a high abundance in many tumors, correlating with increased metastatic potential and poor clinical prognosis.(10−12) HSPGs and their associated proteins and enzymes are thus attractive drug targets because of their promotion of tumor progression at multiple levels: proliferation, invasion, angiogenesis, and metastasis.(3−7) The highly anionic nature of heparin and HS means they are associated in vivo with physiologically relevant cations, similar to nucleic acids.(13−15) Cation association affects the biomolecule conformation and, in some cases, facilitates heparin–protein interactions such as $Ca^{2+}$-dependent heparin–annexin A2 binding.(16) More broadly, $Cu^{2+}$ promotes angiogenesis, although the detailed mechanism is not defined.(17,18) Growth factors are also copper-dependent, with a slightly higher affinity for FGF-1 compared to FGF-2.(19,20) Aquated $Ca^{2+}$, $Mg^{2+}$, $Fe^{3+}$, and $Zn^{2+}$ ions, at higher than physiological concentrations, reduce FGF-1 interactions with HS–



www.manaraa.com

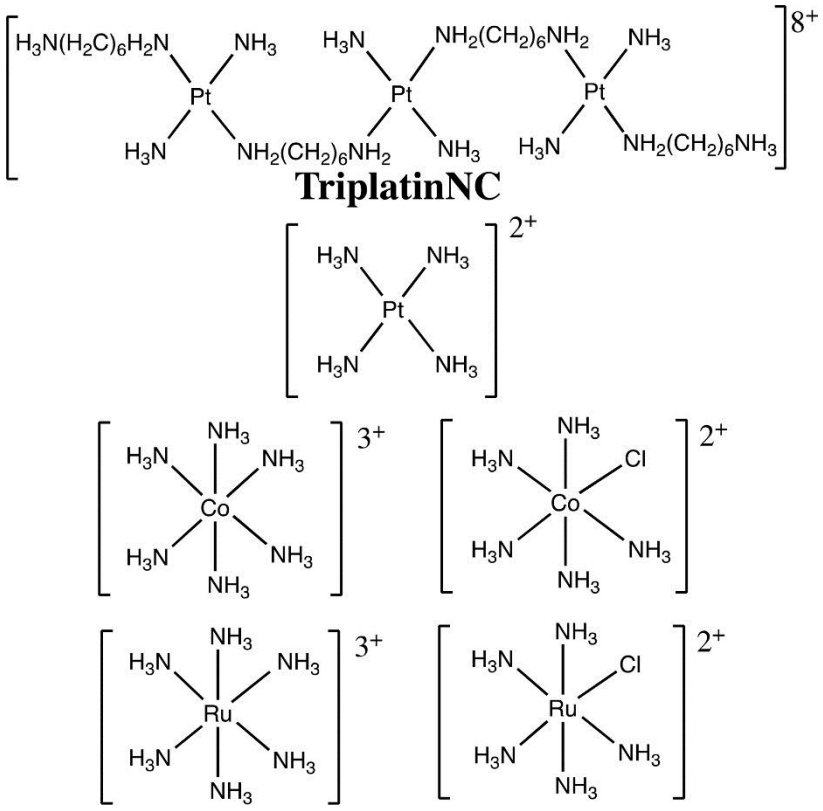


Figure 3.2. Structures of TriplatinNC and metal–ammine compounds used in this study. Counterions are omitted for clarity.



www.manaraa.com

heparin.(13) For heparin and HS, there are no strong donor atoms such as the heterocycle nitrogen atoms of purines and pyrimidines or even sulfur and nitrogen donors of amino acids such as cysteine and histidine available for binding to metal centers, suggesting that harder acids may preferentially bind and/or the oligosaccharides can enter into "noncovalent" electrostatic or hydrogen-bonding interactions (Figure 3.1). In recent papers, we have suggested that metalloglycomics, defined as the study of metal ion–oligosaccharide interactions, can be expanded beyond the study of physiologically relevant aquated metal cations to use defined coordination compounds.(21−24)

Using coordination compounds, alteration of the oxidation state, coordination number, and geometry and substitution lability of ligands allows for the study of a wide variety of structural types to examine the structure and function of sulfated oligosaccharides, extending bioinorganic chemistry to this third major class of biomolecules after DNA/RNA and proteins. Specifically, HSPGs act as receptors for cellular accumulation of the highly cationic polynuclear platinum complexes (PPCs).(21) Molecular recognition of a compound such as TriplatinNC (Figure 3.2) is effected through electrostatic and hydrogen-bonding interactions with the sulfate groups on the HS chains, analogous to the phosphate clamp formed by the same complex on DNA (Figure 3.1a,b).(22−24) This high-affinity sulfate binding, or metalloshielding, has functional consequences including stabilization of the sulfate moieties, in a defined sequence octasaccharide, from dissociation in the gas phase.(23) In biophysical studies, PPC metalloshielding inhibits oligosaccharide backbone cleavage by both bacterial (heparinase I) and mammalian (heparanase) enzymes.(22,23) Growth factor binding to HS is inhibited in the presence of TriplatinNC with consequent effects on downstream kinase signaling.(22) Overall, these interactions lead to the inhibition of cellular angiogenesis and eventually the inhibition of in vivo metastasis (Figure 3.1c).(25,26)

The molecular-level explanation of these events requires a detailed understanding of PPC–glycan interactions. The identity and conformation of the sugar and the number and positions of sulfation make GAGs highly complex systems, with significantly more variability than DNA, also with



www.manaraa.com

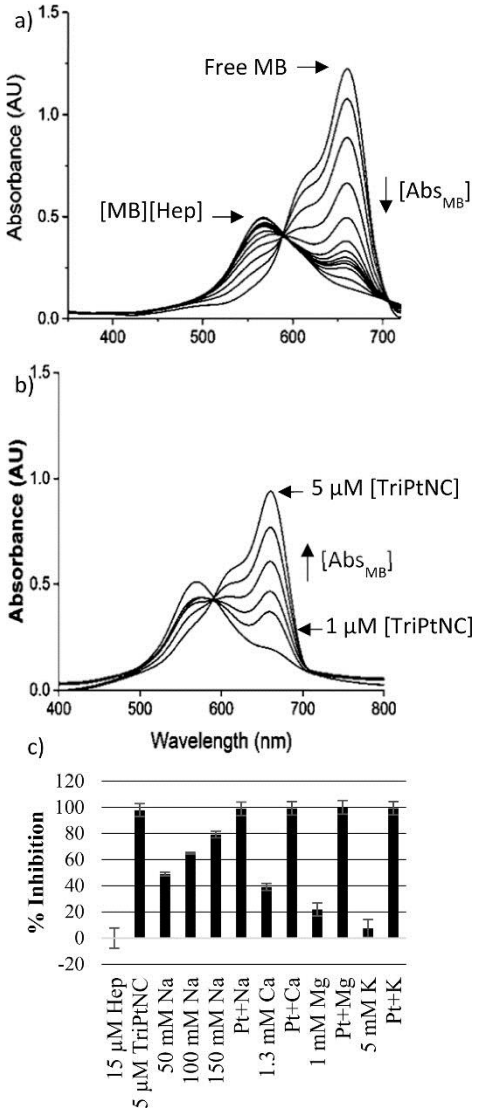


Figure 3.3. MB competition assay for assessment of heparin MW ~18000 binding. (a) The absorbance of a constant concentration of free MB ([AbsMB]) at 664 nm decreases with increasing heparin concentration (from top to bottom with 0–15 µM) with a concomitant increase in the absorbance of [MB][Hep] at 560 nm. (b) At a constant concentration of 15 µM heparin in the presence of varying concentrations of TriplatinNC (from bottom to top with 0–5 µM), MB binding is inhibited, reflected in the change of [AbsMB]. (c) The percent inhibition of MB (18.6 µM) binding to heparin (15 µM) by TriplatinNC (5 µM) in the presence of physiologically relevant concentrations of cations is observed at 664 nm. Charges are omitted for clarity.



www.manaraa.com

respect to non-bond-forming interactions. As polyelectrolytes, heparin and DNA have strong electrostatic interactions that, for heparin and other glycans such as HS, are influenced by the positions and amount of sulfation. Heparin is often used as a model for a highly sulfated HS and is considered to have the highest negative charge density of any biomolecule at an average of 2.7 sulfate groups per disaccharide.(3) This paper evaluates spectroscopic and biophysical approaches to examine metal ion–heparin interactions, especially in the case of substitution-inert PPCs such as TriplatinNC. The fundamental unit of TriplatinNC is the mononuclear tetraam(m)ineplatinum(II), and charge-related effects may be examined by a comparison of mononuclear and poly(tri)nuclear species. The generality of these approaches is exemplified by extension to other mononuclear metal–ammine complexes based on cobalt and ruthenium. The fluorescent properties of $[Ru(bpy)_3]^{2+}$ and its analogues have been used as analytical probes to examine the heparin concentration and even content in cells.(27−29) In this paper, we therefore compared the relative reactivities of the chosen set of compounds toward both biomolecules (DNA and heparin) and in a novel competition assay showed that heparin is a competitor for metal complex–DNA binding. The overall results emphasize the relevance of glycan interactions for understanding the biological properties of coordination compounds and the potential for extending bioinorganic chemistry to this important class of biomolecules.

**3.3 Results and Discussion:**

We first examined the binding of TriplatinNC and subsequently extended the studies to the cobalt and ruthenium systems (Figure 3.2).

**The Case of TriplatinNC**

**Indirect Assays: Methylene Blue (MB) Competition (Absorbance)**

The cationic dye MB has been used to quantify heparin content and examine heparin binding interactions.(30−32) MB interaction with heparin causes a concentration-dependent reduction in



www.manaraa.com

(a)
The Scatchard model was applied to calculate the association constant of MB to heparin by plotting $\frac{n}{[L]}$ versus n, using $\frac{n}{[L]} = \frac{(A_{max}-A)}{(A-A_{min})C_x}$ , where [L] was the concentration of free MB, and where n was the average number of binding sites ($n = \frac{(A_{max}-A)}{\Delta\varepsilon C_x}$; $\Delta\varepsilon$ was the calculated difference in molar absorptivity between free and bound methylene blue in water at 664 nm, and $C_x$ was the concentration of heparin added).[1]

(b)
To determine the $K_{a(app)}$ of metal complexes-heparin, the absorbance values were converted to the percentage of the control (minimum and maximum absorbance) and a competitive model of $\frac{1}{K_{a(app)}} = IC_{50} \times \frac{2K_{dL}[S_L-(B_L)_o]}{[(B_L)_o{}^2+2S_LK_{dL}-3S_L(B_L)_o]}$, ($K_{dL}$ is the dissociation constant for the labeled ligand (MB) and binding site (heparin), $S_L$ is the total concentration of the labeled ligand, and $(B_L)_o$ is the labeled ligand equilibrium value when competitor concentration is zero $(B_L)_o=B_{max}$).[2]

(c)
To determine the $K_d$ of TAMRA-$R_9$ to heparin, the fluorescence data was fitted to a sigmoidal plot using the equation $F = \frac{a-\sqrt{a^2-4[R_T][L_T]}}{2[L_T]}$ (where $a = K_d + [R_T] + [L_T]$, and F is the measured fluorescence, $K_d$ is the dissociation constant for the fluorescent probe (TAMRA-$R_9$) and binding site (heparin), $R_T$ is the total concentration of the heparin, and $L_T$ is the total concentration of the TAMRA-$R_9$.[3]

Equation 3.1. The dissociation constants and apparent binding constants were calculated by the Scathcard model[1] for (a) MB-heparin binding, the competitive model[2] for (b) metal-ammine compounds-heparin binding using MB as a reporter, and the nonlinear curve fitting[3] for (c) TAMRA-$R_9$ -heparin binding.



www.manaraa.com

its absorbance. With increasing heparin concentration, the MB absorbance at 664 and 614 nm decreases while that at 570 nm increases, allowing for calculation of the affinity constants (Figure 3.3a).(30) The Scatchard model (eq 1a) gave a dissociation constant ($K_d$) value for the MB–heparin interaction of 351 nM, comparable to a previously reported value of 578 nM (reported originally as the association constant) measured between MB and chondroitin sulfate (another type of GAG).(33)

In the presence of heparin bound to varying concentrations of TriplatinNC, the absorbance of added MB dye (at a constant concentration) varies depending on how much TriplatinNC is released due to competitive dye binding: [Hep][TriplatinNC] + MB ⇌ [Hep][MB] + TriplatinNC (Figure 3.3b). The disruption of TriplatinNC binding by MB can be reported as $IC_{50}$, the concentration of the complex necessary to give 50% of free dye, as monitored by MB absorbance (Table 3.1). By using MB as a reporter for competitive inhibition in a three-species system, the $K_d$value between TriplatinNC and heparin was calculated to be 66.4 ± 1.3 nM (Table 3.1 and eq 1b).

We also evaluated the competitive binding interactions between TriplatinNC and MB in the presence of other physiologically relevant cations. The presence of physiological concentrations of other cations affects the absorbance of the dye in the MB–heparin interaction.(34) The change in absorbance varies depending on the degree of cation release due to competitive dye binding, and this release is based on the concentration, charge, and ionic radius of the cations.(34) High concentrations of $Na^+$ showed the greatest effect on MB binding, followed by $Ca^{2+}$ > $Mg^{2+}$ > $K^+$(Figure 3.3). With the addition of TriplatinNC (at a constant concentration), MB binding is further inhibited with no observed difference from the TriplatinNC–heparin binding in the presence of other cations, although the increase in inhibition is consequently smaller in the case of the highest concentrations of $Na^+$ at 150 mM. There is a difference between the $Na^+$ effects on DNA, where concentrations above 600 mM were needed to completely restore condensed DNA to the relaxed form in the presence of TriplatinNC, which is a very effective DNA condensing agent.(35,36) We note that the SPR data to be discussed below were obtained in the presence of



www.manaraa.com

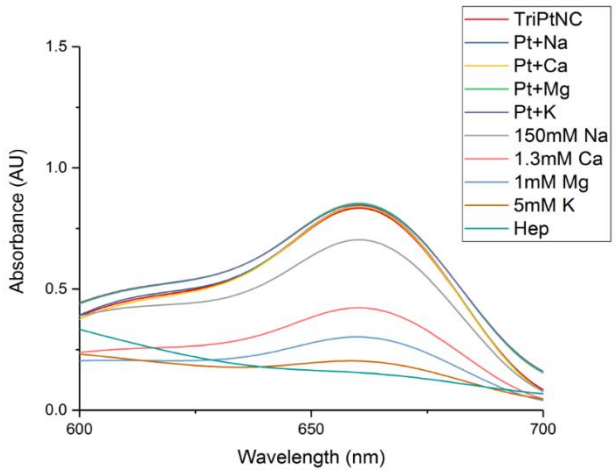


Figure 3.4. Observed absorbance change of binding between MB and heparin with a constant concentration of 18.6 µM MB, 15 µM heparin, 5 µM TriplatinNC, and physiological relevant concentrations of cations; absorbance changes with added concentrations of cations, while no change between the Pt and heparin binding was observed. Aqueous solutions of methylene blue chloride (at a constant final concentration of 18.6 µM), heparin MW 18000 (at a constant final concentration of 15 µM), and TriplatinNC (at a constant final concentration of 5 µM) were used for evaluating the absorbance change of MB-heparin binding by physiological relevant concentrations of cations (Sodium Chloride: 150 mM, Potassium Chloride: 5 mM, Calcium Chloride: 1.3 mM, and Magnesium Chloride: 1 mM).

| | MB | | TAMRA-$R_9$ |
|---|---|---|---|
| **metal complex** | **$IC_{50}$ (µM)[a]** | **$K_{d(app)}$[b]** | **$IC_{50}$ (µM)[a]** |
| $TriplatinNC^{8+}$ | 3.1 ± 0.1 | 66.4 ± 1.3 nM | 62.9 ± 1.1 |
| $[Co(NH_3)_6]^{3+}$ | 16.9 ± 0.4 | 367 ± 9.0 nM | 77.8 ± 3.2 |
| $[Ru(NH_3)_6]^{3+}$ | 46.4 ± 0.7 | 1.0 ± 0.1 µM | N/A |
| $[Pt(NH_3)_4]^{2+}$ | 265 ± 6 | 5.8 ± 0.1 µM | 255 ± 12 |
| $[CoCl(NH_3)_5]^{2+}$ | 392 ± 1 | 8.5 ± 0.1 µM | 539 ± 23 |
| $[RuCl(NH_3)_5]^{2+}$ | 553 ± 14 | 12.0 ± 0.3 µM | 832 ± 28 |

Table 3.1. $IC_{50}$ and $K_d$ values of TriplatinNC and Metal-ammine compounds in competitive inhibition assays using MB or TAMRA-$R_9$.
[a]The $IC_{50}$ value was determined as the concentration of complex required for half-maximal binding of the dye (18.6 µM or 100 nM) to heparin MW ~18000 (15 or 625 µM) for MB or TAMRA-$R_9$ binding assays, respectively.
[b]Dissociation constants were calculated from the MB assay for TriplatinNC and metal–ammine compound binding to heparin MW ~18000 using a competitive inhibitor model.



www.manaraa.com

150 mM NaCl, confirming that TriplatinNC is capable of binding to heparin at physiologically relevant concentrations of small cations.

**Indirect Assays: TAMRA-$R_9$ Competition (Fluorescence)**

TAMRA-$R_9$ is a polycationic, nona-L-arginine peptide linked to a fluorescent TAMRA moiety. In this case, the fluorescence of TAMRA-$R_9$ at 590 nm (emission) increases with increasing heparin concentration, and a $K_d$ value of 109 nM for TAMRA-$R_9$–heparin binding has been previously reported.(37) In our hands, we obtained a $K_d$ value of 405.9 nM, and the difference may be attributed to the use of a larger heparin (MW 18000) than that previously reported (Figure 3.5a). There is also slight variability in the $K_d$ values under similar conditions because heparin preparations can be very heterogeneous.(3,37) We have previously used the fluorescence of TAMRA-$R_9$ as a reporter to identify HSPGs as receptors for platinum complex cellular internalization.(21) Analogous to the enhanced fluorescence of an intercalator such as ethidium bromide (EtBr) upon DNA binding, TAMRA-$R_9$ fluorescence increases when bound to heparin. Again, in the presence of heparin bound to varying concentrations of TriplatinNC, the addition of TAMRA-$R_9$ (at a constant concentration) results in the observation of fluorescence proportional to the amount of TAMRA-$R_9$–heparin binding with TriplatinNC release: [Hep][TriplatinNC] + TAMRA-$R_9$ ⇌ [Hep][TAMRA-$R_9$] + TriplatinNC (Figure 3.5b). The ability of TriplatinNC to compete with TAMRA-$R_9$ for heparin binding can be reported as the $IC_{50}$ required to produce 50% fluorescence compared to control of heparin dye in the absence of the complex (Table 3.1).

**Direct Assays: Surface Plasmon Resonance (SPR)**

For direct analysis, SPR was used to estimate the TriplatinNC–heparin affinity. SPR is a label-free, real-time quantification of the interaction between the immobilized ligand on the sensor chip and the analyte being injected in a continuous flow over the ligand.(38) When the ligand and analyte interact, the refractive index changes, and the response is reported as response units (RU). SPR has been used for determining the heparin concentration, metal–heparin binding, and metal–heparin binding effects on the growth factor and growth factor receptor recognition.(13,39) A mixture of metal ions reduced the affinity of FGF-1 binding to heparin from $K_d$ = 22 to 350



www.manaraa.com

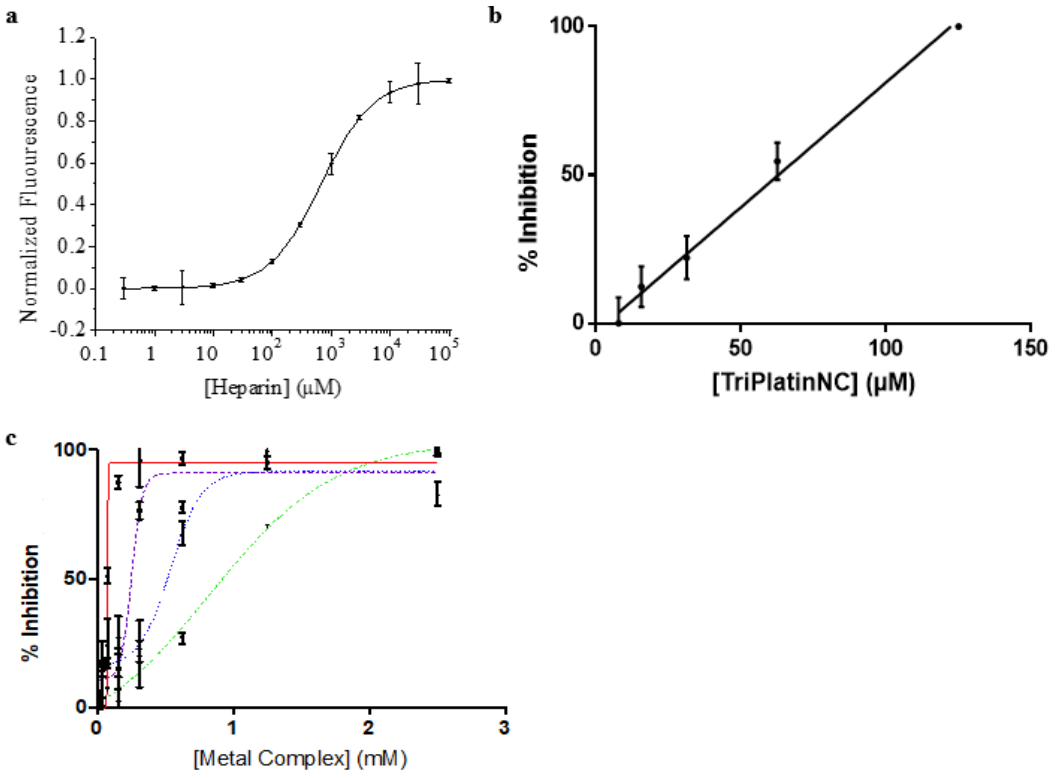


Figure 3.5. TAMRA-$R_9$ competition assay with metal-ammine compounds binding to heparin. (a) Normalized fluorescence spectra of TAMRA-$R_9$ (100 nM) changes with various concentrations of heparin. TAMRA-$R_9$ binding to heparin is inhibited with increasing concentrations of metal complex. Normalized Fluorescence spectra of TAMRA-$R_9$ were changed to a percentage of maximum and minimum fluorescence with % inhibition correlated to a decrease in fluorescence. (b) Concentrations for TriplatinNC were the following: 125, 62.5, 31.3, 15.6, and 7.8 μM. (c) Concentrations for metal-ammines were the following (red) $Co(NH_3)_6]^{3+}$; (purple) $[Pt(NH_3)_4]^{2+}$; (blue) $[CoCl(NH_3)_5]^{2+}$; and (green) $[RuCl(NH_3)_5]^{2+}$: 2500, 1250, 625, 312.5, 156.3, 78.1, 39.1, and



www.manaraa.com

nM.(13)In the study of heparin–protein interactions by SPR, heparin is preferentially immobilized onto the sensor chip rather than the protein because this more closely mimics natural biological systems, where HS is found at the cell surface as a proteoglycan and binds to target proteins.(40,41) A common method for heparin immobilization is to use a biotinylated heparin and a streptavidin-coated sensor chip.(40) The high charge of TriplatinNC caused significant nonspecific binding to both the dextran sensor chip surface and streptavidin. Therefore, in collaboration with Reichert Technologies, a Neutravidin-coated mixed self-assembled monolayer (mSAM) sensor chip was used to minimize the background noise and resulted in significantly lower nonspecific binding of TriplatinNC to the sensor surface, although there is still some binding to the reference, causing some distortion in the binding curves (Figure 3.6). At the lowest 111 nM concentration, there was a large (repeatable) decrease in the signal, which may be due to random adsorption of the highly charged molecule in the system. An analysis of the binding curves for the interaction between heparin and TriplatinNC was generated using the *TraceDrawer* program. Although a global fit was not possible, a one-site model and 1:1 TriplatinNC–heparin stoichiometr, gave a $K_d$ value of 340 ± 30 nM (Figure 3.6). Because the immobilized heparin had MW 15000, it is plausible that there could be multiple binding sites, which may affect the estimated $K_d$ values.

**Direct Assays: Isothermal Titration Calorimetry (ITC)**

ITC accurately determines the thermodynamic contributions of both enthalpy ($\Delta H$) and entropy ($-T\Delta S$) changes to the free energies of binding ($\Delta G$). ITC measures the heat released or absorbed into the system upon the binding of two molecules and is proportional to the overall strength of binding.(42) ITC has been used in heparin growth factor assays and in defining the thermodynamic parameters from these interactions.(43,44) A mixture of heterogeneous heparin chains interacting with FGF-1 gave $K_d$ values of 1.1–3 μM.(45) Using a smaller (MW 3000) heparin, we studied the heparin–TriplatinNC interaction by ITC. As TriplatinNC was titrated into the reaction cell containing heparin (Figure 3.7), the produced peaks were integrated to yield the heat released per titration. Using a one-site model for TriplatinNC–heparin gave a $K_d$ value of 33.1 ± 2 nM (Figure 3.7). The enthalpy term reflects the strong electrostatic and hydrogen-bonding interactions



www.manaraa.com

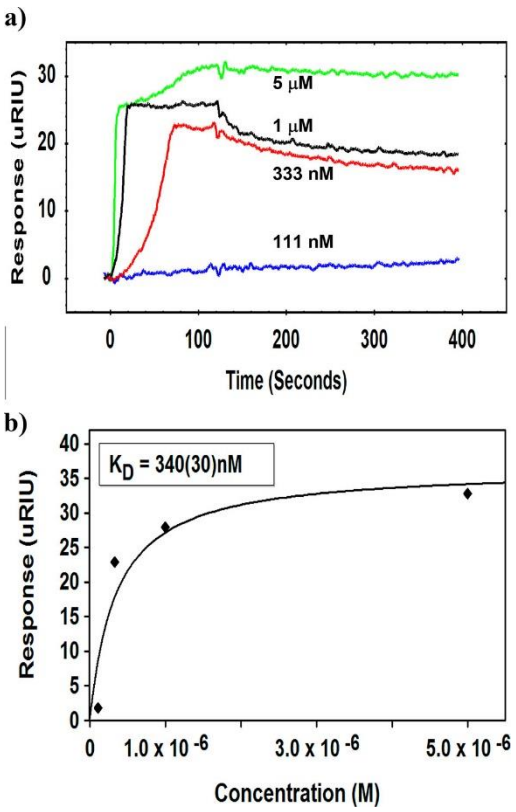


Figure 3.6. Determination of the TriplatinNC–heparin binding affinity by SPR using a biotinylated heparin (MW ~15000) immobilized to Neutravidin on a planar mSAM chip. (a) After injection of 5, 1, 0.333, and 0.111 μM of TriplatinNC, the solution was allowed to flow over the chip for 5 min to allow binding; a buffer was then injected, and after flowing for 5 min, dissociation was assessed. (b) The amount of TriplatinNC bound at equilibrium was corrected for background and plotted versus input TriplatinNC concentration. Analysis by equilibrium parameters using a 1:1 binding model yielded a *K*d value of 340 ± 30 nM.



www.manaraa.com

occurring between the sulfates and ammines, while the entropic term reflects the possible release of water molecules as well as the loss of conformational mobility of the iduronic acid ring.(42) This loss of conformational mobility results in a high entropy value and commonly reflects the phenomenon of entropy–enthalpy compensation.(46) Overall, the interactions observed produce a spontaneous and favorable binding between TriplatinNC and heparin ($\Delta G$ = −10.1 ± 0.1 kJ/mol).

**Summary**

Overall, the results from MB and TAMRA-$R_9$ reporter assays demonstrated strong TriplatinNC–heparin interactions, which were confirmed by SPR and ITC. MB and TAMRA-$R_9$ dyes had similar estimated $K_d$ values for binding to heparin itself, 351 and 405.9 nM, respectively. The TriplatinNC–heparin binding gave similar $K_d$ values of 66.4 ± 1.3 and 33.1 ± 2 nM from the MB assay and ITC system, respectively, whereas the SPR system displayed a magnitude weaker affinity (340 ± 30 nM). Because the SPR system measured TriplatinNC interacting with heparin immobilized to the surface of the sensor chip, this immobilization may reduce the degrees of freedom of the heparin molecule to interact and thus affect the kinetics and affinity of the TriplatinNC–heparin interaction.(47) However, the heparin immobilization more closely mimics natural biological systems where the HS chains are covalently attached to core proteins as HSPGs. There are few small molecule–heparin binding data for comparison by SPR and ITC because the majority of studies have been on protein–heparin interactions.

**Comparison of the PPC–Heparin and PPC–DNA Affinities**

The $K_d$ values with heparin from the indirect reporter assays and the direct SPR and ITC techniques raise questions about the relative affinity of TriplatinNC for DNA or heparin. TriplatinNC and substitution-inert complexes in general bind with high affinity to DNA with a measured $K_{d(app)}$value of 17.7 nM (reported as $K_{a(app)}$).(48) Given the highly anionic nature of both biomolecules, what are the relative affinities of a molecule such as TriplatinNC for DNA or heparin? As mentioned, heparin is considered to have an average of 2.7 sulfate groups *per* disaccharide compared to that of two phosphate groups *per* base pair for DNA. We



www.manaraa.com

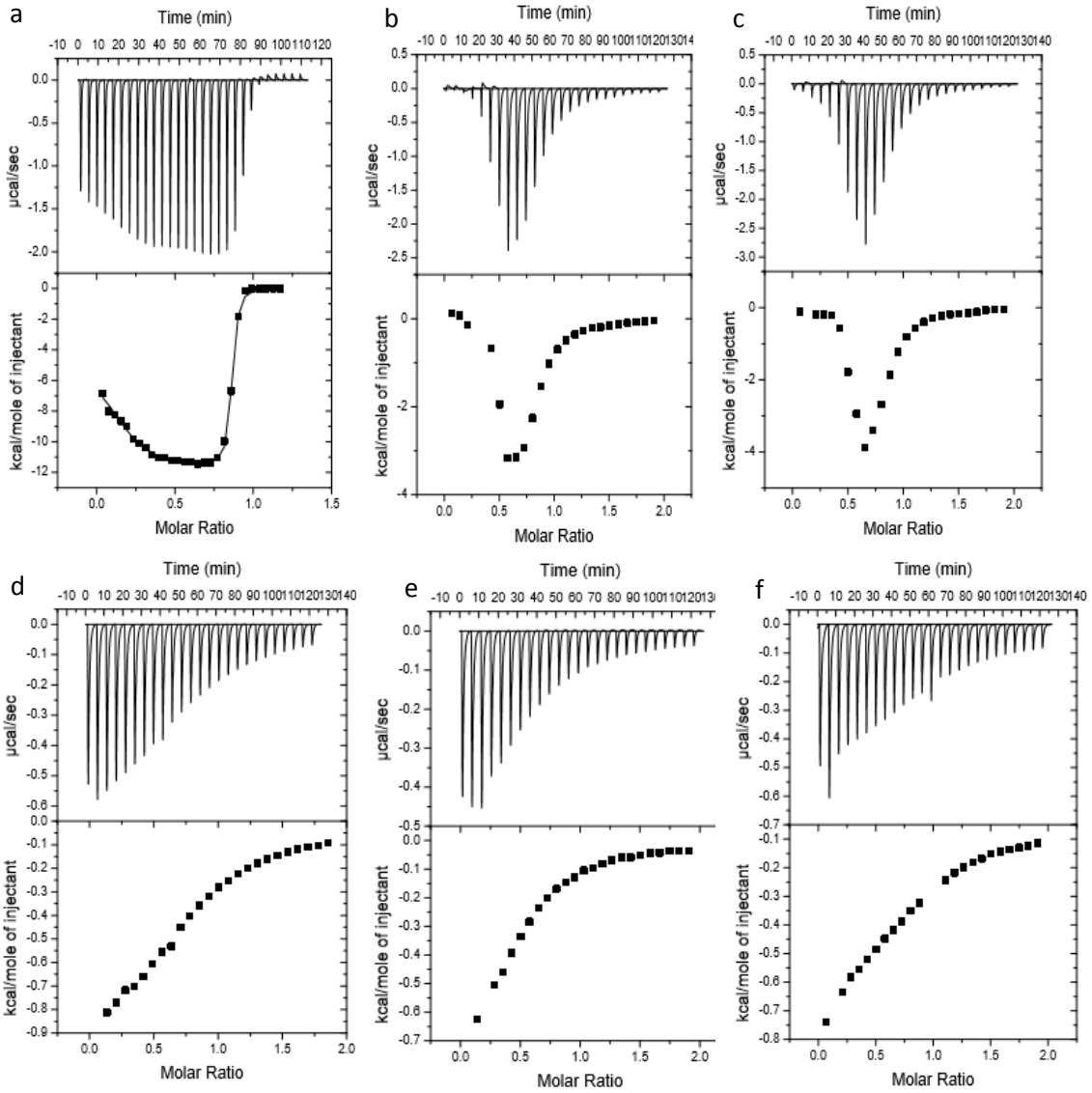


Figure 3.7. Isothermal titration calorimetry measured the heat released by titrations of (a) TriplatinNC, (b) $[Co(NH_3)_6]^{3+}$, (c) $[Ru(NH_3)_6]^{3+}$, (d) $[Pt(NH_3)_4]^{2+}$, (e) $[CoCl(NH_3)_5]^{2+}$, and (f) $[RuCl(NH_3)_5]^{2+}$ into the heparin solution.



www.manaraa.com

therefore developed a number of competitive binding assays to answer this question and to complement the indirect and direct HS–PPC assays. Fluorescence polarization, EtBr, and circular dichroism (CD) competition assays compared the ability of heparin to compete with DNA for the binding of charged metal complexes.

**DNA Competition Assay**

A fluorescence polarization assay measures the tumbling motion of molecules to describe binding events. Typically, the assay incorporates a small fluorescently labeled molecule, such as a DNA oligonucleotide, and an interacting molecule of similar or higher molecular weight, such as a protein. Upon binding, the rotation of the fluorescent molecule decreases, which is measured by emission fluorescence passing through parallel and perpendicular polarized light paths.(38) For our purposes, we examined whether changes in the rotation of a small fluorescently labeled DNA hairpin (DNA-Fl; 23nt; MW 7705) could be detected upon binding of the lower-molecular-weight metal complex, TriplatinNC (MW 1650).

Reproducible saturation binding curves were established with the concentration of drug required for half-maximal binding determined to be $EC_{50}$ = 1.92 μM (Figure 3.8a and Tables 3 and 4). When the same unlabeled DNA hairpin was subsequently titrated into the reactions, a predicTable 3.shift of the curve occurred as unlabeled DNA competed with labeled DNA for binding of TriplatinNC with concomitant increases in the apparent $EC_{50}$ values (Figure 3.8a and Table4). The fold changes of the apparent $EC_{50}$ values were 1.1, 1.9, and 11.6 with changing DNA/DNA-Fl ratios of 0.2:1, 2.11:1, and 21.2:1, respectively (Table 3.4). When heparin MW ~3000 was used as the competitor ligand, the $EC_{50}$ values similarly increased relative to the control DNA-Fl (Figure 3.8b and Table 3.3). In comparison, the fold increases in the $EC_{50}$ values were 1, 2.1, and 10.3 upon the addition of increasing concentrations (0.2–21.2 μM) of heparin, closely comparable to the DNA/DNA-Fl ratios used. These results therefore suggest a similar affinity for TriplatinNC between low-molecular-weight heparin and DNA substrates.

For a second competition assay, we used an adaptation of the well-known EtBr fluorescence assay to measure the binding affinities of metal complexes.(22,48) The fluorescence from intercalator



www.manaraa.com

| Metal Complex | $K_d$ (μM) | ΔG (kJ/mol) | ΔH (kJ/mol) | -TΔS (kJ/mol) |
|---|---|---|---|---|
| TriplatinNC$^{8+}$ | 0.0331 ±0.002 | -10.1 ±0.01 | -11.9 ±0.07 | 1.74 |
| $[Co(NH_3)_6]^{3+}$ | 15.75 ±1.74 | -6.65 ±0.10 | -4.62 ±0.22 | -1.93 |
| $[Ru(NH_3)_6]^{3+}$ | 14.77 ±2.25 | -6.58 ±0.10 | 4.85 ±0.29 | -1.83 |
| $[Pt(NH_3)_4]^{2+}$ | 84 ±4.80 | -5.56 ±0.02 | -1.09 ±0.02 | -4.47 |
| $[CoCl(NH_3)_5]^{2+}$ | 84 ±5.93 | -5.57 ±0.10 | -1.22 ±0.07 | -4.35 |
| $[RuCl(NH_3)_5]^{2+}$ | 199 ±13.45 | -5.06 ±0.10 | -1.27 ±0.06 | -3.79 |

Table 3.2. A comparison of dissociation constants and Gibbs free energy by the enthalpy and entropy of the calorimetric data fitted to a single site-binding model for TriplatinNC and metal-ammine complexes.



www.manaraa.com

binding to DNA is quenched when the intercalator is displaced upon TriplatinNC–DNA binding. Upon the addition of increasing concentrations of heparin, TriplatinNC is sequestered and the nucleic acid now becomes available to bind the intercalator, with a resultant increase in fluorescence (Table 3.5). From Figure 3.8c, we can see that a concentration of 12.5 μM TriplatinNC reduced EtBr fluorescence to approximately 25% of the control value. A concentration of 20.5 μM heparin increases fluorescence to approximately 50%, while full fluorescence is restored in the 35–40 μM range. The experiment allows us to define $EC_{50}$ as the sequestration concentration of heparin required to restore 50% EtBr binding (Table 3.5). This experiment again confirms the similar affinities of the two biomolecules for TriplatinNC.

**CD Assay**

The competitive binding of heparin and DNA can also be easily envisaged by CD spectroscopy monitoring of the conformational changes during each event. The CD spectrum of the DNA structure influenced by its environment and changes such as TriplatinNC binding can be monitored without the need for labels. The positive CD band of DNA centered at approximately 270 nm is decreased in the presence of TriplatinNC (Figure 3.9). Upon the addition of heparin to the DNA–TriplatinNC mixture, the positive band is restored in a heparin concentration-dependent manner through sequestration of TriplatinNC and restoration of DNA to its original conformation. Neither heparin nor heparin–TriplatinNC mixtures show any CD absorbance in the 250–280 nm range, and thus the changes observed are direct visualizations of competitive binding.

**Summary**

Electrostatic and hydrogen-bonding interactions with noncovalent metal complexes observed on DNA translate to heparin–HS interactions. To determine the relative affinity of TriplatinNC for heparin and/or DNA, competition assays were used with reporters for the TriplatinNC–DNA interaction. Fluorescence polarization and EtBr competition assays showed that TriplatinNC has a broadly similar affinity for both unlabeled heparin and DNA.



www.manaraa.com

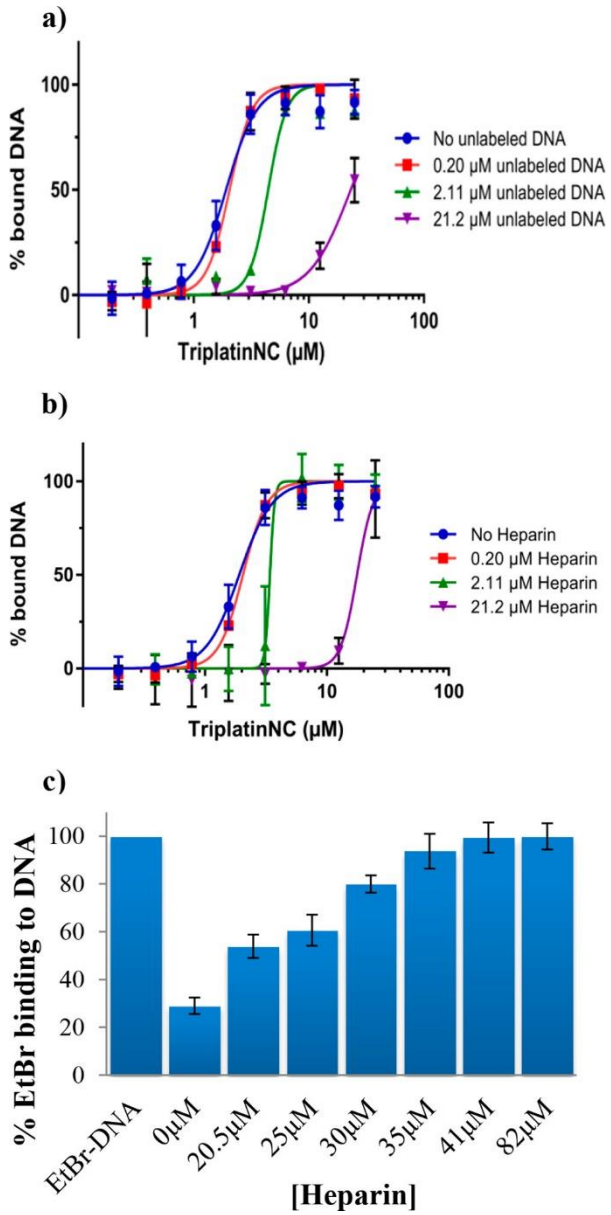


Figure 3.8. Heparin, a competitive inhibitor of TriplatinNC–DNA binding. (a) Unlabeled DNA (0–21.2 μM) competed with fluorescently labeled DNA (23nt and MW 7705) for TriplatinNC binding. (b) Analogously, the binding of TriplatinNC to the fluorescently labeled-DNA was reduced upon the addition of heparin MW ~3000 (0–21.2 μM). (c) EtBr bound to ct-DNA was displaced upon the addition of TriplatinNC, while increasing the concentration of heparin MW ~18000 sequestered TriplatinNC from DNA, allowing EtBr–DNA binding to occur. EtBr bound to DNA was normalized to 100% with EtBr only as 0%.



www.manaraa.com

**Affinity of HS Binding to Metal–Ammine Complexes**

Trinuclear complexes are modular in nature, and the strong interactions of TriplatinNC with heparin led us to explore the individual contributions of the mononuclear tetraam(m)ineplatinum(II) units and further compare charge-related effects based on cobalt and ruthenium analogues (Figure 3.1). While, in principle, the chloropentaammine complexes of cobalt(III) and ruthenium(III) can enter into covalent interactions through Co–Cl or Ru–Cl substitution, the nature of the assays developed and the kinetic inertness of substitution on the cobalt(III) and ruthenium(III) centers suggests that any trends observed across the series of compounds will be most likely due to simple differences in charge.

**MB Assay**

In MB assay, $[Co(NH_3)_6]^{3+}$ and $[Ru(NH_3)_6]^{3+}$ of the mononuclear metal–ammine compounds exhibited the highest affinity to heparin, although the $IC_{50}$ values were significantly higher than that for TriplatinNC (Table 3.1 and Figure 3.10). The efficacy of inhibition is charge-dependent, and the 2+ compounds $[Pt(NH_3)_4]^{2+}$, $[RuCl(NH_3)_5]^{2+}$, and $[CoCl(NH_3)_5]^{2+}$ required over 10-fold more compound for inhibition than $[Co(NH_3)_6]^{3+}$ with increasing $IC_{50}$ (Table 3.1). Similar trends were observed for TAMRA-$R_9$ assay (Table 3.1 and Figure 3.5c).

**ITC Assay**

The ITC titrations of metal–ammine species to heparin did not give well-defined isotherms, perhaps because of the inherently lower affinity as measured by the MB reporter assay, and were not analyzed in detail. Affinity values derived from ITC can also vary depending on the nature of the heparin as noted above.(45)

**DNA Competition Assays**

Metal-ion interactions with nucleic acids have been widely studied;(49) more specifically, the chosen cobalt and ruthenium complexes bind tightly to DNA.(50−54) Thus, we compared the affinities of metal–ammine compounds for DNA and heparin. Using the fluorescently labeled DNA-Fl, as was previously done, and heparin MW ∼3000 as the competitor, we examined the relative binding affinity of metal–ammines for these two substrates. Overall, the metal–ammine



www.manaraa.com

| | TriplatinNC$^{8+}$ | $[Co(NH_3)_6]^{3+}$ | $[Pt(NH_3)_4]^{2+}$ | $[RuCl(NH_3)_5]^{2+}$ | $[CoCl(NH_3)_5]^{2+}$ |
|---|---|---|---|---|---|
| | | | Competitor $EC_{50}$ (μM)[a] | | |
| none | 1.9 | 45.5 | 330 | 388 | 293 |
| 0.20 μM heparin | 2.1 | 49.7 | 340 | 395 | 234 |
| 2.11 μM heparin | 4.0 | 68.2 | 419 | 479 | 281 |
| 21.2 μM heparin | 19.6 | 233 | 655 | 697 | 345 |
| | | | Competitor Fold Change $EC_{50}$[b] | | |
| 0.20 μM heparin | 1.1 | 1.1 | 1.2 | 1.0 | 0.8 |
| 2.11 μM heparin | 2.1 | 1.5 | 1.3 | 1.2 | 1.0 |
| 21.2 μM heparin | 10.3 | 5.1 | 2.0 | 1.8 | 1.2 |

Table 3.3. Fluorescence Polarization Assays Showing That Heparin Is a Competitor for Metal–Ammine Compound Binding to DNA

[a]$EC_{50}$ was determined as the concentration of the complex required for half-maximal binding to fluorescently labeled DNA using heparin MW ~3000 as a competitor.
[b]The fold change $EC_{50}$ was calculated as ($EC_{50}$ of the sample with a competitor)/($EC_{50}$of the sample without a competitor).

| Competitor (μM) | $EC_{50}$ (μM) | fold change $EC_{50}$ |
|---|---|---|
| None | 1.9 | |
| 0.20 unlabeled DNA | 2.1 | 1.1 |
| 2.11 unlabeled DNA | 3.7 | 1.9 |
| 21.2unlabeled DNA | 22.3 | 11.6 |

Table 3.4. TriplatinNC bound to fluorescently labeled DNA competes with "cold" unlabeled DNA. Upon addition of unlabeled-DNA, the $EC_{50}$ of TriplatinNC binding to labeled-DNA increases. The $EC_{50}$ was determined as the concentration of complex required for half-maximal binding to DNA. The fold change $EC_{50}$ is calculated as the ($EC_{50}$ of sample with competitor)/ ($EC_{50}$ of the sample without competitor).



www.manaraa.com

compounds exhibited at least a 2-fold increase in $EC_{50}$ for the highest heparin–DNA ratios, with the largest fold increase of 5.1 observed for $[Co(NH_3)_6]^{3+}$ (Table 3.2 and Figure 3.11). Compared to TriplatinNC, the $EC_{50}$ values of the metal–ammine compounds binding to DNA were higher (TriplatinNC$^{8+}$ < $[Co(NH_3)_6]^{3+}$ < $[CoCl(NH_3)_5]^{2+}$ < $[Pt(NH_3)_4]^{2+}$ ≈ $[RuCl(NH_3)_5]^{2+}$), indicating the expected lower binding affinity to DNA. Upon competition with heparin, the higher fold increase in $EC_{50}$ is a measure of the higher heparin affinity, independent of the actual concentrations used for each compound to achieve half-maximal DNA binding. In this case, the trend suggests a strong charge effect, with TriplatinNC$^{8+}$ and $[Co(NH_3)_6]^{3+}$ showing the highest relative affinities. The (smaller) one to 2-fold changes for the lower-charged species may reflect inherently stronger binding to DNA rather than a diminished heparin affinity, as can be seen in indirect MB and TAMRA-$R_9$ assays (Table 3.1).

Because previous studies demonstrated $[Pt(NH_3)_4]^{2+}$- and $[Co(NH_3)_6]^{3+}$-induced DNA conformational change using CD,(53,54) we employed this method to observe metal–ammine compound binding to DNA and then the effects of the addition of heparin observed by the return of the DNA conformation. The potential covalent metal–ammine compounds (up to a concentration of 500 μM) did not change the DNA conformation at 280 nm, indicating little interaction, even in comparison to the square-planar $[Pt(NH_3)_4]^{2+}$ (data not shown).

For EtBr competition assay, at a concentration identical with that of the intercalator, a much larger concentration of 500 μM was needed for the mononuclear metal–ammine compounds to displace the EtBr compared to TriplatinNC (12.5 μM; Table 3.5 and Figure 3.12). Care must be taken in analyzing these trends across a range of compounds because the inherent affinities of the compounds themselves for DNA as a starting point differ widely. Further, the different assays themselves represent different phenomena. The dangers in extrapolating across a series such as the one studied here is demonstrated for $[Pt(NH_3)_4]^{2+}$, which has demonstrably low affinity for DNA.(55) In principle, charge effects (2+) should be the same as those for the $[CoCl(NH_3)_5]^{2+}$ and $[RuCl(NH_3)_5]^{2+}$ compounds, as seen in fluorescence polarization assay (Table 3.3 and Figure 3.8). An apparently higher affinity for heparin in EtBr assay compared to fluorescence polarization



www.manaraa.com

| metal complex | $EC_{50}$ (μM) |
|---|---|
| TriplatinNC$^{8+}$ | 24.6 ± 1.4 |
| $[Pt(NH_3)_4]^{2+}$ | <100 |
| $[Co(NH_3)_6]^{3+}$ | 689 ± 17 |
| $[Ru(NH_3)_6]^{3+}$ | 853 ± 186 |
| $[RuCl(NH_3)_5]^{2+}$ | >1000 |
| $[CoCl(NH_3)_5]^{2+}$ | >1000 |

Table 3.5. EtBr Competition Assay for Comparison of Metal–Ammine Binding to DNA and Heparin

[a]$EC_{50}$ is defined as the sequestration concentration of heparin MW ~18000 required to return 50% EtBr binding to DNA from the bound metal–ammine compound. EtBr bound to DNA was normalized to 100%, with EtBr only as 0%.

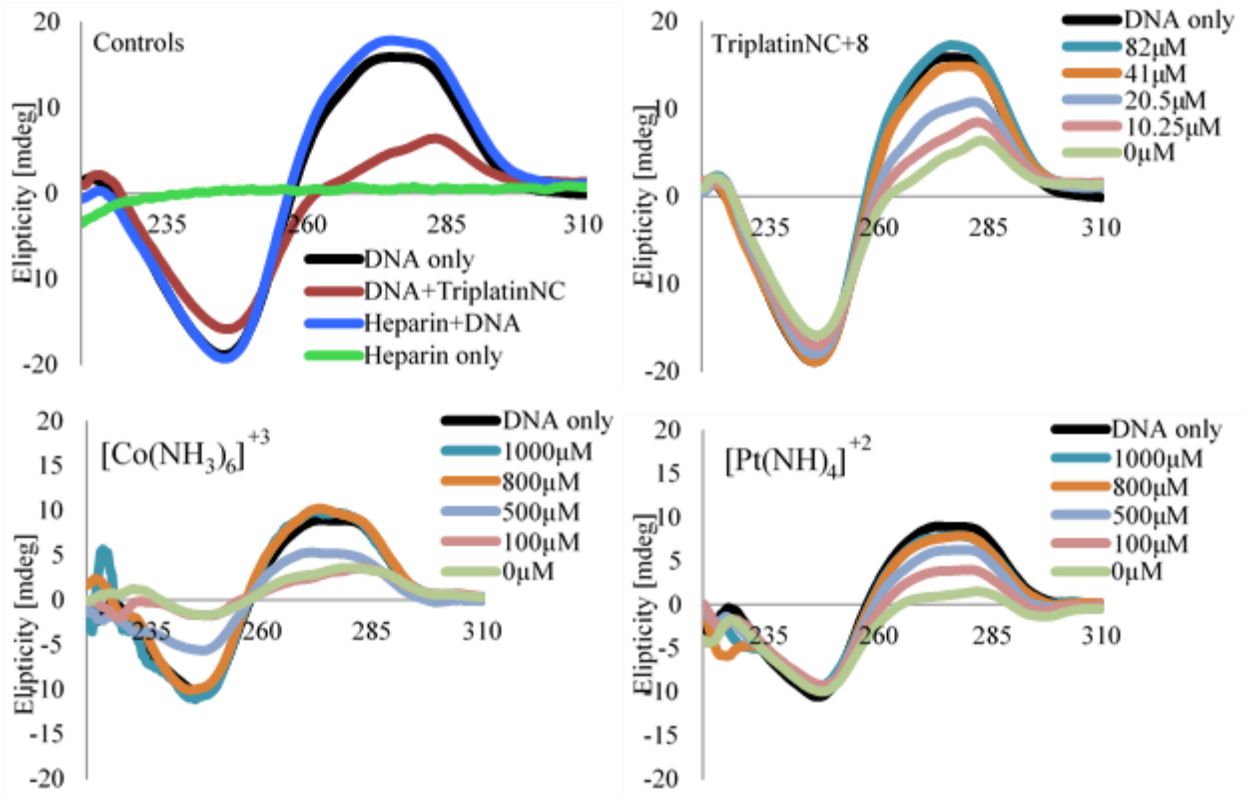


Figure 3.9. CD spectra of ct-DNA in presence and absence of heparin and metal-ammine compounds (0-82μM for TriplatinNC, and 0-1000μM for metal-ammines, MW 18000). DNA-compound conformation (measured by the 280nm absorbance specific for ct-DNA) is restored upon increasing heparin concentrations. HEPES buffer effects are observed below 230nm for DNA.



www.manaraa.com

assay may reflect its reduced ability to displace the intercalator, perhaps because of its smaller square-planar geometry versus the octahedral geometry of the cobalt and ruthenium systems, giving an apparently (but false) higher heparin affinity. This anomaly emphasizes the need to employ more than one approach to assess accurately the questions of relative affinity of heparin and DNA for coordination compounds.

**Summary**

We observed broadly similar trends for metal–ammine compound interaction with heparin across the dye reporter techniques and DNA comparison assays. Slight discrepancies can be accounted for by the nature of the technique. Another caveat is the complexity across the experiments where the ITC system is a simple two-species system, heparin–dye reporter assays are three-species system, and DNA comparison assays are four-species systems. Given these caveats, these results are a testament to the relative accuracy of these methods for determining trends of coordination compound interaction with heparin.

### 3.4 Conclusions:

Overall, oligosaccharide interactions with metal-based compounds are understudied in bioinorganic chemistry. Molecular crowding in the interior of the cell breeds an environment in which molecules must compete with each other,(56) and small molecules such as cisplatin may encounter many possible binding partners, affecting biodistribution and metabolism, a reflection perhaps of the accepted fact that such a small fraction (<5%) of administered drug is considered to bind to its DNA target.(24) The overall results discussed here suggest comparable affinities for heparin relative to DNA for charged substitution-inert coordination compounds, regardless of their intrinsic nucleic acid affinity. This comparison should be capable of extrapolation to glycosoaminoglycans such as HS. The presence of HS on the cell surface and its relatively similar affinity to DNA would suggest that glycan binding is thus a competitive cellular event for many coordination compounds.(21) These results extend our understanding of the importance of the



www.manaraa.com

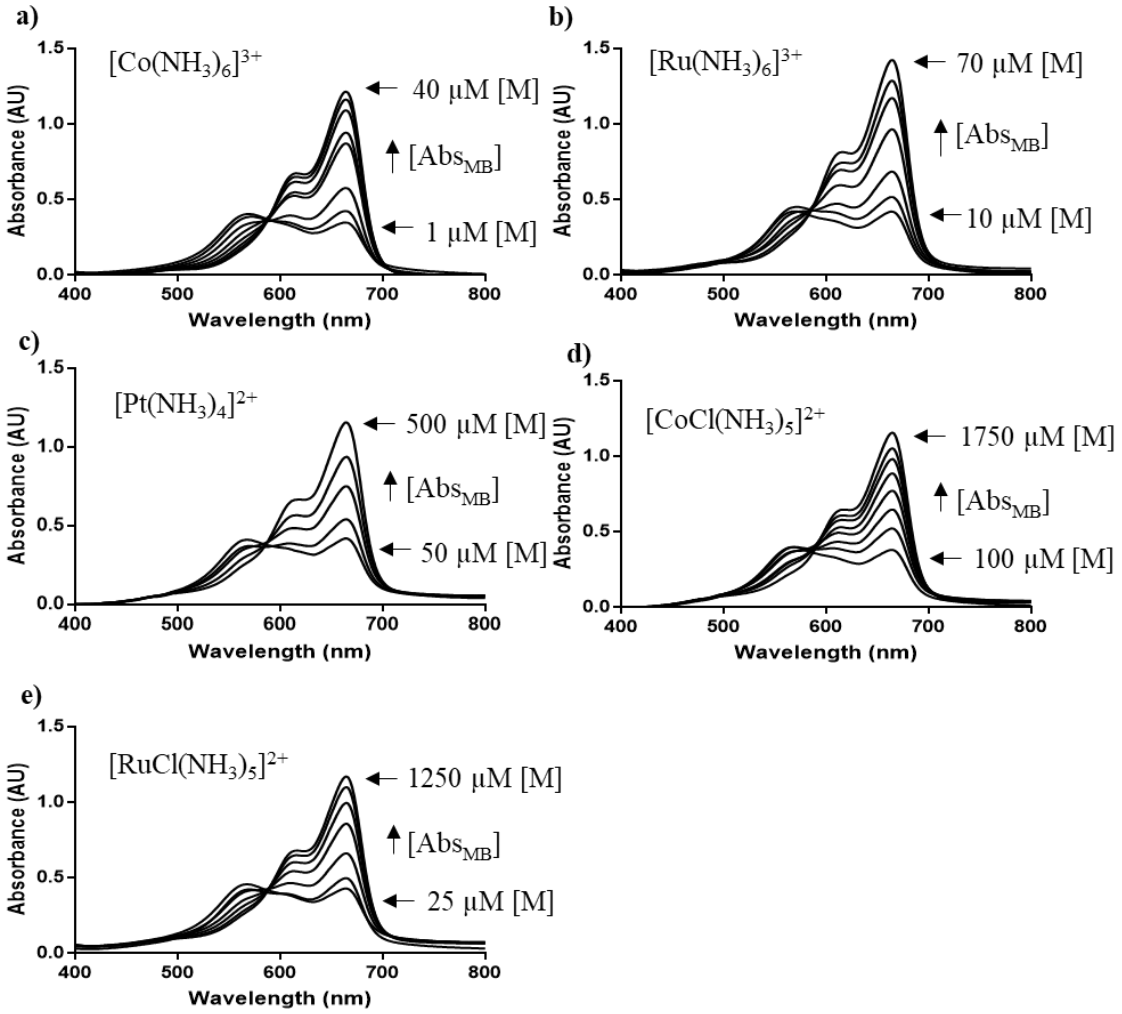


Figure 3.10. Metal-ammine compounds inhibit methylene blue from binding to heparin. Concentrations for metal-ammines were the following from top to bottom at 664 nm with highest and lowest concentrations shown: (a) $[Co(NH_3)_6]^{3+}$ 40, 35, 30, 25, 20, 15, and 1 µM; (b) $[Ru(NH_3)_6]^{3+}$ 70, 60, 50, 40, 30, 20, and 10 µM; (c) $[Pt(NH_3)_4]^{2+}$ 500, 375, 250, 100 and 50 µM; (d) $[CoCl(NH_3)_5]^{2+}$ 1250, 1000, 750, 500, 250, and 100 µM; (e) $[RuCl(NH_3)_5]^{2+}$ 1750, 1500, 1250, 1000, 750, 500, 250, 100, and 25 µM.



www.manaraa.com

interactions of physiologically relevant aquated metal cations with heparin to defined coordination compounds. The available coordinating moieties on HS–heparin are the oxygen-donor atoms of the hard carboxylate and sulfate bases. New patterns of metal-ion binding can be achieved by the interplay and application of hard–soft acid–base concepts. Further, in considering the concept of metalloglycomics, a phrase first coined by Codd,(57) coordination compounds can be manipulated to modify the oxidation state, ligand lability, and coordination number and geometry to produce a diverse inorganic library.

### 3.5 Experimental:

#### Materials

Heparin sodium salts from porcine intestinal mucosa of MW 3000 and 18000, pentaamminechlorocobalt(III) chloride, hexaammineruthenium(III) chloride, and hexaamminecobalt(III) chloride were purchased from Sigma-Aldrich (USA). Pentaamminechlororuthenium(III) chloride was purchased from Aithace Chemical Corp. (USA). TAMRA-$R_9$ and methylene blue chloride were purchased from Anaspec (USA) and Fisher Scientific (USA), respectively. TriplatinNC and tetraammineplatinum(II) chloride were synthesized according to published methods from refs (58) and (59), respectively. The concentrations of heparin were calculated using the dimer IdoA(2S)–GlcNS(6S) with a molecular weight of 609.46 g/mol unless otherwise noted.

#### MB Binding Assay

All heparin–MB binding studies were performed in triplicate on an Agilent 8453 diode-array spectrophotometer in a submicrometer quartz cuvette with a path length of 10 mm. Aqueous solutions of methylene blue chloride (at a constant final concentration of 18.6 μM) and heparin MW 18000 (1–25 μM) were prepared for determination of the optimal heparin–MB binding. A final concentration of 15 μM heparin was used for evaluating the inhibition of MB binding by



www.manaraa.com

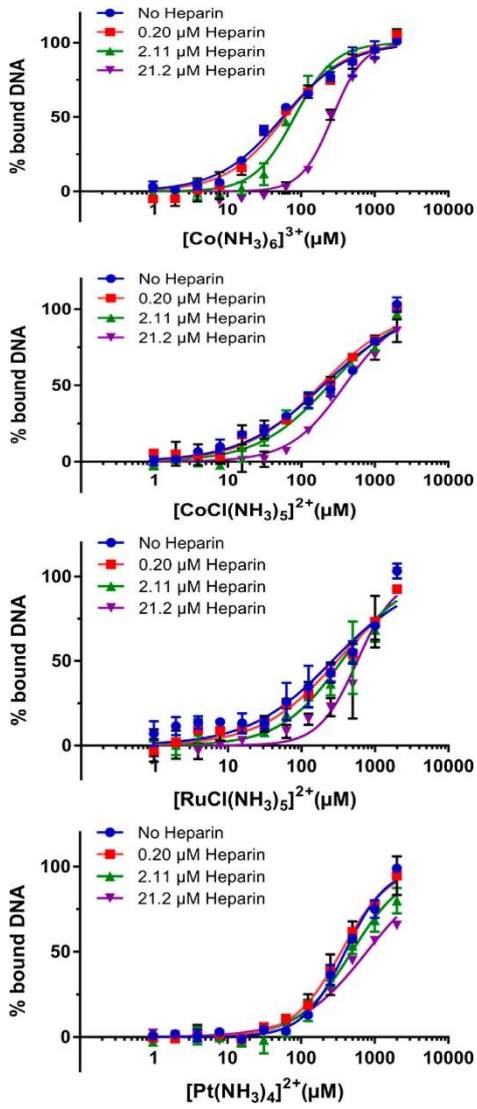


Figure 3.11. Heparin, a competitor for DNA binding to metal–ammine compounds. The binding of metal–ammine compounds to fluorescently labeled DNA is reduced upon the addition of MW ~3000 heparin (0–21.2 μM).



www.manaraa.com

TriplatinNC (1–5 μM), whereas the metal–ammine compounds were studied at the higher 1 μM to 1.75 mM range. The heparin and metal complexes were incubated at room temperature for 15 min before the addition of methylene blue chloride. Aqueous solutions of methylene blue chloride (at a constant final concentration of 18.6 μM), heparin (MW 18000; at a constant final concentration of 15 μM), and TriplatinNC (at a constant final concentration of 5 μM) were used to evaluate the inhibition of TriplatinNC–heparin binding by physiological relevant concentrations of cations (sodium chloride, 50, 100, and 150 mM; potassium chloride, 5 mM; calcium chloride, 1.3 mM; magnesium chloride, 1 mM).

**TAMRA-$R_9$ Binding Assay**

All heparin–TAMRA-$R_9$ binding studies were carried out in triplicate. Solutions of TAMRA-$R_9$ (100 nM) and heparin 18000 MW (3 μM to 10 mM) in cacodylate buffer (200 mM, pH 7.4) were prepared to determine the heparin concentration for optimal fluorescence. Heparin (625 μM) and metal–ammine compounds (in the range 7.8 μM to 2.5 mM) were incubated for 15 min at room temperature for compound–heparin binding before the addition of TAMRA-$R_9$ (100 nM) and measurement of the fluorescence.

**SPR**

Binding experiments were carried out at 25 °C on a Reichert Technologies (Depew, NY) SR7500DC two-channel system equipped with a Neutravidin-coated mSAM sensor chip (Reichert Technologies, part 13306065) using 10 mM 4-(2-hydroxyethyl)-1-piperazineethanesulfonic acid (HEPES), 150 mM NaCl, and 0.005% Tween-20 (HBST) as the running buffer. Prior to heparin capture, the Neutravidin-coated mSAM sensor chip was preconditioned with three consecutive injections of 50 mM NaOH for 1 min, respectively. Biotinylated heparin (MW ~15000, Sigma) at a concentration of 100 μg/mL was subsequently injected onto the avidin surface on the left channel and captured to a level of 110 μRIU (~110 RU), whereas the right channel was left as the bare avidin surface to serve as a reference for nonspecific binding of TriplatinNC. Under a flow rate of 25 μL/min, TriplatinNC was injected over both channels at concentrations of 5, 1, 0.33, and 0.11



www.manaraa.com

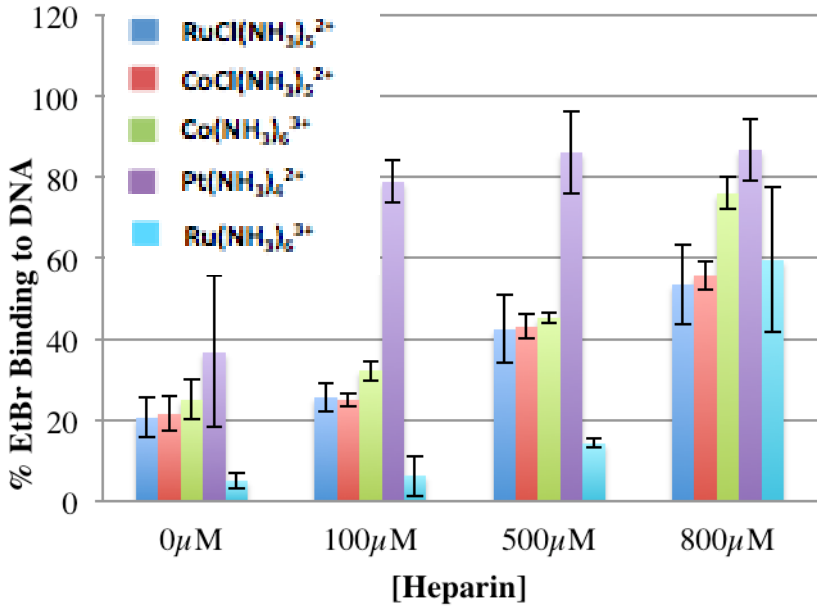


Figure 3.12. Ethidium bromide competition assay for comparison of metal-ammine compounds binding to ct-DNA and heparin (MW ~18000). EtBr displaced by metal-ammine compound-DNA binding rebinds to DNA upon the concentration-dependent sequestration of the metal-ammine compound (500 μM) by heparin. EtBr bound to DNA was normalized to 100% with EtBr only as 0%.



www.manaraa.com

mM, respectively, for 2 min followed by a 5 min dissociation in a HBST running buffer. The kinetic data were analyzed using *TraceDrawer* (Ridgeview Instruments) with a 1:1 model, while the equilibrium data were fit using Scrubber (Biologic Software) to a 1:1 binding model.

**ITC**

Calorimetric data were collected using a VP-ITC microcalorimeter (MicroCal, LLC). All samples were degassed for 5 min using a ThermoVac (MicroCal, LLC). For all titrations, injections of TriplatinNC and metal–ammine compounds (0.546 and 4 mM, respectively) were pipetted automatically into the reaction cell containing 1.3 mL of heparin MW 3000 (0.1 and 0.4 mM) at 300 s intervals from a 300 μL syringe with stirring at 75 rpm. In all experiments, a 100 mM cacodylate buffer (pH 7.4) was used at 25 °C, and the thermal reference cell contained 1.3 mL of 100 mM cacodylate buffer (pH 7.4). Integration of the thermogram peaks was carried out using the software supplied with the calorimeter (*Origin 7.0*). The heat released was fitted using *Origin 7.0* to determine $K_a$, $\Delta H$, and $\Delta S$. $\Delta G$ was obtained using Gibbs free energy equation.

**Fluorescence Polarization**

50 μL binding reactions were carried out at room temperature in 96-well, low-binding, black plates (Greiner) using 100 nM to 25 μM of each compound in 1.25 mM NaCl, 0.125 mM HEPES (pH 7.2), and 1 μM 3′ fluorescein-labeled hairpin DNA (GGGGCGACTGGTGAGTACGCCCC; MW = 7705; Sigma). Readings were recorded immediately after mixing (for no competitor readings). Subsequently, 1 μL of 10 μM heparin (MW = approximately 3000; Sigma) was titrated into each reaction. Readings were recorded immediately. This was followed by titrations of 1 μL of 100 μM heparin and then 1 μL of 1 mM heparin, with immediate readings after each addition. The $EC_{50}$calculation was based on the average of three separate experiments.

**Ethidium Bromide (EtBr) Displacement Assay with Heparin**

Calf-thymus DNA (ct-DNA) was dissolved and dialyzed in HEPES buffer (80 mM HEPES, pH 7.2). Buffer exchanges occurred three times every 12 h. The DNA concentration was determined by UV–vis with absorbance at 260 nm and the average molecular weight of a nucleotide (333



www.manaraa.com

g/mol). EtBr at 5 mM in water was diluted in HEPES buffer and incubated with ct-DNA in HEPES buffer for 5 min at room temperature. An aliquot of 1 mM TriplatinNC (4 mM for other compounds) in water was diluted in HEPES buffer and incubated for 1 h to reduce fluorescence to approximately 30% (20–25% for other compounds). Finally, increasing concentrations of heparin MW 18000 in buffer from 20.5 to 82 μM final (100–1000 μM final for other compounds) were incubated for an additional 1 h. Final concentrations were the following: EtBr, 12.5 μM; ct-DNA, 10 μM; TriplatinNC, 12.5 μM (500 μM for other compounds). All samples were read (after a total of 2 h 5 min) in a 96-well plate at 530/590 nm using a microplate reader (Bio-Tek instruments). Samples were normalized to the controls (EtBr only as 0% and EtBr–DNA as 100%). All incubations were done at 37 °C.

**CD Studies**

TriplatinNC ($r_i$ = 0.075 compound/DNA ratio) or metal–ammine compounds ($r_i$ = 5) were incubated with 100 μM ct-DNA for 1 h at 37 °C in HEPES buffer (80 mM HEPES, pH 7.2). Then heparin MW ~18000 was added with 10.25–230 μM final concentrations (only 10.25–82 μM are shown) and incubated for an additional 1 h at 37 °C. Final concentrations after heparin addition were the following: 100 μM ct-DNA and 7.5 μM TriplatinNC ($r_i$ = 0.075) or 500 μM ($r_i$ = 5). After the incubations, samples were placed in a 10 mm submicro cuvette to record the CD spectra at room temperature using a Jasco J600 spectropolarimeter.

**3.6 Acknowledgements:**

The authors gratefully acknowledge Eric Ginsburg for synthesizing tetraammineplatinum(II) chloride and Daniel Lee for synthesizing TriplatinNC. This research was supported, in part, by Grant NIH RO1CA78754. This project has been partly supported by pilot funding from the Massey Cancer Center, VCU, with funding, in part, from NIH–NCI Cancer Center Support Grant P30 CA016059.



www.manaraa.com

**3.7 References:**


1. A. Varki, R. D. Cummings, J. D. Esko, H. H. Freeze, P. Stanley, C. R. Bertozzi, G. W. Hart, M. Etzler..*Essentials of Glycobiology*, 2nd ed.; Cold Spring Harbor Laboratory Press: Cold Spring Harbor, NY, **2009**.
2. R. D. Cummings, J. M. Pierce. *Chem. Biol.* **2014**, *21*, 1– 15.
3. I. Capila, R. J. Linhardt, *Angew. Chem. Int. Ed.* **2002**, 41, 390–412; *Angew. Chem.* **2002**, 114, 426–450.
4. D. E. Humphries, G. W. Wong, D. S. Friend, M. F. Gurish, W. T. Qiu, C. Huang, A. H. Sharpe, R. L. Stevens. *Nature* **1999**,*400*, 769– 772.
5. M. C. Z. Meneghetti, A. J. Hughes, T. R. Rudd, H. B. Nader, A. K. Powell, E. A. Yates, M. A. Lima. *J. R. Soc., Interface* **2015**, 12, 20150589.
6. P. Chiodelli, A. Bugatti, C. Urbinati, M. Rusnati. *Molecules* **2015**, *20*, 6342–6388.
7. D. Xu, J. D. Esko. *Annu. Rev. Biochem*. **2014**, 83, 129−57.
8. J. E. Hudak, C. R. Bertozzi. *Chem. Biol.* **2014**, *21*, 16– 37.
9. L. Jia, S. Ma. *Eur. J. Med. Chem.* **2016**, *121*, 209– 220.
10. I. Vlodavsky, Y. Friedmann, M. Elkin, H. Aingorn, R. Atzmon, R. Ishai-Michaeli, M. Bitan, O. Pappo, T. Peretz, I. Michal, L. Spector, I. Pecker. *Nat. Med.* **1999**, *5*, 793– 802.
11. L. Baraz, Y. Haupt, M. Elkin, T. Peretz, I. Vlodavsky. *Oncogene* **2006**, *25*, 3939– 3947.
12. C. Pisano, I. Vlodavsky, N. Ilan, F. Zunino, *Biochem. Pharmacol.* **2014**, 89, 12–19.
13. F. Zhang, X. Liang, J. M. Beaudet, Y. Lee, R. J. Linhardt. *J. Biom. Technol. Res.* **2014**, *1*, 6000101.
14. Y. Seo, M. R. Schenauer, J. A. Leary. *Int. J. Mass Spectrom.* **2011**, *303*, 191– 198.
15. I. Stevic, N. Parmar, N. Paredes, L.R. Berry, A. K. C. Chan. *Cell Biochem. Biophys.* **2011**, *59*, 171– 178.
16. C. Shao, F. Zhang, M. M. Kemp, R. J. Linhardt, D. M. Waisman, J. F. Head, B. Seaton. *J. Biol. Chem.* **2006**, *281*,31689– 31695.
17. H. Xie, Y. J. Kang. *Curr. Med. Chem.* **2009**,*16*, 1304– 1314.
18. L. D. D'Andrea, A. Romanelli, R. Di Stasi, C. Pedone. *Dalt. Trans*.**2010**, *39*, 7625– 7636.
19. T. R. Rudd, M. A. Skidmore, S. E. Guimond, M. Guerrini, C. Cosentino, R. Edge, A. Brown, D. T. Clarke, G. Torri, J. E. Turnbull, R. J. Nichols, D. G. Fernig, E. A. Yates. *Carbohydr. Res.* **2008**, *343*, 2184– 2193.




www.manaraa.com

20. K. W. Hung, T. K. S. Kumar, K. M. Kathir, P. Xu, F. Ni, H. H. Ji, M. C. Chen, C. C. Yang, F. P. Lin, I. M. Chiu, C. Yu. *Biochemistry* **2005**, *44*, 15787– 15798.

21. H. Silva, F. Frézard, E. J. Peterson, P. Kabolizadeh, J. J. Ryan, N. P. Farrell. *Mol. Pharmaceutics* **2012**, *9*, 1795– 1802.

22. E. J. Peterson, A. G. Daniel, S. J. Katner, L. Bohlmann, C. W. Chang, A. Bezos, C. R. Parish, M. von Itzstein, S. J. Berners-Price, N. P. Farrell. *Chem. Sci.* **2017**, 8, 241−252.

23. J. B. Mangrum, B. J. Engelmann, E. J. Peterson, J. J. Ryan, S. J. Berners-Price, N. P. Farrell. *Chem. Commun.* **2014**, 50, 4056−4058.

24. N. P. Farrell. *Chem. Soc. Rev*. **2015**, 44, 8773−8785.

25. S. J. Katner, E. J. Petson, E. Katsuta, S. C. DeMasi, J. Koblinski, K. Takabe, N. P. Farrell. *Proceedings of the AACR*, Washington, DC, 2017; Abstract 17.

26. E. Katsuta, E. J. Peterson, S. J. Katner, N. P. Farrell, K. Takabe. *Proceedings of the AACR*, Washington, DC, 2017; Abstract 5117.

27. L. N. Waller, N. Fox, K. F. Fox, A. Fox, R. L. Price. *J. Microbiol. Methods* **2004**, *58*, 23– 30.

28. G. I. Rozenberg, J. Espada, L. L. de Cidre, A. M. Eijan, J .C. Calvo, G. E. Bertolesi. *Electrophoresis* **2001**, *22*, 3– 11.

29. T. T. Cheng, J. L. Yao, X. Gao, W. Sun, S. Shi, T. M. Yao. *Analyst* **2013**, *138*, 3483– 3489.

30. Q. C. Jiao, Q. Liu, C. Sun, H. He. *Talanta* **1999**, *48*, 1095– 1101.

31. L. Tan, S. Yao, Q. Xie. *Talanta* **2007**, 71, 827−832.

32. H. Chu, N. R. Johnson, N. S. Mason, Y. A. Wang. *J. Controlled Release* **2011**, 150, 157−163.

33. L. Zhang, N. Li, F. Zhao, K. Li. *Anal. Sci*. **2004**, 20, 445−450.

34. K. Hibino, Y. Yoshikawa, S. Murata, T. Saito, A. A. Zinchenko, K. Yoshikawa. *Chem. Phys. Lett.* **2006**, *426*, 405– 409.

35. J. Malina, N. P. Farrell, V. Brabec. *Angew. Chem., Int. Ed.* **2014**, *53*, 12812–12816.

36. J. Malina, N. P. Farrell, V. Brabec. *Inorg. Chem.* **2014**, *53*, 1662– 1671.

37. S. M. Fuchs, R. T. Raines, *Biochemistry* **2004**, 43, 2438–2444.

38. X. Du, Y. Li, Y. L. Xia, S. M. Ai, J. Liang, P. Sang, X. L. Ji, S. Q. Liu. *Int. J. Mol. Sci.* **2016**, *17*, 144.

39. K. Gaus, E. A. H. Hall. *J. Colloid Interface Sci.* **1997**,*194*, 373– 378.



www.manaraa.com

40. R. I. W. Osmond, W. C. Kett, S. E. Skett, D. R. Coombe. *Anal. Biochem.* **2002**, *310*, 199– 207.

41. S. Cochran, C. P. Li, V. Ferro. *Glycoconjugate J.* **2009**, *26*, 577– 587.

42. S. Leavitt, E. Freire. *Curr. Opin. Struct. Biol.* **2001**, 11, 560–566.

43. A. K. Dutta, J. Rosgen, K. Rajarathnam. *Methods Mol. Biol.* **2015**, *1229*,315– 324.

44. M. W. Pantoliano, R. A. Horlick, B. A. Springer, D. E. Van Dyk, T. Tobery, D. R. Wetmore, J. D. Lear, A. T. Nahapetian, J. D. Bradley, W. P. Sisk. *Biochemistry* **1994**, *33*, 10229– 10248.

45. A. Brown, C. J. Robinson, J. T. Gallagher, T. L. Blundell. *Biophys. J.* **2013**, 104, 1720–1730.

46. A. Brown. *Int. J. Mol. Sci.* **2009**, *10*, 3457–3477.

47. A. K. Powell, E. A. Yates, D. G. Fernig, J. E. Turnbull. Glycobiology **2004**, 14, 17R–30R.

48. A. Prisecaru, Z. Molphy, R. G. Kipping, E. J. Peterson, Y. Qu, A. Kellett, N. P. Farrell. *Nucleic Acids Res.* **2014**, *42*, 13474– 13487.

49. T. Biver. *Coord. Chem. Rev.* **2013**, *257*, 2765– 2783.

50. D. Bharanidharan, S. Thiyagarajan, N. Gautham. *Acta Crystallogr., Sect. F: Struct. Biol. Cryst. Commun.* **2007**, *63*, 1008– 1013.

51. E. Tselepi-Kalouli, N. Katsaros. *J. Inorg. Biochem.* **1989**, *37*, 271– 282.

52. D. Matulis, I. Rouzina, V. A. Bloomfield. *J. Mol. Biol.* **2000**, *296*, 1053– 1063.

53. H. Deng, V. A. Bloomfield. *Biophys. J.* **1999**, *77*, 1556– 1561.

54. B. I. Kankia, V. Buckin, V. A. Bloomfield. *Nucleic Acids Res.* **2001**, *29*, 2795– 2801.

55. N. Carte, F. Legendre, E. Leize, N. Potier, F. Reeder, J. C. Chottard, A. Van Dorsselaer. *Anal. Biochem.* **2000**, *284*, 77–86.

56. S. R. McGuffee, A. H. Elcock. *PLoS Comput. Biol.* **2010**, *6*, e1000694.

57. R. Codd. *Chem. Commun.* **2004**, 2653– 2655.

58. A. L. Harris, X. Yang, A. Hegmans, L. Povirk, J. J. Ryan, L. Kelland, N. P. Farrell. *Inorg. Chem.* **2005**, *44*, 9598– 9600.

59. G. B. Kauffman, D. O. Cowan. In *Inorganic Synthesis*; J. Klienberg. Eds.; McGraw-Hill Book Co., Inc.: New York, **1963**; Vol. 7, Chapter 63, pp 239– 245.



www.manaraa.com

www.manaraa.com

This work to be published with the following contributions:

HPSE cleavage by Erica Peterson and David Hampton.

**Chapter 4: Cobalt Complexes Interactions with the HS Mimetic Fondaparinux and Their Dual Therapeutic Potential.**

**Wyatt E. Johnson, J. David Hampton, Erica J. Peterson, James F. Beaton, and Nicholas P. Farrell**



www.manaraa.com

## 4.1 Abstract

Spectroscopic and biophysical approaches were developed to examine the affinity and stoichiometry of simple cobalt complexes for Fondaparinux (FPX) as a model for Heparan Sulfate (HS). HSs play vital roles in both cancer cell proliferation, angiogenesis, metastasis, and differentiation; and viral particle attachment. Cobalt containing complexes, like CTC-96, were shown to inhibit Herpes Simplex Virus 1 replication through HS binding, and this work extends FPX binding to these simple cobalt complexes. Cobalt complexes are competitive inhibitors of methylene blue (MB)–FPX binding, and the change in absorbance of the dye in the presence or absence of sulfated FPX was used as an indirect reporter of cobalt-FPX affinity. The dissociation constant ($K_d$) was also directly measured using Isothermal Titration Calorimetry (ITC). Stoichiometry and sulfate protection was determined using electrospray ionization mass spectrometry (ESI-MS). Cleavage of HS by the enzyme heparanase also modulates tumor angiogenesis, cell invasion, and metastasis. Metalloshielding of HS cleavage by these cobalt complexes will effectively inhibit tumor-related events. Studies using P. heparinus heparanase I showed that these cobalt complexes inhibit the cleavage activity of the enzyme. These results will further the understanding of the metalloglycomics concept into the third important class of biomolecules from the well-studied protein and DNA/RNA and their interactions.

## 4.2 Introduction

Proteoglycans containing Heparan Sulfate (HS), a sulfated glycosaminoglycan, play a major role in the cell signaling process, adhesion and migration.(1,2) Heparan sulfate proteoglycans (HSPGs) are HSs conjugated with proteins and can be found on the cell surface or in the extracellular matrix.(1,2) HSPGs are over-expressed on the surface of many cancer cells.(3,4) The sulfate residues on HS are the recognition site for many different protein substrates including pro-angiogenic growth factors, similar to the phosphate clamp-arginine fork motif.(5-10) Fibroblast



www.manaraa.com

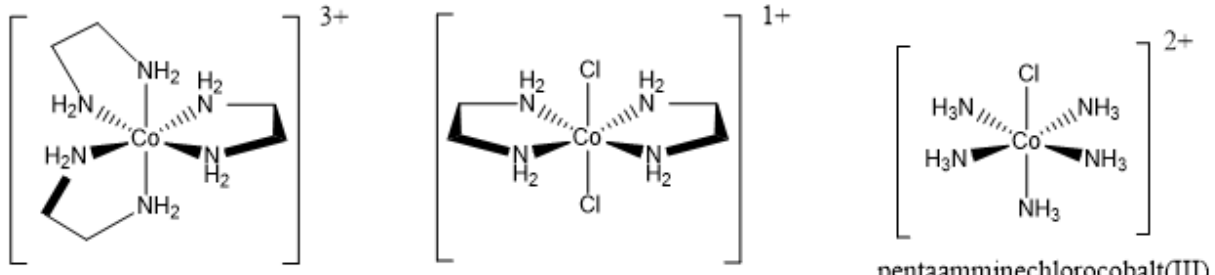


Figure 4.1. Structures of cobalt complexes used. Counterions are omitted for clarity.

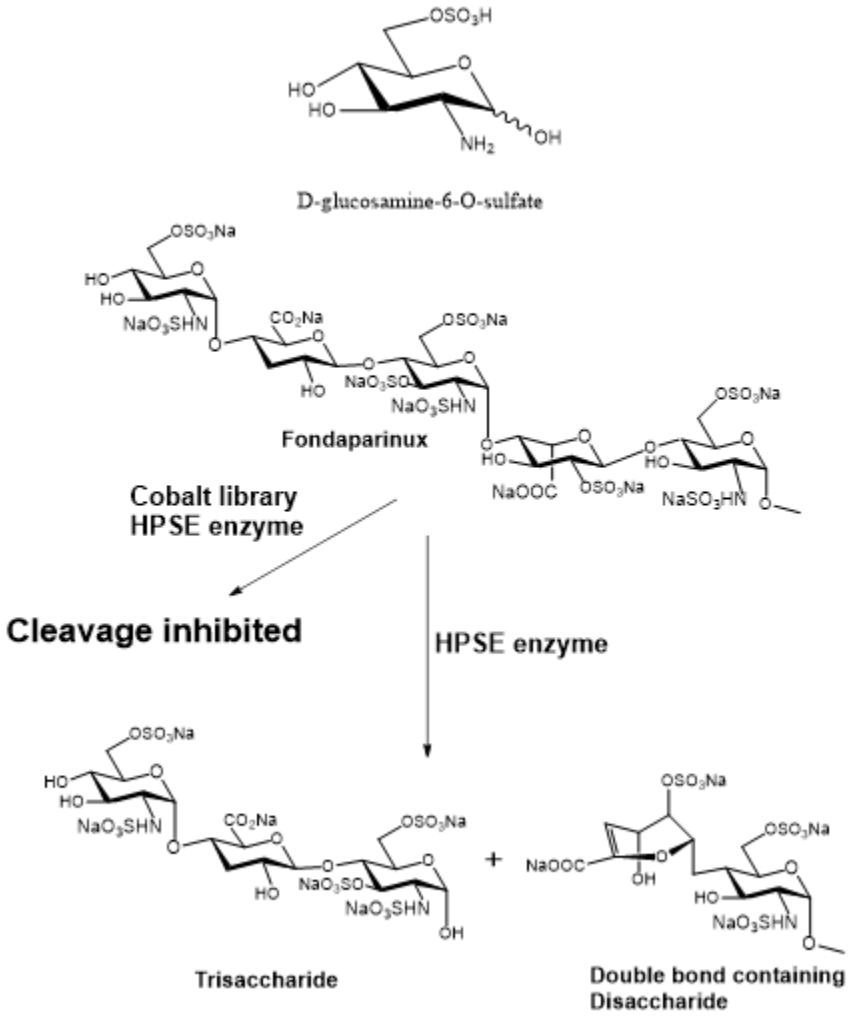


Figure 4.2. Structures of D-Glucosamine-6-O-sulfate, Fondaparinux, and cleavage products by P. *heparinum heparinase I*. In the presence of cobalt complexes, cleavage was inhibited.



www.manaraa.com

growth factors (FGF) directly stimulates the cancer cell's growth, metastasis and survival.(6) Enzymatic cleavage of HSPG at the glycosidic linkages by heparanase (HPSE) causes release of angiogenic growth factors initiating the angiogenic cascade.(11-13) HPSE is also over-expressed in tumors with significant correlation between metastatic potential and heparanase activity.(14) Furthermore, HS plays a vital role in the attachment of viral envelope glycoproteins to the cell surface.(15) Viral particles attach to HS by their glycoproteins causing subsequent interactions with specific cell entry receptors leading to viral cell replication.(15) Cobalt containing complexes binding HS has been shown to disrupt synthesis of viral structural proteins.(15) HS is thus an attractive drug target to inhibit tumor cell progression and viral replication. We have shown that "metalloshielding" or sulfate cluster masking of HS by metal complexes protect HS from enzymatic cleavage by the mammalian heparanase, prevents growth factors from binding to HS and/or prevents release of bound growth factors.(6, 7) We hypothesize that such binding by cobalt complexes may also act at the point of viral entry; preventing viral particle attachment and thus inhibiting the replication of the viral cells.

In order to determine the importance of structure-activity relationship on the "metalloshielding" potential of the metal complex library, affinity and cleavage inhibition studies were performed on Fondaparinux, as a model HS-like substrate. Fondaparinux is a well-defined, octasulfated pentasaccharide with a single point of cleavage for both bacterial and human HPSE.(11,13) We have previously presented spectroscopic and biophysical approaches to examine the affinity of metal−ammine coordination complexes for heparin.(16) Metal−ammine compounds are competitive binders to heparin. Results have shown that simple cobalt compounds bind with relatively high affinity, even greater than that of the simple platinum compound, tetraammineplatinum(II).(16) To further explore the less cytotoxic cobalt, as compared to platinum, and its interactions with HS, the differences between covalent and non-covalent interactions will be examined. New patterns of cobalt-heparin binding can be achieved by the application of hard–soft acid–base concepts.



www.manaraa.com

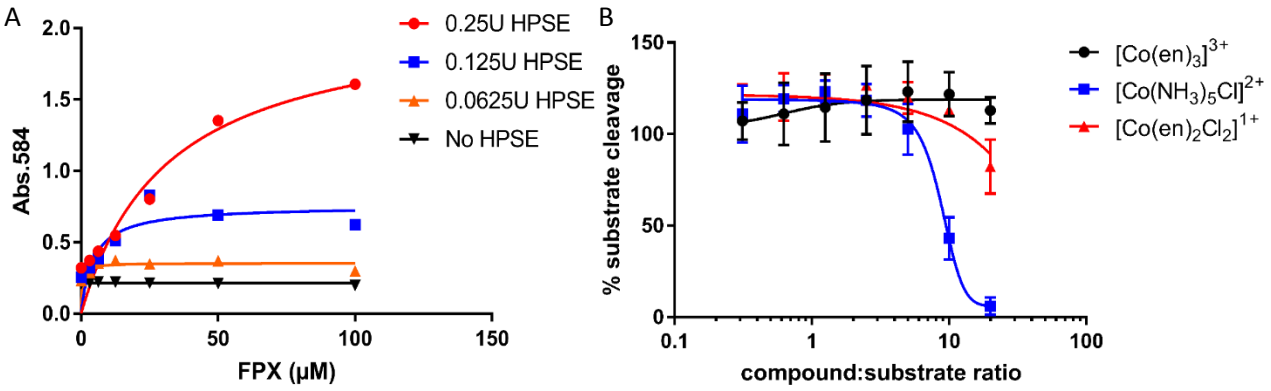


Figure 4.3. A) Fondaparinux cleavage by heparinase I. B) Pentamminechlorocobalt (III) inhibits heparinase I cleavage of fondaparinux more effectively than t-dichlorobis(ethylenediamine)cobalt (III) or tris(ethylenediamine)cobalt (III).

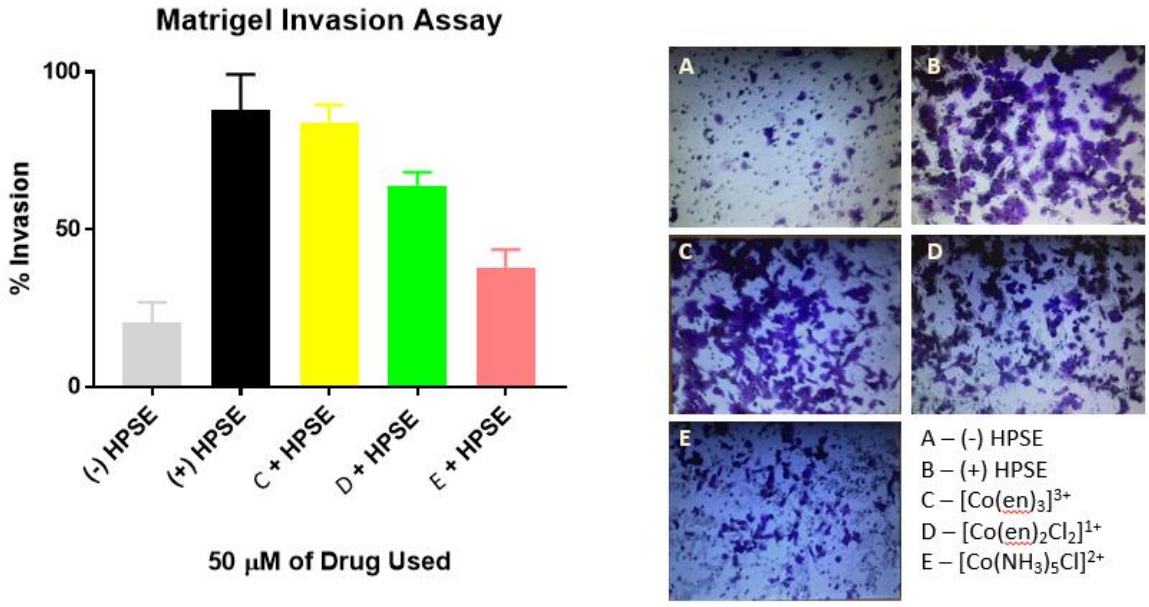


Figure 4.4. Pentamminechlorocobalt (III) inhibits the heparinase I induced invasion of matrigel by MDA-MB231 cells more than t-dichlorobis(ethylenediamine)cobalt(III) or tris(ethylenediamine)cobalt (III).



www.manaraa.com

To develop the structure-activity relationships, we have chosen a small library of cobalt complexes to examine the effects of covalent and non-covalent interactions on their interactions with FPX. In this paper, we describe cleavage inhibition studies in the presence/absence of the cobalt library using bacterial HPSE.(17) A competition assay using methylene blue (MB) as a reporter describes an approach to measure the affinity of each compound for FPX and compare that to a direct titration of each cobalt complex into FPX using isothermal titration calorimetry (ITC). Binding stoichiometry and type of binding to compare covalent and non-covalent interactions were examined using mass spectrometry (MS) and nuclear magnetic resonance (NMR). The overall results emphasize the importance of understanding the properties of glycan interactions with coordination complexes.

**4.3 Results and Discussion**

The library of simple cobalt compounds is shown in Figure 4.1. The compounds were chosen to study the covalent interactions between hard base oxygens on the glycan chain with the hard acid cobalt metal. These covalent interactions will also be compared to a non-covalent compound to determine strength of binding and overall stoichiometry.

The cleavage patterns for bacterial heparinase I (often used as a model for the mammalian enzyme) are shown in Figure 4.2. Colorimetric assays for enzymatic activity and inhibitor screening have been developed.(18) We therefore adapted the assay to examine the inhibitory effect of cobalt complexes on the enzymatic (heparinase) degradation of Fondaparinux. The pentasaccharide substrate was incubated with cobalt complex prior to enzyme exposure and cleavage measured versus control in absence of added complex. Inhibition of heparinase cleavage is effective for the non-covalent compound, pentaamminechlorocobalt(III), followed by the covalent t-dichlorobis(ethylenediamine)cobalt(III), Figure 4.3.

Cellular invasion through the extracellular matrix (ECM) requires degradation of the matrix by HPSE, and cell motility in response to growth factors. The ability of cobalt complexes to inhibit



www.manaraa.com

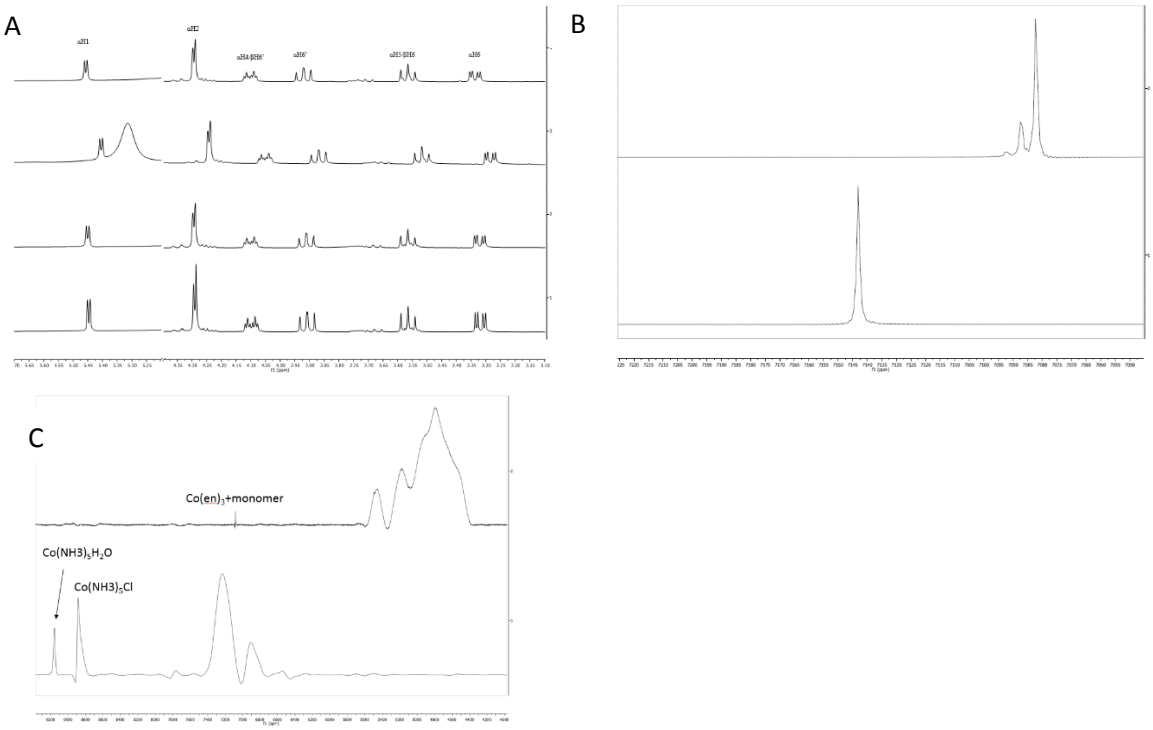


Figure 4.5. A) $^{1}H$ NMR spectra of 1:1 mixtures of D-glucosamine-6-O-sulfate and various cobalt complexes from top to bottom: tris(ethylenediamine)cobalt(III), *t*-dichlorobis(ethylenediamine)cobalt(III), pentaamminechlorocobalt(III), and D-glucosamine-6-O-sulfate. B) $^{59}Co$ NMR spectrum of tris(ethylenediamine)cobalt(III) (bottom) and 1:1 mixture of D-glucosamine-6-O-sulfate and tris(ethylenediamine)cobalt(III) (top). C) $^{59}Co$ NMR spectrum of 1:1 mixture of D-glucosamine-6-O-sulfate and *t*-dichlorobis(ethylenediamine)cobalt(III) (top) and 1:1 mixture of D-glucosamine-6-O-sulfate and pentaamminechlorocobalt(III) (bottom).

| | **Δδ = δ(monomer : Co) – δ(monomer/Co) (ppm)** | | | | | | |
|---|---|---|---|---|---|---|---|
| | **αH1** | **αH2** | **αH4/βH6'** | **αH6'** | **αH5/βH6** | **αH6** | **$^{59}$Co** |
| $[Co(en)_3]^{3+}$ | 0.010 | 0.018 | 0.000 | 0.012 | 0.004 | 0.003 | -61 |
| $[Co(en)_2Cl_2]^{1+}$ | -0.042 | -0.034 | -0.047 | -0.039 | -0.047 | -0.049 | -4164 |
| $[Co(NH_3)_5Cl]^{2+}$ | 0.004 | 0.002 | 0.001 | 0.002 | 0.002 | 0.003 | -1983 |

Table 4.1. $^{1}H$ and $^{59}Co$ chemical shift changes (Δδ = δ(monomer : Co) – δ(monomer/Co)) after incubation of Co complexes with D-glucosamine-6-O-sulfate.



www.manaraa.com

cell invasion through matrigel basement membrane was accessed using a Boyden-chamber assay.(19) Serum-starved cells were seeded into the top chamber onto a matrigel membrane with heparinase I or without (migration control). Complex was added to the top chamber in serum-free media. The bottom chamber was filled with media containing 10% serum (no drug). In Figure 4.4, pentaamminechlorocobalt(III) shows minimal cell migration at the 50 μM. The results of the two heparinase cleavage assays clearly distinguishes that the pentaamminechlorocobalt(III) exhibits the greatest inhibition of heparinase cleavage followed by t-dichlorobis(ethylenediamine)cobalt(III) with minimal inhibition by the tris(ethylenediamine)cobalt(III).

The NMR chemical shift changes of D-glucosamine-6-O-sulfate (monomer) in the presence of cobalt complexes were investigated to delineate the binding interactions. Addition of cobalt complexes shifted the protons of the monomer, Figure 4.5 A. Upon measurements performed from the freshly prepared 1:1 Co:Monomer complexed mixture, distinct shifts were observed due to fast interactions. It is readily apparent that only small downfield shifts (.000 to .018 Δppm) are observed disregarding t-dichlorobis(ethylenediamine)cobalt(III), Table 4.1. These weaker shifts are due to the non-covalent interactions produced by these cobalt complexes. However, t-dichlorobis(ethylenediamine)cobalt(III) produced shifts (-.034 to -.049 Δppm) that were at least 4 fold greater than any other cobalt complex shift. The covalent interactions produced larger shifts by coordination of the cobalt to the sulfate or any other oxygen on the monomer. Due to the lack of solubility pentaamminechlorocobalt(III) peaks did not shift considerably.

59Co NMR spectra of cobalt complexes with monomer were also obtained. Tris(ethylenediamine)cobalt(III) peak was observed similar to previously published data, Table 4.2, at 7144 ppm (literature - 7145 ppm).(20) Upon measurements performed from the freshly prepared 1:1 Co:Monomer complexed mixture, distinct shifts were observed due to fast interactions, Table 4.1. It is readily apparent that only a small upfield shift of -61 ppm, Figure 4.5 B. However, pentaamminechlorocobalt(III) and t-dichlorobis(ethylenediamine)cobalt(III) produced shifts of -1983 and -4164 ppm respectively, that were considerably greater than the non-



www.manaraa.com

| Composition* | NMR Chemical Shift | |
|---|---|---|
| | Observed | Published |
| $[Co(en_3)]$ | 7144 | 7145 |
| $[Co(NH_3)_5Cl]$ | 8885 | 8887 |
| $[Co(NH_3)_5H_2O]$ | 9155 | 9147 |
| *c*-$[Co(en_2)Cl_2]$ | 8961 | 8974 |

Table 4.2. Species detected using $^{59}Co$ NMR. *charges were omitted for clarity. Published chemical shifts were obtained from ref. 20.

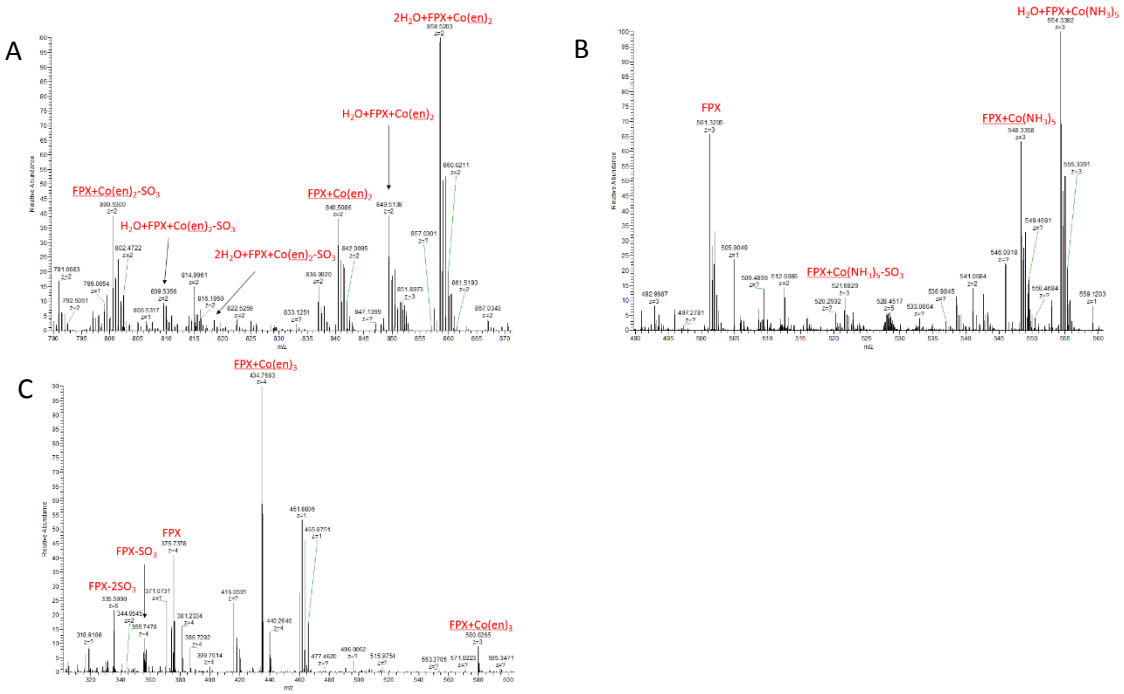


Figure 4.6. ESI-MS of 1:1 adducts of FPX and A) *t*-dichlorobis(ethylenediamine)cobalt(III) in the 2- charge state, both covalent and non-covalent interactions are observed with loss of sulfates, B) pentaamminechlorocobalt(III) in the 3- charge state, both covalent and non-covalent interactions are observed with loss of sulfate with the parent peak of FPX also observed, and C) tris(ethylenediamine)cobalt(III) in the 3- and 4- charge states. Parent peak of FPX with loss of sulfates was also observed at the 4- charge state.



www.manaraa.com

covalent cobalt complex shifts, Figure 4.5 C. The covalent interactions of the cobalt coordinating to the sulfate or any other oxygen on the monomer produced larger shifts. The pentaamminechlorocobalt(III) peak was observed at 8885 ppm (8887 ppm), while the pentaammineaquacobalt(III) was shifted downfield to 9155 ppm (9147 ppm).(20) After addition of monomer to the solution, the peak representing two monomers, one bound covalently and one bound non-covalently to the cobalt complex, is upfield shifted to 6909 ppm, while the peak representing a coordinated water with a two non-covalent monomers was observed at 7231 ppm. This 1:2 Co:monomer stoichiometry follows the trend observed in the monomer mass spectrometry data. Since the t-dichlorobis(ethylenediamine)cobalt(III) rapidly isomerizes in aqueous solutions with a greater abundance of cis being formed, we only observed the cis chloride isomer at 8961 ppm (8974 ppm). Due to the complexity of the spectra, we used tris(ethylenediamine)cobalt(III) as a standard, which agreed to the previous spectra. After addition of monomer, we again observed a similar shift of tris(ethylenediamine)cobalt(III). High symmetry complexes have narrower lines while low symmetry complexes have broader lines, cis is broader than trans, therefore all peaks are attributed to a cis geometry due to the broad nature observed.(20) Again, following the mass spectrometry data, there will be a 1:2 binding stoichiometry of Co:monomer. An upfield shift was observed at 5400 ppm attributed to c-diaquabis(ethylenediamine)cobalt(III) with 2 non-covalently bound monomers. Further upfield at 5200 ppm, a peak was observed of covalently bound water and monomer with another non-covalent bound monomer. A very broad peak was observed at 4797 ppm, which is likely due to both a bidentate bound monomer with a non-covalent bound monomer and bismonomer covalently bound.

The analysis of the NMR spectra are based largely on the chemical shifts of the peaks and the quadrupole splitting. The former measures electron density around the 1H nucleus when the chloride ligand is replaced by sulfate from the monomer. Furthermore, Co(III) chemical shifts are heavily influenced by the nephelauxetic effect in the 59Co NMR spectra.(21) This refers to a decrease in the Racah interelectronic repulsion parameter when the cobalt forms a covalent



www.manaraa.com

| Composition* | Formula | m/z (charge) | MW | |
|---|---|---|---|---|
| | | | Observed | Calculated |
| FPX+[Co($en_3$)] | $C_{37}H_{70}CoN_9O_{49}S_8$ | 434.77 (4-) | 1739.08 | 1739.04 |
| FPX+[Co($en_3$)]-$SO_3$ | $C_{37}H_{70}CoN_9O_{46}S_7$ | 414.78 (4-) | 1659.12 | 1659.08 |
| FPX+[Co($en_3$)]+Na | $C_{37}H_{69}CoN_9NaO_{49}S_8$ | 440.26 (4-) | 1761.04 | 1761.02 |
| FPX+[Co($en_3$)] | $C_{37}H71CoN_9O_{49}S_8$ | 580.03 (3-) | 1740.09 | 1740.04 |
| | | | | |
| FPX+[Co($NH_3$)$_5$] | $C_{31}H_{61}CoN_8O_{49}S_8$ | 410.99 (4-) | 1643.96 | 1643.96 |
| FPX+[Co($NH_3$)$_5$]+$H_2O$ | $C_{31}H_{63}CoN_8O_{50}S_8$ | 415.50 (4-) | 1662.00 | 1661.97 |
| FPX+[Co($NH_3$)$_5$] | $C_{31}H_{62}Co\ N_8O_{49}S_8$ | 548.34 (3-) | 1645.02 | 1644.97 |
| FPX+[Co($NH_3$)$_5$]-$SO_3$ | $C_{31}H_{62}CoN_8O_{46}S_7$ | 521.68 (3-) | 1565.04 | 1565.01 |
| FPX+[Co($NH_3$)$_5$]+$H_2O$ | $C_{31}H_{64}CoN_8O_{50}S_8$ | 554.34 (3-) | 1663.02 | 1662.98 |
| FPX+[Co($NH_3$)$_5$] | $C_{31}H_{63}Co\ N_8O_{49}S_8$ | 823.01 (2-) | 1646.02 | 1645.98 |
| FPX+[Co($NH_3$)$_5$]+$H_2O$ | $C_{31}H_{65}CoN_8O_{50}S_8$ | 832.01 (2-) | 1664.02 | 1663.99 |
| | | | | |
| FPX+[Co($en_2$)] | $C_{35}H_{63}CoN_7O_{49}S_8$ | 560.00 (3-) | 1680.00 | 1679.98 |
| FPX+[Co($en_2$)]-$SO_3$ | $C_{35}H_{63}CoN_7O_{46}S_7$ | 533.35 (3-) | 1600.05 | 1600.02 |
| FPX+[Co($en_2$)]+$H_2O$ | $C_{35}H_{65}CoN_7O_{50}S_8$ | 566.01 (3-) | 1698.03 | 1697.99 |
| FPX+[Co($en_2$)]+2$H_2O$ | $C_{35}H_{67}CoN_7O_{51}S_8$ | 571.99 (3-) | 1715.97 | 1715.99 |
| FPX+[Co($en_2$)] | $C_{35}H_{64}CoN_7O_{49}S_8$ | 840.51 (2-) | 1681.02 | 1680.98 |
| FPX+[Co($en_2$)]-$SO_3$ | $C_{35}H_{64}CoN_7O_{46}S_7$ | 800.53 (2-) | 1601.06 | 1601.03 |
| FPX+[Co($en_2$)]-2$SO_3$ | $C_{35}H_{64}CoN_7O_{43}S_6$ | 760.55 (2-) | 1521.10 | 1521.07 |
| FPX+[Co($en_2$)]-3$SO_3$ | $C_{35}H_{64}CoN_7O_{40}S_5$ | 720.57 (2-) | 1441.14 | 1441.11 |
| FPX+[Co($en_2$)]-4$SO_3$ | $C_{35}H_{64}CoN_7O_{37}S_4$ | 680.59 (2-) | 1361.18 | 1361.16 |
| FPX+[Co($en_2$)]-5$SO_3$ | $C_{35}H_{64}CoN_7O_{34}S_3$ | 640.61 (2-) | 1281.22 | 1281.20 |
| FPX+[Co($en_2$)]-6$SO_3$ | $C_{35}H_{64}CoN_7O_{31}S_2$ | 600.51 (2-) | 1201.02 | 1201.24 |
| FPX+[Co($en_2$)]+$H_2O$ | $C_{35}H_{66}CoN_7O_{50}S_8$ | 849.51 (2-) | 1699.02 | 1698.99 |
| FPX+[Co($en_2$)]+$H_2O$-$SO_3$ | $C_{35}H_{66}CoN_7O_{47}S_7$ | 809.84 (2-) | 1619.68 | 1619.04 |
| FPX+[Co($en_2$)]+2$H_2O$ | $C_{35}H_{68}CoN_7O_{51}S_8$ | 858.52 (2-) | 1717.04 | 1717.00 |
| FPX+[Co($en_2$)]+2$H_2O$-$SO_3$ | $C_{35}H_{68}CoN_7O_{48}S_7$ | 818.52 (2-) | 1637.04 | 1637.05 |
| FPX+2[Co($en_2$)] | $C_{39}H_{76}Co_2N_{11}O_{49}S_8$ | 928.25 (2-) | 1856.50 | 1856.02 |
| | | | | |
| 2Monomer+[Co($en_3$)] | $C_{18}H_{48}CoN_8O_{16}S_2$ | 755.19 (1+) | 755.19 | 755.19 |
| 2Monomer+[Co($en_2$)] | $C_{16}H_{40}CoN_6O_{16}S_2$ | 695.12 (1+) | 695.12 | 695.13 |
| Monomer+[Co($en_2$)$Cl_2$] | $C_{10}H_{28}Cl_2CoN_5O_8S$ | 507.26 (1-) | 507.26 | 507.04 |

Table 4.3. Species detected on the ESI-MS spectra. *protons and charges were omitted for clarity. FPX represent the parent Fondaparinux species and Monomer represents D-glucosamine-6-O-sulfate.



www.manaraa.com

interaction with the monomer, producing less repulsion between two electrons in a doubly occupied d-orbital.(19) This repulsion parameter likely arises from one or two causes, the effective positive charge on the metal has decreased from a negative bound ligand and/or an increase in orbital size from a covalent interaction. The latter is sensitive to the symmetry of the structural environment around the transition metal, specifically the symmetrical tris(ethylenediamine)cobalt(III) when bound to multiple monomers loses symmetry and multiple peaks are observed. The racemic $[Co(en)_3]^{3+}$ ion pairs with D-glucosamine-6-O-sulfate, resulting in the diastereomeric ion pairs having clearly distinct chemical shifts.(22) Comparison of NMR to MS gives a clear picture of binding stoichiometry between these cobalt complexes and monomer. Negative mode electrospray ionization (ESI) is commonly used for identification and analysis of heparin. We have previously shown through ESI-MS studies that FPX undergoes sulfate loss in the gas phase.(9) Analysis regarding the retention of labile sulfate groups on the heparin backbone has shown metal cations stabilize sulfate groups.(23) In the present work we examine the stoichiometry of cobalt complexes bound to FPX and their ability to protect against sulfate loss. We again compare the difference in covalent and non-covalent interactions, Table 4.3.

Peaks corresponding to a hydrogen bonding interaction between tris(ethylenediamine)cobalt(III) and FPX were observed at 434.77 m/z (4-) and 580.03 m/z (3-), Figure 4.6. Peaks were also observed corresponding to a retained sodium ion at 440.26 m/z (4-) and loss of one sulfate at 414.78 m/z (4-). The cobalt compounds may coordinate to water resulting in a noncovalent interaction, or may coordinate to the sulfates resulting in a covalent interaction since the chloride would be dissociated from the compound. Pentaamminechlorocobalt(III) and t-dichlorobis(ethylenediamine)cobalt(III) have the ability to interact both covalently and non-covalently, Figure 4.6. Covalent and non-covalent interactions were both observed for pentaamminechlorocobalt(III) at the 2-, 3-, and 4- charge states. The cobalt compounds may coordinate to water resulting in a noncovalent interaction, or may coordinate to the sulfates resulting in a covalent interaction since the chloride would be dissociated from the compound. A 1:1 binding interaction was observed covalently at 823.01 m/z (2-), 548.34 m/z (3-) along with



www.manaraa.com

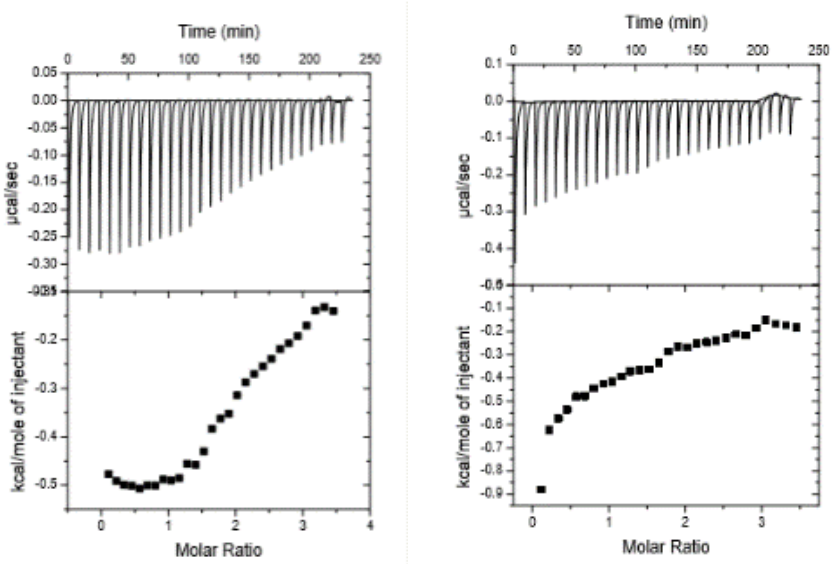


Figure 4.7. A trace of calorimetric titration (upper panel) and integrated isotherms (lower panel). The first peak represents a pre-injection that was omitted in the binding calculations. A) ITC analysis of FPX by direct titration of tris(ethylenediamine)cobalt(III). B) ITC analysis of FPX by direct titration of pentaamminechlorocobalt(III).

| | **$K_d$ (µM)** | **ΔG (kJ/mol)** | **ΔH (J/mol)** | **-TΔS (kJ/mol*K)** |
|---|---|---|---|---|
| $[Co(en)_3]^{3+}$ | 18.6 ± 3.0 | -6.5 ± 0.1 | -374.8 ± 7.5 | -6.1 |
| $[Co(NH_3)_5Cl]^{2+}$ | 87.7 ± 17.7 | -5.5 ± 0.3 | -345.7 ± 20.2 | -5.2 |

Table 4.4. ITC analysis showing the obtained binding parameters: dissociation constants ($K_d$); free energy of binding (ΔG); enthalpy of binding (ΔH); and entropy of binding (-TΔS) between cobalt compounds and FPX. The standard error from 3 measurements is indicated.



www.manaraa.com

loss of one sulfate at 521.68 m/z (3-), and 410.99 m/z (4-). The non-covalent interaction uses hydrogen bonding either between the ammines or coordinated water of the cobalt and the sulfates of the FPX. The non-covalent interaction was also observed with a coordinated water at 832.01 m/z (2-), 554.34 m/z (3-), and 415.50 m/z (4-). Covalent and non-covalent interactions were both observed for t-dichlorobis(ethylenediamine)cobalt(III) at the 2- and 3- charge states. The cobalt compounds may coordinate to the sulfates producing a covalent interaction since the chlorides are dissociated from the compound. Water may also coordinate to one of the free ligand sites, still allowing a covalent interaction between cobalt and FPX. The non-covalent interaction uses hydrogen bonding either between the ammines or bound water of the cobalt and the sulfates of the FPX since water is coordinated to both of the free ligand sites of the cobalt compound. A 1:1 binding interaction was observed covalently at 560.00 m/z (3-) and with one coordinated water at 566.01 m/z (3-), and non-covalently with 2 coordinated waters at 571.99 m/z (3-). Loss of one sulfate was also observed at 533.35 m/z (3-) with no coordinated water. A 1:1 binding interaction was observed covalently at 840.51 m/z (2-) and with one coordinated water at 849.51 m/z (2-), and non-covalently with 2 coordinated waters at 858.52 m/z (2-). Loss of one to six sulfates was also observed at 800.53, 760.55, 720.57, 680.59, 640.61, and 600.51 m/z (2-) respectively with no coordinated water, while at loss of one sulfate was observed both covalently with one coordinated water at 809.84 m/z (2-) and non-covalently with two coordinated waters at 818.52 m/z (2-). A 2:1 binding stoichiometry of Co:FPX was observed at 928.25 m/z (2-) with no coordinated waters.

We also observed more sulfate loss with covalent interactions, since hydrogen bonding interactions allow for sulfate cluster interactions more sulfates are protected. While the covalent interactions would only protect one sulfate from loss. Non-covalent interactions protect more sulfates as compared to covalent interactions likely due to the non-covalent interaction's ability to "metalloshield" a larger group of sulfate clusters, while the covalent interaction may only protect one sulfate through bidentate binding.

To compare the binding stoichiometry observed in the monomer NMR, monomer binding with cobalt complexes was also studied. Peaks were observed for an interaction between



www.manaraa.com

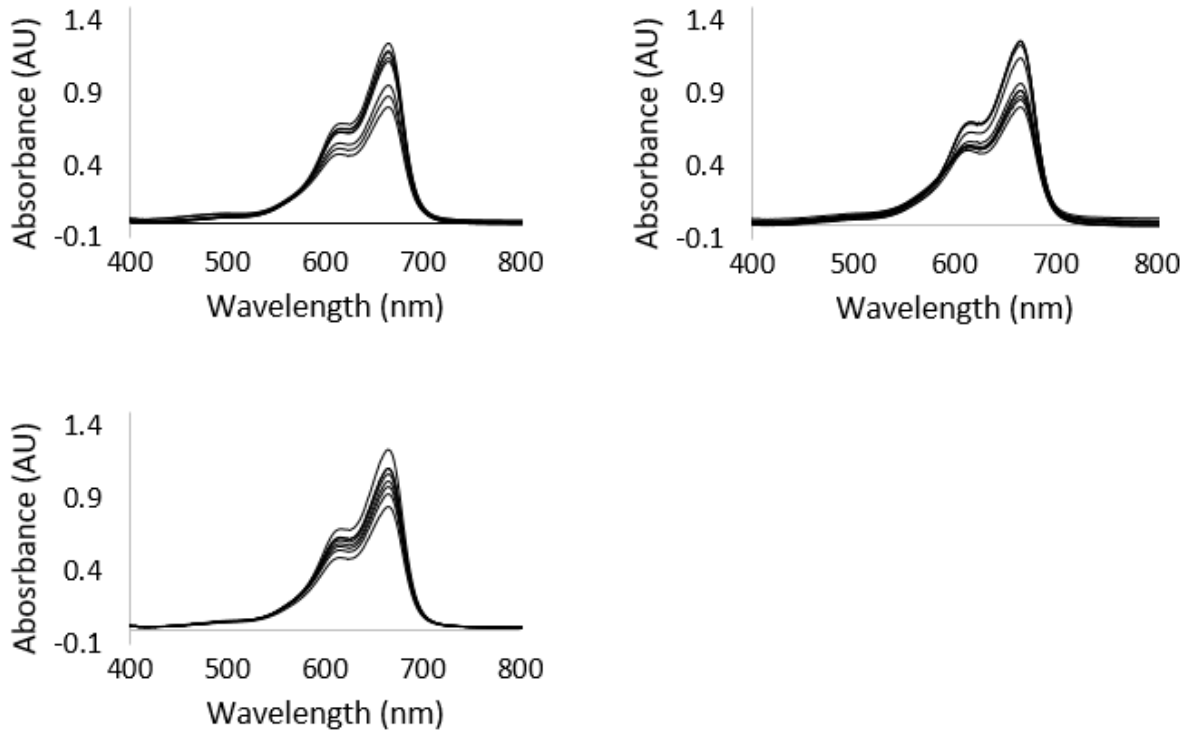


Figure 4.8. MB competition assay for assessment FPX binding. At a constant concentration of FPX (15 μM) in the presence of varying concentrations of A) tris(ethylenediamine)cobalt(III) (from bottom to top with 30, 40, 50, 80, 90, 100, 250, 500 μM), B) *t*-dichlorobis(ethylenediamine)cobalt(III) (from bottom to top with 40, 50, 60, 70, 80, 90, 200, 300, 400, 500 μM), and C) pentaamminechlorocobalt(III) (from bottom to top with 40, 50, 60, 70, 80, 90, 100, 200 μM); MB binding is inhibited, reflected in the change of [AbsMB] at 664 nm.

| | **$IC_{50}$ (μM)[a]** | **$K_{d(app)}$ (μM)[b]** |
|---|---|---|
| $[Co(en)_3]^{3+}$ | 71.0 ± 2.9 | 33.3 ± 1.4 |
| $[Co(en)_2Cl_2]^{1+}$ | 116.1 ± 1.6 | 54.4 ± 0.8 |
| $[Co(NH_3)_5Cl]^{2+}$ | 75.6 ± 1.2 | 35.4 ± 0.5 |

Table 4.5. $IC_{50}$ and $K_d$ values of cobalt complexes in competitive inhibition assays using MB.
[a]The $IC_{50}$ value was determined as the concentration of complex required for half-maximal binding of the dye (18.6 μM) to FPX (15 μM).
[b]Dissociation constants were calculated from the MB assay for cobalt complexes binding to FPX using a competitive inhibitor model.



www.manaraa.com

tris(ethylenediamine)cobalt(III) and monomer at a 1:2 Co:monomer stoichiometry at 755.19 m/z (1+). A 1:2 covalent binding interaction was observed between t-dichlorobis(ethylenediamine)cobalt(III) and monomer at 695.12 m/z (1+), while a 1:1 non-covalent binding interaction was observed at 507.26 m/z (1-) with no dissociated chlorides.

ITC measures the amount of heat energy released or absorbed into the system upon the interaction of two molecules. ITC determines the thermodynamic influences of both the change in enthalpy (ΔH) and entropy (ΔS) changes to calculate the free energy of binding (ΔG). ITC assays were performed to determine the binding constants between FPX and the cobalt compound library. Covalent and non-covalent interactions contribute to the enthalpy term, while conformational freedom changes and solvation upon complexation contribute to the entropy term.(24,25)

While the major contribution for the derived thermodynamic binding parameters arose from the entropy term, binding interactions can still be evaluated from the enthalpy binding term, Table 4.4. Tris(ethylenediamine)cobalt(III) produced a Kd (18.6 µM) and greatest Gibbs Free energy (-6.5 kJ/mol), this is likely due to the hydrogen bonding ability and larger overall size compared to other ligands, Figure 4.7. Pentaamminechlorocobalt(III) produced a Kd of 87.8 µM and the weakest Gibbs Free energy (-5.5 kJ/mol), Figure 4.7. The calculated binding parameters of pentaamminechlorocobalt(III) are likely weaker due to its ability to only interact with one sulfate covalently. The ITC titrations of t-dichlorobis(ethylenediamine)cobalt(III) to FPX did not give a well-defined isothermal trace, perhaps due to the rapid isomerization of t-dichlorobis(ethylenediamine)cobalt(III) in aqueous solutions. The major contribution arose from the entropy term, produced by the release of solvent molecules from FPX upon binding. While the enthalpy terms are similar between the two cobalt complexes showing similar strength of hydrogen bonding, the difference in the entropy term produces a discrepancy in the dissociation constant.

Methylene blue (MB) has been used to quantify sulfate content on heparin chains and to examine heparin binding interactions.(26-29) The MB absorbance at 664 nm and 614 nm decreases proportionally with increasing sulfate concentration from addition of FPX to the solution. We have previously shown that with addition of FPX to a solution containing a constant concentration of



www.manaraa.com

MB, the absorbance decreases as free MB is bound to increasing concentrations of FPX.(17) The association constant between FPX and MB was previously calculated using a Scatchard plot (4.1 x $10^4$ $M^{-1}$).(16, 17)

We again used the MB assay to study the ability of the cobalt library to inhibit MB binding through metalloshielding of FPX. With increasing concentrations of cobalt compounds in solution, FPX is metalloshielded from MB interacting with the FPX allowing more free-MB to be in solution resulting in an increase of absorbance. The ability for these cobalt compounds to "metalloshield" was calculated as an IC50 value, the concentration of cobalt compound required to inhibit 50% of the MB to bind to the FPX. Pentaamminechlorocobalt(III) and tris(ethylenediamine)cobalt(III) both have the ability to 'metalloshield' multiple sulfate clusters from binding to MB resulting in similar concentrations required (75.6 and 71.0 µM respectively), Table 4.5 and Figure 4.8. Again, we observed a higher concentration required for the covalent interaction of t-dichlorobis(ethylenediamine)cobalt(III) (116.1 µM) which may be due to the one sulfate covalent protection over hydrogen bonding cluster interactions or to the rapid isomerization artificially increasing the concentration needed, Figure 4.8. By using MB as a reporter, we are able to calculate the apparent dissociation constant (Kd(app)) between the cobalt complexes and FPX.

## 4.4 Conclusions

The focused small library studied here begins to elucidate structure–activity relationships. The stark contrast between *t*-dichlorobis(ethylenediamine)cobalt(III) and pentaamminechlorocobalt(III) in inhibiting the HS cleavage emphasizes the importance of hydrogen bonding in sulfate cluster protection. The overall results discussed here suggest comparable affinities for cobalt complexes binding to FPX as previously discussed.(16, 17) ITC shows that cobalt complexes interacting with FPX, $K_d$s of 18.6 to 90.1 µM, are comparable to a mixture of heterogeneous heparin chains complexing with FGF-1, $K_d$s of 1.1 to 3 µM.(30,31) MB and MS assays suggest that covalent interactions of these cobalt compounds may only interact



www.manaraa.com

with a single sulfate, while non-covalent hydrogen bonding may interact with a cluster of sulfates. This was observed using MB as a reporter, requiring a higher concentration of covalently interacted cobalt complexes over the non-covalent complexes. This was also observed in the MS with a greater number of sulfates lost through the covalent interaction of *t*-dichlorobis(ethylenediamine)cobalt(III) with up to six sulfates lost from FPX in the 2- charge state, while the non-covalent interaction showed lower abundance of lost sulfates. Therefore "metalloshielding" of FPX through sulfate clusters would be greater in the non-covalent compounds over the covalent interactions. However, the NMR results show that covalent interactions, using application of hard–soft acid–base concepts, occur much stronger than the non-covalent interactions. These assays give an estimate of the strength of the FPX–cobalt binding and provide a relative calculation of affinities. However, given clear disparities in the quantitation of dissociation constants, care should be taken in extrapolating across the assays discussed due to the inherent differences in the nature of these assays. Thus, whereas ITC is a "two-body" system, the MB competition assay becomes a "three-body" system, and is consequently more difficult to interpret. Overall, the results validate the importance of the metalloglycomics concept in developing new classes of molecules for study of glycan structure and function, further emphasizing the need to explore the dual- function therapeutic nature of the less cytotoxic cobalt complexes.

## 4.5 Experimental Section

### Synthesis and Materials

D-glucosamine-6-O-sulfate was purchased from Carbosynth Ltd.(USA). Fondaparinux and pentaamminechlorocobalt(III) chloride were purchased from Sigma-Aldrich (USA). Methylene blue chloride was purchased from Fisher Scientific (USA). Tris(ethylenediamine)cobalt(III) chloride, *t*-dichlorobis(ethylenediamine)cobalt(III) chloride, and potassium



www.manaraa.com

hexacyanocobaltate(III) were synthesized according to published methods from refs 32, 33, and 34, respectively.

**Heparinase Studies**

**Colorimetric HPSE activity assay**

The indicated concentration of each compound was incubated for 15 min. at room temperature with 50 µM fondaparinux in buffer containing 40mM NaOAc, pH 5. After addition of 0.25U heparinase I for 1h at 37°C, the reactions were stopped by adding 100 µl 1.69mM WST-1 (Dojindo). After heating the plate to 60°C for 30 min., absorbance readings at 584 nm were collected using a spectrophotometer (Biotek). The points on the graph represent the mean of two independent experiments containing two replicates for each concentration.

**Matrigel Invasion HPSE assay**

**Drug + Heparinase Incubation**

Growth factor reduced matrigel chambers (Corning) were treated with either PBS (-HPSE and +HPSE) or 50 µM of cobalt compound for 1 hour. Following treatment, chambers were then treated with additional PBS (-HPSE) or 0.3 units of heparinase I (+HPSE and Drug + HPSE). Matrigel chambers were then placed in 37°C incubator for 16 hours to allow heparinase digestion of matrigel to take place. Following this digestion, matrigel inserts were washed 10x times with PBS in order to remove remaining enzyme or drug. Inserts were then filled with DMEM:F12 media (Gibco) containing low percentage of FBS (0.2%). Inserts were then placed into new wells containing chemoattractant (10%FBS).

**Cell Invasion**

Next, 8x104 serum starved MDA-MB231 cells were seeded into each chamber. Cells were then placed into the incubator for 12 hours to allow for invasion to occur. Following this, cells which had invaded were fixed and stained using methanol/crystal violet, imaged, and counted manually. Percent invasion was determined by normalizing cells invaded through matrigel to cells which migrated through control insert.

**Direct Binding Assays:**



www.manaraa.com

**Isothermal Titration Calorimetry**

Calorimetric data was collected using a VP-ITC Microcalorimeter (MicroCal, LLC). All samples were degassed for 5 minutes using a ThermoVac (MicroCal, LLC). For all titrations, injections of cobalt complexes were pipetted automatically into the reaction cell containing 1.3 mL of FPX at 300 second intervals from a 300 µL syringe while stirring at 75 rpm. In all experiments, 100 mM cacodylate buffer (pH 7.4) was used at 25°C and the thermal reference cell contained 1.3 mL of 100 mM cacodylate buffer (pH 7.4). Integration of the thermogram peaks were carried out using the software supplied with the calorimeter (Origin 7.0). The heats were fitted to a one site model using Origin 7.0 to determine $K_d$, $\Delta H$, and $\Delta S$. $\Delta G$ was obtained using Gibbs free energy equation.

**NMR Studies**

$^{1}H$ NMR spectroscopy was performed in an Ascend 400 MHz NMR spectrometer (Bruker), data being collected and analyzed with the TOPSPIN software (Bruker). Monomer (23 mM) was pre-incubated for 10 min with each of the cobalt compounds (23 mM) in the cobalt library (Figure 4.1) in deuterated water.

$^{59}Co$ NMR spectroscopy was performed in an Ascend 400 MHz NMR spectrometer (Bruker), data being collected and analyzed with the TOPSPIN software (Bruker). Monomer (23 mM) was pre-incubated for 10 min with each of the cobalt compounds (23 mM) in the cobalt library (Figure 4.1) in deuterated water. Chemical shifts are reported relative to $Co(CN)_6^{3-}$.

**Mass Spectrometry**

Mass spectra were acquired on a Thermo Electron Corporation Orbitrap Velos mass spectrometer (Waltham, MA). Samples were introduced by flow injection at flow rates of 0.5 to 0.7 µL/min using a syringe pump. Electrospray source condition were kept constant with a capillary temperature of 230°C and capillary voltage between 2.3 and 2.5 kV. FPX and cobalt complexes were reconstituted in DI water to a stock concentration of 40 µM. Samples were mixed at a 1:1 molar ratio and were incubated at room temperature for 20 minutes. Samples were diluted with addition of Milli-Q methanol for a final concentration of 1:10 methanol:water.

**Competitive Binding Assays:**



www.manaraa.com

**Methylene Blue Reporter Method**

A change in absorbance of MB at 664 nm accompanies it binding to the sulfates on FPX. This change was used to quantitate the affinity of MB (at a constant final concentration of 21.98 µM) for FPX in water. Varying concentrations of cobalt complexes were incubated with constant concentration of FPX (at a constant final concentration of 15 µM) for 15 mins at room temp. To each sample was added constant concentration of MB. All binding studies were performed in triplicate on an Agilent 8453 diode array spectrophotometer in a sub-micro quartz cuvette with a path length of 10 mm.

$IC_{50}$ and $K_{a(app)}$ values for binding of cobalt complexes to FPX were calculated by converting the MB absorption values to a normalized value (minimum and maximum absorbance) and the $K_{a(app)}$ was determined using the following equation:

$$\frac{1}{K_{a(app)}} = IC_{50}x\frac{2K_{dL}[S_L-(B_L)_o]}{[(B_L)_o{}^2+2S_LK_{dL}-3S_L(B_L)_o]},$$

where $K_{dL}$ is the dissociation constant for the labeled ligand (MB) and binding site (FPX), $S_L$ is the total concentration of the labeled ligand, and $(B_L)_o$ is the equilibrium of labeled ligand value when competitor concentration is zero.

## 4.6 References


1. A. Varki, R. D. Cummings, J. D. Esko, H. H. Freeze, P. Stanley, C. R. Bertozzi, G. W. Hart, M. Etzler..*Essentials of Glycobiology*, 2nd ed.; Cold Spring Harbor Laboratory Press: Cold Spring Harbor, NY, **2009**.

2. R. D. Cummings, J. M. Pierce. *Chem. Biol.* **2014**, *21*, 1– 15.

3. P. Chiodelli, A. Bugatti, C. Urbinati, M. Rusnati. *Molecules* **2015**, *20*, 6342–6388.

4. C. Pisano, I. Vlodavsky, N. Ilan, F. Zunino. *Biochem. Pharmacol.* **2014**, *89*, 12– 19.

5. M. C. Z. Meneghetti, A. J. Hughes, T. R. Rudd, H. B. Nader, A. K. Powell, E. A. Yates, M. A. Lima. *J. R. Soc., Interface* **2015**, 12, 20150589.

6. P. Chiodelli, A. Bugatti, C. Urbinati, M. Rusnati. *Molecules* **2015**, 20, 6342−6388.




www.manaraa.com

7. D. Xu, J. D. Esko. *Annu. Rev. Biochem*. **2014**, 83, 129−57.

8. E. J. Peterson, A. G. Daniel, S. J. Katner, L. Bohlmann, C. W. Chang, A. Bezos, C. R. Parish, M. von Itzstein, S. J. Berners-Price, N. P. Farrell. *Chem. Sci.* **2017**, 8, 241−252.

9. J. B. Mangrum, B. J. Engelmann, E. J. Peterson, J. J. Ryan, S. J. Berners-Price, N. P. Farrell. *Chem. Commun.* **2014**, 50, 4056−4058.

10. N. P. Farrell. *Chem. Soc. Rev*. **2015**, 44, 8773−8785.

11. J. C. Wilson, A. E. Laloo, S. Singh, V. Ferro. *Biochem. Biophys. Res. Commun.* **2014**, 443, 185–188.

12. L. Bohlmann, C. W. Chang, I. Beacham, M. von Itzstein. *ChemBioChem* **2015**, 16, 1205–1211.

13. E. Hammond, C. P. Li, V. Ferro. *Anal. Biochem*. **2010**, 396, 112–116.

14. F. Levy-Adam, N. Ilan, I. Vlodavsky. *Semin. Cancer Biol* **2010**, 20, 153-160.

15. J. A. Schwartz, E. K. Lium, S. J. Silverstein. *J Virol.* **2001**, 75, 4117-4128.

16. S. J. Katner, W. E. Johnson, E. J. Peterson, P. Page, N. P. Farrell. *Inorg. Chem*. **2018**, 57, 3116-3125.

17. A. K. Gorle, S. J. Katner, W. E. Johnson, D. E. Lee, A. G. Daniel, E. P. Ginsburg, M. von Itzstein, S. J. Berners-Price, N. P. Farrell. *Chem. Eur. J.* **2018**, 24, 6606-6616.

18. E. Hammond, C. P. Li, V. Ferro. *Anal Biochem*. **2010**, 396, 112–116.

19. M. D. Hulett, C. Freeman, B. J. Hamdorf, R. T. Baker, M. J. Harris, C. R. Parish. *Nat. Med.* **1999**, 5, 803–809.

20. S. C. F. Au-Yeung, D. R. Eaton. *Can. J. Chem*. **1983**, 61, 2431-2441.

21. J. C. C. Chan, S. C. F. Au-Yeung. *J. Chem. Soc., Faraday Trans*., **1996**, 92, 1121-1128.

22. L. L. Borer, J. G. Russell, R. E. Settlage. *J. Chem. Ed*. **2002**, 79, 494-497.

23. M. J. Kailemia, L. Li, Y. Xu, J. Liu, R. J. Linhardt, I. J. Amster. *Anal. Chem*. **2012**, 84, 5475–5478.



www.manaraa.com

24. A. Brown. *Int. J. Mol. Sci.* **2009**, 10, 3457–3477.

25. S. Leavitt, E. Freire. *Curr. Opin. Struct. Biol.* **2001**, 11, 560–566.

26. Q. C. Jiao, Q. Liu, C. Sun, H. He. *Talanta* **1999**, *48*, 1095– 1101.

27. L. Tan, S. Yao, Q. Xie. *Talanta* **2007**, 71, 827−832.

28. H. Chu, N. R. Johnson, N. S. Mason, Y. A. Wang. *J. Controlled Release* **2011**, 150, 157−163.

29. L. Zhang, N. Li, F. Zhao, K. Li. *Anal. Sci*. **2004**, 20, 445−450.

30. A. Brown, C. J. Robinson, J. T. Gallagher, T. L. Blundell. *Biophys. J.* **2013**, 104, 1720–1730.

31. A. K. Powell, E. A. Yates, D. G. Fernig, J. E. Turnbull. Glycobiology **2004**, 14, 17R–30R.

32. J. A. Broomhead, F. P. Dwyer, J. W. Hogarth. *Inorg. Syn*., **1960**, 6, 183-186.

33. J. C. Bailar Jr. *Inorg. Synth*. **1946**, 2, 222-225.

34. P. S. Poskozim. *J. Chem. Educ*. **1969**, 46, 384-385.



www.manaraa.com

## Chapter 5: Interactions of Non-covalent Metal Complexes with Fondaparinux

### 5.1 Results and Discussion

Negative mode electrospray ionization (ESI) is commonly used for characterization of heparin due to its highly acidic nature. We have previously shown through ESI-MS studies that FPX undergoes sulfate loss in the gas phase. (1) Analysis regarding the retention of labile sulfate groups on the heparin backbone has shown metal cations stabilize sulfate groups. (2) In this work we examine the stoichiometry of metal complexes bound to FPX and the ability of these metal complexes to protect against sulfate loss, Table 5.1.

Peaks corresponding to a hydrogen bonding interaction between hexaamminecobalt(III) and FPX were observed at 415.25 *m/z* (4-), 554.01 *m/z* (3-), and 831.52 *m/z* (2-), Figure 5.1. Peaks were also observed corresponding to a retained sodium ion at 561.33 *m/z* (3-) and one to three retained sodium ions at 842.51, 853.50, and 864.49 *m/z* (2-) respectively. A 2:1 binding stoichiometry of Co:FPX was also observed at 910.55 *m/z* (2-). Continuing with Werner's complex, one peak corresponding to a hydrogen bonding interaction between Werner's Complex and FPX with a 2:2 binding stoichiometry was observed at 816.59 *m/z* (5-), Figure 5.1. Switching to an electrostatic compound rather than a hydrogen bonding compound, peaks corresponding to tris(2,2'-bipyridine)cobalt(III) and FPX were observed at a 1:2 Co:FPX stoichiometry at 620.99 *m/z* (6-), 745.39 *m/z* (5-), 931.98 *m/z* (4-), and 1242.98 *m/z* (3-), Figure 5.1. A 1:1 binding stoichiometry was also observed 1110.99 *m/z* (2-). Continuing with tris(2,2'-bipyridine)ruthenium(II), peaks corresponding to an electrostatic bonding interaction between tris(2,2'-bipyridine)ruthenium(II) and FPX were observed with a 2:1 Ru:FPX stoichiometry at 660.55 *m/z* (4-), 881.08 *m/z* (3-), and 1321.62 *m/z* (2-), Figure 5.1. A peak was also observed corresponding to a retained sodium ion at 892.74 *m/z* (3-). An 1:1 binding stoichiometry was also observed at 517.76 *m/z* (4-), 690.68 *m/z* (3-), and 1036.52 *m/z* (2-). Peaks were also observed corresponding to a retained sodium ion at 698.67 (3-) and to one and two retained sodium ions at 1047.51 and 1058.51 *m/z* (2-) respectively.



www.manaraa.com

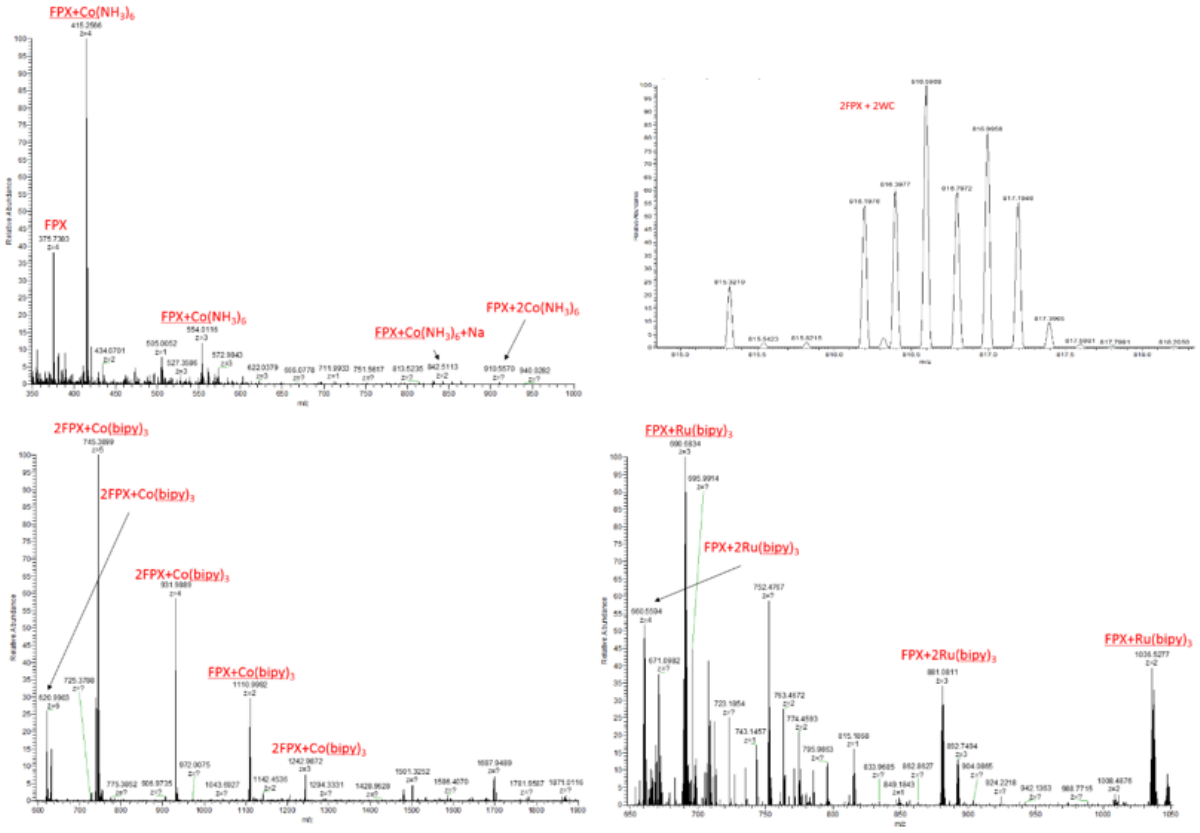


Figure 5.1. ESI-MS of 1:1 adducts of FPX and A) hexaamminecobalt(III) in the 2-, 3-, and 4- charge states with the parent peak of FPX also observed at the 4- charge state with a 2:1 Co:FPX stoichiometry at the 2- charge state, B) Werner's complex in the 5- charge state with an observed 2:2 Co:FPX stoichiometry, C) tris(2,2'-bipyridine)cobalt(III) in the 2- through 6- charge states with observed 1:1 and 1:2 Co:FPX stoichiometry and loss of 1 sulfate, and D) tris(2,2'-bipyridine)ruthenium(II) in the 2- through 4- charge states with observed 1:1 and 2:1 Co:FPX stoichiometry.



www.manaraa.com

A peak was also observed with one retained sodium ion and loss of sulfate at 1007.48 (2-). We also observed more sulfate loss with electrostatic interactions, since hydrogen bonding interactions allow for sulfate cluster interactions, more sulfates are protected. Cobalt complexes with the ability to interact through hydrogen bonding were able to protect the FPX from sulfate loss through sulfate cluster interaction with an ability to "metalloshield" a larger group of sulfate clusters where one ammine can interact with multiple oxygens. Conversely, sulfate loss was observed after interactions with the electrostatic complexes. The compounds using only electrostatic interactions will have more of dispersed charge with larger ligands that produces a weaker interaction between the metal complexes and FPX.

ITC measures the amount of heat energy released or absorbed into the system upon the interaction of two molecules. ITC determines the thermodynamic influences of both the change in enthalpy ($\Delta H$) and entropy ($\Delta S$) changes to calculate the free energy of binding ($\Delta G$). ITC assays were performed to determine the binding constants between FPX and the metal compound library. Electrostatic and hydrogen bonding interactions contribute to the enthalpy term, while conformational freedom changes and solvation changes that occur upon complexation contribute to the entropy term. (3, 4)

While the major contribution for the derived thermodynamic binding parameters arose from the entropy term, binding interactions can still be evaluated from the enthalpy binding term, Table 5.2. Hexaamminecobalt(III) has an intermediate $K_d$ (59.5 µM) and Gibbs Free energy (-5.8 kJ/mol) which is likely due to the hydrogen bonding ability and smaller size of the coordinated ligands, Figure 5.2. WC had the greatest $K_d$ and Gibbs Free energy (296 nM and -8.78 kJ/mol, respectively). This is due to the overall 6+ charge and largest size, which displaces the most solvent molecules and forces a FPX conformational change. Tris(2,2'-bipyridine)cobalt(III) has the lowest $K_d$ (90.1 µM) and the weakest Gibbs Free energy (-5.5 kJ/mol), Figure 5.2. The less favorable binding parameters of tris(2,2'-bipyridine)cobalt(III) likely arise from the lack of hydrogen bonding interactions. ITC titrations of tris(2,2'-bipyridine)ruthenium(II) into FPX did not give a well-defined isothermal trace, perhaps due to weak binding arising from a lack of hydrogen bonding



www.manaraa.com

| Composition* | Formula | m/z (charge) | MW | |
|---|---|---|---|---|
| | | | Observed | Calculated |
| FPX+[Co(NH$_3$)$_6$] | $C_{31}H_{64}CoN_9O_{49}S_8$ | 415.25 (4-) | 1661.00 | 1660.99 |
| FPX+[Co(NH$_3$)$_6$] | $C_{31}H_{65}CoN_9O_{49}S_8$ | 554.01 (3-) | 1662.03 | 1662.00 |
| FPX+[Co(NH$_3$)$_6$]+Na | $C_{31}H_{64}CoN_9NaO_{49}S_8$ | 561.33 (3-) | 1683.99 | 1683.98 |
| FPX+[Co(NH$_3$)$_6$] | $C_{31}H_{66}CoN_9O_{49}S_8$ | 831.52 (2-) | 1663.04 | 1663.00 |
| FPX+[Co(NH$_3$)$_6$]+Na | $C_{31}H_{65}CoN_9NaO_{49}S_8$ | 842.51 (2-) | 1685.02 | 1684.99 |
| FPX+[Co(NH$_3$)$_6$]+2Na | $C_{31}H_{64}CoN_9Na_2O_{49}S_8$ | 853.50 (2-) | 1707.00 | 1706.97 |
| FPX+[Co(NH$_3$)$_6$]+3Na | $C_{31}H_{63}CoN_9Na_3O_{49}S_8$ | 864.49 (2-) | 1728.98 | 1728.95 |
| FPX+2[Co(NH$_3$)$_6$] | $C_{31}H_{81}Co_2N_{15}O_{49}S_8$ | 910.55 (2-) | 1821.10 | 1821.07 |
| | | | | |
| 2FPX+2WC | $C_{62}H_{173}Co_8N_{30}O_{110}S_{16}$ | 816.19 (5-) | 4080.95 | 4080.91 |
| | | | | |
| FPX+[Co(bipy)$_3$] | $C_{61}H_{73}CoN_9O_{61}S_8$ | 1110.99 (2-) | 2221.98 | 2221.99 |
| 2FPX+[Co(bipy)$_3$] | $C_{92}H_{123}CoN_{12}O_{110}S_{16}$ | 620.99 (6-) | 3725.94 | 3725.93 |
| 2FPX+[Co(bipy)$_3$] | $C_{92}H_{124}CoN_{12}O_{110}S_{16}$ | 745.39 (5-) | 3726.95 | 3726.93 |
| 2FPX+[Co(bipy)$_3$] | $C_{92}H_{125}CoN_{12}O_{110}S_{16}$ | 931.98 (4-) | 3727.92 | 3727.94 |
| 2FPX+[Co(bipy)$_3$] | $C_{92}H_{126}CoN_{12}O_{110}S_{16}$ | 1242.98 (3-) | 3728.94 | 3728.95 |
| | | | | |
| FPX+[Ru(bipy)$_3$] | $C_{61}H_{71}N_9O_{49}RuS_8$ | 517.76 (4-) | 2071.04 | 2071.01 |
| FPX+[Ru(bipy)$_3$] | $C_{61}H_{72}N_9O_{49}RuS_8$ | 690.68 (3-) | 2072.04 | 2072.02 |
| FPX+[Ru(bipy)$_3$]+Na | $C_{61}H_{71}N_9NaO_{49}RuS_8$ | 698.67 (3-) | 2096.01 | 2096.02 |
| FPX+[Ru(bipy)$_3$] | $C_{61}H_{73}N_9O_{49}RuS_8$ | 1036.52 (2-) | 2073.04 | 2073.03 |
| FPX+[Ru(bipy)$_3$]+Na | $C_{61}H_{72}N_9NaO_{49}RuS_8$ | 1047.51 (2-) | 2095.02 | 2095.01 |
| FPX+[Ru(bipy)$_3$]+Na-SO$_3$ | $C_{61}H_{72}N_9NaO_{46}RuS_7$ | 1007.48 (2-) | 2014.96 | 2015.05 |
| FPX+[Ru(bipy)$_3$]+2Na | $C_{61}H_{71}N_9Na_2O_{49}RuS_8$ | 1058.51 (2-) | 2117.02 | 2116.99 |
| FPX+2[Ru(bipy)$_3$] | $C_{91}H_{96}N_{15}O_{49}Ru_2S_8$ | 660.55 (4-) | 2642.20 | 2642.13 |
| FPX+2[Ru(bipy)$_3$] | $C_{91}H_{97}N_{15}O_{49}Ru_2S_8$ | 881.08 (3-) | 2643.24 | 2643.14 |
| FPX+2[Ru(bipy)$_3$]+Na | $C_{91}H_{109}N_{15}O_{49}Ru_2S_8$ | 892.74 (3-) | 2678.22 | 2678.22 |
| FPX+2[Ru(bipy)$_3$] | $C_{91}H_{97}N_{15}O_{49}Ru_2S_8$ | 1321.62 (2-) | 2643.24 | 2643.14 |

Table 5.1. Species detected on the ESI-MS spectra. *protons and charges were omitted for clarity. FPX represent the parent Fondaparinux species.



www.manaraa.com

interactions, consistent with what was observed in the following MB assay. The major contribution arose from the entropy term in the case of the simple cobalt complexes. This was produced by the release of solvent molecules from FPX upon binding. The "U"-shaped traces that were observed are indicative of a strong conformational change produced by WC interacting with FPX and a weaker conformational change produced by hexaamminecobalt(III) with FPX.

The NMR chemical shift changes of D-glucosamine-6-O-sulfate (monomer) in the presence of cobalt complexes were investigated to delineate the binding interactions. Addition of cobalt complexes shifted the proton signals of the monomer, Figure 5.3. Upon measurements performed from the freshly prepared 1:1 Co:Monomer mixture, distinct shifts were observed due to fast interactions. Only small downfield shifts (.000 to .007 ppm) are observed for the non-covalent interactions disregarding Werner's Complex, Table 5.3. Werner's Complex produced shifts (up to .017 ppm) that were at least 2 fold greater than any other non-covalent cobalt complex shift. Werner's Complex produced larger shifts due to the stronger binding of the complex to the monomer. Since no considerable shifts were observed in the case of tris(2,2'-bipyridine)cobalt(III) due to electrostatic interactions with no hydrogen bonding, tris(2,2'-bipyridine)ruthenium(II) was not investigated. The major shifts were observed through the sulfate interaction between Werner's Complex and FPX, while a non-discriminate binding to both sulfate and hydroxy groups were observed for hexaamminecobalt(III).

Methylene blue (MB) has been used to quantify sulfate content on heparin chains and to examine heparin binding interactions.(5-8) The MB absorbance at 664 nm and 614 nm decreases proportionally with increasing sulfate concentration from addition of FPX to the solution. We have previously shown that with addition of FPX to a solution containing a constant concentration of MB, the absorbance decreases as free MB is bound to increasing concentrations of FPX. (9) The association constant between FPX and MB was previously calculated using a Scatchard plot (4.1 x $10^4$ $M^{-1}$). (9, 10)

We again used the MB assay to study the ability of the metal library to inhibit MB binding through



www.manaraa.com

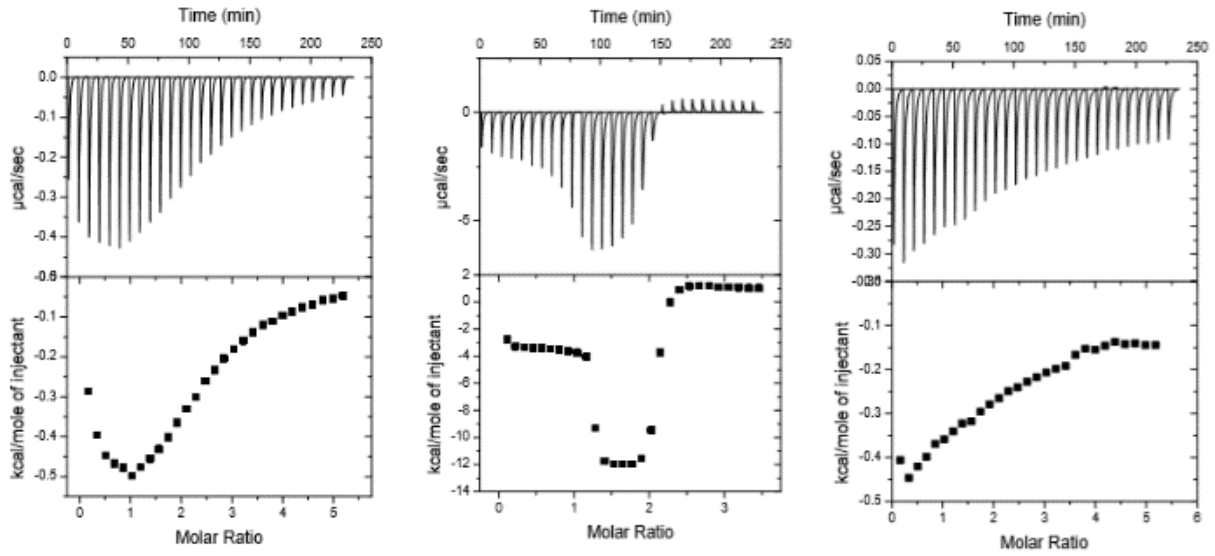


Figure 5.2. ITC analysis of FPX by direct titration with A) hexaamminecobalt(III) B) Werner's complex and C) tris(2,2'-bipyridine)cobalt(III). A trace of calorimetric titration (upper panel) and integrated isotherms (lower panel). The first peak represents a pre-injection that was omitted in the binding calculations.

| | $K_d$ | ΔG (kJ/mol) | ΔH (J/mol) | -TΔS (kJ/mol*K) |
|---|---|---|---|---|
| $[Co(NH_3)_6]^{3+}$ | 59.5 ± 7.8[a] | -5.8 ± 0.2 | -557.1 ± 15.7 | -5.2 |
| $WC^{6+}$ | 296 ± 34[b] | -8.78 ± 0.1 | -1336 ± 8 | -7.4 |
| $[Co(bipy)_3]^{3+}$ | 90.1 ± 20.3[a] | -5.5 ± 0.5 | -526.9 ± 51.1 | -4.9 |

Table 5.2. ITC analysis showing the obtained binding parameters: dissociation constants ($K_d$); free energy of binding (ΔG); enthalpy of binding (ΔH); and entropy of binding (-TΔS) between cobalt compounds and FPX. The standard error from 3 measurements is indicated.

[a] $K_d$ measured in µM.
[b] $K_d$ measured in nM.



www.manaraa.com

metalloshielding of FPX. With increasing concentrations of metal compounds, FPX is metalloshielded from MB, allowing more free-MB to be in solution, resulting in an increase of absorbance at 664 nm. The ability of these metal compounds to "metalloshield" was calculated as an $IC_{50}$ value, the concentration of metal compound required to inhibit 50% of the MB to bind to the FPX. Werner's Complex and tris(2,2'-bipyridine)cobalt(III) required the lowest concentrations to inhibit MB binding (41.4 and 36.4 µM respectively), Figure 5.4 and Table 5.4. The similarity in concentrations is attributed to the overall larger size of the ligands and their ability to spatially inhibit MB binding to the sulfates. A higher concentration was required for the smaller hexaamminecobalt(III) compound (64.5 µM). Similarly to the ITC assay, a greater concentration of tris(2,2'-bipyridine)ruthenium(II) (676.2 µM) was required to inhibit MB binding to FPX. These weak interactions by tris(2,2'-bipyridine)ruthenium(II) arise from the lower charge and lack of hydrogen bonding. By using MB as a reporter, we are able to calculate the apparent dissociation constant ($K_{d(app)}$) between the cobalt complexes and FPX.

## 5.2 Experimental

### Mass Spectrometry

Mass spectra were acquired on a Thermo Electron Corporation Orbitrap Velos mass spectrometer (Waltham, MA). Samples were introduced by flow injection at flow rates of 0.5 to 0.7 µL/min using a syringe pump. Electrospray source condition were kept constant with a capillary temperature of 230ºC and capillary voltage between 2.3 and 2.5 kV. FPX and cobalt complexes were reconstituted in DI water to a stock concentration of 40 µM. Samples were mixed at a 1:1 molar ratio and were incubated at room temperature for 20 minutes. Samples were diluted with addition of Milli-Q methanol for a final concentration of 1:10 methanol:water.

### Isothermal Titration Calorimetry

Calorimetric data was collected using a VP-ITC Microcalorimeter (MicroCal, LLC). All samples were degassed for 5 minutes using a ThermoVac (MicroCal, LLC). For all titrations, injections of



www.manaraa.com

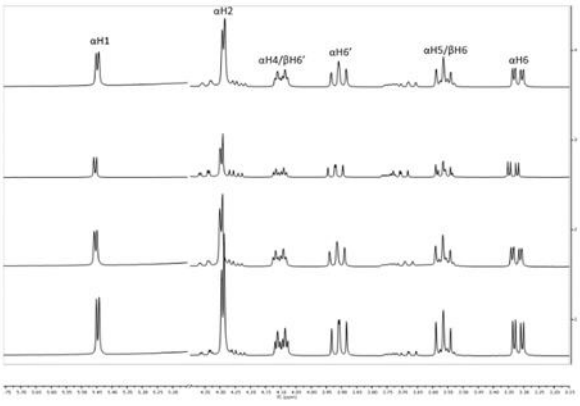


Figure 5.3. $^{1}$H NMR spectra of 1:1 mixtures of D-glucosamine-6-O-sulfate and various metal complexes from top to bottom: hexaamminecobalt(III), Werner's complex, tris(2,2'-bipyridine)cobalt(III), and D-glucosamine-6-O-sulfate.

| | Δδ = δ(monomer : Co) – δ(monomer) (ppm) | | | | | |
|---|---|---|---|---|---|---|
| | αH1 | **αH2** | **αH4/βH6'** | **αH6'** | **αH5/βH6** | **αH6** |
| [Co(NH3)6]3+ | 0.007 | 0.006 | 0.001 | 0.006 | 0.006 | 0.006 |
| WC6+ | 0.009 | 0.005 | 0.005 | 0.012 | 0.000 | 0.017 |
| [Co(bipy)3]3+ | 0.001 | 0.002 | 0.000 | 0.001 | 0.000 | 0.002 |

Table 5.3. $^{1}$H chemical shift changes (Δδ = δ(monomer : Co) – δ(monomer)) after incubation of metal complexes with D-glucosamine-6-O-sulfate.



www.manaraa.com

cobalt complexes were pipetted automatically into the reaction cell containing 1.3 mL of FPX at 300 second intervals from a 300 µL syringe while stirring at 75 rpm. In all experiments, 100 mM cacodylate buffer (pH 7.4) was used at 25°C and the thermal reference cell contained 1.3 mL of 100 mM cacodylate buffer (pH 7.4). Integration of the thermogram peaks were carried out using the software supplied with the calorimeter (Origin 7.0). The heats were fitted to a one site model using Origin 7.0 to determine $K_d$, ΔH, and ΔS. ΔG was obtained using Gibbs free energy equation.

**NMR Studies**

$^1$H NMR spectroscopy was performed in an Ascend 400 MHz NMR spectrometer (Bruker), data being collected and analyzed with the TOPSPIN software (Bruker). Monomer (23 mM) was pre-incubated for 10 min with each of the cobalt compounds (23 mM) in the cobalt library (Figure 5.5) in deuterated water.

**Methylene Blue Reporter Method**

A change in absorbance of MB at 664 nm accompanies it binding to the sulfates on FPX. This change was used to quantitate the affinity of MB (at a constant final concentration of 21.98 µM) for FPX in water. Varying concentrations of cobalt complexes were incubated with constant concentration of FPX (at a constant final concentration of 15 µM) for 15 mins at room temp. To each sample was added constant concentration of MB. All binding studies were performed in triplicate on an Agilent 8453 diode array spectrophotometer in a sub-micro quartz cuvette with a path length of 10 mm.

$IC_{50}$ and $K_{a(app)}$ values for binding of cobalt complexes to FPX were calculated by converting the MB absorption values to a normalized value (minimum and maximum absorbance) and the $K_{a(app)}$ was determined using the following equation:

$$\frac{1}{K_{a(app)}} = IC_{50}x \frac{2K_{dL}[S_L-(B_L)_o]}{[(B_L)_o{}^2+2S_LK_{dL}-3S_L(B_L)_o]}$$



www.manaraa.com

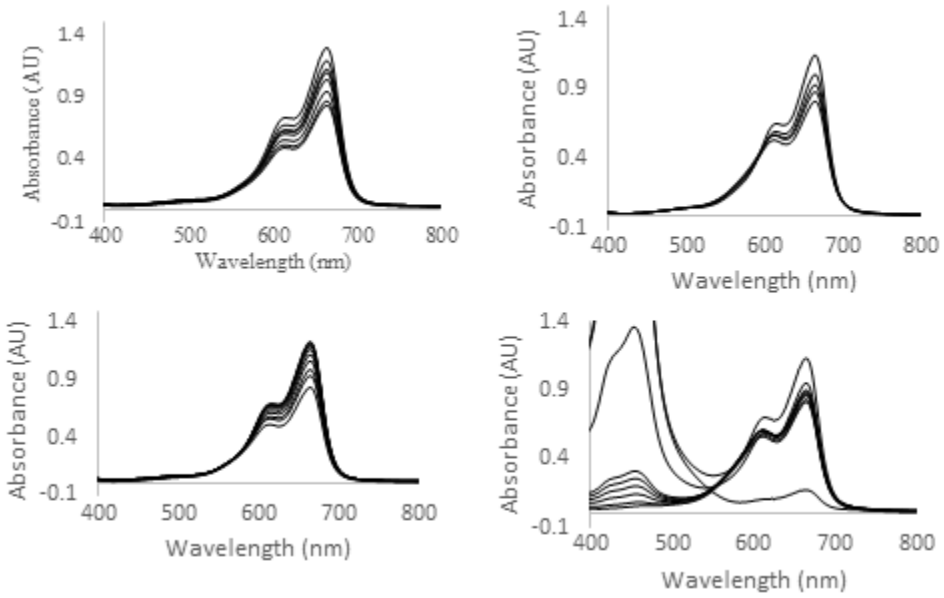


Figure 5.4. MB competition assay for assessment FPX binding. At a constant concentration of 15 μM FPX in the presence of varying concentrations of A) hexaamminecobalt(III) (from bottom to top with 30, 40, 50, 60, 70, 80, 90, 100 μM), B) Wener's complex (from bottom to top with 10, 20, 30, 40, 50 μM), C) tris(2,2'-bipyridine)cobalt(III) (from bottom to top with 10, 20, 30, 40, 50, 60, 70, 80, 90, 100 μM) D) tris(2,2'-bipyridine)ruthenium(II) (from bottom to top with Ruthenium only (1 mM), 10, 20, 40, 60, 80, 100, 500, 1000 μM); MB binding is inhibited, reflected in the change of [AbsMB] at 664 nm.

| | $IC_{50}$ (μM)[a] | $K_{d(app)}$ (μM)[b] |
|---|---|---|
| $[Co(NH_3)_6]^{3+}$ | 64.5 ± 1.1 | 30.2 ± 0.5 |
| $WC^{6+}$ | 41.4 ± 0.1 | 20.1 ± 0.2 |
| $[Co(bipy)_3]^{3+}$ | 36.4 ± 0.9 | 17.7 ± 0.4 |
| $[Ru(bipy)_3]^{2+}$ | 676.2 ± 17.3 | 316.8 ± 8.1 |

Table 5.4. $IC_{50}$ and $K_{d(app)}$ Values of metal compounds in the competitive inhibition assay using MB as a reporter.

a) The $IC_{50}$ value was determined as the concentration of complex required for half-maximal binding of the dye (21.98 μM) to FPX (15 μM) for the MB binding assay.

b) Dissociation constants were calculated from the MB assay for metal compounds binding to FPX using a competitive inhibitor model.



www.manaraa.com

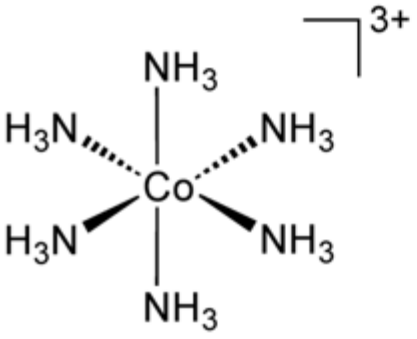


Hexamminecobalt(III)

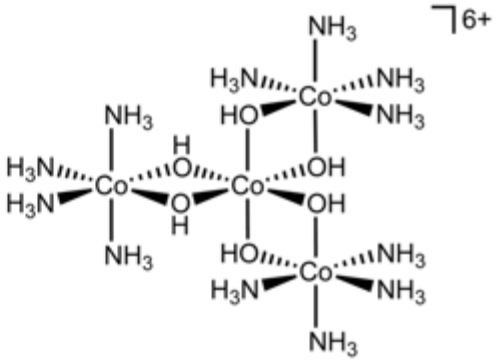


Werner's hexol

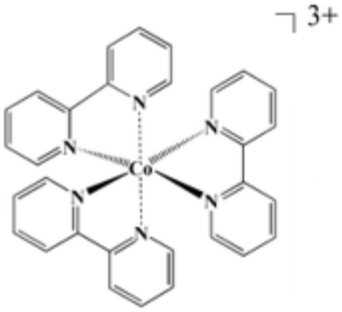


Tris(2,2'-bipyridine)cobalt(III)

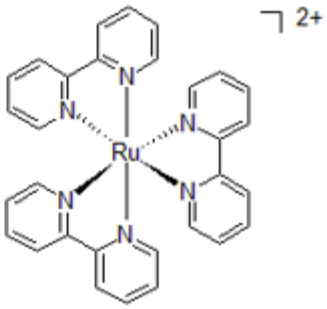


Tris(2,2'-bipyridine)ruthenium(II)

Figure 5.5. Library of cobalt complexes used. Counterions omitted for clarity.



www.manaraa.com

where $K_{dL}$ is the dissociation constant for the labeled ligand (MB) and binding site (FPX), $S_L$ is the total concentration of the labeled ligand, and $(B_L)_o$ is the equilibrium of labeled ligand value when competitor concentration is zero.

### 5.3 References


1. J. B. Mangrum, B. J. Engelmann, E. J. Peterson, J. J. Ryan, S. J. Berners-Price, N. P. Farrell. *Chem. Commun.* **2014**, 50, 4056−4058.
2. M. J. Kailemia, L. Li, Y. Xu, J. Liu, R. J. Linhardt, I. J. Amster. *Anal. Chem*. **2012**, 84, 5475–5478.
3. A. Brown. *Int. J. Mol. Sci.* **2009**, 10, 3457–3477.
4. S. Leavitt, E. Freire. *Curr. Opin. Struct. Biol.* **2001**, 11, 560–566.
5. Q. C. Jiao, Q. Liu, C. Sun, H. He. *Talanta* **1999**, 48, 1095−1101.
6. L. Tan, S. Yao, Q. Xie. *Talanta* **2007**, 71, 827−832.
7. H. Chu, N. R. Johnson, N. S. Mason, Y. A. Wang. *J. Controlled Release* **2011**, 150, 157−163.
8. L. Zhang, N. Li, F. Zhao, K. Li. *Anal. Sci*. **2004**, 20, 445−450.
9. A. K. Gorle, S. J. Katner, W. E. Johnson, D. E. Lee, A. G. Daniel, E. P. Ginsburg, M. von Itzstein, S. J. Berners-Price, N. P. Farrell. *Chem. Eur. J.* **2018**, 24, 6606-6616.
10. S. J. Katner, W. E. Johnson, E. J. Peterson, P. Page, N. P. Farrell. *Inorg. Chem*. **2018**, 57, 3116-3125.




www.manaraa.com

This work to be published with the following contributions:

Synthesis by Wyatt Johnson, MB and MS by Wyatt Johnson and Marjon Mashid, HPSE cleavage by Wyatt Johnson, Marjon Mashid, and Erica Peterson. Text by Wyatt Johnson.

## Chapter 6: Metalloglycomics: Probing the Metalloshielding Interactions of Simple Metal Complexes with Fondaparinux

**Wyatt E. Johnson, Marjon Mashid, James F. Beaton, Erica J. Peterson and Nicholas P. Farrell**

Department of Chemistry and Massey Cancer Center, Virginia Commonwealth University (VCU), Richmond, Virginia 23284, United States



www.manaraa.com

## 6.1 Abstract

The interaction between simple metal cations and fondaparinux leads to sulfate cluster binding, thus providing a simple platform to investigate "metalloshielding" of sulfates using a reporter dye, stabilization of sulfates using ESI-MS, and cleavage inhibition of glycosidic linkages using bacterial heparinase.

## 6.2 Introduction

Heparan sulfate proteoglycans (HSPGs) are found in the extracellular matrix or on the cell surface once proteins associate with heparan sulfate (HS), a sulfated glycosaminoglycan. HSPGs play a major role in the cell recognition process, adhesion, and migration.(1,2) Cancer cells over-express HSPGs on their cell surface. HS sulfate residues are the recognition site for many different protein substrates including pro-angiogenic growth factors, interacting similar to the phosphate clamp-arginine fork motif. Fibroblast growth factors (FGFs) directly stimulate the growth, metastasis and survival of cancer cells.(3) HSPG enzymatic cleavage at glycosidic linkages by heparanase (HPSE) causes release of angiogenic growth factors initiating the angiogenic cascade. HPSE is also over-expressed in tumors with significant correlation between metastatic potential and heparanase activity.(4-7) HS is, thus, an attractive drug target to inhibit tumor cell progression through "metalloshielding" or sulfate cluster masking of HS by metal complexes protecting HS from enzymatic cleavage by the mammalian heparanase, and preventing growth factors from binding to HS and/or preventing release of bound growth factors.

The highly anionic nature of HSs means they are associated with physiologically relevant cations.(8-10) Cation association affects the biomolecule conformation and can facilitate heparin−protein interactions such as $Ca^{2+}$-dependent heparin−annexin A2 binding.(11) Growth factors are also copper-dependent, with a slightly higher affinity of HS for FGF-1 compared to FGF-2.(12-15) Aquated $Ca^{2+}$, $Mg^{2+}$, $Fe^{3+}$, and $Zn^{2+}$ ions, at higher than physiological



www.manaraa.com

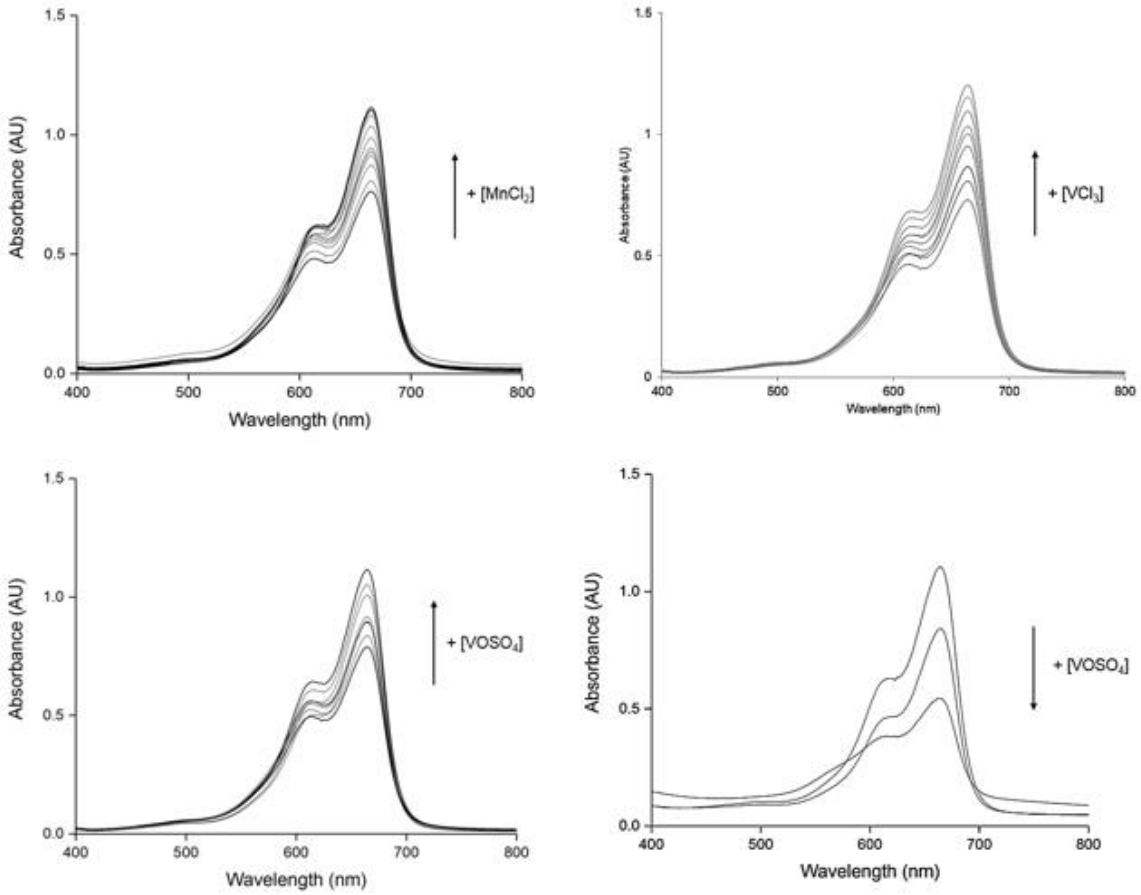


Figure 6.1. MB competition assay for assessment FPX binding. At a constant concentration of 15 μM FPX and 21.98 μM MB in the presence of varying concentrations of A) Manganese(II) chloride (from bottom to top with 10, 20, 30, 50, 60, 70, 80, 200, 300, 400, and 500 μM), B) Vanadium(III) chloride (from bottom to top with 10, 20, 30, 70, 80, 90, 200, 300, 400, and 500 μM), C) Vanadyl(III) sulfate (from bottom to top with 50, 60, 70, 80, 90, 100, 250, 300, and 400 μM) and D) absorption spectrum of MB and Vanadyl(III) sulfate (from bottom to top with 100, 250, and 500 μM); MB binding is inhibited, reflected in the change of [AbsMB] at 664 nm.



www.manaraa.com

concentrations, reduce FGF-1 interactions with HS.(8) In order to determine the importance of hard-soft acid-base concepts on the "metalloshielding" potential of the metal complex library, binding and cleavage inhibition studies were performed using Fondaparinux as a model HS-like substrate. Fondaparinux (FPX) is a well-defined octasulfated pentasaccharide with a single point of cleavage for bacterial HPSE. New patterns of metal-heparin binding can be achieved by the application of hard–soft acid–base concepts.

To develop the HSAB concepts, we have chosen a small library of metal complexes to examine their effects with FPX. This communication describes cleavage inhibition studies in the presence and absence of Manganese(II) chloride using bacterial HPSE. A competition assay was implemented using methylene blue (MB) as a reporter to measure the "metalloshielding" of MB for each compound. Sulfate stability was examined using mass spectrometry (MS). The overall results emphasize the importance of understanding the properties of glycan interactions with metal complexes, to expand bioinorganic chemistry into this important class of biomolecules.

**6.3 Results and Discussion**

Methylene blue (MB) has been used to quantify sulfate content on heparin chains and to examine heparin binding interactions.(16-18) With increasing sulfate concentration from addition of FPX to the solution, the MB absorbance at 664 nm and 614 nm decreases proportionally. It has been previously shown that upon addition of FPX to a solution of MB, the absorbance decreases as more MB is bound to FPX.(19) The association constant between FPX and MB was previously calculated using a Scatchard plot ($4.1 \times 10^4$ $M^{-1}$).(19)

The MB assay was used to study the ability of the metal library to inhibit MB binding through "metalloshielding" of FPX. Varying concentrations of metal complexes were incubated with constant concentration of FPX (15 μM) for 15 mins at room temperature. MB was added to each (to a constant final concentration of 21.98 μM). With increasing concentrations of metal compounds in solution, FPX is "metalloshielded" from MB, preventing interaction with FPX. The additional free-MB in solution resulting in an absorbance increase, Figure 6.1. The ability of these



www.manaraa.com

| | $IC_{50}$ (μM)[a] | $IC_{50}$ (μM)[b] |
|---|---|---|
| $MnCl_2$ | 333 ± 1 | 354 ± 78 |
| $VCl_3$ | 264 ± 1 | NA |
| $VOSO_4$ | 535 ± 1 | NA |

Table 6.1. $IC_{50}$ values of metal compounds in the competitive inhibition assay using MB as a reporter.

a) The $IC_{50}$ value was determined as the concentration of complex required for half-maximal binding of the dye (21.98 μM) to FPX (15 μM) for the MB binding assay.
b) The $IC_{50}$ value was determined as the concentration of complex required to inhibit 50% of HPSE cleavage on FPX.

| Composition* | Formula | m/z (charge) | MW | |
|---|---|---|---|---|
| | | | Observed | Calculated |
| FPX+Mn+Na | $C_{31}H_{47}MnN_3NaO_{49}S_8$ | 526.28 (3-) | 1578.87 | 1578.83 |
| FPX+Mn | $C_{31}H_{49}MnN_3O_{49}S_8$ | 778.94 (2-) | 1557.88 | 1557.86 |
| FPX+Mn-$SO_3$ | $C_{31}H_{49}MnN_3O_{46}S_7$ | 738.98 (2-) | 1477.96 | 1477.90 |
| | | | | |
| FPX+V | $C_{31}H_{46}N_3O_{49}S_8V$ | 387.72 (4-) | 1550.88 | 1550.84 |
| FPX+V+Na | $C_{31}H_{47}N_3NaO_{49}S_8V$ | 787.43 (2-) | 1574.86 | 1574.84 |
| FPX+V | $C_{31}H_{48}N_3O_{49}S_8V$ | 776.44 (2-) | 1552.88 | 1552.86 |
| FPX+V-$SO_3$ | $C_{31}H_{48}N_3O_{46}S_7V$ | 736.46 (2-) | 1472.92 | 1472.90 |
| | | | | |
| FPX+VO+Na | $C_{31}H_{48}N_3NaO_{50}S_8V$ | 530.63 (3-) | 1591.89 | 1591.84 |
| FPX+VO+Na-$SO_3$ | $C_{31}H_{48}N_3NaO_{47}S_7V$ | 503.97 (3-) | 1511.91 | 1511.88 |
| FPX+VO | $C_{31}H_{49}N_3O_{50}S_8V$ | 523.30 (3-) | 1569.90 | 1569.86 |
| FPX+VO-$SO_3$ | $C_{31}H_{49}N_3O_{47}S_7V$ | 496.65 (3-) | 1489.95 | 1489.90 |
| FPX+VO-2$SO_3$ | $C_{31}H_{49}N_3O_{44}S_6V$ | 496.99 (3-) | 1490.97 | 1409.95 |
| FPX+VO-3$SO_3$ | $C_{31}H_{49}N_3O_{41}S_5V$ | 443.34 (3-) | 1330.02 | 1329.99 |
| FPX+VO+Na | $C_{31}H_{49}N_3NaO_{50}S_8V$ | 796.45 (2-) | 1592.90 | 1592.85 |
| FPX+VO+Na-$SO_3$ | $C_{31}H_{49}N_3NaO_{47}S_7V$ | 756.47 (2-) | 1512.94 | 1512.89 |
| FPX+VO+Na-2$SO_3$ | $C_{31}H_{49}N_3NaO_{44}S_6V$ | 716.49 (2-) | 1432.98 | 1432.94 |
| FPX+VO+Na-3$SO_3$ | $C_{31}H_{49}N_3NaO_{41}S_5V$ | 676.51 (2-) | 1353.02 | 1352.98 |
| FPX+VO | $C_{31}H_{50}N_3O_{50}S_8V$ | 785.46 (2-) | 1570.92 | 1570.87 |
| FPX+VO-$SO_3$ | $C_{31}H_{50}N_3O_{47}S_7V$ | 745.48 (2-) | 1490.96 | 1490.91 |
| FPX+VO-2$SO_3$ | $C_{31}H_{50}N_3O_{44}S_6V$ | 705.50 (2-) | 1411.00 | 1410.95 |
| FPX+VO-3$SO_3$ | $C_{31}H_{50}N_3O_{41}S_5V$ | 665.52 (2-) | 1331.04 | 1331.00 |

Table 6.2. Species detected on the ESI-MS spectra. *protons and charges were omitted for clarity. FPX represent the parent Fondaparinux species.



www.manaraa.com

metal compounds to "metalloshield" was calculated as an $IC_{50}$ value, the concentration of metal compound required to inhibit 50% of MB binding, Table 6.1. The higher charged Vanadium(III) requires the lowest concentration, 264 µM, while Vanadyl(III) requires the highest concentration, 535 µM, due to the decrease in overall charge of the complex due to the presence of negatively charged oxygen. Manganese(II) requires an intermediate concentration, 333 µM. While the V(III) and Mn(II) complexes interact covalently with protection proportional to the charge of each metal; the VO, while still covalent, requires a higher concentration due to the oxygen being retained, both lowering the overall charge of the complex and limiting the number of available interaction sites on the Vanadium. Due to MB's ability to interact with sulfates, we also measured the absorbance change of MB in the presence of Vanadyl(III) sulfate. An analogous change in absorbance was observed using similar concentrations of Vanadyl(III) sulfate to those used in the inhibitory MB assay. This would artificially decrease the absorbance requiring a higher concentration of metal required to inhibit MBs binding to FPX.

Negative mode electrospray ionization (ESI) is commonly used for identification and analysis of heparin. We have previously shown through ESI-MS studies that FPX undergoes sulfate loss in the gas phase.(19) Analysis regarding the retention of labile sulfate groups on the heparin backbone has shown metal cations stabilize sulfate groups.(20) In the present work, the stoichiometry of metal complexes bound to FPX and their ability to protect against sulfate loss. FPX and metal complexes were reconstituted in DI water to a stock concentration of 40 µM. Samples were mixed at a 1:1 molar ratio and were incubated at room temperature for 20 minutes. Samples were diluted with addition of Milli-Q methanol for a final concentration of 1:9 methanol:water. Peaks corresponding to a covalent interaction between Manganese(II) and FPX were observed at 778.9447 *m/z* (2-) with loss of one sulfate at 738.9751 *m/z* (2-), Table 6.2. A Peak was also observed corresponding to the previous interaction with a retained sodium ion at 526.2888 *m/z* (3-). Peaks corresponding to a covalent interaction between Vanadium(III) and FPX were observed



www.manaraa.com

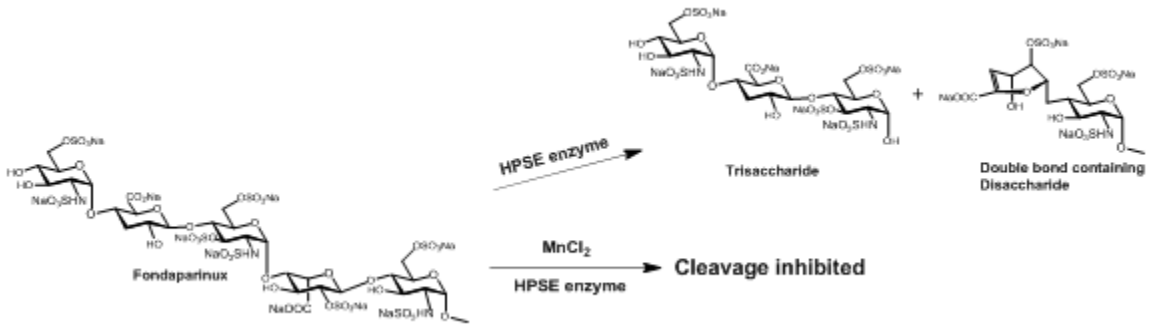


Figure 6.2. Structure of Fondaparinux, and cleavage products by *P. heparinus heparinase I*. In the presence of Manganese(II) chloride, cleavage was inhibited.

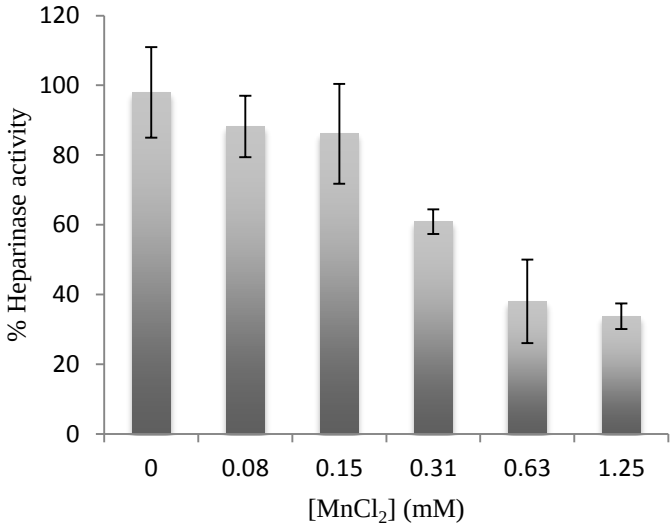


Figure 6.3. Inhibition of heparinase I through interaction of Manganese(II) chloride with FPX. Data are expressed as percentages relative to controls containing no Manganese(II) chloride.



www.manaraa.com

at 387.7184 *m/z* (4-) and 776.4411 *m/z* (2-) with loss of one sulfate at 736.4632 *m/z* (2-), Table 6.2. A Peak was also observed corresponding to a retained sodium ion at 787.4316 *m/z* (2-). Peaks corresponding to a covalent interaction between Vanadyl and FPX with a retained sodium were observed at 398.22067 *m/z* (4-) with loss of one sulfate at 378.2310 *m/z* (4-), Table 6.2. Peaks of the previous interaction were also observed at 523.6379 *m/z* (3-) and loss of sulfate at 496.9847 *m/z* (3-), along with peaks corresponding to a retained sodium ion at 531.2971 *m/z* (3-) and loss of one sulfate at 504.6441 *m/z* (3-). Peaks were also observed corresponding to Vanadyl and FPX covalent interaction at 785.9596 *m/z* (2-) with loss of one, two, and three sulfates at 745.9811, 706.0016, and 666.0220 *m/z* (2-), respectively. Again, retained sodium was observed at 797.4489 *m/z* (2-) with loss of one to three sulfates at 757.4705, 717.4907, and 677.5122 *m/z* (2-), respectively.

The interaction peaks observed were relatively weak compared to the parent FPX peaks. Greater sulfate loss was observed in the case of Vanadyl, since the negative oxygen was retained. The oxygen was retained due to the strong interaction between Vanadium and oxygen using HSAB chemistry. The positive charge of the Vanadium complex would be lowered concomitantly inhibiting the Vanadium from interacting with a greater number of sulfates.

The cleavage patterns for the interactions between FPX and mammalian heparanase or bacterial heparinase I (often used as a model for the mammalian enzyme) are shown in Figure 6.2.(21) A colorimetric assay was adapted to examine the inhibitory effect of metal complexes on the enzymatic heparinase degradation of FPX. Manganese(II) chloride was incubated for 15 min at room temperature with 50 µM FPX in 40mM NaOAc buffer, pH 5. After addition of 0.25 U heparinase I for 1 hour at 37 °C. The reactions were stopped by adding 100 µL 1.69 mM WST-1 (Dojindo), and absorbance readings were recorded at 584 nm. The pentasaccharide substrate was incubated with metal complex prior to enzyme exposure and cleavage was measured *versus* control in absence of added complex. Inhibition of heparinase cleavage is effective in a concentration-dependent manner for Manganese(II) chloride, Figure 6.3 and Table 6.1. Time course studies show that Manganese(II) chloride instantly inhibited activity with little



www.manaraa.com

or no variation with time, while the Vanadium(III) complexes interacted with the assay and did not produce reportable results.

Overall, these results emphasize that the study of simple cations with oligosaccharides has substantial potential in the new area of metalloglycomics. Simple metal cations such as $Zn^{2+}$ and $Ca^{2+}$ affect the activity and conformation of heparin mimetics. Our results highlight the potential "metalloshielding" effect by metal complexes of heparin mimetics through modification of metal oxidation state and substitution lability of ligands, and use of HSAB concepts. Vanadium, a hard acid, reacts with oxygen, a hard base, forming a stronger bond than Manganese, an intermediate acid, with oxygen. Vanadium also produces a stronger interaction than Manganese due to a higher overall charge of the complex and due to its ability to interact with more sulfate groups. Vanadyl, containing oxygen, lowered the overall charge of the metal complex and limited the amount of "metalloshielding". The study of simple metal cations extends the application of bioinorganic chemistry from protein and DNA-RNA interactions into the new era of metalloglycomics.

### 6.4 References


1. A. Varki, R. D. Cummings, J. D. Esko, H. H. Freeze, P. Stanley, C. R. Bertozzi, G. W. Hart, M. Etzler..*Essentials of Glycobiology*, 2nd ed.; Cold Spring Harbor Laboratory Press: Cold Spring Harbor, NY, **2009**.
2. R. D. Cummings, J. M. Pierce. *Chem. Biol.* **2014**, *21*, 1– 15.
3. P. Chiodelli, A. Bugatti, C. Urbinati, M. Rusnati. *Molecules* **2015**, *20*, 6342–6388.
4. L. Jia, S. Ma. *Eur. J. Med. Chem.* **2016**, *121*, 209– 220.
5. I. Vlodavsky, Y. Friedmann, M. Elkin, H. Aingorn, R. Atzmon, R. Ishai-Michaeli, M. Bitan, O. Pappo,T. Peretz, I. Michal, L. Spector, I. Pecker. *Nat. Med.* **1999**, *5*, 793– 802.
6. L. Baraz, Y. Haupt, M. Elkin, T. Peretz, I. Vlodavsky. *Oncogene* **2006**, *25*, 3939– 3947.
7. C. Pisano, I. Vlodavsky, N. Ilan, F. Zunino. *Biochem. Pharmacol.* **2014**, *89*, 12– 19.




www.manaraa.com

8. F. Zhang, X. Liang, J. M. Beaudet, Y. Lee, R. J. Linhardt. *J. Biom. Technol. Res.* **2014**, *1*, 6000101.

9. Y. Seo, M. R. Schenauer, J. A. Leary. *Int. J. Mass Spectrom.* **2011**, *303*, 191– 198, .

10. I. Stevic, N. Parmar, N. Paredes, L. R. Berry, A. K. C. Chan. *Cell Biochem. Biophys.* **2011**, *59*, 171– 178.

11. C. Shao, F. Zhang, M. M. Kemp, R. J. Linhardt, D. M. Waisman, J. F. Head, B. Seaton. *J. Biol. Chem.* **2006**, *281*, 31689– 31695.

12. H. Xie, Y. J. Kang. *Curr. Med. Chem.* **2009**, *16*, 1304– 1314.

13. L D. D'Andrea, A. Romanelli, R. Di Stasi, C. Pedone. *Dalt. Trans.***2010**, *39*, 7625– 7636.

14. T. R. Rudd, M. A. Skidmore, S. E. Guimond, M. Guerrini, C. Cosentino, R. Edge, A. Brown, D. T. Clarke, G. Torri, J. E. Turnbull, R. J. Nichols, D. G. Fernig, E. Yates. *Carbohydr. Res.* **2008**, *343*, 2184– 2193.

15. K. W. Hung, T. K. S. Kumar, K. M. Kathir, P. Xu, F. Ni, H. H. Ji, M. C. Chen, C. C.Yang, F. P. Lin, I. M. Chiu, C. Yu. *Biochemistry* **2005**, *44*, 15787– 15798.

16. Q. C. Jiao, Q. Liu, C. Sun, H. He. *Talanta* **1999**, *48*, 1095– 1101.

17. L. Tan, S. Yao, Q. Xie. *Talanta* **2007**, *71*, 827– 832.

18. H. Chu, N. R. Johnson, N. S. Mason, Y. A. Wang. *J. Controlled Release* **2011**, *150*, 157– 163.

19. A. K. Gorle, S. J. Katner, W. E. Johnson, D. E. Lee, A. G. Daniel, E. P. Ginsburg, M. von Itzstein, S. J. Berners-Price, N. P. Farrell. *Chem. Eur. J.* **2018**, 24, 6606-6616.

20. M. J. Kailemia, L. Li, Y. Xu, J. Liu, R. J. Linhardt, I. J. Amster. *Anal. Chem*. **2012**, 84, 5475–5478.

21. R. A. Ruhayel, B. A. Corry, C. Braun, D. S. Thomas, S. J. Berners-Price, N. P. Farrell. *Inorg. Chem*. **2010**, 49, 10815–10819.



www.manaraa.com

## Chapter 7: Synthesis and Characterization of Werner's Complex

### 7.1 Synthesis

Ammonium carbonate (7.0 g, 0.0728 mol) was dissolved in 20.0 mL of water, 20.0 mL of concentrated aqueous ammonia was then added. In a second container, cobalt (II) nitrate hexahydrate (5.0 g, 0.017 mol) was dissolved in 10.0 mL of water. The two solutions were combined with stirring. Slowly, 3.0 mL of the 30% hydrogen peroxide solution was added. Once the hydrogen peroxide has been added, the solution was evaporated to a volume of 30 mL. During the evaporation time, ammonium carbonate (1.7 g, 0.0173 mol) was added to the solution. When the solution volume was about 30 mL, the solution was filtered and the filtrate was cooled on ice. Red/purple crystals of product formed. These crystals were collected and washed with a few milliliters of ice-cold water and then ethanol, and dried. 2.0 g of the product was dissolved in 55 mL of 0.6 M nitric acid. The solution was then treated with 25 mL of ethanol, slowly. The resulting precipitate was filtered off. 2.0 g of the product was dissolved in 25 mL of 0.2 M aqueous ammonia. After 24 hours purple/black crystals began to form. After 3 days the crystals were collected. 2.0 g, 40.8% recovered.

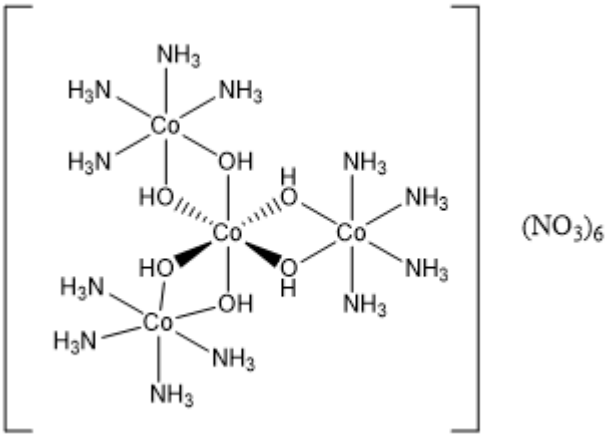


Figure 7.1. Werner's Complex



www.manaraa.com

## 7.2 Characterization

**1H NMR:**

Theoretical:

2.49ppm DMSO

2.95 and 4.29 ppm (3:3) axial and equatorial NH3

3.34 ppm (1.2) waters of crystallization

-1.69 ppm (1) OH

Experimental:

2.49ppm DMSO

2.9 and 4.3 ppm (3.02:3) axial and equatorial NH3

3.3 ppm (6.56) waters of crystallization

-1.7 ppm (.98) OH

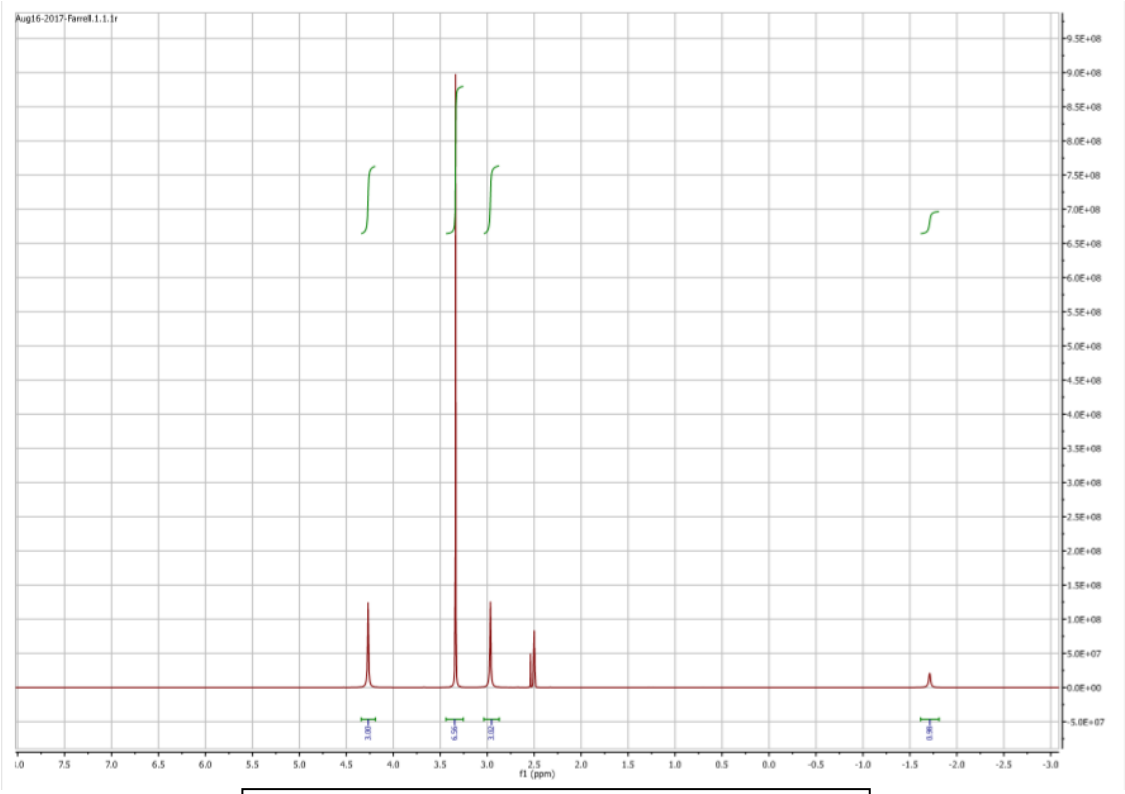


Figure 7.2. 1H NMR of Werner's Complex in DMSO.



www.manaraa.com

**UV:**

Theoretical:

311(4.95x10^3), 504(212), 627(126) wavelength (mol-1 cm-1)

Experimental:

311(4.79x10^3), 504(204), 627(127) wavelength (mol-1 cm-1)

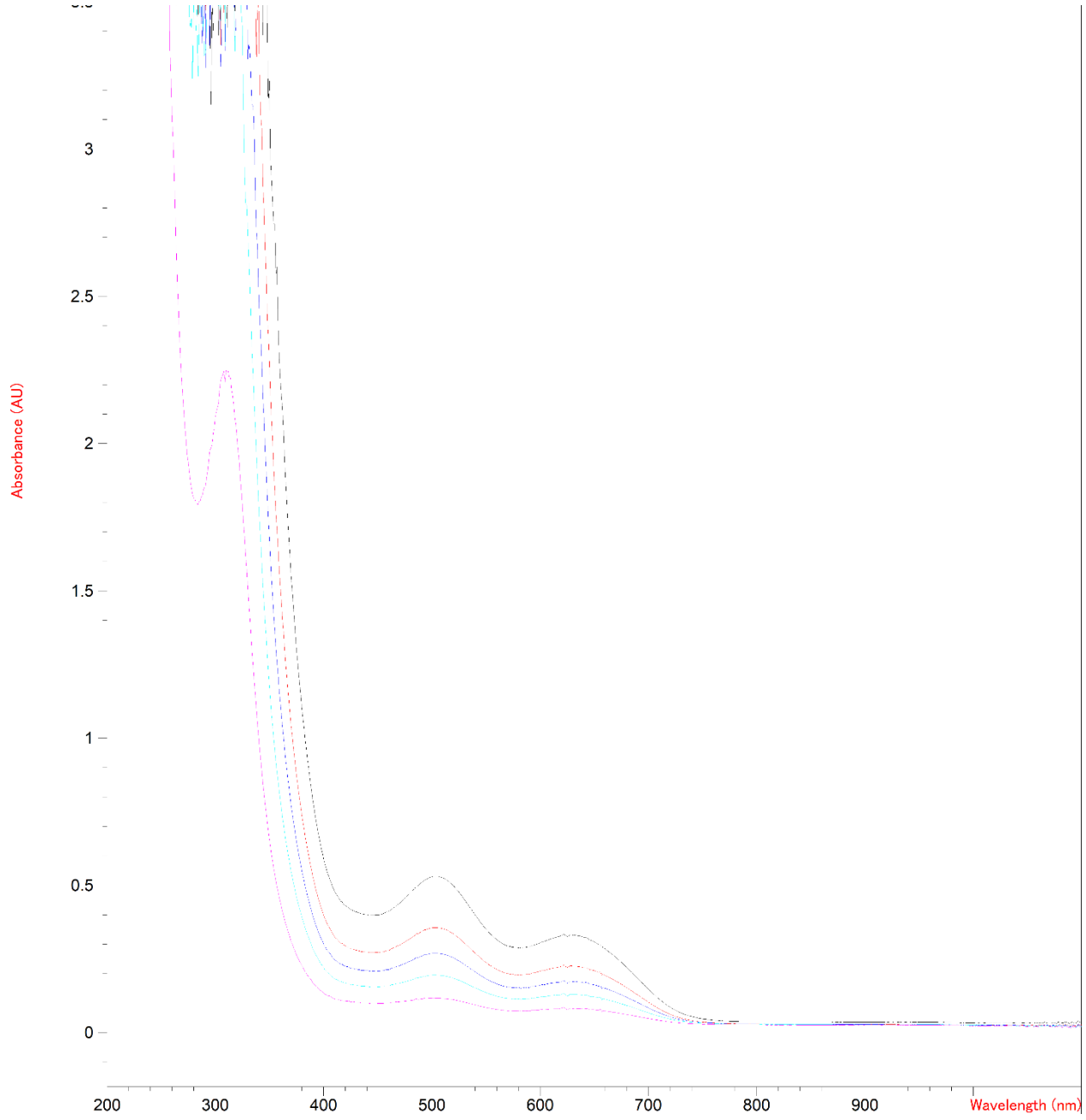


Figure 7.3. UV spectra of Werner's Complex in water.



www.manaraa.com

**IR:**

Present:

OH stretch 3600-3300

NH4 stretch 2375 and 3169, 1626, 817

NO3 stretch 1329

Co-N stretch 462

Co-O stretch 543

Not present:

SO4 stretch 1115

CO3 stretch 1715, 1240

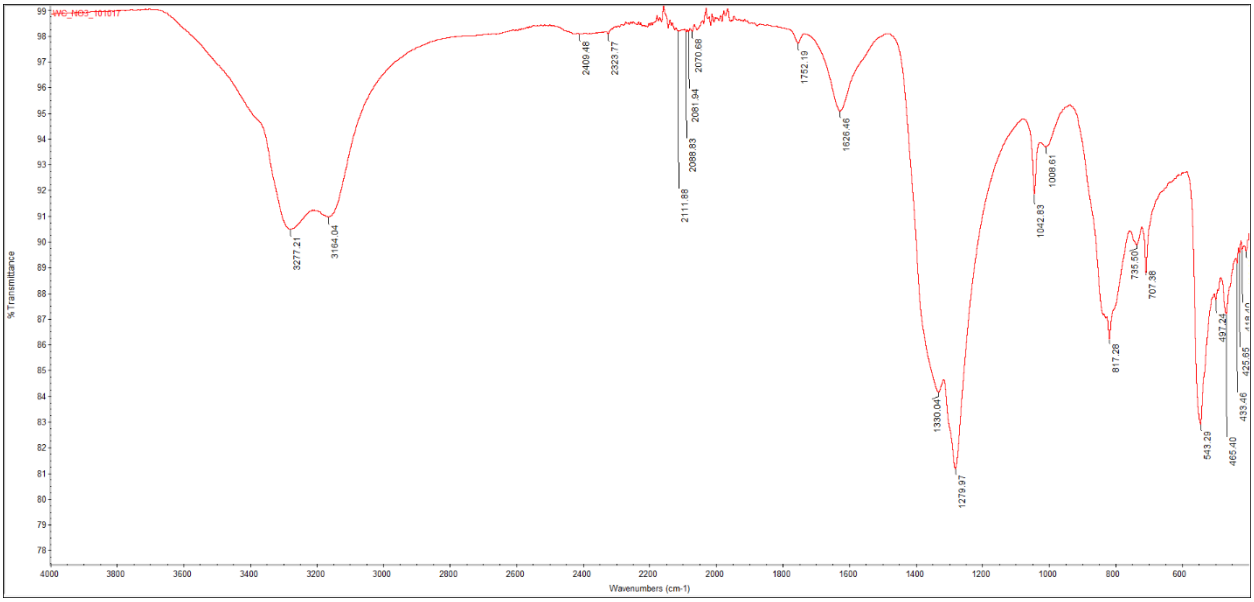


Figure 7.4. IR spectra of Werner's Complex.

**Elemental Analysis:**

Theoretical for $Co_4H_{42}N_{18}O_{24}$: C 0.00, H 5.19, N 25.24. Experimental: C <0.10, H 4.78, N 25.24



www.manaraa.com

**7.3 References:**


1. I. Bernal, J. Cetrullo, S. Berhane. *J. Coord. Chem.* **2000**, *52*, 185-205.

2. R. J. Angelici. Syntheses and Techniques in Inorganic Chemistry. W. B. Saunders: Philadelphia, 1977, 13.

3. A. M. Greenaway, R. J. Lancashire. *J. Chem. Educ*. **1982**, 59, 419.

4. A. Werner. *Z. Anorg. Chem*., **1893**, 3, 267; translated by G. B. Kauffman in "Classics in Coordination Chemistry Part 1," Dover Publications, Inc., N.Y. 1968, 9-88.

5. P. Pfeiffer. *J. Chem. Edu*. **1928**, 5, 1090.

6. A. Werner, V. L. King. *Chem. Berichte* **1911**, 44, 1887. Translated by G. B. Kauffman in "Classics in Coordination Chemistry Part 1," Dover Publications, Inc., N.Y. *1968*, 159-73.

7. A. Werner. *Chem. Berichte* **1914**, 47, 3087.

8. S. M. Jorgensen. *Z. Anorg. Chem*. **1898**, 16, 184.

9. A. Werner, E. Berl. *Chem. Berichte* **1907**, 40, 2103.

10. G. B. Kauffman, R. P. Pinnell. Inorganic Syntheses V, **1960**, 176.

11. G. Pass, H. Sutcliffe. "Practical Inorganic Chemistry," Chapman and Hall, Second Editio, **1974**.

12. H. A. Goodwin, E. C. Gyarfas, D. P. Mellor. *Aust. J. Chem*, **1958**, 11,426.

13. S. F. Mason, J. W. Wood. *J. Chem. Soc. Chem. Comm.* **1967**, 209.




www.manaraa.com

## Chapter 8: Conclusions

The results on heparin and Fondaparinux interactions with metal complexes can be extrapolated to glycosoaminoglycans such as HS. This emphasizes the relevance of glycan interactions in understanding the biological properties of coordination compounds and the utility of the metalloglycomics concept for extending bioinorganic chemistry to this class of important biomolecules.

The focused small library of PPCs studied here begins to elucidate structure–activity relationships. The stark contrast between $[Pt(NH_3)_4]^{2+}$ and MonoplatinNC in inhibiting the HS cleavage emphasizes the importance of dangling amine moieties as well as increased charge dispersion. The relative efficacy of the polynuclear set again shows that positive charge dispersion through dangling amines and Pt coordination spheres play important roles in masking the HS fragments and protecting them against enzymatic cleavage. The ability to form a "sulfate clamp" from the interaction of am(m)ines in a Pt coordination unit are likely to be more effective in masking than the single positive charge of the dangling amine—nevertheless the two structural features do contribute to the overall effect. Trends were assessed, affinity is related to charge and in general these substitution- inert complexes show broadly similar affinity to FPX and DNA. The approaches to inhibition of HS or DNA function are formally analogous since both protect the "substrate" from enzyme and/or protein processing. High- affinity DNA binding through the phosphate clamp efficiently inhibits transcription factors such as TBP (TATA box binding proteins) and restriction enzymes. While, the $K_d$ values found for PPC–FPX interactions are broadly similar to those found for growth factor–oligosaccharide interactions in the nM range. This suggests that metalloshielding will also be effective in inhibition of oligosaccharide- protein function as shown for the effect of TriplatinNC on FGF- heparin interactions.

The small library of simple metal ammine complexes, along with the lead compound TriPtNC, confirmed the generality of metal complexes and their affinity for HS. The $K_d$ values found for metal ammine–FPX interactions are broadly similar to those found for growth factor–



www.manaraa.com

oligosaccharide interactions in the μM range. Again, the overall results suggest comparable affinities for heparin relative to DNA for charged metal compounds, regardless of their intrinsic nucleic acid affinity. The presence of HS on the cell surface and its relatively similar affinity to DNA would suggest that glycan binding is thus a competitive cellular event for many coordination compounds. These results extend our understanding of the importance of the interactions of physiologically relevant aquated metal cations with heparin to defined coordination compounds. The available coordinating moieties on HS–heparin are the oxygen-donor atoms of the hard carboxylate and sulfate bases. Therefore, new patterns of metal-ion binding can be achieved by the interplay and application of hard–soft acid–base concepts. Further, in considering the concept of metalloglycomics, coordination compounds can be manipulated to modify the oxidation state, ligand lability, and coordination number and geometry to produce a diverse inorganic library. These studies also confirm the affinity of simple coordination complexes with heparin, using a series of mononuclear cobalt, ruthenium, and platinum compounds with affinity for heparin ordered Co > Ru > Pt. This suggests that cobalt complexes may be more effective at metalloshielding oligosaccharide-protein function.

Simple cobalt compounds bind with relatively high affinity to heparin, even greater than that of the simple platinum compound, tetraammineplatinum(II), extending this work into a library of cobalt complexes. The contrast between *t*-dichlorobis(ethylenediamine)cobalt(III) and pentaamminechlorocobalt(III) in inhibiting HS cleavage of FPX and matrix emphasizes the importance of hydrogen bonding in sulfate cluster protection. The overall results discussed here suggest comparable affinities for cobalt complexes binding to FPX as previously discussed. ITC shows that cobalt complexes interacting with FPX, $K_d$s of 18.6 to 90.1 μM, are comparable to a mixture of heterogeneous heparin chains complexing with FGF-1, $K_d$s of 1.1 to 3 μM. MB and MS assays suggest that covalent interactions of these cobalt compounds may only interact with a single sulfate, while non-covalent hydrogen bonding may interact with a cluster of sulfates. This was observed using MB as a reporter, requiring a higher concentration of covalently interacted cobalt complexes over the non-covalent complexes. This was also observed in the MS with a



www.manaraa.com

greater number of sulfates lost through the covalent interaction of *t*-dichlorobis(ethylenediamine)cobalt(III) with up to six sulfates lost from FPX in the 2- charge state, while the non-covalent interaction showed lower abundance of lost sulfates. Therefore "metalloshielding" of FPX through sulfate clusters would be greater in the non-covalent compounds over the covalent interactions. However, the NMR results show that covalent interactions, using application of hard–soft acid–base concepts, occur much stronger than the non-covalent interactions. These assays give an estimate of the strength of the FPX–cobalt binding and provide a relative calculation of affinities. This suggests that cobalt complexes with hydrogen bonding ability will be more effective at metalloshielding oligosaccharide-protein function.

Interactions between non-covalent cobalt complexes and FPX were also studied. More sulfate loss was observed with electrostatic interactions, while cobalt complexes with the ability to interact through hydrogen bonding were able to protect the FPX from sulfate loss through sulfate cluster interaction with an ability to "metalloshield" a larger group of sulfate clusters where one ammine can interact with multiple oxygens. The compounds using only electrostatic interactions will have more of dispersed charge with larger ligands that produces a weaker interaction between the metal complexes and FPX. Further, electrostatic interactions between cobalt and FPX were stronger as compared to electrostatic interactions between ruthenium complexes and FPX. ITC titrations of tris(2,2'-bipyridine)ruthenium(II) into FPX did not give a well-defined isothermal trace, perhaps due to weak binding arising from a lack of hydrogen bonding interactions, consistent with what was observed in the MB assay. The multinuclear Werner's Complex exhibited similar association as the PPCs for FPX. Again, this suggests that multinuclear cobalt complexes with hydrogen bonding ability will be more effective at metalloshielding oligosaccharide-protein function.

In addition, simple metal complexes interact with Fondaparinux and may be considered in the development of future antimetastatic drugs in application of hard-soft acid-base concepts. Vanadium, a hard acid, reacts with oxygen, a hard base, forming a stronger bond than Manganese, an intermediate acid, with oxygen. Vanadium also produces a stronger interaction than Manganese due to a higher overall charge of the complex and due to its ability to interact with more sulfate



www.manaraa.com

groups. Vanadyl, containing oxygen, lowered the overall charge of the metal complex and limited the amount of "metalloshielding". New patterns of metal-ion binding can be achieved by the interplay and application of hard–soft acid–base concepts.

Further studies should be performed using the less cytotoxic cobalt complexes to confirm their strength of interactions to HS. Assays using ITC would show the competitive binding of cobalt complexes vs growth factors binding to FPX. Linear, multinuclear cobalt complexes should also be studied, mimicking the lead compounds TriplatinNC or BBR3464. These linear cobalt complexes should interact relatively similarly as the PPCs with the anionic HS while maintaining the low cytotoxic profile. A BBR3464 mimic would allow strong covalent interactions between the hard acid of cobalt and the hard base of oxygen, while the non-covalent hydrogen bonding would allow sulfate cluster interactions for strong metalloshielding. Furthermore, the poor pharmacokinetic results that plagued BBR3464 should be overcome by limiting the inactivation of sulfur containing biomolecules and producing a target that is overexpressed on cancer cells. Overall, these results demonstrate the utility of the metalloglycomics concept in developing new classes of molecules for study of glycan structure and function. It is clear that oligosaccharides represent a viable alternative cellular target to oligonucleotides and these results further emphasize the unique dual-function nature of metal complexes.



www.manaraa.com

## Appendix

### Synthesis and Characterization

trisethylenediaminecobalt(III) chloride

Cobalt(II) chloride hexahydrate (6.0 g, 25.0 mmol) was dissolved in 17.5 mL of water. Another solution was prepared by dissolving 4.51 mL of anhydrous ethylenediamine (2.7 eq, 67.5 mmol) in 12.5 mL of water and cooled to 0 °C on ice and neutralized partially with 4.35 mL of 6 M HCl (25.5 mmol). Both solutions were mixed together and 5 mL of 30% hydrogen peroxide was added with stirring. The solution was then boiled to a volume of approximately 30.0 mL. 30 mL of 12 M HCl was added, followed by addition of 60 mL of ethanol and allowed to cool to room temperature for 30 mins. The solution was cooled to 0 °C and the precipitate was collected and washed with ice-cold ethanol and ether (10 mL each). The final product was dried in air. Yellow crystals collected 4.3 g 61.7%.



www.manaraa.com

**1H NMR:**

Theoretical:

4.80 ppm $D_2O$

5.2 and 4.8 ppm (6:6) $NH_2$

2.8 ppm (12) $CH_2$

Actual:

5.2 ppm (6) $NH_2$ and 4.8 ppm (under $D_2O$)

2.8 ppm (12) $CH_2$

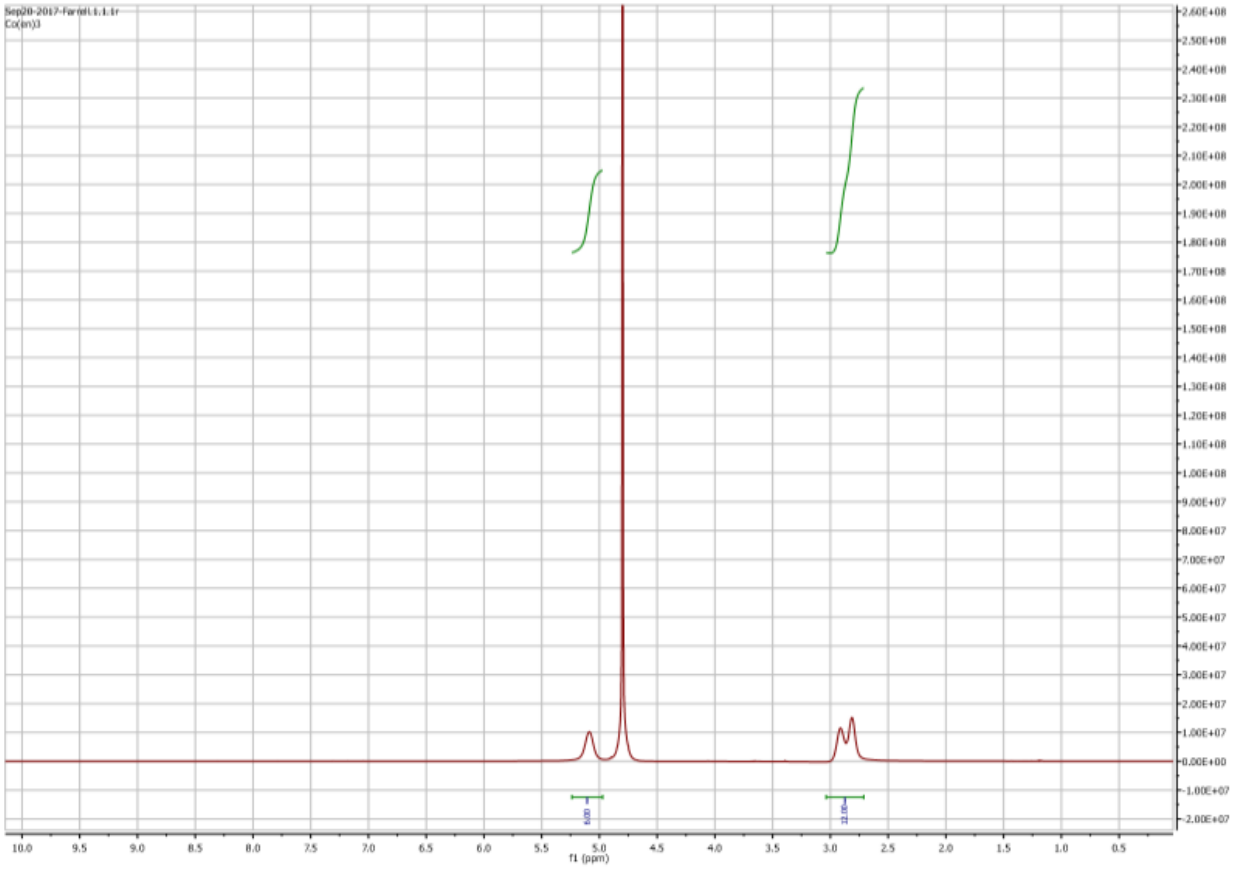


Figure A.1. 1H NMR of $Co(en)_3Cl_3$ in water.



www.manaraa.com

*trans*-dichlorobis(ethylenediamine)cobalt(III) chloride

300 mL of water was heated in a 600 mL beaker and maintained at a moderate boil. In an evaporating dish, 4.0g of Cobalt (II) Chloride Hexahydrate (16.6 mmol) was combined with 10 mL of water. To this was added 15 mL of 10% ethylenediamine (en) (0.23 mmol). The evaporating dish was placed on top of the beaker of boiling water. The mixture was stirred over this steam bath for 40 minutes; the volume of the solution was maintained at about 5 mL by occasionally adding small portions of water. During this process, the $Co^{2+}$ was oxidized to $Co^{3+}$ by the oxygen in the air. Good agitation was necessary to promote solvation of the oxygen. To the solution, 12 mL of Concentrated 12 M HCl was added. Heating and stirring was continued without addition of water until a thin slurry of crystals was formed. The slurry was cooled to Room Temperature by setting the evaporating dish on the lab bench and stirred occasionally for 15 minutes. The mixture was collected using a Buchner funnel with Side-Arm Flask attached to an aspirator. The precipitate was washed with a minimal amount of 6 M HCl (2 mL) and air dried. 1.19 g collected green precipitate (20.8%).



www.manaraa.com

**1H NMR:**

Theoretical:

4.80 ppm $D_2O$

5.2 (1) $NH_2$

2.8 ppm (1) $CH_2$

Actual:

5.2 ppm (1) $NH_2$

2.8 ppm (1) $CH_2$

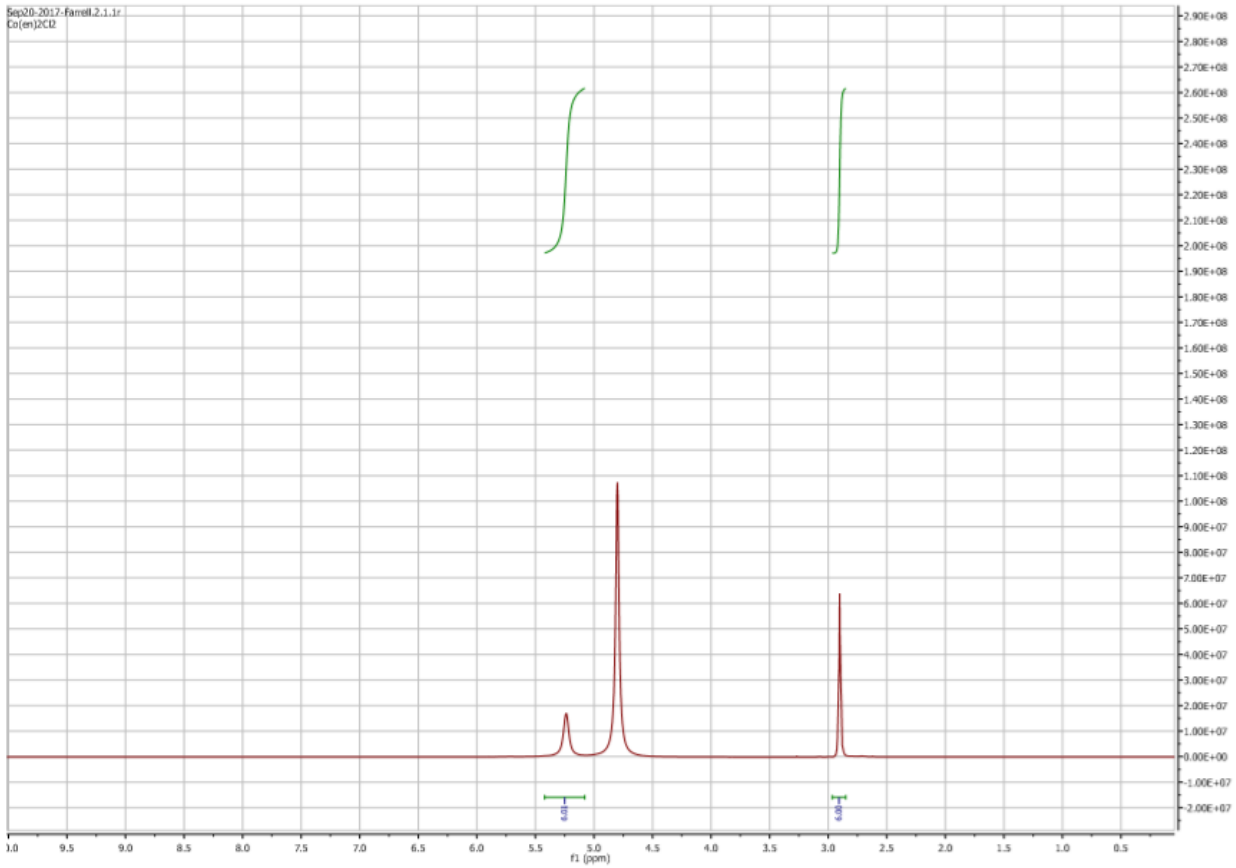


Figure A.2. 1H NMR of $Co(en)_2Cl_2Cl$ in water.



www.manaraa.com

**UV-VIS $\lambda_{maz}$:**

Theoretical

cis: 390, 530 nm

trans: 450, 625 nm

Actual

cis: 380, 520 nm

trans: 450, 625 nm

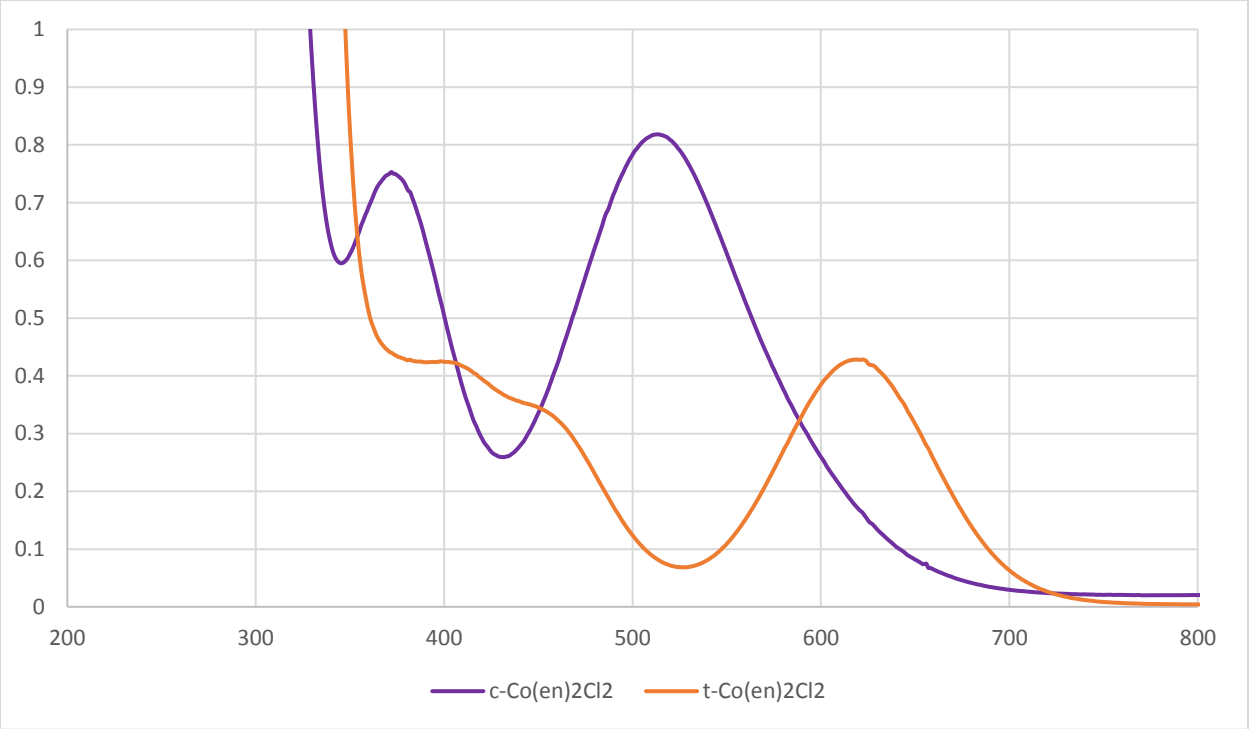


Figure A.3. UV-VIS spectra of isomerization of $Co(en)_2Cl_2Cl$ in water.



www.manaraa.com

**Isothermal Titration Calorimetry**

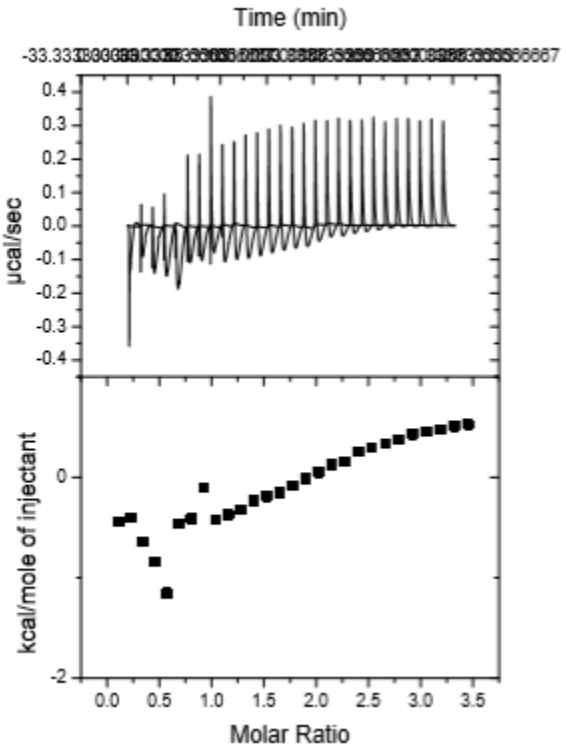


Figure A.4. ITC of isomerization of $Co(en)_2Cl_2Cl$ in water.



www.manaraa.com

**References**


1. J. A. Broomhead, F. P. Dwyer, J. W. Hogarth. *Inorg. Syn.* **1960**, 6, 183-186.

2. J. C. Bailar Jr. *Inorg. Synth*. **1946**, 2, 222-225.

3. P. S. Poskozim. *J. Chem. Educ*. **1969**, 46, 384-385.




www.manaraa.com

# Vita

Wyatt E. Johnson was born in Moseley, Virginia. He received his Bachelor of Science degree in Biology and his Master of Science in Curriculum and Instruction with Science Speacialization from Pensacola Christian College in 2011 and 2013. He then enrolled in the graduate program at Virginia Commonwealth University. He recently started working at Evonik as a formulation chemist. Publications include:

Katner, S.J., Johnson, W.E., Peterson, Page, P., and Farrell, N.P. (in press). Comparison of metal-ammine compounds binding to DNA and heparin. Glycans as ligands in bioinorganic chemistry. Inorg. Chem, 2018.

Gorle A.K., Katner, S.J., Johnson, W.E., Lee, D.E., Daniel, A.G., Ginsburg, E.P., Itzstein, M., Berners-Price, S.J., and Farrell, N.P. (in press). Substitution-inert Polynuclear Platinum Complexes as Metalloshielding Agents for Heparan Sulfate. Chem. Eur. J, 2018.

In Preparation:

Johnson, W.E., Hampton, J.D., Peterson, E.J., Beaton, J.F., and Farrell, N.P. Cobalt Complexes Interactions with the HS Mimetic Fondaparinux and Their Dual Therapeutic Potential.

Johnson, W.E., Mashid, M., Beaton, J.F., Peterson, E.J., and Farrell, N.P Metalloglycomics: Probing the Metalloshielding Interactions of Simple Metal Complexes with Fondaparinux.

Interactions of Non-covalent Metal Complexes with Fondaparinux.

To be submitted to Inorganic Chemistry



www.manaraa.com